Trinity College Dublin
Coláiste na Tríonóide, Baile Átha Cliath
The University of Dublin

**Ph.D. Drug Development**

**May 2024**

# Investigating the therapeutic utility of Olaparib in Metachromatic Leukodystrophy and Krabbe Disease

**Marianna Mekhaeil**

Submitted to Trinity College Dublin for the degree of Doctor of Philosophy

Primary Supervisor: Prof. Kumlesh Dev

Secondary Supervisor: Dr. Melissa Conroy

## Declaration

I declare that this thesis has not been submitted as an exercise for a degree at this or any other university and it is entirely my own work. I agree to deposit this thesis in the University's open-access institutional repository or allow the Library to do so on my behalf, subject to Irish Copyright Legislation and Trinity College Library conditions of use and acknowledgment. I consent to the examiner retaining a copy of the thesis beyond the examining period, should they so wish (EU GDPR May 2018).

## Abstract

Leukodystrophies encompass a diverse group of genetically-based disorders that impact the development and preservation of myelin in the central nervous system's white matter. These conditions, affecting approximately 1 in 7,700 live births, exhibit significant variability in clinical presentation and disease progression, manifesting symptoms like motor dysfunction, cognitive impairment, and ataxia. Recent advancements in genetic medicine and imaging have shed light on the specific genetic and biochemical abnormalities associated with individual leukodystrophies, such as Metachromatic Leukodystrophy (MLD) and Krabbe disease (KD), which are characterized by the accumulation of toxic substances, sulfatide, and psychosine, respectively.

Traditionally, it was believed that mutations in myelin- or oligodendrocyte-specific genes were solely responsible for leukodystrophies. However, contemporary research has expanded our understanding, revealing that these disorders are linked to defects in astrocytes, microglia, axons, and blood vessels. Despite limited knowledge of their underlying mechanisms, symptomatic treatments have been developed to alleviate some of the burdens associated with leukodystrophies. Nevertheless, effective cures for these conditions remain elusive, prompting exploration into addressing neuroinflammation as a promising therapeutic strategy.

Poly (ADP-ribose) polymerase 1 (PARP-1) has emerged as a central player in chronic inflammation, operating not only in immune cells but also in astrocytes, endothelial cells, and fibroblasts, contributing to inflammation across various tissues. Some FDA-approved PARP-1 inhibitors, including Olaparib and Veliparib, have exhibited cytoprotective and anti-inflammatory effects in preclinical models of non-oncological diseases, such as neurological conditions (e.g., stroke, Parkinson's disease, Alzheimer's disease, multiple sclerosis), diabetes, and myocardial infarction. However, there is currently no direct evidence of PARP-1 involvement in leukodystrophies like KD or MLD, and no PARP-1 inhibitors are under clinical investigation for these conditions.

In the context of MLD, research has focused on the interplay between sulfatide and Olaparib in astrocytes, which play a crucial role in inflammation and myelination. Studies have established a concentration-dependent model of sulfatide-induced astrocyte toxicity, with Olaparib effectively mitigating these effects. Sulfatide has also been found to induce impairments in ROS production, mitochondrial stress, and Ca2+ signaling in human astrocytes, all of which are alleviated by Olaparib treatment. Additionally, using an *ex vivo* model of murine-derived organotypic cerebellar slices, it was demonstrated that sulfatide induces demyelination, which can be attenuated by Olaparib treatment.

In the case of KD, characterized by psychosine accumulation and chronic inflammation, a connection between psychosine toxicity and PARP-1 overactivation in both astrocytes and murine-derived organotypic cerebellar slices has been revealed. Psychosine-induced toxicity involves neuroinflammation, immune cell migration, ROS production impairments, Ca2+ signaling disturbances, demyelination, axonal degeneration, and oligodendrocyte loss. Olaparib treatment significantly mitigates the toxic effects of psychosine.

In conclusion, this study provides compelling evidence that psychosine and sulfatide-induced neurotoxicity are mediated by PARP-1 activation, resulting in oligodendrocyte loss, heightened pro-inflammatory cytokine expression, increased ROS levels, and enhanced recruitment of NK and T cells. Furthermore, the findings suggest that Olaparib treatment may hold therapeutic potential in alleviating toxin-induced pathology in both MLD and KD. This research underscores the importance of exploring novel treatment avenues for rare demyelinating diseases and the potential of PARP-1 inhibitors as a promising therapeutic approach.

## Acknowledgments

First and foremost, I would like to express my heartfelt appreciation to Prof. Kumlesh Dev, my supervisor, for his consistent mentorship, invaluable guidance, and unwavering encouragement in fostering my independent work. His vast expertise and boundless patience have steered me through every phase of my research project, offering unparalleled support on academic fronts.

My sincere gratitude extends to Dr. Melissa Conroy, whose steadfast support and encouragement have been a constant beacon. Her guidance and advice, both scientific and personal, have been generously shared with a smile, and I am thankful for the substantial amount of time she has dedicated to me and my project.

To all the Ph.D. students, research assistants, and MD students I've had the privilege to collaborate with in recent years – Sybille Bechet, Sean Lonergan, Joanna Laskowska, Kapil Sharma, Eimear Mylod, Caroline Marion, Emily Keenan, Paraskevi Papakyriakopoulou, and Stamatia Trygoni – I am profoundly grateful. Our endless coffee breaks and lengthy lunches on the benches outside have been both enjoyable and nourishing for my academic spirit.

My sincere appreciation also goes out to the entire Department of Physiology for their warm hospitality and assistance, with special mention to Mr. Aidan Kelly. I am equally thankful to Dr. Gavin McManus for his invaluable assistance with confocal microscopy and IMARIS analysis.

Lastly, I want to express my deep gratitude to my family and friends for their unwavering support throughout my academic journey.

# Outputs

## Publications - Accepted

*First author*

- Existing Evidence for the Repurposing of PARP-1 Inhibitors in Rare Demyelinating Diseases. Authors: **Marianna Mekhaeil**, Kumlesh K. Dev, Melissa J. Conroy. Cancers (Basel), 2022.
- Olaparib Attenuates Demyelination and Neuroinflammation in an Organotypic Slice Culture Model of Metachromatic Leukodystrophy. Authors: **Marianna Mekhaeil**, Melissa J. Conroy, Kumlesh K. Dev. Neurotherapeutics, 2023.
- Elucidating the therapeutic utility of Olaparib in sulfatide-induced human astrocyte toxicity and neuroinflammation. Authors: **Marianna Mekhaeil**, Melissa J. Conroy, Kumlesh K. Dev. Journal of Neuroimmune Pharmacology, 2023.

*Authored*

- Investigating the Effects of Olaparib on the Susceptibility of Glioblastoma Multiforme Tumour Cells to Natural Killer Cell-Mediated Responses. Authors: Jennifer Moran*, Eimear Mylod*, Laura E. Kane, Caroline Marion, Emily Keenan, **Marianna Mekhaeil**, Joanne Lysaght, Kumlesh K. Dev, Jacintha O'Sullivan, Melissa J. Conroy. Pharmaceutics, 2023.
- Inhibition of microglial β-glucocerebrosidase hampers the microglia-mediated antioxidant and protective response in neurons. Authors: Elettra Brunialti, Alessandro Villa, **Marianna Mekhaeil**, Federica Mornata, Elisabetta Vegeto, Adriana Maggi, Donato Di Monte, Paolo Ciana. Journal of Neuroinflammation, 2021.

## Publications - Under Revision/Preparation

*First author*

- Identifying a Novel Role of PARP-1 in Psychosine-Induced Astrocyte Toxicity, Inflammation and Demyelination. Authors**: Marianna Mekhaeil**, Sean Lonerghan, Melissa J. Conroy, Kumlesh K. Dev Target Journal: Journal of Neuroinflammation.

## Poster presentations at conferences

- **Annual Scientific Meeting of the Irish Society of Clinical Neurophysiology**, Cork, 2nd – 3rd March 2023, Title: Elucidating the therapeutic utility of Olaparib in sulfatide-induced human astrocyte toxicity and neuroinflammation.
- **European Glial Meeting 2023**, Berlin, Germany, 8th – 11th July 2023, Title: Elucidating the therapeutic utility of Olaparib in Metachromatic Leukodystrophy.

## Awards

- Ermenegildo Zegna Award (2021, 2022, 2023) a highly prestigious doctoral fellowship for Italian citizens undertaking their postgraduate studies outside Italy.
- Trinity Trust Travel Grant for travel to GLIA conference 2023, Berlin, Germany.
- Prize for best confocal image – Physiology Friday 2022.
- ImmunoTools Special Award, 2021

Table of Contents

**List of Figures**

**List of tables**

# Abbreviations

| | |
|---|---|
| ACM | Astrocyte Conditioned Media |
| AIF | Apoptosis-Inducing Factor 1 |
| AMD | Auto-Modification Domain |
| AQP4 | Water Channel Aquaporin 4 |
| ARSA | Arylsulfatase A |
| ART | ADP-Ribosyl Transferase |
| ATP | Adenosine Triphosphate |
| AUC | Area Under Curve |
| BBB | Blood Brain Barrier |
| BRCT | BRCA1 C Terminus |
| BSA | Bovine Serum Albumin |
| Ca2+ | Calcium |
| CCL | C-C Motif Chemokine Ligand |
| CNS | Central Nervous System |
| Ctrl | Control |
| CX3CL1 | C-X3-C Motif Ligand 1 |
| DCFDA | 2′,7′-Dichlorofluorescein Diacetate |
| DCFH-DA | Diacetyldichlorofluorescein |
| DMEM | Dulbecco’s Modified Eagle Medium |
| DMSO | Dimethylsulfoxide |
| DNA | Deoxyribonucleic Acid |
| EAE | Experimental Autoimmune Encephalomyelitis |
| ELISA | Enzyme-Linked Immunosorbent Assay |
| FACS | Fluorescent Activated Cell Sorting |
| FBS | Foetal Bovine Serum |
| FDA | Food And Drug Administration |
| GALC | Galactocerebrosidase |
| GFAP | Glial Fibrillary Acidic Protein |
| HBSS | Hanks' Balanced Salt Solution |
| HD | Helical Sub-Domain |
| HEPES | 4-(2-Hydroxyethyl)-1-Piperazineethanesulfonic Acid |
| HPR | Horseradish Peroxidase |
| Iba1 | Ionized Calcium-Binding Adapter Molecule 1 |
| ICAM-1 | Intercellular Adhesion Molecule 1 |

| | |
|---|---|
| IFN-γ | Interferon Gamma |
| IL | Interleukin |
| iNOS | Inducible Nitric Oxide Synthase |
| JC-1 | 5,5,6,6'-Tetrachloro-1,1',3,3' Tetraethylbenzimi-Dazoylcarbocyanine Iodide |
| KD | Krabbe Disease |
| KO | Knock-Out |
| LFA-1 | Lymphocyte Function-Associated Antigen 1 |
| MBP | Myelin Basic Protein |
| Mg2+ | Magnesium |
| MIF | Macrophage Migration Inhibitory Factor |
| MLD | Metachromatic Leukodystrophy |
| MOG | Myelin Oligodendrocyte Glycoprotein |
| MTT | 3-(4,5-Dimethylthiazol-2-Yl)-2,5-Diphenyltetrazolium Bromide |
| NAD | Nicotinamide Adenine Dinucleotide |
| NFH | Neurofilament Heavy |
| NF-κB | Nuclear Factor Kappa-Light-Chain-Enhancer Of Activated B Cells |
| NK cell | Natural Killer Cell |
| NMDA | N-Methyl-D-Aspartate |
| OCS | Mouse Organotypic Cerebellar Slice |
| OCSCM | Conditioned media from OCS |
| pADPr | Poly-ADP-Ribosylation |
| PAR | Poly-ADP-Ribose |
| PARG | Poly-ADP-Ribose Glycohydrolase |
| PARP | Poly-ADP-Ribose Polymerase |
| PBMC | Peripheral Blood Mononuclear Cells |
| PBS | Phosphate Buffered Saline |
| Pen/Strep | Penicillin/Streptomycin |
| PFA | Paraformaldehyde |
| Psychosine | Galactosylsphingosine |
| PVDF | Polyvinylidene Difluoride |
| RIPA | Radioimmunoprecipitation Assay |
| ROI | Region Of Interest |
| ROS | Reactive Oxygen Species |
| RPMI | Roswell Parks Memorial Institute Media |
| SD | Standard Deviation |

| | |
|---|---|
| SDS-PAGE | Sodium Dodecyl-Sulphate Polyacrylamide Gel Electrophoresis |
| SEM | Standard Error Of The Mean |
| SSB | DNA Single-Strand Break |
| Sulfatide | Galactosylceramide-3-O-Sulfate |
| TNF-α | Tumour Necrosis Factor Alpha |
| VCAM-1 | Vascular Adhesion Molecule 1 |
| VLA-4 | Very Late Antigen 4 |
| XRCC1 | X-Ray Repair Cross-Complementing 1 |
| α-syn | α -Synuclein |

# Chapter 1 – Introduction

## 1.1 Poly (ADP-ribose) polymerase 1

In response to environmental challenges, intrinsic DNA repair pathways are engaged to uphold cellular functionality and viability [1]. Dysfunctional DNA repair mechanisms can compromise genomic stability, escalate the risk of errors during RNA and protein synthesis, and closely correlate with various cancers [1,2]. The Poly (ADP-ribose) polymerase (PARP) family, comprising 17 human enzymes **[Table 1.1]**, takes charge of crucial cellular processes such as DNA repair, transcriptional control, cell cycle progression, oncogene activity, and mitochondrial function. These functions are facilitated through a post-translational modification called PARylation, where ADP-ribose units derived from nicotinamide adenine dinucleotide ($NAD^+$) are covalently added to target proteins, aiding in the rescue of DNA damage [3,4].

At the forefront of PARylation stands PARP-1, responsible for over 90% of PARylation activity [5]. Its most well-established role involves the recognition and mending of DNA single-strand breaks (SSBs). PARP-1 catalyzes the attachment of poly (ADP-ribose) (PAR) units not only to itself but also to other pivotal proteins such as DNA ligase II, DNA polymerase, and XRCC1 topoisomerases **[Figure 1.1A]** [6,7]. These enzymes are essential custodians of genomic integrity, steering the course of SSB repair. Poly (ADP-ribose) glycohydrolase (PARG) steps in to conclude the DNA repair process by detaching PAR from target proteins [8]. The failure to rectify SSBs could lead to the progression of double-strand breaks, often culminating in cellular demise and contributing to the emergence and advancement of a spectrum of diseases [9] **[Table 1.1]**.

Upon the initiation of programmed cell death pathways, such as apoptosis, PARP-1 is cleaved and deactivated by activated caspases [10]. Deficiencies in PARP-1 inactivation or prolonged DNA damage can trigger excessive activation of PARP-1, depleting $NAD^+$ and adenosine

triphosphate (ATP) levels [10,11]. In such scenarios, cells might undergo necrosis or a less common form of cell demise termed "PARthanatos" [10]. PARthanatos is implicated in the etiology of several brain-related disorders, including neurodegeneration and neuroinflammation [10]. This process unfolds with the translocation of free PAR to the cytoplasm, where it binds to mitochondrial receptors, culminating in the release of apoptosis-inducing factor 1 (AIF). AIF translocates to the nucleus, triggering DNA fragmentation [10] [**Figure 1.1B**].

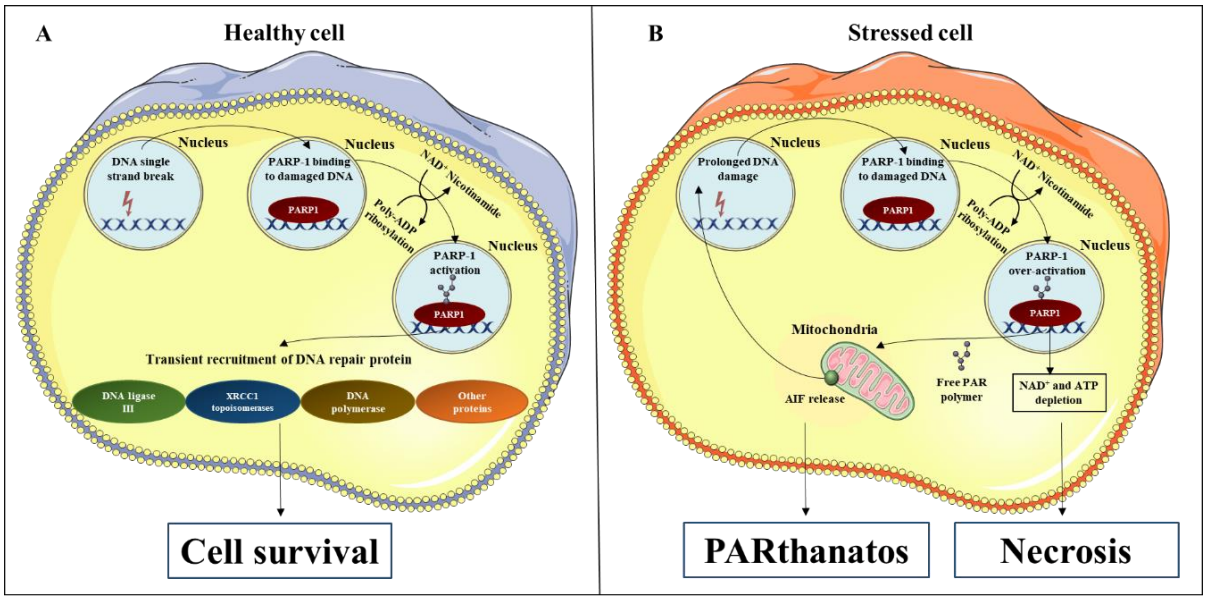


**Figure 1.1: PARP-1 signaling in healthy and stressed cells. (A)** PARP-1 activation requires $NAD^+$ to catalyse the addition of PAR to itself. This same pathway is also used for PARP-1 to add PAR to DNA repair proteins including DNA ligase II, DNA polymerase, and XRCC1 topoisomerases. **(B)** Prolonged DNA damage induces over-activation of PARP-1, leading to $NAD^+$ and ATP depletion, which may promote cell necrosis. In addition, some PAR may translocate to the cytosol and bind to mitochondrial receptors, causing the release of AIF, which diffuses to the nucleus and triggers DNA fragmentation. This form of cell death is known as “PARthanatos”. Parts of the figure were generated using images from Servier Medical Art.

| PARP enzyme | Function | Localization | Catalysed reaction | Associated pathology |
|---|---|---|---|---|
| PARP-1 | DNA break repair, chromatin regulation and transcription, cell cycle, metabolic regulation, inflammation | Nucleus | Poly-ADP-ribosylation | Most malignancies, neurodegenerative diseases, brain injury, inflammatory-based diseases, metabolic disorders, Diphtheria, Xeroderma Pigmentosum, Complementation Group A |
| PARP-2 | DNA break repair, chromatin regulation and transcription, cell cycle, metabolic regulation, inflammation | Nucleus, Cytoplasm | Poly-ADP-ribosylation | Most malignancies, neuroinflammation, brain injury, metabolic disorders, Osebold-Remondini Syndrome, Cockayne Syndrome |
| PARP-3 | DNA break repair, chromatin regulation and transcription, cell cycle | Nucleus, Cytoplasm | Mono-ADP-ribosylation | Osebold-Remondini Syndrome, Arthrogryposis, Renal Dysfunction, Cholestasis 1 |
| PARP-4 | Tumorigenesis, immune response | Nucleus, Cytoplasm | Mono-ADP-ribosylation | Osebold-Remondini Syndrome, primary thyroid, breast cancer |
| TNKS1 | Regulation of telomeres and mitosis, inflammation, metabolic regulation, stress response | Cytoplasm | Poly-ADP-ribosylation | Cherubism, Lung Acinar Adenocarcinoma, Herpes simplex and Epstein Barr viral infections, severe obesity |
| TNKS2 | Regulation of telomeres and mitosis, inflammation, metabolic regulation | Cytoplasm | Poly-ADP-ribosylation | Cancer, Cherubism, systemic sclerosis, severe obesity, Arthrogryposis, Renal Dysfunction, Cholestasis 1 |
| PARP-6 | DNA break repair, tumour suppressor, dendrite morphogenesis in neuron | Cytoplasm | Mono-ADP-ribosylation | Microencephaly, Intellectual disabilities, Epilepsy, Renal cancer, Cervical cancer, Colorectal cancer, Porokeratosis |
| PARP-7 | DNA break repair, chromatin regulation and transcription, innate immune response, neuronal function | Nucleus, Cytoplasm | Mono-ADP-ribosylation | Retinitis Pigmentosa, Breast cancer |
| PARP-8 | Assembly or maintenance of membranous organelles | Cytoplasm | Mono-ADP-ribosylation | Developmental And Epileptic Encephalopathy, Arthrogryposis, Renal Dysfunction, Cholestasis |
| PARP-9 | DNA break repair, chromatin regulation and transcription, immune response, cell migration | Nucleus, Cytoplasm | Mono-ADP-ribosylation | B-Cell Lymphoma, Lymphoma |
| PARP-10 | DNA break repair, chromatin regulation and transcription, RNA processing, immune response | Cytoplasm, Golgi apparatus | Mono-ADP-ribosylation | Diphtheria, Arthrogryposis, Renal Dysfunction, Cholestasis 1 |
| PARP-11 | DNA break repair, chromatin regulation and transcription, nuclear envelope stability, immune response | Nucleus, Cytoplasm | Mono-ADP-ribosylation | Osteogenesis Imperfecta, Arthrogryposis, Renal Dysfunction, Cholestasis 1 |
| PARP-12 | DNA break repair, chromatin regulation and transcription, RNA processing, stress response, immune response | Cytoplasm | Mono-ADP-ribosylation | Renal and liver cancer, Osebold-Remondini Syndrome, Osteogenesis Imperfecta |

**Table 1.1: Classification of PARP enzymes and associated pathologies.** The PARP family includes 17 enzymes in humans. Most PARPs are localized in nucleus and cytoplasm and contribute to genome integrity, metabolic regulation, and immune response. Mutations or dysfunction in PARP activity are associated with distinct pathologies. Sources: Genecards.org; Proeinatlas.org.

Structurally, PARP-1 has a C-terminal catalytic domain, composed of a helical sub-domain (HD) and ADP-ribosyl transferase (ART) fold [12]. Its function is to oxidize nicotinamide as a substrate to add PAR on target proteins. PARP-1 also has a Trp-Gly-Arg (WGR) domain and an N-terminal DNA-binding domain (DBD) containing three zinc finger motifs (Zn1, Zn2, and Zn3) [12]. Together, these domains allow PARP-1 to detect DNA breaks and physically interact with chromatin [13]. In addition, there is a central auto-modification domain (AMD) constituted by BRCA1 C terminus (BRCT) motif, which acts as the target of covalent auto-modification [13] **[Figure 1.2]**.

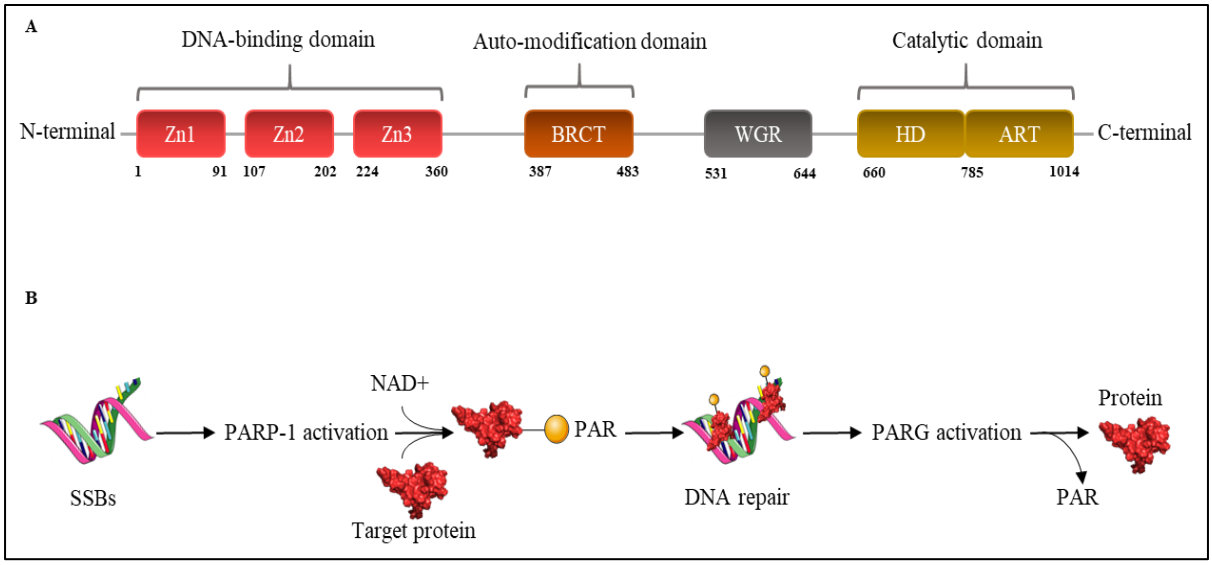


**Figure 1.2: Scheme of PARP-1 structure and mechanism of action. (A)** PARP-1 is comprised of three main domains starting from N-terminal to C-terminal: DNA binding domain characterized by zinc finger motifs Zn1, Zn2, and Zn3; auto-modification domain with the BRCT motif; WGR domain; catalytic domain formed by HD and ART; **(B)** DNA SSBs are recognized by PARP-1, which become activated and use $NAD^+$ to catalyse the addition of PAR to target proteins that contribute to DNA's reparation. The reaction is ended by PARG's recruitment that removes PAR from target proteins. Parts of the Figure were generated using images from Servier Medical Art.

## 1.2 The Pharmacology of PARP-1 Inhibitors

The chronic activation of PARP-1 has been closely linked to the development of diverse malignancies including breast, ovarian, uterine, lung, skin, and prostate cancers, as well as colorectal cancer, pediatric central nervous system cancer, Non-Hodgkin's Lymphoma, glioblastoma multiforme, Ewing's sarcoma, and testicular germ cell tumours [14,15]. While PARP-1's pivotal role in tumourigenesis underscores its attractiveness as a therapeutic target, the precise mechanisms through which it contributes to cancer are yet to be fully elucidated. A prevailing hypothesis suggests that both cancer cells and non-cancer cells experiencing prolonged oxidative stress, substantial DNA damage, or inflammatory conditions elevate PARP-1 expression. This up-regulation aids in the repair of mildly damaged DNA and fosters the accumulation of carcinogenic mutations that fuel tumour progression [15]. Furthermore, PARP-1 significantly contributes to chronic inflammation and genomic instability, which are cardinal hallmarks of cancer [14]. Additionally, PARP-1 displays disease-specific functions, as exemplified by its binding to estrogen receptor (ER) and progesterone receptor (PR) in breast and prostate cancer, respectively, leading to the activation of ER- or PR-associated genes [16].

At present, PARP-1 inhibitors constitute targeted therapies for treating BRCA-mutated ovarian and breast cancers [13]. The rationale behind developing these inhibitors predominantly lies in their ability to target cancer cells characterized by high replication rates and/or deficiencies in DNA repair mechanisms [13]. In the context of BRCA mutations, tumour cells with such mutations harbour unrepaired SSBs. In this scenario, PARP-1 activation becomes pivotal for rectifying DNA damage and preventing cell death. Thus, inhibiting PARP-1 is cytotoxic to cancer cells, leading to its use as a monotherapy or in combination with chemotherapy [17,18].

The inaugural PARP-1 inhibitor was nicotinamide, a product released during the PAR synthesis process from $NAD^+$ [19]. Subsequent PARP-1 inhibitors have been designed based on the nicotinamide structure, featuring a carboxamide group linked to an aromatic ring that competes

with $NAD^+$ for the catalytic pocket of PARP-1 [19]. As of 2021, the US Food and Drug Administration (FDA) and the European Medicines Agency (EMA) have sanctioned four PARP-1 inhibitors – Olaparib (IC50 = 13 nM), Rucaparib (IC50 = 80 nM), Niraparib (IC50 = 35 nM), and Talazoparib (IC50 = 3 nM), for use as anti-cancer therapies in breast and ovarian cancers [19] **[Figure 1.3]**. These drugs induce cancer cell death through dual mechanisms. Firstly, PARP-1 inhibitors compete with $NAD^+$ at the catalytic domain of PARP-1 enzymes, inhibiting their activity and leading to elevated DNA repair errors, particularly in rapidly dividing cancer cells [20]. Secondly, these inhibitors impede auto-PARylation, consequently suppressing the release of PARP-1 and reducing DNA repair capacity in cancer cells [21]. Their marked selectivity, oral availability, pharmacokinetic and pharmacodynamic attributes, and potency place PARP-1 inhibitors as potential therapeutics for a spectrum of cancers marked by high replication and genomic instability [21]. However, while the clinical promise of PARP-1 inhibitors is undeniable, with over 100 ongoing clinical trials spanning solid tumours and hematologic malignancies (clinicaltrials.gov checked on 2-09-2023), many inhibitors exhibit limited selectivity [22,23]. Notably, their affinity for PARP-2 is often reported due to the catalytic domain's high homology and sequence similarity between PARP-1 and PARP-2 [23]. Consequently, off-target inhibition of PARP-2 is likely to contribute to the efficacy of PARP-1 inhibitors [13]. Paradoxically, PARP-2 inhibition could give rise to adverse effects such as haematological and gastrointestinal toxicities [24]. Consequently, substantial interest revolves around refining the specificity and potency of PARP-1 inhibitors, as evidenced by compounds like NMS-P118. This selective agent inhibits PARP-1 80-fold more potently than PARP-2, effectively quelling the growth of breast cancer cells and pancreatic ductal adenocarcinoma xenografts [25].

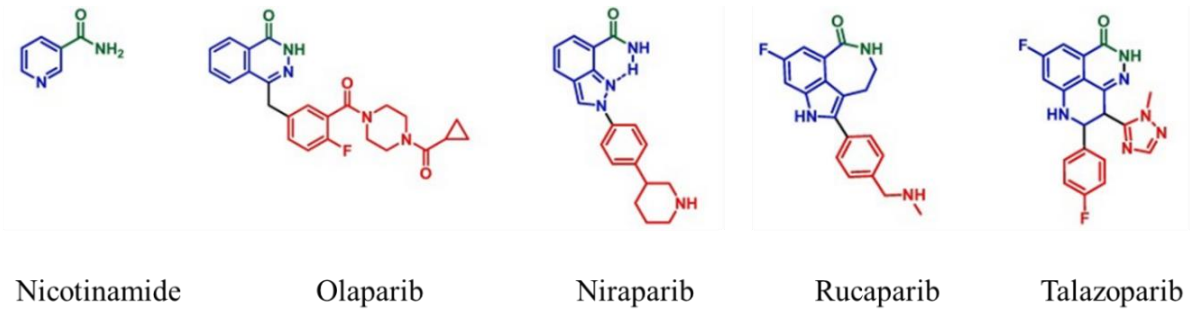


**Figure 1.3: Structure of FDA-approved PARP inhibitors.** Chemical structures of currently approved PARP inhibitors. Nicotinamide, a $NAD^+$ moiety, is shown to illustrate the chemical similarities between PARP inhibitors and the endogenous ligand.

### 1.3 Role of PARP-1 in Inflammation

PARP-1 plays a pivotal role in the context of chronic inflammation associated with inflammatory-driven pathologies and tumourigenesis [26]. The significance of this role is underscored by findings from studies employing PARP-1 knock-out (KO) mice or mice treated with PARP-1 inhibitors, which have demonstrated resistance to various forms of inflammatory stimuli, including lipopolysaccharide-induced septic shock [27,28]. Notably, PARP-1's pro-inflammatory effects extend beyond immune cells and encompass diverse cell types such as astrocytes, endothelial cells, and fibroblasts, thereby holding potential to contribute to the inflammatory cascade in virtually all tissues [29,30].

PARP-1 exerts these effects through two principal pathways. Firstly, it co-activates nuclear factor kappa-light-chain-enhancer of activated B cells (NF-κB), initiating the transcription of genes encoding proteins including inducible nitric oxide synthase (iNOS), tumour necrosis factor-α (TNFα), cell adhesion molecules like intercellular adhesion molecule-1 (ICAM-1) and vascular adhesion molecule-1 (VCAM-1), interleukin-1 (IL-1), interleukin-6 (IL-6), and pro-metastatic cytokines [31,32]. The collective action of these molecules amplifies the inflammatory response, culminating in heightened generation of reactive oxygen species (ROS), increased genomic instability, and heightened sensitivity of neighbouring cells to

oxidative stress [32]. Additionally, the activation of NF-κB further triggers PARP-1 activation, creating a persistent cycle of oxidative stress [33]. Secondly, excessive PARP-1 activation leads to extensive PAR synthesis, depletion of $NAD^+$ and ATP, and eventual cell death [32] **[Figure 1.4]**.

Considering the ubiquity of PARP-1's role in cellular physiology, its potential as a therapeutic target extends beyond oncology. Research studies have uncovered the cytoprotective and anti-inflammatory attributes of several FDA-approved PARP-1 inhibitors, notably Olaparib and Veliparib, in preclinical models of non-oncological disorders, encompassing lung inflammatory conditions, neurological ailments (e.g., stroke, Parkinson's disease, Alzheimer's disease, multiple sclerosis), diabetes, and myocardial infarction [34,35,36]. In chronic inflammatory diseases, the application of PARP-1 inhibitors contributes to a reduction in oxidative stress, attenuates PAR synthesis and the subsequent release of apoptosis-inducing factor (AIF) by mitochondria, prevents $NAD^+$ depletion and cell death, diminishes NF-κB activation, and curtails the expression of adhesion molecules and lymphocyte infiltration [14,15,37]. This multi-faceted approach targeting various pathways in tandem leads to synergistic effects, elucidating why lower doses of PARP-1 inhibitors suffice to confer efficacy in non-oncological conditions compared to their use in cancer therapy [15]. These investigations provide a compelling rationale for repurposing PARP-1 inhibitors for non-oncological indications, particularly in cases where therapeutic options are limited.

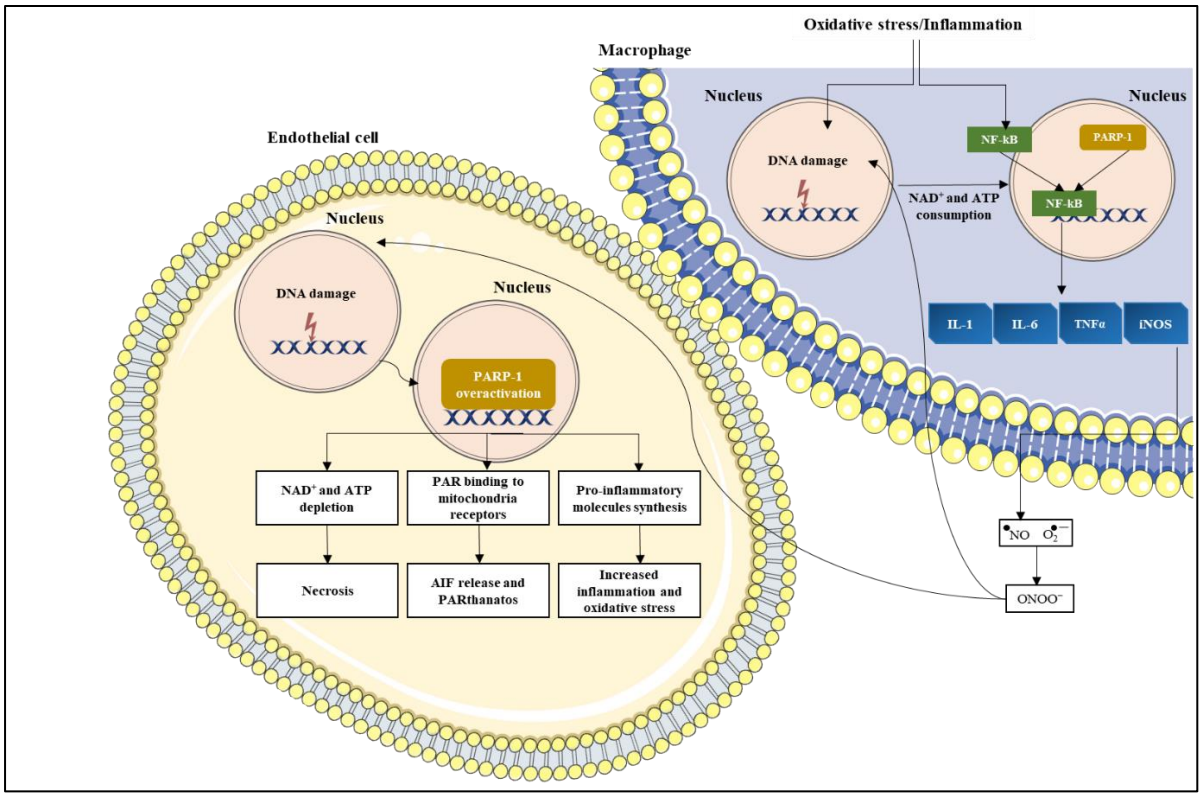


**Figure 1.4: PARP-1 role in inflammation.** Macrophages under inflammatory or oxidative stress conditions, activate PARP-1, which in turn positively regulates NF-κB transcription. NF-κB induces the transcription of pro-inflammatory genes including IL-1, IL-6, TNFα, and iNOS. The consequent synthesis of NO that reacts with the superoxide anion to form peroxynitrite (ONOO−), causes DNA damage in other cells such as endothelial cells, triggering PARP-1 overactivation. This ultimately leads to cell death through necrosis or AIF release and eventual PARthanatos. Parts of the Figure were generated using images from Servier Medical Art.

## 1.4 Role of PARP-1 in the Central Nervous System

The presence of PARP-1 in the central nervous system (CNS) is pervasive, being expressed by various brain cell types [38]. In addition to its primary involvement in PAR synthesis, PARP-1 assumes multifaceted roles within the CNS encompassing processes like cell differentiation, cholinergic and glutamatergic signaling regulation, and memory formation [39,40]. Herein, we present the current understanding of PARP-1's implications in the CNS, its associations with CNS disorders, and its potential as a therapeutic target in neurological inflammatory and demyelinating ailments.

### 1.4.1 Neuronal Expression of PARP-1

Neurons, owing to their susceptibility to free radical generation during cell respiration, oxidative stress, and neurotransmission, are vulnerable to DNA damage and ensuing PARP-1 activation [41]. PARP-1, under basal conditions, participates in signaling pathways essential for neuronal viability and synaptic plasticity, involving Akt, extracellular signal-regulated kinases (ERKs), and cyclic AMP response element-binding protein (CREB) [42]. During acute neuronal injuries, PARP-1 activation has been implicated in instigating neuronal demise through the nuclear translocation of apoptosis-inducing factor (AIF) from mitochondria [43]. Notably, N-methyl-D-aspartate (NMDA) receptor-mediated excitotoxicity, induced by nitric oxide (NO) synthesis and its reaction with superoxide anion to yield peroxynitrite ($ONOO^-$), culminates in neuronal DNA damage and PARP-1 activation [44,45]. Remarkably, PARP-1 inhibitors such as Rucaparib, Veliparib, Talazoparib, Olaparib, and DPQ have demonstrated potential in rescuing neuronal cells from oxidative stress and NMDA-induced cell death, suggesting their utility in neuronal pathologies [43,45].

Persistent activation of PARP-1, a hallmark of various CNS disorders, contributes not only to neuronal demise via apoptotic-independent pathways but also to axonal degeneration [46]. The ensuing depletion of $NAD^+$ and ATP, vital for neuronal health and growth, coupled with cytotoxic expression of glutamate-type Ca2+-permeable AMPA receptors, underpins neuronal vulnerability [47,48]. Collectively, targeting PARP-1 emerges as a promising strategy to mitigate neuronal loss and bolster axonal regeneration in chronic brain injuries [49,50].

### 1.4.2 Oligodendrocyte Expression of PARP-1

Oligodendrocytes, composing a subset of the glial cell population (5–10%), play a pivotal role in axonal myelination, critical for preserving axonal integrity and rapid neuronal

communication [51,52]. During CNS development, PARP-1 expression escalates in oligodendrocytes, influencing the positive regulation of oligodendrocyte differentiation and maturation [53,54]. Notably, PARP-1 KO mice exhibit reduced oligodendrocyte density and essential myelin proteins, suggesting its participation in maintaining myelination [55]. Although diverse reports exist regarding the implications of PARP-1 in oligodendrocytes, its potential as a factor influencing differentiation, viability, and myelination warrants attention [56,57,58].

### 1.4.3 Microglial Expression of PARP-1

Microglia, the immune guardians of the CNS, hold a pivotal role in orchestrating neuroinflammation and safeguarding the brain from various insults [59]. PARP-1 interacts with NF-κB to regulate microglial functions including migration, activation, proliferation, and the production of pro-inflammatory molecules and reactive oxygen species (ROS) [59]. Selective PARP-1 inhibition or deletion in microglia has demonstrated neuroprotection against injuries and inhibited microglial migration towards sites of injury, suggesting a role for microglial PARP-1 in inflammatory responses [60,61,62].

### 1.4.4 Astrocytic Expression of PARP-1

Astrocytes, abundant CNS glial cells, assume multifunctional roles in maintaining CNS homeostasis and responding to diverse challenges [63,64]. Notably, PARP-1's contribution to astrocyte activation and pro-inflammatory cytokine production has been recognized [65,66]. While some studies underscore the involvement of PARP-1 in astrocyte cell death and impairment of astrocytic glutamate transporters, complexities and contradicting observations

warrant further investigation [67,68,69]. Collectively, unravelling the intricate roles of PARP-1 across diverse CNS cell types informs potential therapeutic avenues for ameliorating CNS disorders and promoting neurological health.

### 1.5 Evidence for PARP-1 as a Drug Target for Neurodegenerative Diseases

The pathological mechanisms underlying several neurological conditions, encompassing Alzheimer's disease, Parkinson's disease, and multiple sclerosis, is rooted in persistent inflammation and DNA damage [70]. Multiple sclerosis, an autoimmune and demyelinating ailment of the central nervous system (CNS), exemplifies this paradigm [71]. In the murine experimental allergic encephalomyelitis (EAE) model of multiple sclerosis, PAR, a hallmark of PARP-1 activation, accumulates around demyelinated plaques in astrocytes, oligodendrocytes, microglia, and neurons [72]. Employing selective inhibitors (PJ34 or INH2BP) to curb PARP-1 activity in the EAE model attains a reduction in disease advancement and an improvement in symptoms. This is achieved through the downregulation of inflammatory cytokines like TNF-α, IL-1β, interferon-γ (IFN-γ), interleukin-2 (IL-2), and iNOS in the spinal cord [73,74] **[Table 1.2]**. Additionally, PARP-1 inhibitors demonstrate efficacy in restricting immune cell infiltration by modulating the blood-brain barrier (BBB) and inhibiting PARP-1 activity within monocytes [75]. This constrained immune cell transmigration across the BBB is likely attributed to altered integrin conformation such as VLA-4 and LFA-1, which in turn diminishes immune cell adherence to cerebral endothelium [76,77].

Parkinson's disease, characterized by α-synuclein (α-syn) fibril accumulation and heightened oxidative stress, potentially involves PARP-1 activation [78]. Intracerebral injection of preformed α-syn fibrils in murine brains triggers PAR accumulation, possibly via intensified

PARP-1 enzyme activity, in neurons of the substantia nigra and striatum. Subsequently, the augmented PAR interacts with α-syn, instigating a self-propelling loop that accelerates fibrillization. Genetic PARP-1 deletion or treatment with Rucaparib or Veliparib counteracts α-syn aggregation, spread, and neurotoxicity in primary neuronal cells [79] **[Table 1.2]**. Additionally, compelling insights suggest an excessive PARP-1 activation in Alzheimer's disease-afflicted brains [80,81]. Notably, PARP-1 inhibition utilizing nicotinamide or PJ34, though deemed as modest inhibitors [82], ameliorates brain pathology in transgenic Alzheimer's disease mouse models by diminishing β-amyloid production [83]. Collectively, these preclinical observations substantiate the therapeutic promise of PARP-1 inhibitors in neuroinflammation, neurological pathologies, and neurodegenerative disorders **[Figure 1.5]**.

| Disease/ Unhealthy condition | In vivo pre-clinical model | Effects of PARP-1 inhibitor | In vitro pre-clinical model | Effect of PARP-1 inhibitor |
|---|---|---|---|---|
| Parkinson's disease | MPTP mouse model | Benzamide show protective effects against the catecholamine depletions induced by MPTP in cortex and striatum and prevents $NAD^+$ and ATP depletion. | Neurons purified from a Parkinson's disease mouse model injected with preformed α-synuclein fibrils | Rucaparib or Veliparib reduces α-synuclein phosphorylation and aggregation, spreading and neurotoxicity |
| Alzheimer's disease | 3×Tg-AD mouse model | Nicotinamide reduces levels of phosphorylated species of tau and β-amyloid in the hippocampus and cerebral cortex and restores cognitive functions. | Rat pheochromocytoma (P C12) cells treated with 1 μM Aβ 1–42 oligomers<br><br>Neuroblastoma cells (SH-SY5Y) treated with $A\beta_{25-35}$ fragment | PJ-34 enhances transcription of antioxidant genes and regulation of mitochondria function.<br><br>MC2050 diminishes NF-κB activation, ROS production, and pro-apoptotic proteins. |
| Stroke | Mouse model of middle cerebral artery occlusion (MCAO)<br><br>Mouse model of transient middle cerebral artery occlusion<br><br>MCAO rat model injected with thrombin | PJ34 alleviates post-stroke neuro-inflammation and neurological deficits and suppresses microglial activation.<br><br>Olaparib reduces infarct size, immunoglobulin G extravasation, and ameliorates neurological deficits.<br><br>HYDAMTIQ reduces neurological impairment by up to 40%<br><br>INO-1001 reduces infarct volume by 86%, prevents AIF migration to the nucleus | Cultured human neurons exposed to oxygen–glucose deprivation (OGD) | Olaparib reduces OGD-induced neuronal cell death. |
| Multiple sclerosis | A primary demyelination mouse model, induced by a copper chelator cuprizone in weanling mice, results in multi-focal demyelination and loss of oligodendrocytes in the corpus callosum and superior cerebellar peduncle<br><br>EAE mouse model<br><br>EAE mouse model | 4-hydroxyquinazoline (4HQ) protects against cuprizone-induced demyelination in the brain, prevents weight loss, decreases AIF-mediated cell death.<br><br>PJ34 suppresses the development of clinical signs of EAE, reduces CNS Inflammation in the spinal cord, and limits BBB disruption.<br><br>INH2BP delays onset and reduces severity of EAE reducing the expression of pro-inflammatory molecules and immune cells infiltration. | Primary mouse neurons exposed to chondroitin sulfate proteoglycans (CSPGs) | PJ34, 4HQ, or 3AB promote neurite outgrowth |

**Table 1.2: Pre-clinical studies of PARP-1 inhibitors in neurodegenerative diseases.** Table displaying examples of *in vitro* and *in vivo* models of brain disorders in which PARP-1 inhibitors have shown efficacy.

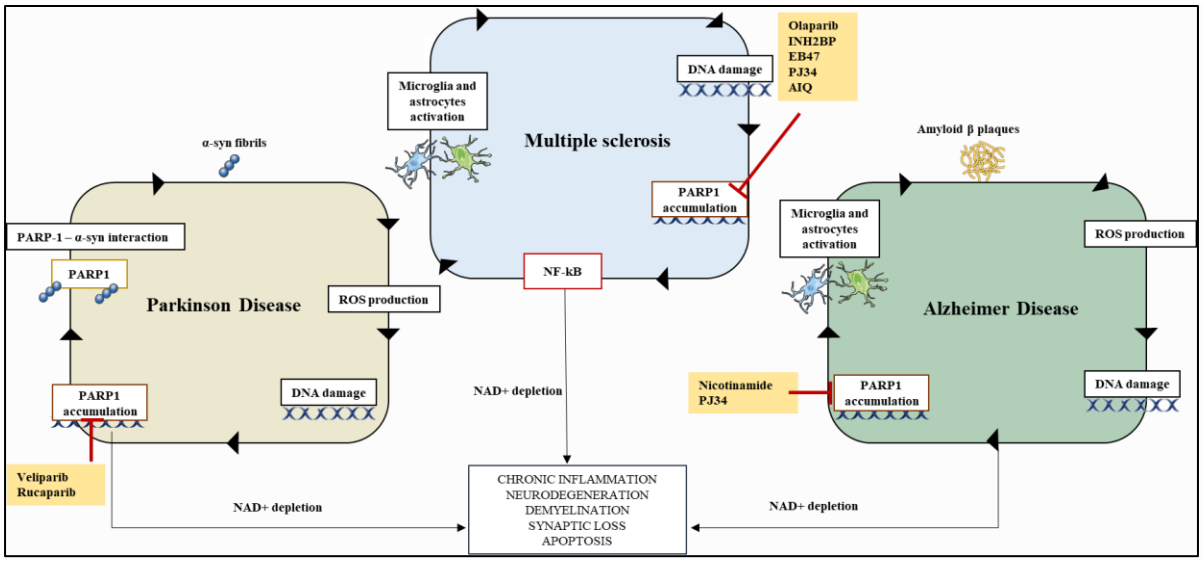


**Figure 1.5: Overactivation and pre-clinical evidence of PARP-1 inhibitor efficacy for Parkinson's disease, Alzheimer's disease, and multiple sclerosis.** Fibrillary α-syn in Parkinson's disease causes PAR accumulation, a marker of PARP-1 activation, in neurons in the substantia nigra and in the striatum, which subsequently interacts with α-syn and accelerates its fibrillization. PARP-1 selective inhibition with Rucaparib or Veliparib, reduced α-syn aggregation, spreading, and neurotoxicity in a Parkinson's disease mouse model. In multiple sclerosis, PAR accumulation is measured in cells surrounding demyelinated plaques. PARP-1 inhibition with selective inhibitors PJ34 or INH2BP in the EAE model markedly reduces neuro-inflammation by preventing NF-κB, microglia, and astrocytes over-activation. In Alzheimer's disease, amyloid β plaques enhance ROS production, leading to PARP-1 over-activation which, in different transgenic mouse models, is rescued by the treatment with nicotinamide or PJ34. Parts of the Figure were generated using images from Servier Medical Art.

## 1.5 Potential Utility of PARP-1 Inhibitors in Leukodystrophies

### 1.5.1 The Clinical Challenge and Therapeutic Landscape of Leukodystrophies

Leukodystrophies are a group of heterogeneous, genetically-based disorders affecting the development or maintenance of the myelin in the white matter of the CNS [84]. Collectively, leukodystrophies have an incidence of 1 in 7700 live births and can present at any age from infancy to adulthood, with a considerable variability in disease progression and clinical presentation [84]. Patients with leukodystrophies experience a large array of significant and disabling symptoms including motor impairment, dysautonomia, cognitive impairment, and ataxia [85]. Most of the diagnoses for leukodystrophies are not precise and are based on a combination of history, expected prevalence, physical and neurologic features, and radiological examination [86]. More promisingly, recent advances in genetic medicine and imaging have led to the identification of specific genetic and biochemical defects associated with individual leukodystrophies including MLD and X-linked adrenoleukodystrophy, which are the most frequent diagnosed among leukodystrophies, and KD [87].

In the past decades, existing dogma has been questioned suggesting that mutations within myelin- or oligodendrocyte-specific genes were the sole causative factors behind leukodystrophies [88]. Nowadays, leukodystrophies are linked to defects in astrocytes, microglia, axons, and blood vessel function [88]. Causes of leukodystrophies have also been associated with pathological mechanisms that share features with the archetypical demyelinating disease, multiple sclerosis, including BBB disruption, disorders of DNA transcription, translation, production of essential proteins for myelin, and neuroinflammation [89]. Both diagnosis and treatment of leukodystrophies possess a significant challenge due to the limited information regarding the mechanisms behind their pathologies. Symptomatic treatments can decrease the burden of events and assist somewhat in the quality of life [87]. To

date, however, effective cures for patients with leukodystrophies are greatly lacking. In this scenario, reducing neuroinflammation, which plays a pivotal role in leukodystrophy progression presents a desirable strategy, either possibly as a monotherapy or part of a combinatorial approach. The repurposing of approved drugs with a clinically proven ability to attenuate inflammation could be an attractive strategy to pursue. This thesis will explore the role of PARP-1 and the utility of PARP-1 inhibitors in two models of leukodystrophy disease: MLD and KD.

### 1.5.2 Metachromatic Leukodystrophy – The Role of Sulfatides

Metachromatic Leukodystrophy (MLD), a demyelinating disorder of autosomal recessive inheritance, emerges as an exemplar model of leukodystrophy, with its prevalence pegged at approximately 1–2 per 100,000 births and an incidence of 1 in 40,000 births [90]. This progressive disease is characterised by impairments in both motor and cognitive function, alongside gradual visual deterioration [90,91]. The trajectory of life often hangs upon the timing of diagnosis, with the late infantile iteration resulting in demise within 5–6 years, while the juvenile and adult forms may extend survival to early adulthood or beyond [91]. This pathology finds its roots in mutations within the aryl-sulfatase A gene (ARSA), bestowing a deficient activity of the arylsulfatase A lysosomal enzyme [92]. The consequential shortfall in ARSA enzymatic function sets the stage for sulfatide accumulation within oligodendrocytes, precipitating dysfunction and deterioration of the neuronal myelin sheaths [92]. Beyond the confines of the CNS, sulfatide accretion ripples through visceral organs, colonizing the pancreas, liver, adrenal glands, lymph nodes, and ovaries [90].

Chronic inflammation underpins MLD's progression and wields significant influence. Evidenced by elevated levels of CCL2, interleukin-1 receptor antagonist (IL-1Ra), interleukin-

8 (IL-8), and macrophage inflammatory protein 1β (MIP-1β) in the cerebral spinal fluid of MLD patients, inflammatory processes underly the dynamics of this progressive disease [93]. Beyond molecular signatures, a murine MLD model unveils a tapestry of excessive glial cell proliferation and hyperactivation of microglia, which amplifies the inflammation [94]. Autopsies of MLD and adrenoleukodystrophy patient specimens have uncovered the pivotal role played by DNA fragmentation in microglial death, a process that precedes the onset of demyelination [95]. Insights from models of multiple sulfatase deficiency support the hypothesis of inflammation's central role in MLD, as sulfatide build up induces a pro-inflammatory response, marked by increased TNF-α mRNA expression and T-cell infiltration [96].

An array of therapeutic strategies has been interrogated within experimental animal models of MLD. Despite this robust exploration, a definitive curative avenue has not been discovered. Various therapeutic approaches to MLD have been tested in experimental animal models, but so far, no curative treatment is available. Among the promising approaches with potential clinical utility are: (i) enzyme-replacement therapy (ERT); (ii) bone marrow transplant (BMT); (iii) gene therapy by *ex vivo* transplantation of genetically modified hematopoietic stem cells (HSC); and (iv) AAV-mediated gene therapy directly to the CNS [92].

### 1.5.3 Krabbe Disease – A Psychosine-Driven Disorder

Globoid Cell Leukodystrophy (Krabbe Disease) is a rare and aggressive neurodegenerative disorder with poor prognosis, emerging with an approximate frequency of 1 in 100,000 live births [97]. Krabbe disease (KD) is characterized by an early onset, rapid progression, and inescapable fatality, particularly within the infantile demographic [98]. The majority (85–90%)

of cases are of the infantile form and are characterized by symptoms including irritability, hypersensitivity, psychomotor arrest, and hypertonia, followed by optic atrophy, rapid mental and motor deterioration, and seizures [97]. Typically, death usually ensues within the first 2 years of life [99,100]. KD is caused by a mutation in the lysosomal enzyme galactosylceramidase (GALC) [101], resulting in the accumulation of a toxic lipid metabolite psychosine (galactosylsphingosine) and, to a lesser extent, β-galactosylceramide [102]. Progressive accumulation of psychosine in the brains of KD patients is thought to be the major driver of this illness [99]. Pathological features of KD include profound demyelination and almost complete loss of oligodendrocytes in the white matter, reactive astrocytosis, and infiltration of numerous multinucleated macrophages termed "globoid cells" [99]. Several reports have demonstrated that the cellular cytotoxicity caused by psychosine is in part mediated by inflammatory molecules, such as NF-κB, AMP-activated protein kinase (AMPK), prostaglandin D, iNOS, and pro-inflammatory cytokines such as TNF-α and IL-6 [103]. There is currently no cure for KD, except for hematopoietic stem cell transplantation, which is effective only if performed at the early stage of the disease [104]. Our group have already demonstrated the therapeutic potential of the oral multiple sclerosis drug, fingolimod, in the twitcher mouse model of KD and here we will examine the utility of Olaparib in this poor prognosis neurological disorder [105].

### 1.6 Conclusions

PARP-1 is an essential player in DNA integrity maintenance, cellular energy metabolism, and inflammation. Dysregulation of PARP-1 is not limited to the malignant setting and has been associated with the chronic inflammation underpinning multiple neurological diseases. Inhibition of PARP-1 in cancer has led to the marketing of four PARP-1 inhibitors for breast cancer and ovarian cancer, namely, Olaparib, Rucaparib, Niraparib, and Talazoparib. PARP-1

inhibitors hold promise extended utility in multiple neurological disorders including Parkinson's disease, Alzheimer's disease, and multiple sclerosis. These data lead us to hypothesize putative mechanisms through which PARP-1 signaling might drive the progression of two rare demyelinating diseases; KD and MLD, for which no therapeutic options currently exist. Targeted drugs with potential to penetrate the BBB and attenuate neuroinflammation are highly desirable for these poor prognosis diseases. Therefore, here we propose that PARP-1 inhibitors are worthy candidates for repurposing for such rare diseases, either as monotherapies or as combination therapies. Further insights into the function of PARP-1 in brain homeostasis and dysregulation in pathological states may assist in the development of PARP-1 inhibitors for rare demyelinating diseases such as leukodystrophies.

# Chapter 2 – Materials and Methods

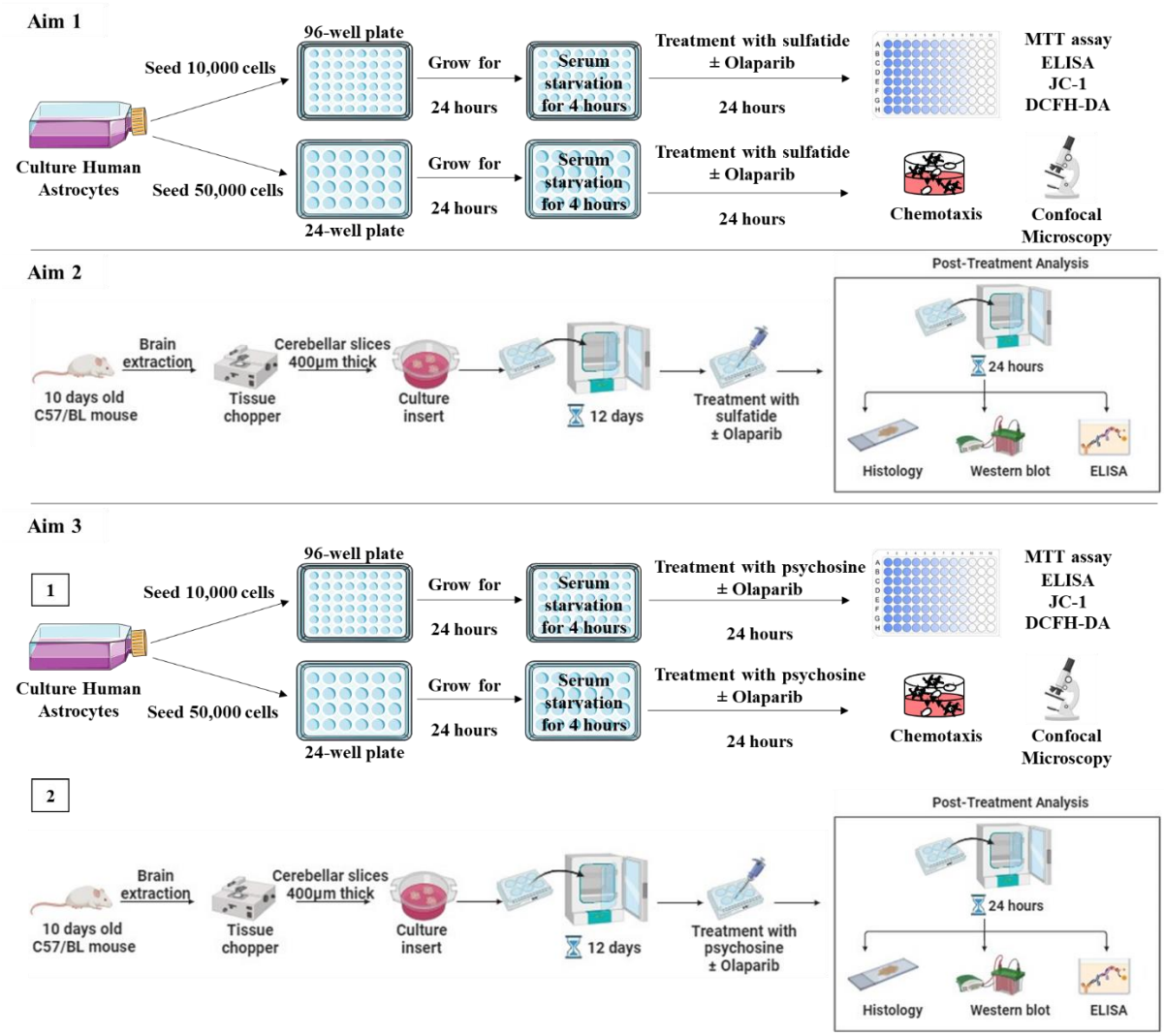


**Figure 2.1 Study Schematic Aims. Aim 1:** Human astrocytes were grown in T75 flasks and then seeded in either a 24-well plate or a 96-well plate before treatment with sulfatide (1µM, 5µM, 10µM, 20µM, 50µM, 100µM, 500µM, 1mM, 10mM) in the presence or absence of Olaparib (100nM) for 24 hours. MTT assay, ELISA, JC-1 and ROS assay, chemotaxis assay, and confocal microscopy were performed to evaluate the toxic effect of sulfatide and the therapeutic utility of Olaparib in cultured human astrocytes**. Aim 2:** Organotypic cultures of cerebellar slices were obtained from 10 days C57/CL mice. After culture at 37°C, 5% CO2 for 12 days, slices were treated with sulfatide (5µM, 10µM, 20µM, 50µM, 100µM) with or without Olaparib (100nM) for 24 hours. Immunofluorescence, western blot, and ELISA assay were engaged to assess the effect of sulfatide and Olaparib on myelin state and glial activation. **Aim 3:** Human astrocytes and organotypic cultures of cerebellar slices were used to evaluate the extended utility of Olaparib (100nM) in existing models of KD obtained through the treatment of cultures with psychosine (10µM, 20µM). The therapeutic effect of Olaparib was evaluated through a combination of techniques including MTT assay, ELISA, JC-1 and ROS assay, chemotaxis assay, confocal microscopy, and western blot.

## 2.1 Materials

| Purpose | Media | Ingredients |
|---|---|---|
| Splenocytes/PBMC | RPMI media | 500ml RPMI 1640 (Gibco, UK)<br>10% FBS (Sigma, USA)<br>1% Pen/Strep (Lonza, Switzerland) |
| Human Astrocyte | DMEM media | 500mL DMEM/F12 (Agilent, USA)<br>1% Pen/Strep (Lonza, Switzerland)<br>1% Astrocyte Growth Supplement (ScienceCell, USA)<br>10% FBS (Sigma, USA) |
| | Serum-starve DMEM media | 500mL DMEM/F12 (Agilent, USA)<br>1% Pen/Strep (Lonza, Switzerland)<br>1% Astrocyte Growth Supplement (ScienceCell, USA) |
| Organotypic slice culture | Media day 0-4 | 100mL Opti-MEM (Gibco, UK)<br>50mL HBSS (Gibco, UK)<br>50mL Horse Serum (Sigma, USA)<br>2.2mL Glutamax (Agilent, USA)<br>2.2mL D-glucose (Agilent, USA)<br>2mL HEPES (Agilent, USA)<br>2mL Pen/Strep (Lonza, Switzerland) |
| | Media day 4+ | 196mL Neurobasal A (Gibco, UK)<br>4mL B27 (Gibco, UK)<br>2.2mL D-glucose (Agilent, USA)<br>2.2mL Glutamax (Agilent, USA)<br>2mL Pen/Strep (Lonza, Switzerland)<br>2mL HEPES (Agilent, USA) |
| | **Buffer** | **Ingredients** |
| Flow Cytometry | FACS Buffer | 500ml PBS (Lonza, Switzerland)<br>2% FBS (Sigma, USA)<br>0.01% sodium azide (Sigma, USA) |
| | FACS Blocking Buffer | 50% FACS Buffer 50% FBS |
| Western blot | RIPA buffer (Roche, Germany) | 50mM TRIS 150mM NaCl<br>0.02% NaN3 1% NP-40<br>0.5% Sodium Deoxycholate 0.1% SDS |
| | 10% Separating gel (Roche, Germany) | 4.02mL dH20 100µL 10% SDS<br>3.33mL Bis Acrylamide 10µL TEMED<br>2.5mL Tris-HCL 50µL 10% APS |
| | 12% Separating gel (Roche, Germany) | 3.35mL dH20 100µL 10% SDS<br>4mL Bis Acrylamide 10µL TEMED<br>2.5mL Tris-HCL 50µL 10% APS |
| | 4% Stacking gel (Roche, Germany) | 3.05mL dH20 50µL 10% SDS<br>0.65mL Bis Acrylamide 8µL TEMED<br>1.25mL Tris-HCL 25µL 10% APS |
| | Running buffer | 60.4g Tris Base (Sigma, USA)<br>20g SDS (Sigma, USA)<br>288g Glycine (Sigma, USA) |
| | Transfer buffer | 60.4g Tris Base (Sigma, USA)<br>288g Glycine (Sigma, USA) |

**Table 2.1: Ingredients of buffers and cell culture media.**

### 2.1.1 Pharmacological compounds

All compounds are summarised in **[Table 2.2]**. Sulfatide comprises the major glycolipid components of myelin and was prepared as a 10mM stock solution dissolved in 90% dimethyl sulfoxide (DMSO, Sigma; D8418). Psychosine was prepared as a 10mM stock solution dissolved in 90% DMSO. Olaparib (is a PARP-1 inhibitor (IC50 = 13nM) [106] with partial binding affinity for PARP-2 that was prepared as a 20 mM stock solution in 90% DMSO.

| **Compound** | **Details** | **Working concentration** |
|---|---|---|
| Sulfatide | Sigma, 383906-24-9 | 1µM, 5µM, 10µM, 20µM, 50µM, 100µM, 500µM, 1mM, 10mM |
| Psychosine | Santa Cruz, sc-202781 | 10µM, 20µM |
| Olaparib | Bioscience; AZD2281 | 1nM, 10nM, 100nM, 1µM |

**Table 2.2: List of compounds used.**

### 2.1.2 Antibodies

All antibodies used for immunohistochemistry (IHC), or western blot (WB) are summarised in **[Table 2.3]**. Primary antibodies used were PARP-1, pADPr, vimentin, myelin basic protein (MBP), myelin oligodendrocyte glycoprotein (MOG), neurofilament heavy H (NFH), ionized calcium-binding adapter molecule 1 (Iba1), SMI-32, glial fibrillary acidic protein (GFAP), Olig2, F4/80, and CD3e. Secondary antibodies used were: goat anti-rabbit Alexa Fluor 488, goat anti-mouse Alexa Fluor 488, goat anti-mouse Alexa Dylight 549, goat anti-chicken IgY Alexa Fluor 633, HRP-conjugated anti-rabbit, HRP-conjugated anti-mouse, Alexa 488 anti-goat.

| PRIMARY ANTIBODIES | | | | | |
|---|---|---|---|---|---|
| **Target** | **Purpose** | **Host** | **Supplier** | **Cat No.** | **Dilution** |
| Vimentin | IHC, WB | Mouse | Santa Cruz | sc-373717 | 1/500, 1/1000 |
| MOG | IHC, WB | Mouse | Millipore | MAB5680 | 1/1000, 1/2000 |
| MBP | IHC, WB | Rabbit | Abcam | ab40390 | 1/1000, 1/2000 |
| NFH | IHC | Chicken | Millipore | AB5539 | 1/1000 |
| Iba-1 | IHC, WB | Rabbit | Wako | 19-19741 | 1/1000 |
| Olig2 | IHC, WB | Rabbit | Abcam | ab109186 | 1/500, 1/1500 |
| pADPr | IHC | Mouse | Santa Cruz | sc-56198 | 1/500 |
| PARP-1 | IHC, WB | Mouse | Santa Cruz | sc-8007 | 1/300 |
| SMI-32 | IHC | Mouse | Millipore | NE1023 | 1/1000 |
| CD3e | IHC, | Mouse | Biosciences | 557306 | 1/500 |
| GFAP | IHC, WB | Chicken | Abcam | ab4674 | 1/1000, 1/2000 |
| F4/80 | IHC, WB | Mouse | Invitrogen | MF48000 | 1/300, 1/1000 |
| Actin | WB | Mouse | Abcam | ab3280 | 1/3000 |
| **SECONDARY ANTIBODY** | | | | | |
| **Target** | **Purpose** | **Host** | **Supplier** | **Cat No.** | **Dilution** |
| Alexa 488 anti-rabbit | IHC | Goat | Invitrogen | A11008 | 1/1000 |
| Alexa 488 anti-mouse | IHC | Goat | Invitrogen | A11001 | 1/1000 |
| Alexa 633 anti-chicken | IHC | Donkey | Invitrogen | A21103 | 1/1000 |
| Alexa 549 anti-mouse | IHC | Donkey | JIR | 115-506-068 | 1/1000 |
| HRP-conjugated anti-rabbit | WB | Goat | VWR | NA934 | 1/5000 |
| HRP-conjugated anti-mouse | WB | Goat | Fisher | A16066 | 1/5000 |
| Alexa 488 anti-goat | WB | Donkey | Sigma | SAB4600127 | 1/2000 |

**Table 2.3: List of primary and secondary antibodies used.**

### 2.1.3 Dyes

Nuclear stain Hoechst 34580 (Invitrogen, H21486) to stain nuclei. MTT (3-(4,5-Dimethylthiazol-2-yl)-2,5-diphenyltetrazolium bromide) to perform viability assay (Invitrogen, M6494). Cal-520AM (Abcam, ab171868) was used to perform calcium imaging on human astrocytes. JC-1 (Abcam, ab113850) was used to perform mitochondrial stress assay. 2′,7′-dichlorofluorescein diacetate (DCFDA) (Merck; D6883), to measure ROS activity within the cell.

## 2.2 Cell culture

### 2.2.1 Aseptic technique

All *in vitro* procedures were carried out in strictly aseptic techniques. All instruments were sterilized before and after use by autoclaving and sprayed with 70% ethanol before placing them back inside the laminar flow hood (Mason Technologies, Ireland). Cell laboratory coat and gloves sprayed with 70% ethanol were used at all times. The interior of the laminar flow hood with the instruments inside were exposed to germicidal UV lamp, emitting at 253.7 nm to ensure sterility after use. Cell culture preparation and treatments were carried out under the laminar flood hood and cells were kept in an incubator, with temperature and $CO_2$ concentration stable at 37 °C (in the case of human astrocytes) or 35.5 °C (in the case of murine cerebellar slice culture) and 5% $CO_2$ concentration.

### 2.2.2 Human astrocyte cell culture

Human astrocytes from fetal brains were purchased from ScienCell Research Laboratory, USA (1800, Lot Nos. 9063 and 11065), as per the ethics outlined by the supplier and as we have described previously [107,108]. Human astrocytes were cultured at 37 °C and 5% CO2 in a

humidified incubator and grown in standard DMEM/F12 media supplemented with 1% astrocyte growth supplement, 10% fetal bovine serum (FBS) and 1% penicillin/streptomycin (pen/strep) in T75 culture flasks (Corning) unless otherwise indicated in the Fig. legends. Human astrocytes were grown for 14 days until 80% confluent and then seeded into 24-well or 96-well plates or split into T75 flasks until 80% confluent.

### 2.2.3 Cell counting

Cells were diluted 1 in 10 with trypan blue (Sigma, USA) and 10µL was added to the hemocytometer (Neubauer glass hemocytometer 0.01 mm depth, Marienfeld-Superior). Viable cells with an intact membrane do not take up the trypan blue dye, while dead cells lacking an intact membrane will take up the dye and thus are blue when visualized under the microscope. Unstained cells were visualized at 20X magnification under a light microscope (Nikon Eclipse E200) and counted in the four corners of the hemocytometer. The number of cells per ml was calculated as follows:

$$\text{Avg. no. of cells x } 10\text{^}4 \text{ x dilution factor} = \text{no. of cells/ml}$$

### 2.2.4 Drug treatments of astrocytes

Human astrocytes were seeded into either 24-well or 96-well plates at a cellular density of 50,000 cells/well in 500µL or 10,000 cells/well in 100µL of DMEM **[Table 2.1]**. Subsequent to a 24-hour incubation period at 37 °C and under 5% $CO_2$ conditions, the cells underwent a serum-starvation phase lasting 4 hours in a medium specifically designed for serum deprivation **[Table 2.1]**. Following this, the cells were exposed to sulfatides, which were appropriately

diluted in DMEM medium, at various concentrations: 1µM, 5µM, 10µM, 20µM, 50µM, 100µM, 500µM, 1mM, and 10mM. The exposure durations were 6, 24, and 48 hours. Alternatively, the cells were treated with psychosine at concentrations of 10 µM and 20 µM for a duration of 24 hours to induce toxicity. To assess the therapeutic effect of Olaparib in sulfatide or psychosine-induced astrocyte toxicity, human astrocytes were co-treated with sulfatides (1µM, 5µM, 10µM, 20µM, 50µM, 100µM, 500µM, 1mM, and 10mM) and Olaparib (1nM, 10nM, 100nM, 1µM) or psychosine (10µM, 20µM) and Olaparib (100nM).

### 2.2.5 Peripheral blood mononuclear cell preparation – Ethical approval

Healthy donors provided informed consent for sample blood acquisition and the study received full ethical approval from the Faculty of Health Sciences Ethics Committee at Trinity College Dublin. Blood samples were pseudonymized to protect the privacy rights of the donors.

### 2.2.6 Collection of human blood and Preparation of peripheral blood mononuclear cells

Whole blood was collected in red top vacutainer tubes suitable for collecting serum (BD Biosciences, USA). Blood was centrifuged at 10000 RPM for 10 minutes. The upper layer consisting of the serum was pipetted into labelled cryovials and stored at -80 °C for future use. Peripheral blood mononuclear cell (PBMC) isolation was carried out using density gradient centrifugation in a laminar flow hood under sterile conditions. Blood was diluted 1:2 with phosphate-buffered saline (PBS). For PBMC isolated from buffy packs, 500µL of EDTA (Sigma, USA) was added per 50mL of blood. Using a Pasteur pipette, 35mL of diluted blood was slowly layered on top of 15mL of ficoll paque (GE, USA) in a 50mL tube **[Figure 2.2]**. This was centrifuged at 400g for 25 minutes with the brake off. The cloudy buffy layer found underneath the plasma layer was transferred to a new 50 mL tube, using a Pasteur pipette, and

topped up to 50mL with PBS **[Figure 2.2]**. Cells were centrifuged at 800 × g for 10 minutes. The PBS layer was discarded by inverting the tube and the pellet was vortexed. Fifty millilitres of fresh PBS were added and cells were centrifuged at 400 × g for 5 minutes. The PBS was discarded by inverting the tube and the pellet was vortexed. The pellet was resuspended in 1ml of cRPMI and cells were counted as per section 2.2.3.

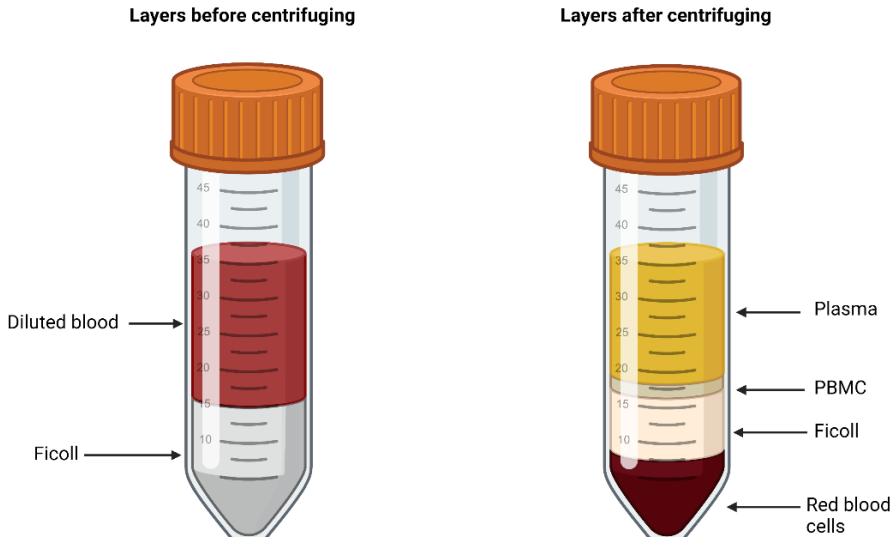


**Figure 2.2: Isolation of PBMC using density gradient centrifugation.** Schematic showing the isolation of PBMC from blood using ficoll paque before (left) and after (right) centrifugation. After centrifugation, the blood separates out into distinct layers based on their relative densities. This allows for the PBMC layer which lies between the plasma and ficoll layers to be removed by pipetting. Created with BioRender.com by Dr. Eimear Mylod.

### 2.2.7 Ethical approval for mouse organotypic cerebellar slice and murine splenocyte culture

All experiments were conducted in accordance with EU guidelines and protocols approved by the Trinity College Dublin ethics committee. The project was authorised by the Health Products Regulatory Authority (HPRA), under the project authorization number AE19136/I712.

### 2.2.8 Murine splenocyte cell culture

Spleens were isolated from postnatal day 10 C57BL/6 mice (P10) provided by BioResources Unit, Trinity College Dublin (Ireland). Following the sacrifice of the mice by decapitation, the spleen was removed and washed three times using Hank's buffered salt solution (HBSS). The spleen was pulverized using a rubber syringe plunger and pushed through a 70 μm sterile wire mesh screen in PBS. The red blood cells were removed using a lysis buffer (Biosciences; 555899) and the spleen cell suspensions were washed twice using the PBS solution and suspended in RPMI, which was supplemented with 10% FBS and 1% pen/strep. Cell counting was performed as per section 2.2.3.

### 2.2.9 Drug treatments of murine splenocytes

Murine splenocytes were seeded into 24-well plates at a cellular density of 50,000 cells/well in 500μL RPMI **[Table 2.1]**. After a 24-hour incubation period at 37 °C and under 5% $CO_2$ conditions, the migration of murine immune cells towards conditioned media of mouse organotypic cerebellar slice (OCS) was examined.

### 2.2.10 Mouse organotypic cerebellar slice culture

OCS cultures were generated from postnatal day 10 C57BL/6 mice (P10) provided by BioResources Unit, Trinity College Dublin (Ireland). All tissue was isolated in accordance with EU regulations and internal protocols approved by Trinity College Dublin ethical committee. Mice were sacrificed by decapitation, the skull removed, and the cerebellum separated from the hindbrain. Cerebellum was cut into 400 μm parasagittal sections using a McIlwan tissue chopper. Tissue was placed into Opti-MEM and separated into individual slices under a dissection microscope. Five slices were placed per cell culture insert (PICMORG50, Merk

Millipore, Burlington, MA, USA) and grown at 35.5 °C, 95% humidity, and 5% CO2. Slices were grown for the first 4 days in Day 0-4 medium **[Table 2.1]**. On day 4, the media was changed to a serum-free media containing **[Table 2.1]**. Media was changed again on day 10 and treatment was done on day 12.

### 2.2.11 Drug treatments of OCS

OCS were treated with either sulfatide (10µM, 20µM, 50µM, 100µM) or psychosine (10µM) diluted in Day 4+ medium at day 12 for 24 hours. To test the therapeutic utility of Olaparib in sulfatide or psychosine-induced demyelinating disease at day 12, OCSs were co-treated with sulfatide/psychosine and Olaparib (100nM) for 24 hours.

## 2.3 Functional assays

### 2.3.1 MTT assay

Human astrocytes or murine splenocytes were plated in 96-well plates at a density of 10,000 cells/well and cultured for 24 hours until 80% confluent. The cells were starved with serum-free media (DMEM/F12) for 4 hours, treated with or without compounds, after which the media was removed and replaced by 100µL of fresh, pre-warmed media supplemented with 10µL of 12 mM MTT. The cells were incubated with MTT for 4 hours at 37˚C. After 4 hours of incubation, 75µL of media was removed from each well and 50µL of DMSO was added. The cells were incubated for 10 minutes at 37 ˚C. The plate was shaken and the absorbance read at 540 nm.

### 2.3.2 JC-1 assay

Changes in mitochondrial potential were measured using a commercially available tetraethylbenzimidazolylcarbocyanine iodide (JC-1) assay kit following the manufacturer's instructions. Briefly, astrocytes were seeded in a 24-well plate at a density of 20,000 cells/well and treated with sulfatides (5μM, 10μM, 20μM, 50μM, and 100μM) and Olaparib (100nM). Thirty minutes before the end of each treatment, 1μM JC-1 dye was added to each well. After 30 minutes, the wells were washed twice with dilution buffer. The excitation wavelength was set at 535 ± 17.5 nm and the emission at 590 ± 17.5 nm. Aggregate emission was measured in a BioTek synergy HT microplate reader (BioTek, VT).

### 2.3.3 Reactive Oxygen Species Assay

Human astrocytes were seeded in a 96-well plate at a density of 10,000 cells/well for 24 hours and treated with sulfatides (5μM, 10μM, 20μM, 50μM, and 100μM) and Olaparib (100nM). Cellular ROS was measured using a detection assay kit. In brief, 2′,7′-dichlorofluorescein diacetate (DCFDA) is a fluorogenic dye that measures hydroxyl, peroxyl, and other ROS activity within the cell. After diffusion into the cells, DCFDA was deacetylated by cellular esterases to a non-fluorescent compound, which was later oxidized by ROS into 2′,7′-dichlorofluorescin (DCF), a highly fluorescent compound. Fluorescence from the DCF was detected by a fluorescence microplate reader with maximum excitation and emission spectra of 495 nm and 529 nm, respectively.

### 2.3.4 Live-cell calcium imaging

Human astrocytes were seeded in a 24-well plate and grown for 24 hours in supplemented DMEM/FBS until 80% confluent. Cells were then serum-starved for 4 hours prior to treatment with sulfatides/psychosine with or without 100nM Olaparib for 24 hours. After treatment, cells were incubated with 3μM Cal-520AM dye in HBSS supplemented with 10mM glucose and 25mM HEPES for 90 minutes at 37 °C, followed by 30 minutes at room temperature. Cells were always protected from bright light. Cells were then incubated in HBSS minus $Ca^{2+}$ and $Mg^{2+}$ (HBSS−/−). Time-lapse $Ca^{2+}$ imaging was performed at a rate of 0.99 frames per second. Following a 20-second baseline, cells were stimulated with 300μM ATP for 240 seconds. Intracellular $Ca^{2+}$ imaging experiments were performed with HBSS minus $Ca^{2+}$ and $Mg^{2+}$ (HBSS−/−). Images were acquired using a motorised epifluorescent microscope and a ×20 magnification objective.

Analysis of the recordings was performed using ImageJ software. Briefly, .lif files were exported as .tiff with no LUT. After adjusting threshold, files were made binary and watershed. Particles bigger than 150 $pixels^2$ were analysed and saved as a region of interest (ROI). The whole image sequence was opened, and all ROI mean intensity values were analysed at all time points.

### 2.3.5 Enzyme-linked immunosorbent assay (ELISA)

Human Soluble fractalkine (sCX3CL1), interleukin 6 (IL-6), interleukin 8 (IL-8), and interleukin 17 (IL-17) concentrations in astrocyte-conditioned media were detected with human ELISA kit according to the manufacturer's instructions **[Table 2.4]**. Murine IL-6, tumor necrosis factor-alpha *(*TNF-α) interleukin 17A (IL-17A), macrophage inflammatory protein-1α (MIP-1α/CCL3), macrophage migration inhibitory factor *(*MIF*)*, and interferon-gamma

(IFN-γ), CXCL5, and monocyte chemoattractant protein-1 (MCP-1/CCL2) levels in OCS-conditioned media were detected with mouse ELISA kit according to the manufacturer's instructions **[Table 2.4]**. Briefly, 96-well ELISA plates (Thermo Scientific; 95029780) were coated overnight at 4 °C with capture antibodies diluted in Dulbecco's PBS (dPBS, Sigma; 14190-094). The plates were washed three times with wash buffer (0.05% Tween 20 (Sigma; P7949), 10X PBS, pH 7.4) and then blocked for 2 hours at room temperature with the appropriate reagent diluent. The plates were then washed three times with wash buffer, and any remaining buffer was removed from the wells by aspiration. A standard curve was prepared using serial dilutions of the recombinant protein diluted in the appropriate reagent diluents. The samples and standards were then incubated in the antibody-coated ELISA plate for 2 hours at room temperature. The plate was then washed three times with wash buffer, and a detection antibody (diluted in reagent diluent) was added to each well for 2 hours. Following three more washes, streptavidin-HRP diluted in reagent diluents was added to each well and incubated for 20 minutes at room temperature, protected from light. After an additional three washes, the wells were incubated with substrate solution (R&D systems; DY999) for 15 minutes at room temperature and protected from light. The color reaction was stopped with the addition of 1 M H2SO4, and absorbance was read immediately using a plate reader at 450 nm (Labsystem Multiskan). The standard curve was calculated by plotting the standards against the absorbance values, and the cytokine levels were measured in pg/ml or ng/mL.

| Target | Host | Company | Cat No. |
|---|---|---|---|
| hsCX3CL1 | Human | R&D | DY365 |
| IL-6 | Human | R&D | DY206 |
| IL-8 | Human | R&D | DY208 |
| IL-17 | Human | R&D | DY317 |
| IL-6 | Mouse | R&D | DY406 |
| TNF-α | Mouse | R&D | DY410 |
| CCL3 | Mouse | R&D | DY450 |
| IFN-γ | Mouse | Assay Genie | MOFI00047 |
| CXCL5 | Mouse | R&D | MX000 |
| CCL2 | Mouse | R&D | DY479 |
| IL-17A | Mouse | Assay Genie | MOFI01286 |
| MIF | Mouse | R&D | DY1978 |

**Table 2.4: ELISA Targets.**

### 2.3.6 SDS-PAGE and Western blot

Human astrocyte protein samples were obtained by scraping the cell monolayer in RIPA buffer **[Table 2.1]**. OCS samples were obtained by homogenizing and sonicating OCS in RIPA buffer. Samples were mixed 1:1 dilution with Laemmli sample buffer 2X (BioRad, 161-0737) and boiled at 95 °C for 5 minutes. Simultaneously, 10% or 12% polyacrylamide separating gels with 4% stacking gels were prepared **[Table 2.1]**. Samples were loaded to have 6 µg of total protein per condition. The gels were run in running buffer **[Table 2.1]** at a constant voltage 120V to separate the proteins by their molecular weight. Electrophoresis was followed by a semi-dry transfer to a polyvinylidene difluoride membrane (PVDF; Millipore, IPVH00010) at constant 70V for 3 hours on ice, prior to activation of the PVDF membrane in methanol. Membranes were then blocked in PBS containing 5% BSA and 0.05% Tween-20 for 2 hours at room temperature and incubated with a primary antibody **[Table 2.3]** for 18 hours at 4 °C. After several PBS and PBS-Tween 0.05% washes, membranes were incubated with secondary

antibodies for 2 hours at room temperature. Several washes were then performed and PVDF membranes were developed using a chemiluminescent HRP substrate (Millipore, WBKLS0500).

### 2.3.7 Boyden chamber chemotaxis assays

#### 2.3.7.1 Chemotaxis assay on PBMC

PBMC were isolated from 6 healthy donors as outlined in section 2.2.6 and resuspended at a density of $0.2 \times 10^6$ cells/100µl RPMI supplemented with 1% Pen/Strep and 10% FBS and rested overnight at 37 °C and 5% CO2 in a humidified incubator. Cells were centrifuged at 1300 RPM for 5 minutes; the supernatant was removed, and cells were resuspended in serum-free RPMI. Conditioned media from astrocyte cell cultures (treated with or without sulfatides and with or without Olaparib) were added to the lower chamber of a 5 µm pore Transwell filter system (Corning Inc, Corning, NY, USA). Serum-free DMEM was used as a negative control and DMEM supplemented with 20% FBS was used as a positive control for chemotaxis. PBMC were subsequently added at a density of $0.2 \times 10^6$ cells/100µL RPMI to the upper chamber of the transwell system. This system was incubated for 2 hours at 37 °C, with 5% $CO_2$. Migrated cells were collected from the lower chamber and stained for flow cytometric analysis with CD56-FITC$^{Viobright}$ (Miltenyi Biotec., Germany) and CD3-APC-Cy7 (BioLegend, USA) **[Table 2.5]**. CountBright beads (ThermoFisher, Waltham, MA, United States) were used to enumerate the migrated lymphocytes, $CD56^+CD3^-$ NK (Natural Killer) cells, and $CD56^-CD3^+$ T cells. Cells were acquired using the CANTO II flow cytometer (BD Biosciences) and analysed using FlowJo v10 software (Tree Star).

The frequency of migrated cells was calculated as follows:

$$\frac{\text{No. beads per 10µl x No. of cells acquired}}{\text{Vol. of cells acquired x No. of beads acquired}}$$

| ANTIBODIES USED FOR FLOW CYTOMETRY | | | | | |
|---|---|---|---|---|---|
| **Target** | **Type** | **Host** | **Supplier** | **Cat No.** | **Volume (µl)** |
| CD56-FITC$^{Viobright}$ | Monoclonal | Human | Miltenyi Biotec | 130-114-552 | 1 |
| CD3-APC-Cy7 | Monoclonal | Human | Biolegend | 300318 | 1 |
| NK1.1-APC-Cy7 | Monoclonal | Mouse | Biosciences | 560618 | 1 |
| CD3-FITC | Monoclonal | Mouse | Biolegend | 100203 | 1 |
| F4/80-PE | Monoclonal | Mouse | Biolegend | 123109 | 1 |

**Table 2.5: Antibody panels used for extracellular staining of PBMC or murine splenocytes.**

### 2.3.8 Chemotaxis assay on murine splenocytes

Murine splenocytes were taken from 5 postnatal C57BL/6 mice (P10) at day 10, as described in section 2.2.8. Splenocytes were resuspended in RPMI supplemented with 1% Pen/Strep and 10% FBS and rested overnight at 37 °C and 5% CO2 in a humidified incubator. Conditioned media from OCS (OCSCM) (treated with or without psychosine and with or without Olaparib) were added to the lower chamber of a 5 µm pore Transwell filter system (Corning Inc, Corning, NY, USA). Serum-free RPMI was used as a negative control and RPMI supplemented with 20% FBS was used as a positive control for chemotaxis. Splenocytes were subsequently added at a density of $0.2 \times 10^6$ cells/100 µL serum-free RPMI to the upper chamber of the transwell system. This system was incubated for 2 hours at 37 °C, with 5% $CO^2$. Migrated cells were collected from the lower chamber and surface stained for subsequent flow cytometric analysis with mouse CD3-FITC (BioLegend, USA) and NK1.1-APC-Cy7 (Biosciences, USA), and F4/80-PE (Biosciences, USA) according to manufacturer instructions **[Table 2.5]**. CountBright beads (ThermoFisher, Waltham, MA, United States) were used to enumerate the migrated macrophages, NK cells and T cells. Cells were acquired using the CANTO II flow cytometer (BD Biosciences) and analysed using FlowJo v10 software (Tree Star).

The frequency of migrated cells was calculated as follows:

$$\frac{\text{No. beads per 10µl x No. of cells acquired}}{\text{Vol. of cells acquired x No. of beads acquired}}$$

### 2.3.9 Flow cytometry acquisition and analysis

All experiments were acquired using the FACS CANTO II and FACS Diva software (BD, USA) at the core flow cytometry facility at the Trinity Translational Medicine Institute. Data was analysed using FlowJo Version 10 software (BD, USA). The gating strategy used is as follows: the lymphocyte population was gated on using the SSC-A and FSC-A. Following this to remove doublets single cells were gated on within FSC-H and FSC-A. NK cells were gated as $CD56^{+}CD3^{-}$ or $NK1.1^{+}CD3^{-}$ cells within this gate, and T cells were gated as $CD56^{-}CD3^{+}$ cells or $NK1.1^{-}CD3^{+}$ within this gate. Unstained controls were utilised to decipher positive and negative populations. Compensation beads (Miltenyi Biotec and BD) were used to compensate for spectral overlap as per manufacturer's instructions on the BD FACS CANTO II.

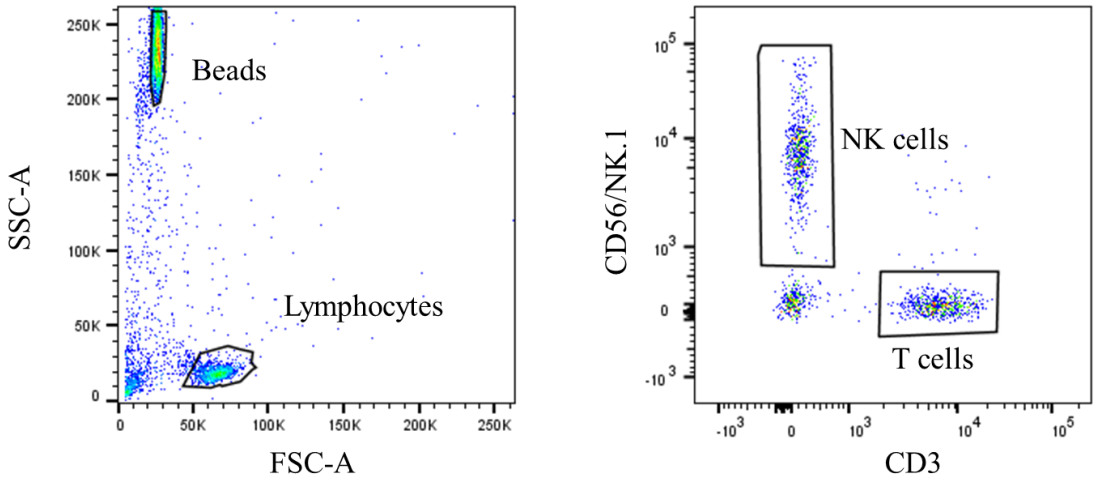


**Figure 2.3: Representative Dot Plot Showing NK Cell and T cell Gating Strategy.** Representative plots showing gating in PBMC or murine splenocytes samples. The lymphocyte population was gated on using the SSC-A and FSC-A (left). Following this NK cells were gated as $CD56^{+}CD3^{-}$ cells and T cells as $CD56^{-}CD3^{+}$ cells within this gate (right).

### 2.3.10 Immunocytochemistry of astrocytes

Human astrocytes were plated in 24-well plates (Corning) and cultured for 24 hours until 80% confluent. After pharmacological treatment, cells were washed in PBS and fixed in 4% paraformaldehyde (PFA) for 5 minutes. Cells were washed for 3 x 7 minutes in PBS and then permeabilized by incubation with 0.1% Triton-X-100 in PBS for 5 minutes at room temperature. Another 3 x 7 minutes PBS washes were performed, and non-reactive sites were blocked by adding 1% bovine serum albumin (Sigma) in PBS for 1 hour. The cells were then incubated in primary antibody **[Table 2.3]** overnight at 4 °C. The primary antibody was removed, and the cells were washed for 3 x 7 minutes PBS after which the secondary fluorescent antibody goat anti-mouse Alexa fluor 488 (Invitrogen), was applied for 1 hour at room temperature. After washing three times in PBS, the cells were then incubated with Hoechst nuclear stain (diluted 1:10,000 in PBS) (Invitrogen) for 10 minutes and washed twice again. The coverslips were then mounted on glass slides in Vectashield (Vector Labs) and the edges were sealed with varnish. Samples were stored at 4 °C in the dark until imaged. Images were captured with a confocal microscope (Leica SP8) in 1024 x 1024 resolution at 200 frames per second (fps).

### 2.3.11 Immunocytochemistry of slice cultures

After treatments, the OCS cultures were fixed in 4% paraformaldehyde (PFA) for 7 minutes. Slices were washed with PBS twice for 10 minutes. Blocking and permeabilization were performed overnight at 4°C in PBS containing 10% BSA + 0.5% Triton X-100. Primary antibodies were diluted in 2% BSA in PBS + 0.1% Triton X-100 and incubated for 48 hours at 4°C **[Table 2.3]**. Slices were washed with PBS for 5 minutes and PBS + 0.1% Triton X-100 buffer three times for 10 minutes. Incubation with secondary antibodies was performed at 4°C

for 18 hours. Slices were washed again, stained with Hoechst nuclear stain (diluted 1:10,000 in PBS) (Invitrogen; H21486), and mounted on microscope slides using ProLong® Gold antifade reagent (Thermo Fisher Scientific, P36934). Samples were stored at 4 °C in the dark until imaging was performed. Images were captured with a confocal microscope (Leica SP8) in 1024 x 1024 resolution at 200 frames per second (fps).

### 2.3.12 Microscopy and Image Analysis

Immunofluorescence images from human astrocytes were captured at ×20 or ×40 magnification using a Leica SP8 confocal microscope. The images were exported as 8-bit.tif files for analysis using the software package FIJI (ImageJ, NIH, version 2.0.0). To analyze astrocyte morphology, FIJI's ROI manager software plugin was used to identify individual cells in each image, enabling the calculation of both fluorescence intensity and cell area. For PARP-1 and PAR, the fluorescence images were processed as follows: ROIs of cellular nuclei automatically generated by ImageJ using the Hoechst field were utilised to quantify the average gray value of the PARP-1 or PAR field.

Immunofluorescence images of OCS cultures were captured at ×20 or ×40 magnification using a Leica SP8 confocal microscope. For each experiment ($n = 5$), there were five slices per treatment group and 5–6 fluorescence images were captured per slice. The areas of the cerebellum captured were kept consistent between treatment groups and cover most of the total area of the cerebellum. The images were exported as 8-bit.tif files for analysis using the software package FIJI (ImageJ, NIH, version 2.0.0). Intensity values were normalized to the average of control for each experiment and each marker. To analyze the expression of SMI-32 in the white matter tracts, a ROI containing predominantly white matter tracts was manually selected in each image and the fluorescence intensity was calculated. The proportion of this

white matter area that stained positive for SMI-32 immunoreactivity (termed SMI-32 surface area) was quantified. For cell count and surface area analysis, FIJI's particle analyzer tool was employed. Briefly, images were converted from 8-bit to binary and a value of 20 pixels was set as the minimum particle size. A mask of the particles detected was generated to check the accuracy of the detection method. A numbered list of particles displaying the fluorescence intensity and the area of each were analysed. For Iba1 Z-stack images the surface volume was calculated using Imaris® software. For astrocyte morphology, FIJI's skeletonized and AnalyzeSkeleton (2D/3D) software plugins were used. The outputs of these plugins summarize cell morphology in terms of astrocyte number of branches.

### 2.4 Statistical analysis

All data were analysed using GraphPad Prism 5 (GraphPad Software). One-way and Two-way analysis of variance (ANOVA) and multiple comparisons post hoc tests were used to assess significant differences between the values obtained for Control, psychosine- and drug-treated astrocytes and splenocytes. The differences were considered significant if $p<0.05$ and all values were expressed as the mean "standard error of the mean" (SEM). For cell experiments, where indicated, 'n' stands for the number of separate experiments carried out. Two or three technical replicates were performed for each condition/drug treatment within each separate experiment. A separate experiment is counted as experiments done with cells from a different passage for human astrocytes.

For organotypic slice culture experiments, the normality of the data was determined using the Shapiro-Wilk test. Where appropriate, histologic and biochemical data were analysed using the parametric one or two-way ANOVA with the Tukey post-hoc test for multiple comparisons to assess significant differences between the values obtained for vehicle control, psychosine-

treated and Olaparib-treated organotypic slice cultures. For Western blot Newman–Keuls multiple comparisons post hoc tests were run in conjunction with one-way ANOVAs and all groups were compared with one another. Mean fluorescence intensity as measured with ImageJ software was used as an arbitrary unit of measure. Raw data sets were normalized and presented as percentages of the control group average. The differences were considered significant if $p<0.05$ and all values were expressed as the mean "standard error of the mean" (SEM). Where indicated, 'n' stands for the number of independent organotypic slice culture preparations performed on different experimental days. For each experiment, there were five technical replicates per treatment group and each experiment was repeated n = 4 or 5 times, as indicated in the appropriate Fig. legend. Separate experiments were counted as slices that were extracted from different brain tissue from different mouse litters on different experimental days. For each slice culture, 25 healthy slices were obtained from the cerebellum of five mouse littermates and randomly separated into five treatment groups. Therefore, if an experiment was repeated n = 5, a total of 25 cerebellar slices were stained and imaged.

# Chapter 3 – Elucidating the therapeutic utility of Olaparib in sulfatide-induced human astrocyte toxicity and neuroinflammation

### 3.1 Hypothesis and Aims

MLD, an autosomal recessive leukodystrophy, lacks a cure due to ARSA gene mutations causing deficient arylsulfatase A enzyme activity, leading to sulfatide build-up in the brain. The impact of sulfatide on astrocytes is not well understood. In the realm of potential therapeutic approaches, PARP inhibitors have demonstrated effectiveness in preclinical models of various neurodegenerative and inflammatory diseases, though their application in MLD has not been explored.

**Hypothesis**

PARP-1 is a key driver of sulfatide-induced toxicity in human astrocytes

**Aims**

1. Elucidate the detrimental effects of sulfatides on human astrocytes.
2. Evaluate the potential utility of Olaparib to ameliorate sulfatide-induced cellular damage in astrocytes

### 3.2 Highlights

- Sulfatide induces human astrocyte death in a concentration-dependent manner ($EC_{50}$~20μM at 24 hours).
- Sulfatide-induced astrocyte toxicity is underpinned by (i) PARP-1 over-expression and over-activation, (ii) pro-inflammatory cytokine release (IL-6, IL-8, IL-17, and CX3CL1), and (iii) enhanced chemoattraction of peripheral blood immune cells.
- Sulfatide causes impairments of ROS production, mitochondrial stress, and $Ca^{2+}$ signaling in human astrocytes, that are indicative of metabolic alterations.
- Sulfatide-induced effects are attenuated by Olaparib treatment ($IC_{50}$~100nM).

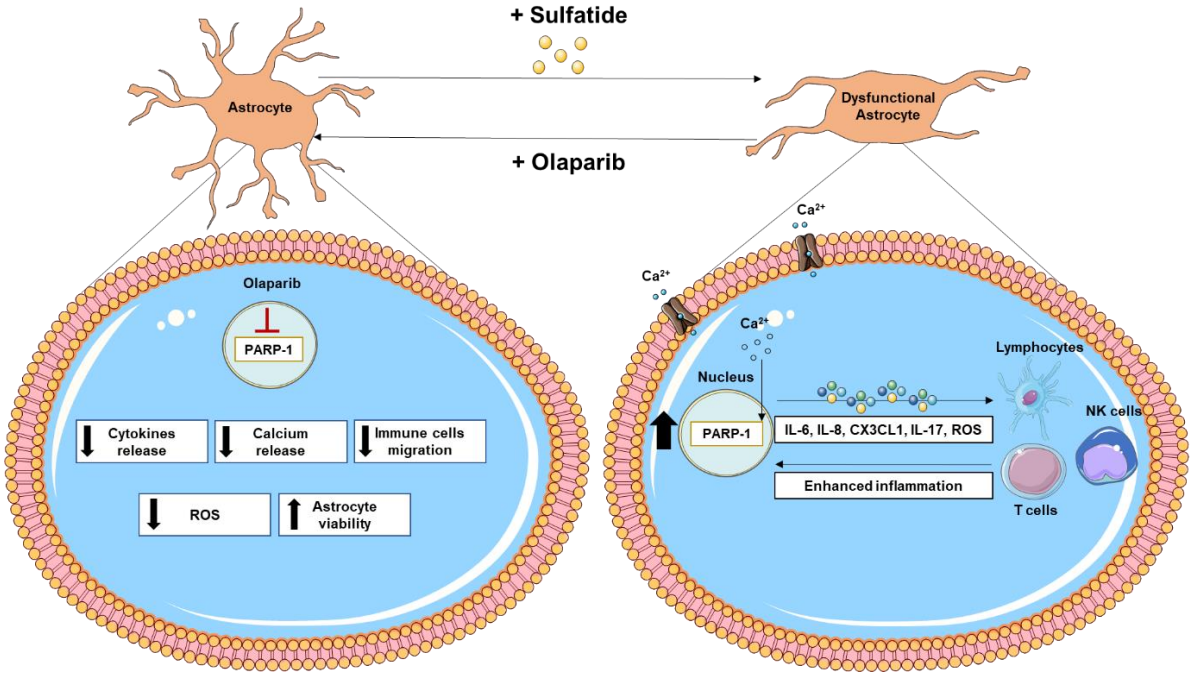


**3.1 Graphical abstract. Proposed mechanism of action of Olaparib in sulfatide-treated astrocytes.** Human astrocytes treated for 24 hours with sulfatides increase PARP-1 expression and die. PARP-1 overexpression is modulated by $Ca^{2+}$ release from the endoplasmic reticulum, thus enhancing intracellular $Ca^{2+}$ concentration. PARP-1 inhibition with Olaparib reduces $Ca^{2+}$ influx and cell death. Olaparib also decreases IL-6, IL-8, IL-17, and CX3CL1 release from sulfatide-stimulated astrocytes, suggesting that PARP-1 plays a role in dampening neuroinflammation in MLD. This is confirmed by the reduction of immune cell migration such as lymphocytes, NK cells, and T cells towards sulfatide-treated astrocytes. Moreover, mitochondrial stress and ROS production induced by sulfatides are rescued by PARP-1 inhibition. Future studies will focus on the signaling cascades triggered by PARP-1-mediated currents in reactive astrocytes and Olaparib as a potential therapeutic target for MLD.

### 3.3 Introduction

MLD is a rare genetic disorder characterized by the progressive loss of myelin, caused by autosomal recessive mutations. It affects approximately 1-2 individuals per 100,000 births, with an incidence of 1 in 40,000 births [90]. Unfortunately, there is currently no curative therapy available for MLD, leading to a significant decline in muscle and cognitive function, along with progressive vision loss [90]. The life expectancy of individuals with MLD varies depending on the age at diagnosis. In cases of late infantile MLD, death typically occurs within 5-6 years, whereas juvenile and adult forms may extend survival until early adulthood or beyond [90].

This devastating disease is a result of mutations in the arylsulfatase A gene (ARSA), leading to deficient activity of the arylsulfatase A lysosomal enzyme [91]. The reduced ARSA enzyme activity leads to the accumulation of sulfatide in the central and peripheral nervous systems [92]. Sulfatide predominantly accumulates in oligodendrocytes, causing dysfunction and destruction of neuronal myelin sheaths and inhibiting the differentiation of oligodendrocytes from precursor cells, thus preventing remyelination [92].

Several studies have implicated sulfatides in MLD neurodegeneration, contributing to various MLD features such as blood-brain barrier disruption, dysfunctional transcription, and translation of essential myelin proteins, and neuroinflammation [91,110]. While previous research has predominantly focused on the role of the ARSA mutation in oligodendrocytes [90,111], investigating the involvement of astrocytes in MLD may offer new insights into the disorder. Astrocytes are crucial for supporting myelination by producing a significant portion of brain cholesterol. Disruption of astrocyte cholesterol production leads to hypomyelination [112]. Additionally, astrocytic end feet expressing aquaporin 4 (AQP4) and the Kir4.1 K+ channel plays a vital role in maintaining blood-brain barrier integrity [113]. Astrocytes also contribute to innate immune responses and neuroinflammation, which are key drivers of MLD

disease progression, as evidenced by elevated levels of inflammatory markers in the cerebral spinal fluid of MLD patients [93]. Moreover, a mouse model of MLD has shown excessive glial cell proliferation and microglia hyperactivation [94]. Thus, it is plausible to hypothesize that sulfatide accumulation affects astrocytes and significantly contributes to axonal degeneration and chronic inflammation in MLD, which we aim to investigate in this study.

PARP inhibitors, initially developed as anti-cancer therapeutics, have demonstrated efficacy in preclinical models of various neurodegenerative and inflammatory diseases, including stroke, Parkinson's disease, Alzheimer's disease, multiple sclerosis, diabetes, and myocardial infarction [34,35,36,114]. Among PARPs, PARP-1 is the most extensively studied member of the nuclear enzyme superfamily, responsible for transferring ADP-ribose units from $NAD^+$ to various acceptor proteins, such as histones and transcription factors. PARP-1 is involved in a wide array of cellular processes, including DNA repair, apoptosis, transcriptional regulation, mitochondrial function, and inflammation. Overactivation of PARP-1 has been implicated in the pathogenesis of several central nervous system (CNS) diseases [72]. PARP-1's role in disease is mediated, in part, through the co-activation of nuclear factor kappa-light-chain-enhancer of activated B cells (NF-κB), leading to the transcription of pro-inflammatory genes, including inducible nitric oxide synthase (iNOS), tumor necrosis factor α (TNF-α), cell adhesion molecules (e.g., intercellular adhesion molecule-1 (ICAM-1), vascular adhesion molecule-1 (VCAM-1)), interleukin-1 (IL-1), and interleukin-6 (IL-6) [31,32]. These molecules collectively promote inflammation, increase reactive oxygen species (ROS) production, induce genomic instability, and sensitize neighbouring cells to oxidative stress [31]. Moreover, NF-κB activation further exacerbates PARP-1 activation, creating a chronic oxidative feedback loop [26]. Overactive PARP-1 also leads to excessive PAR synthesis, $NAD^+$ and ATP depletion, ultimately resulting in cell death [32].

Notably, several FDA-approved PARP inhibitors, such as Olaparib and Veliparib, have shown promise in reducing oxidative stress, preventing excessive PAR synthesis, preserving $NAD^+$ levels, mitigating cell death, suppressing NF-κB activation, and decreasing the expression of adhesion molecules and lymphocyte infiltration in neurological diseases (Scott et al., 2004). Given the evidence of increased DNA fragmentation, oxidative stress, inflammation, mitochondrial dysfunction, and blood-brain barrier disruption in MLD, our study focuses on three main objectives: (i) understanding the impact of sulfatide accumulation on human astrocyte dysfunction and toxicity; (ii) investigating whether Olaparib-mediated PARP inhibition can provide protection against sulfatide-induced astrocyte dysfunction; and (iii) uncovering the mechanisms underlying sulfatide-induced astrocyte toxicity.

## 3.4 Results

### 3.4.1 Sulfatides Induce Human Astrocyte Cell Death

The impact of sulfatides on astrocytes has been relatively unexplored, especially when compared to their well-documented effects on oligodendrocytes. Consequently, we embarked on an extensive investigation to uncover how sulfatides influence human astrocytes, starting with an examination of their effect on astrocyte viability. To investigate this, we subjected cultured human astrocytes to a period of serum starvation lasting 4 hours, followed by exposure to varying concentrations of sulfatides for different durations [**Figure 3.2A**]. Our findings revealed a concentration- and time-dependent reduction in the number of viable human astrocytes following sulfatide exposure. During a 6-hour treatment, we observed a modest decrease in astrocyte survival (Untreated: 100%, 20µM Sulfatide: 92.6%, 50µM Sulfatide: 88.3%, and 100µM Sulfatide: 68.1%, compared to untreated) [**Figure 3.2B and C**]. Interestingly, as the exposure time extended to 24 and 48 hours, a more deep reduction in astrocyte viability became evident (24 hours, Untreated: 100%, 20µM Sulfatide: 74.2%, 50µM Sulfatide: 65.8%, and 100µM Sulfatide: 48.2%, compared to untreated), (48 hours, Untreated: 100%, 20µM Sulfatide: 42.4%, 50 µM Sulfatide: 20.7%, and 100µM Sulfatide: 4.7%, compared to untreated) [**Figure 3.2B and C**]. This data suggests that sulfatides induce dysfunction in astrocytes, potentially contributing to the demyelination process observed in associated diseases.

### 3.4.2 Olaparib reduces Sulfatide-Induced Toxicity in Human Astrocytes

Considering the time-dependent nature of sulfatide-induced astrocytic toxicity, our focus was on evaluating the impact of sulfatide treatment at the 24-hour mark. Subsequently, we examined the protective effects of Olaparib against sulfatide-induced toxicity in human

astrocytes. Human astrocytes were treated with sulfatides (1µM, 5µM, 10µM, 20µM, 50µM, 100µM, 500µM, 1mM, and 10mM) and Olaparib (1nM, 10nM, 100nM, and 1µM) at the time points indicated [**Figure 3.3A**]. Our findings revealed that Olaparib exerted a protective effect at lower doses (1nM, 10nM, and 100nM) on sulfatide-induced astrocyte cell death (1nM Olaparib: 10µM Sulfatide: 83.8% vs 10µM Sulfatide + 1nM Olaparib: 90.6%; 20µM Sulfatide: 74.2% vs 20µM Sulfatide + 1nM Olaparib: 89.6%; 50µM Sulfatide: 65.8% vs 50µM Sulfatide + 1nM Olaparib: 79.2%; 100µM Sulfatide: 48.2% vs 100µM Sulfatide + 1nM Olaparib: 51.2%) [**Figure 3.3B**], (10nM Olaparib: 10µM Sulfatide: 83.8% vs 10µM Sulfatide + 10nM Olaparib: 95.4%; 20µM Sulfatide: 74.2% vs 20µM Sulfatide + 10nM Olaparib: 93.0%; 50µM Sulfatide: 65.8% vs 50µM Sulfatide + 10nM Olaparib: 88.3%; 100µM Sulfatide: 48.2% vs 100µM Sulfatide + 10nM Olaparib: 51.6%) [**Figure 3.3C**], (100nM Olaparib: 10µM Sulfatide: 83.8% vs 10µM Sulfatide + 100nM Olaparib: 99.0%; 20µM Sulfatide: 74.2% vs 20µM Sulfatide + 100nM Olaparib: 97.1%; 50µM Sulfatide: 65.8% vs 50µM Sulfatide + 100nM Olaparib: 96.3%; 100µM Sulfatide: 48.2% vs 100µM Sulfatide + 100nM Olaparib: 59.1%) [**Figure 3.3D and 3.3E**], (1µM Olaparib: 10µM Sulfatide: 83.8% vs 10µM Sulfatide + 1µM Olaparib: 84.4%; 20µM Sulfatide: 74.2% vs 20µM Sulfatide + 1µM Olaparib: 75.3%; 50µM Sulfatide: 65.8% vs 50µM Sulfatide + 1µM Olaparib: 70.9%; 100µM Sulfatide: 48.2% vs 100µM Sulfatide + 1µM Olaparib: 52.7%,) [**Figure 3.3F**]. These results highlight the efficacy of Olaparib in mitigating sulfatide-induced cytotoxicity in human astrocytes, with the most pronounced effect observed at the 100nM dosage of Olaparib. Consequently, we selected this concentration of Olaparib for use in subsequent experiments.

### 3.4.3 Olaparib decreases Sulfatide-Induced PARP-1 Activation in Human Astrocytes

Under normal physiological conditions, PARP-1 activity plays a crucial role in various cellular processes, including the detection and repair of DNA damage, stress response, and chromatin maintenance [115]. However, in neurodegenerative disorders such as Parkinson's disease and multiple sclerosis, the hyperactivation of PARP-1 leads to neuronal death due to the accumulation of PAR polymers and excessive activation of glial cells [46].

Hence, the effects of sulfatides and Olaparib on PARP-1 activation in human astrocytes were investigated by measuring the changes in PARP-1 expression in the nucleus. Treatment of human astrocytes with sulfatides (5μM, 10μM, 20μM, 50μM, 100μM) for 24 hours induced PARP-1 expression in astrocyte nuclei in a concentration-dependent manner [**Figure 3.4A and 3.4B**]. Importantly, these changes in PARP-1 fluorescence were reduced by treatment with Olaparib (100nM) (Untreated: 8.0 vs Olaparib: 7.4; 5μM Sulfatide: 10.4 vs 5μM Sulfatide + Olaparib: 8.6; 10μM Sulfatide: 23.4 vs 10μM Sulfatide + Olaparib: 17.3, p=0.01; 20μM Sulfatide: 38.1 vs 20μM Sulfatide + Olaparib: 16.8, p=0.001; 50μM Sulfatide: 42.9 vs 50μM Sulfatide + Olaparib: 17.8, p=0.002; 100μM Sulfatide: 44.4 vs 100μM Sulfatide + Olaparib: 36.2, p=0.03) [**Figure 3.4C**]. In parallel, we assessed PAR expression as a representative marker of PARP-1 activation. The quantification of PAR expression within astrocyte nuclei exposed to varying sulfatide concentrations (ranging from 5μM to 100μM) in the presence or absence of Olaparib (100 nM) revealed a concentration-dependent increase in PAR expression induced by sulfatides [**Figure 3.4D and E]**. Sulfatide elevation in PAR expression was significantly ameliorated by Olaparib treatment (Untreated: 4.6 vs Olaparib: 2.2; 5μM Sulfatide: 7.7 vs 5μM Sulfatide + Olaparib: 4.6; 10μM Sulfatide: 16.8 vs 10μM Sulfatide + Olaparib: 7.2, p=0.03; 20μM Sulfatide: 25.2 vs 20μM Sulfatide + Olaparib: 11.3, p=0.0005; 50μM Sulfatide: 27.8 vs 50μM Sulfatide + Olaparib: 14.5, p=0.0008; 100μM Sulfatide: 29.7 vs 100μM Sulfatide + Olaparib: 20.5, p=0.007) [**Figure 3.4F**]. In summary, these results

provide support for the notion that sulfatide-induced toxicity involves, at least in part, PARP-1 overactivation and that Olaparib effectively attenuates these detrimental effects.

### 3.4.4 Sulfatide-Induced Impairment in Human Astrocyte Morphology is Partially Reversed by Olaparib

To further investigate the cytotoxic effects of sulfatides and the potential rescue by Olaparib, we examined their impact on changes in astrocyte morphology. Specifically, we assessed the protective effect of Olaparib against sulfatide-induced toxicity through immunocytochemistry using the astrocyte marker vimentin, which is a key player in cytoskeleton formation in astrocytes. Treatment of human astrocytes with sulfatides (5μM, 10μM, 20μM, 50μM, 100μM) for 24 hours resulted in a reduction in vimentin expression in astrocytes, particularly in the cell processes, suggesting deregulation of the cellular cytoskeleton [**Figure 3.5A and Figure 3.5B**]. This change likely reflected the rounding of astrocytes before detachment induced by sulfatides. Importantly, these sulfatide-induced changes in vimentin localization were reduced by treatment with Olaparib (100nM) (Untreated: 3.6 vs Olaparib: 3.4; 10μM Sulfatide: 2.7 vs 10μM Sulfatide + Olaparib: 3.2, p=0.04; 20μM Sulfatide: 1.6 vs 20μM Sulfatide + Olaparib: 2.3, p=0.0007; 50μM Sulfatide: 1.4 vs 50μM Sulfatide + Olaparib: 2.5, p=0.0005, 100μM Sulfatide: 0.7 vs 100μM Sulfatide + Olaparib: 1.3, p=0.02) [**Figure 3.5D**]. The analysis of vimentin intensity fluorescence confirmed that Olaparib reverses sulfatide-induced astrocytes morphology impairment at 10μM sulfatide (70.46% vs 110.43%, p=0.04), 20μM sulfatide (50.24% vs 130.36%, p=0.03), and 100μM sulfatide (10.04% vs 40.20%, p=0.03) [**Figure 3.5C and 3.5E**]. In summary, these findings support the notion that altered cytoskeletal structure, which precedes sulfatide-induced cell death in human astrocytes, can be attenuated by Olaparib treatment.

### 3.4.5 Olaparib Attenuates Sulfatide-Induced Oxidative Stress Damage And Mitochondrial Stress in Human Astrocytes

Next, oxidative stress in human astrocytes was assessed using DCFH-DA. Following exposure to sulfatides (5μM, 10μM, 20μM, 50μM, 100μM), the fluorescence intensity of DCFH-DA was elevated compared to the untreated group [**Figure 3.6A**]. Treatment with 100nM Olaparib significantly attenuated sulfatide-induced reactive oxygen species (ROS) levels (Untreated: 1.0 vs Olaparib:1.08; 5μM Sulfatide: 1.10 vs 5μM Sulfatide + Olaparib: 0.87; 10μM Sulfatide: 1.32 vs 10μM Sulfatide + Olaparib: 0.90, p=0.01; 20μM Sulfatide: 2.31 vs 20μM Sulfatide + Olaparib: 1.29, p=0.009; 50μM Sulfatide: 3.11 vs 50μM Sulfatide + Olaparib: 1.50, p=0.00008; 100μM Sulfatide: 3.16 vs 100μM Sulfatide + Olaparib: 2.27) [**Figure 3.6C**]. Moreover, there is growing evidence suggesting PARP's involvement in alterations in electron transport and the loss of mitochondrial membrane potential (ΔΨm) (Wang et al., 2018). Here, we measured ΔΨm using the membrane-permeant dye tetraethylbenzimidazolylcarbocyanine iodide (JC-1), which accumulates in mitochondria in a potential-dependent manner. An increase in JC-1 monomers signifies a loss of mitochondrial membrane potential. Human astrocytes cultured in serum-starved conditions were treated with sulfatides (ranging from 5μM to 100μM), either with or without Olaparib (100nM). Subsequently, cells were loaded with 1 μM JC-1, and after 30 minutes, emission spectra were measured. Sulfatide treatment led to a loss of ΔΨm compared with the untreated group, indicating increased mitochondrial stress [**Figure 3.6B**]. Significantly, Olaparib treatment attenuated the sulfatide-induced increase in mitochondrial stress (Untreated: 0.0% vs Olaparib: 1.29%; 5μM Sulfatide: 11.16% vs 5μM Sulfatide + Olaparib: 6.76%; 10μM Sulfatide: 35.87% vs 10μM Sulfatide + Olaparib: 21.01%, p=0.005; 20μM Sulfatide: 82.27% vs 20μM Sulfatide + Olaparib: 58.23%, p=0.003; 50μM Sulfatide: 83.44% vs 50μM Sulfatide + Olaparib: 73.84%; 100μM Sulfatide: 97.64% vs 100μM Sulfatide + Olaparib: 76.01%) [**Figure 3.6D**]. These findings provide further evidence of astrocyte cell

damage in the presence of sulfatides and support the notion that PARP-1 is involved in modulating oxidative stress and mitochondrial dysfunction.

### 3.4.6 Olaparib Reduces Calcium Influx in Sulfatide-Stimulated Astrocytes

Activation of PARP-1 has previously been observed to influence the expression of calcium-permeable channels and disrupt mitochondrial calcium homeostasis in conditions like ischemic or traumatic brain injury, as well as in an NMDA toxicity model involving rat primary cortical neurons [47,116]. Our results above show that sulfatides increase PARP-1 expression in human astrocytes [**Figure 3.4**], hence the effects of sulfatides in the presence or absence of Olaparib on activation, influx, and oscillations of $Ca^{2+}$ in human astrocytes were investigated. Astrocyte cultures were pre-treated with sulfatides (5μM, 10μM, 20μM, 50μM, 100μM) with or without Olaparib (100 nM) for 24 hours and then loaded with Cal-520AM calcium dye. Time-lapse $Ca^{2+}$ imaging was performed. After a 20-second baseline recording, cells were treated with 300 μM ATP and imaged for a further 3 minutes (to determine the proportions of astrocytes that display ATP-induced $Ca^{2+}$ oscillations). Sulfatide-treated astrocytes displayed ATP-induced $Ca^{2+}$ peaks that were larger in amplitude than those elicited by astrocytes cotreated with sulfatides and Olaparib [**Figure 3.7A-G**]. Measurement of the area under the curve (AUC) of 20 μM sulfatides group showed the largest AUC $Ca^{2+}$ response to ATP perfusion compared to the untreated group (1321.6 vs 3042.8, p=0.01). Interestingly, Olaparib significantly reduced this sulfatide-induced AUC $Ca^{2+}$ response to ATP perfusion (10μM Sulfatide: 2851.6 vs 10μM Sulfatide + Olaparib: 1293.2, p=0.03; 20μM Sulfatide: 3042.8 vs 20μM Sulfatide + Olaparib: 1630.8, p=0.01) [**Figure 3.7H**]. Sulfatide treatment did not affect the halftime of $Ca^{2+}$ release [**Figure 3.7I**]. Taken together with the data above showing sulfatide-induced PARP-1 overexpression and Olaparib-mediated reductions in $Ca^{2+}$ oscillations in response to ATP in

sulfatide-stimulated astrocytes, we speculate a cross modulation between the PARP-1 expression and $Ca^{2+}$ signaling, that is regulated in an opposing manner by sulfatides and Olaparib.

### 3.4.7 Sulfatides Induce Pro-Inflammatory Cytokine and Chemokine Release From Human Astrocytes

MLD patients exhibit augmented levels of pro-inflammatory cytokines and chemokines including CCL2, IL-1Ra, IL-8, and CCL4 in the cerebral spinal fluid. The levels of pro-inflammatory cytokines IL-6, IL-17, IL-8, and CX3CL1 secreted from human astrocytes treated with sulfatides (5μM, 10μM, 20μM, 50μM, 100μM) for 24 hours, showed a concentration-dependent increase compared to untreated group [**Figure 3.8A-D**]: IL-6 (Untreated 32.8 pg/ml; 10μM Sulfatide: 77.6 pg/ml, p=0.02; 20μM Sulfatide: 125.4 pg/ml, p=0.004; 50μM Sulfatide: 145.3 pg/ml, p=0.006; 100μM Sulfatide: 148.8 pg/ml, p=0.003) [**Figure 3.8A**], IL-17 (Untreated 7.4 pg/ml; 20μM Sulfatide: 78.1 pg/ml, p=0.0003; 50μM Sulfatide: 105.4, p=0.0006; 100μM Sulfatide: 102.8 pg/ml, p=0.0001) [**Figure 3.8B**], IL-8 (Untreated 14.9 pg/ml; 10μM Sulfatide: 72.4 pg/ml, p=0.0006; 20μM Sulfatide: 88.0 pg/ml, p=0.0008; 50μM Sulfatide: 112.1 pg/ml, p=0.0004; 100μM Sulfatide: 98.5 pg/ml, p=0.0006) [**Figure 3.8C**], and CX3CL1 (Untreated 0.68 ng/ml; 20μM Sulfatide: 9.4 ng/ml, p=0.01; 50μM Sulfatide: 10.5 ng/ml, p=0.03; 100μM Sulfatide: 10.7 ng/ml, p=0.02) [**Figure 3.8D**]. Taken together, these data demonstrate that sulfatide exposure promotes inflammatory mediator release by human astrocytes.

### 3.4.8 Olaparib Inhibits Pro-Inflammatory Cytokine and Chemokine Release From Sulfatide-Treated Astrocytes

PARP-1 has a key role in chronic inflammation in the context of many inflammatory-driven pathologies. Therefore, the effects of sulfatide treatment on the expression of IL-6, IL-17, IL-8, and CX3CL1 from human astrocytes were examined in the presence or absence of PARP-1 inhibition. Treating astrocytes with 100 nM Olaparib for 24 hours, in the presence of sulfatides (5μM, 10μM, 20μM, 50μM, 100μM), significantly decreased the release of IL-6 (Untreated 32.8 vs. Olaparib: 25.3 pg/ml; 20μM Sulfatide: 125.4 vs. 20μM Sulfatide + Olaparib: 50.6 pg/ml, p=0.02; 50μM Sulfatide: 145.3 vs. 50μM Sulfatide + Olaparib: 63.0 pg/ml, p=0.006) [**Figure 3.9A**], IL-17 (Untreated 7.4 vs. Olaparib: 10.1 pg/ml; 20μM Sulfatide: 78.1 vs. 20μM Sulfatide + Olaparib: 35.1 pg/ml, p=0.04; 50μM Sulfatide: 105.4 vs. 50μM Sulfatide + Olaparib: 54.4 pg/ml, p=0.03) [**Figure 3.9B**], IL-8 (Untreated 14.9 vs. Olaparib: 24.5 pg/ml; 20μM Sulfatide: 88.0 vs. 20μM Sulfatide + Olaparib: 29.3 pg/ml, p=0.01; 50μM Sulfatide: 112.1 vs. 50μM Sulfatide + Olaparib: 17.9 pg/ml, p=0.03) [**Figure 3.9C**], and CX3CL1 (Untreated 0.68 vs. Olaparib: 0.55 ng/ml; 20μM Sulfatide: 9.4 vs. 20μM Sulfatide + Olaparib: 5.0 ng/ml, p=0.01; 50μM Sulfatide: 10.5 vs. 50μM Sulfatide + Olaparib: 6.0 ng/ml, p=0.01) [**Figure 3.9D**]. Interestingly, the overall expression of these cytokines is negatively correlated with astrocyte survival measured by MTT ($\rho$=-0.7272, p=0.0102) [**Figure 3.9E**]. Taken together, these data demonstrate that Olaparib can attenuate this sulfatide-induced secretion of pro-inflammatory cytokines and chemokines by astrocytes. This suggests that astrocytic PARP-1 overexpression may, therefore, promote CNS neuroinflammation.

### 3.4.9 Olaparib Reduces the Chemoattraction of Human Immune Cells Towards the Soluble Microenvironment of Sulfatide-Treated Astrocytes

To elucidate the effects of sulfatide accumulation on immune cell infiltration to the inflamed CNS, peripheral blood lymphocyte, NK cell, and T cell migration towards human astrocyte-conditioned media was examined. Human astrocytes were treated, for 24 hours, with sulfatides (5μM, 10μM, 20μM, 50μM, 100μM). Migration of the isolated peripheral blood immune cells towards the astrocyte-conditioned medium (ACM) was measured using a transwell chemotaxis assay [**Figure 3.10A**]. Data are presented as fold-change (FC) of lymphocyte, NK cell, and T cell migration towards the lower chamber of the transwell versus Negative Control (DMEM). Data showed migration of immune cells towards the Positive Control (DMEM + 20% FBS) was significantly higher compared with the Negative Control (DMEM) demonstrating the functionality of the chemotaxis system (Lymphocytes, Neg Control: 1 vs Pos Control: 6.16, p=0.03), (T cells, Neg Control: 1 vs Pos Control: 4.80, p=0.03), (NK cells, Neg Control: 1 vs Pos Control: 3.64, p=0.02). The conditioned media from astrocytes treated with sulfatides increased the migration of lymphocytes, T cells, and NK cells towards the lower chamber, compared to the negative control (FC Migration of Lymphocytes, 10μM Sulfatide: 11.34, p=0.03; 20μM Sulfatide: 13.29, p=0.006) [**Figure 3.10B**]; (FC Migration of T cells, 5μM Sulfatide: 18.34, p=0.04; 20μM Sulfatide: 24.85, p=0.007; 50μM Sulfatide: 24.94, p=0.002) [**Figure 3.10C**]; (FC Migration of NK cells, 20μM Sulfatide: 7.92, p=0.03) [**Figure 3.10D**]. Overall, these data suggest that the sulfatide-induced changes in pro-inflammatory response of human astrocytes are paralleled by an increased potential to recruit lymphocytes. Of note, at higher concentrations of sulfatides (100μM), some cytokine release from astrocytes (IL-17 and IL-8) and immune cell migration decreased. Together with the data from cell viability, calcium, and ROS assays, it is likely that this is due to excessive sulfatide-induced astrocyte toxicity.

### 3.4.10 Olaparib Reduces the Chemoattraction of Human Immune Cells Towards the Soluble Microenvironment of Sulfatide-Treated Astrocytes

To elucidate the effects of Olaparib on sulfatide-induced immune cell recruitment, peripheral blood lymphocyte, NK cell, and T cell migration towards human astrocyte conditioned media was examined. Human astrocytes were treated, for 24 hours, with sulfatides (5μM, 10μM, 20μM, 50μM, 100μM) with or without 100nM Olaparib. Migration of the isolated peripheral blood immune cells towards the ACM was measured using a transwell chemotaxis assay [**Figure 3.11A**]. Data are presented as fold-change (FC) of lymphocyte, NK cell, and T cell migration towards the lower chamber of the transwell versus Negative Control (DMEM). Data showed migration of immune cells towards the Positive Control (DMEM + 20% FBS) was significantly higher compared with the Negative Control (DMEM) demonstrating the functionality of the chemotaxis system (Lymphocytes, Neg Control: 1 vs Pos Control: 6.16, p=0.03), (T cells, Neg Control: 1 vs Pos Control: 4.80, p=0.03), (NK cells, Neg Control: 1 vs Pos Control: 3.64, p=0.02). The conditioned media from astrocytes treated with sulfatides increased the migration of lymphocytes, T cells, and NK cells towards the lower chamber, compared to the negative control [**Figure 3.11B-D**]. Importantly, conditioned medium from astrocytes treated with sulfatides and Olaparib significantly attenuated immune cell migration compared to conditioned medium from astrocytes treated with sulfatides: (FC Migration of Lymphocytes, 10μM Sulfatide: 11.34 vs 10μM Sulfatide + Olaparib: 5.01, p=0.02; 20μM Sulfatide: 13.29 vs 20μM Sulfatide + Olaparib: 5.36, p=0.02) [**Figure 3.11B**]; (FC Migration of T cells, 20μM Sulfatide: 24.85 vs 20μM Sulfatide + Olaparib: 11.35, p=0.03; 50μM Sulfatide: 24.94 vs 50μM Sulfatide + Olaparib: 11.84, p=0.04) [**Figure 3.11C**]; (FC Migration of NK cells, 20μM Sulfatide: 7.92 vs 20μM Sulfatide + Olaparib: 0.73, p=0.04) [**Figure 3.11D**]. These data demonstrate that Olaparib can significantly reduce immune cell migration towards the chemotactic cues of sulfatide-treated astrocytes. Overall, these data suggest that

the sulfatide-induced changes in pro-inflammatory response and immune cell recruitment can be attenuated by treatment with Olaparib.

**Figure 3.2**

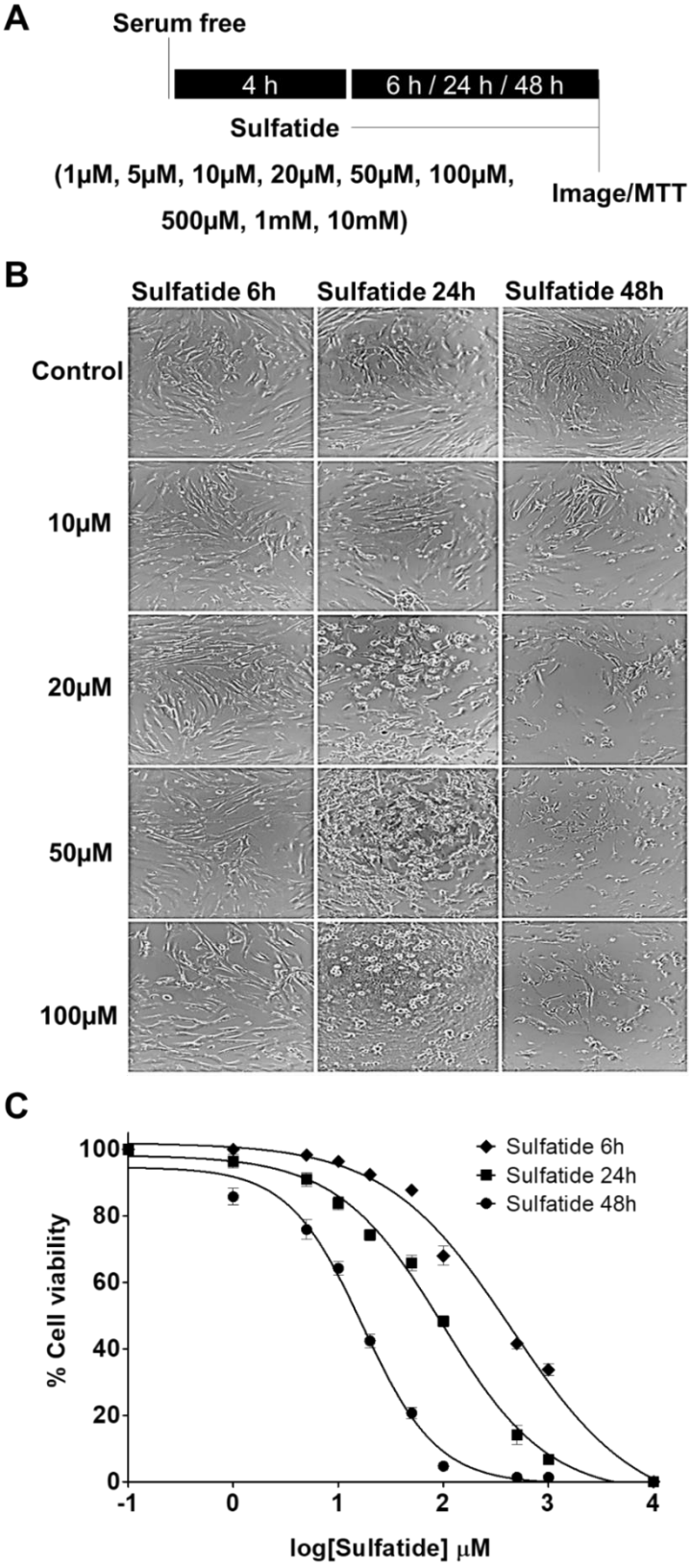
A
Serum free
4 h
6 h / 24 h / 48 h
Sulfatide
(1μM, 5μM, 10μM, 20μM, 50μM, 100μM,
500μM, 1mM, 10mM)
Image/MTT
B
Sulfatide 6h
Sulfatide 24h
Sulfatide 48h
Control
10μM
20μM
50μM
100μM
C
Sulfatide 6h
Sulfatide 24h
Sulfatide 48h
% Cell viability
100
80
60
40
20
0
-1
0
1
2
3
4
log[Sulfatide] μM

**Figure 3.2: Sulfatides induce human astrocyte cell death.** (**A**) Diagram of experimental timeline depicting astrocytes were incubated in serum-free media for 4 hours and treated with sulfatides at concentrations indicated for 6 hours, 24 hours, or 48 hours. (**B**) Representative images of human astrocytes treated with 10µM, 20µM, 50µM, and 100µM sulfatides for either 6 hours, 24 hours, or 48 hours. Cells were imaged under light microscopy. (**C**) Dose-response curves showing that sulfatides decreased human astrocyte viability in a concentration-dependent (5µM, 10µM, 20µM, 50µM, and 100µM) and time-dependent (6 hours (black diamond), 24 hours (black square), 48 hours (black circle)) manner (n = 5-10). Cell viability was quantified using an MTT assay (Vybrant® MTT Cell Proliferation Assay Kit, Life technologies). All values are given as a percentage normalized to the untreated group. Statistical analysis was performed using a log dose-response test with GraphPad Prism 5. Graphical data are presented as mean ± SD.

**Figure 3.3**

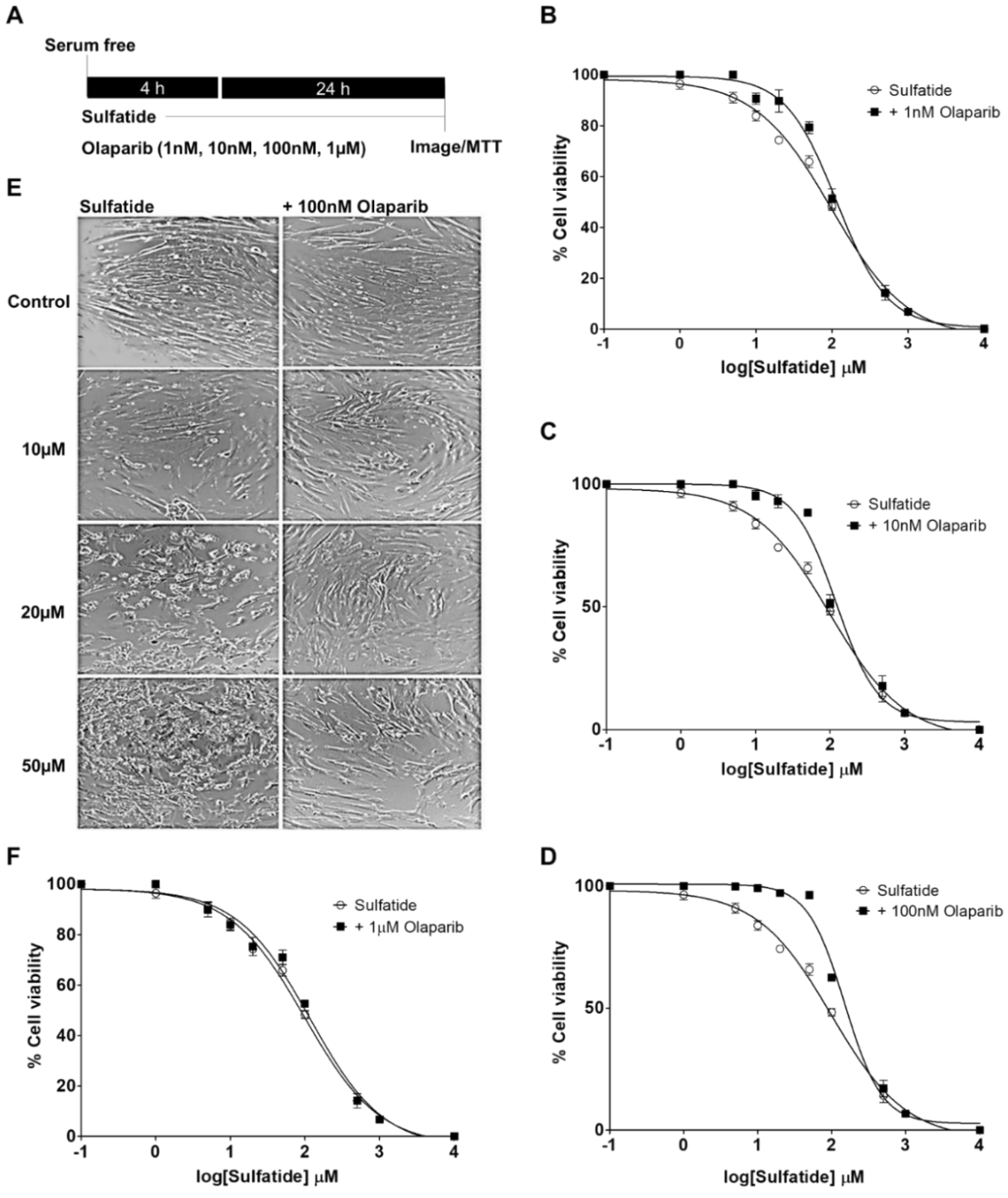
A
Serum free
4 h
24 h
Sulfatide
Olaparib (1nM, 10nM, 100nM, 1μM)
Image/MTT
B
% Cell viability
log[Sulfatide] μM
Sulfatide
+ 1nM Olaparib
C
+ 10nM Olaparib
D
+ 100nM Olaparib
E
Sulfatide
+ 100nM Olaparib
Control
10μM
20μM
50μM
F
+ 1μM Olaparib

**Figure 3.3: Olaparib reduces sulfatide-induced human astrocyte cell death.** (**A**) Diagram of experimental timeline and treatments. Human astrocytes were treated with 5µM, 10µM, 20µM, 50µM, and 100µM sulfatides for 24 hours with or without 100nM Olaparib. (**B**) A dose-response curve showing changes in astrocyte viability after treatment with sulfatides (5µM, 10µM, 20µM, 50µM, and 100µM, clear circle) with or without Olaparib treatment (1nM, black square) for 24 hours (n = 5). (**C**) A dose-response curve showing changes in astrocyte viability after treatment with sulfatides (5µM, 10µM, 20µM, 50µM, and 100µM, clear circle) with or without Olaparib treatment (10 nM, black square) for 24 hours (n = 5). (**D**) A dose-response curve showing changes in astrocyte viability after treatment with sulfatides (5µM, 10µM, 20µM, 50µM, and 100µM, clear circle) with or without Olaparib treatment (100nM, black square) for 24 hours (n = 5). (**E**) Representative images of astrocytes treated with sulfatides (20µM, 50µM, and 100µM) with or without Olaparib (100nM) for 24 hours. Cells were imaged under light microscopy. (**F**) A dose-response curve showing changes in astrocyte viability after treatment with sulfatides (5µM, 10µM, 20µM, 50µM, and 100µM, clear circle) with or without Olaparib treatment (1 µM, black square) for 24 hours (n = 5). Cell viability was quantified using an MTT assay (Vybrant® MTT Cell Proliferation Assay Kit, Life Technologies). Statistical analysis was performed using a log dose-response test with GraphPad Prism 5. Graphical data are presented as mean ± SEM.

**Figure 3.4**

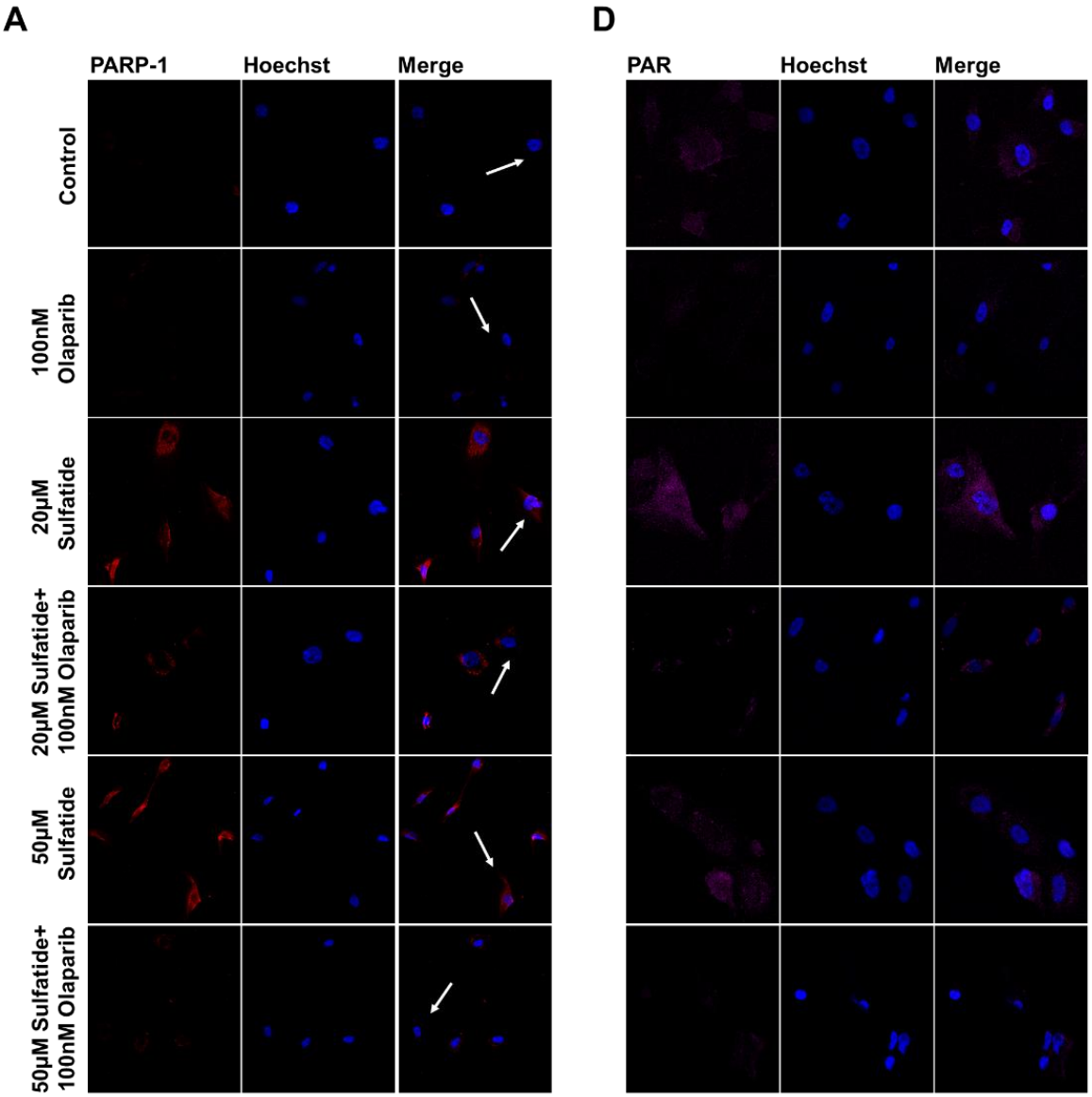
A
PARP-1
Hoechst
Merge
Control
100nM Olaparib
20μM Sulfatide
20μM Sulfatide+ 100nM Olaparib
50μM Sulfatide
50μM Sulfatide+ 100nM Olaparib
D
PAR
Hoechst
Merge

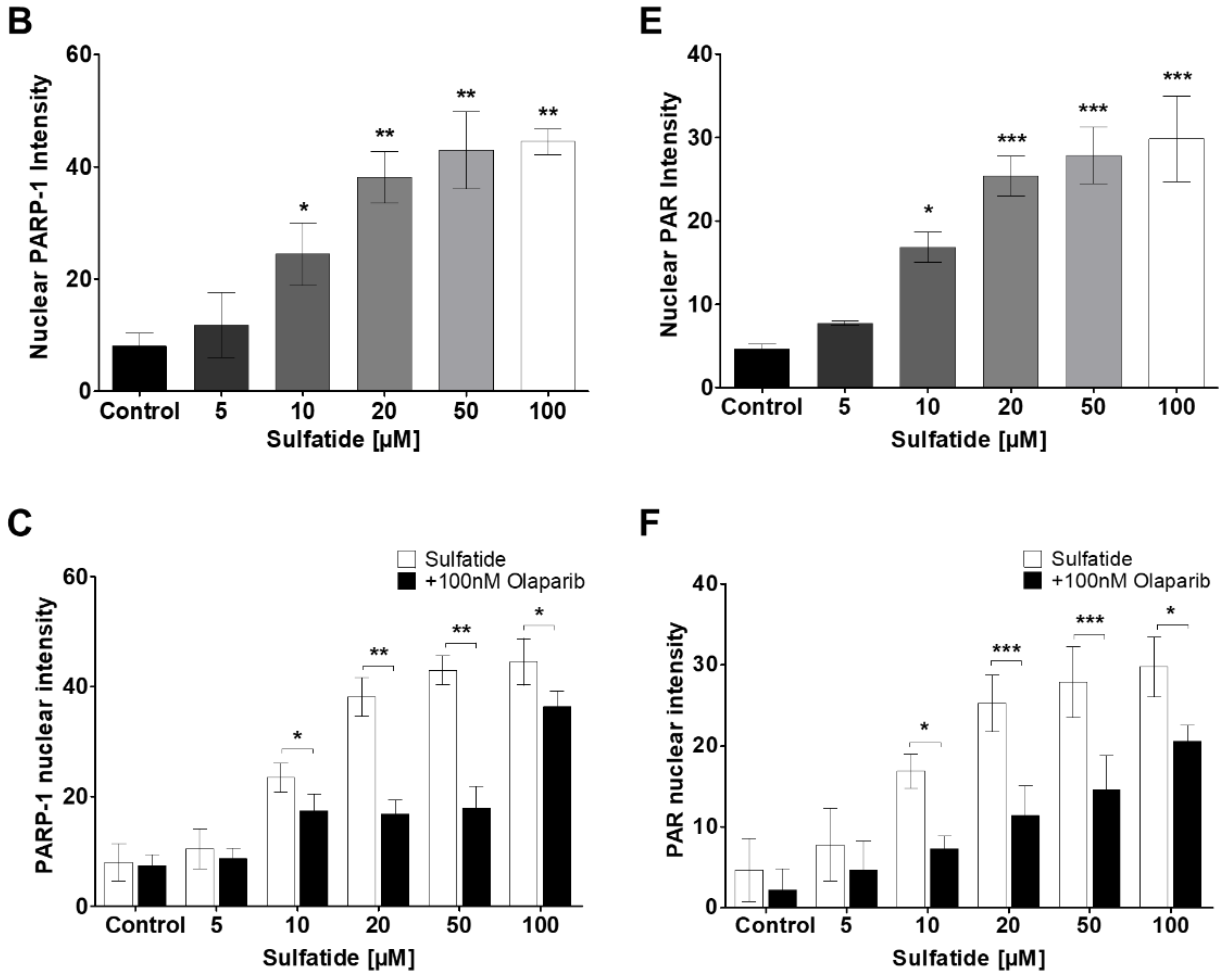


**Figure 3.4: Olaparib decreases sulfatide-induced PARP-1 activation and expression in human astrocytes. (A)** Representative confocal images displaying PARP-1 (red) and Hoechst (blue) immunostaining under treatment conditions indicated. Confocal images were captured at ×40 magnification. **(B)** Treatment with sulfatides induced PARP-1 translocation to nuclei (5µM, 10µM, 20µM, 50µM, and 100µM). **(C)** Treatment with Olaparib (100nM) reduced sulfatide-induced PARP-1 translocation to nuclei (5µM, 10µM, 20µM, 50µM, and 100µM). A number of 15 images were analysed per condition. Semi-quantitative analysis of PARP-1-associated fluorescence in the nuclei of astrocytes. **(D)** Representative confocal images displaying PAR (purple) and Hoechst (blue) immunostaining under treatment conditions indicated. Confocal images were captured at ×63 magnification. **(E)** Treatment with sulfatides induced PAR expression in nuclei (5µM, 10µM, 20µM, 50µM, and 100µM). **(F)** Treatment with Olaparib (100nM) reduced sulfatide-induced PAR expression in nuclei (5µM, 10µM, 20µM, 50µM, and 100µM). A number of 15 images were analysed per condition. Data are presented as mean ± SEM (n = 5), one-way ANOVA followed by Turkey's post hoc test, *p<0.05, **p<0.01, ***p<0.001.

**Figure 3.5**

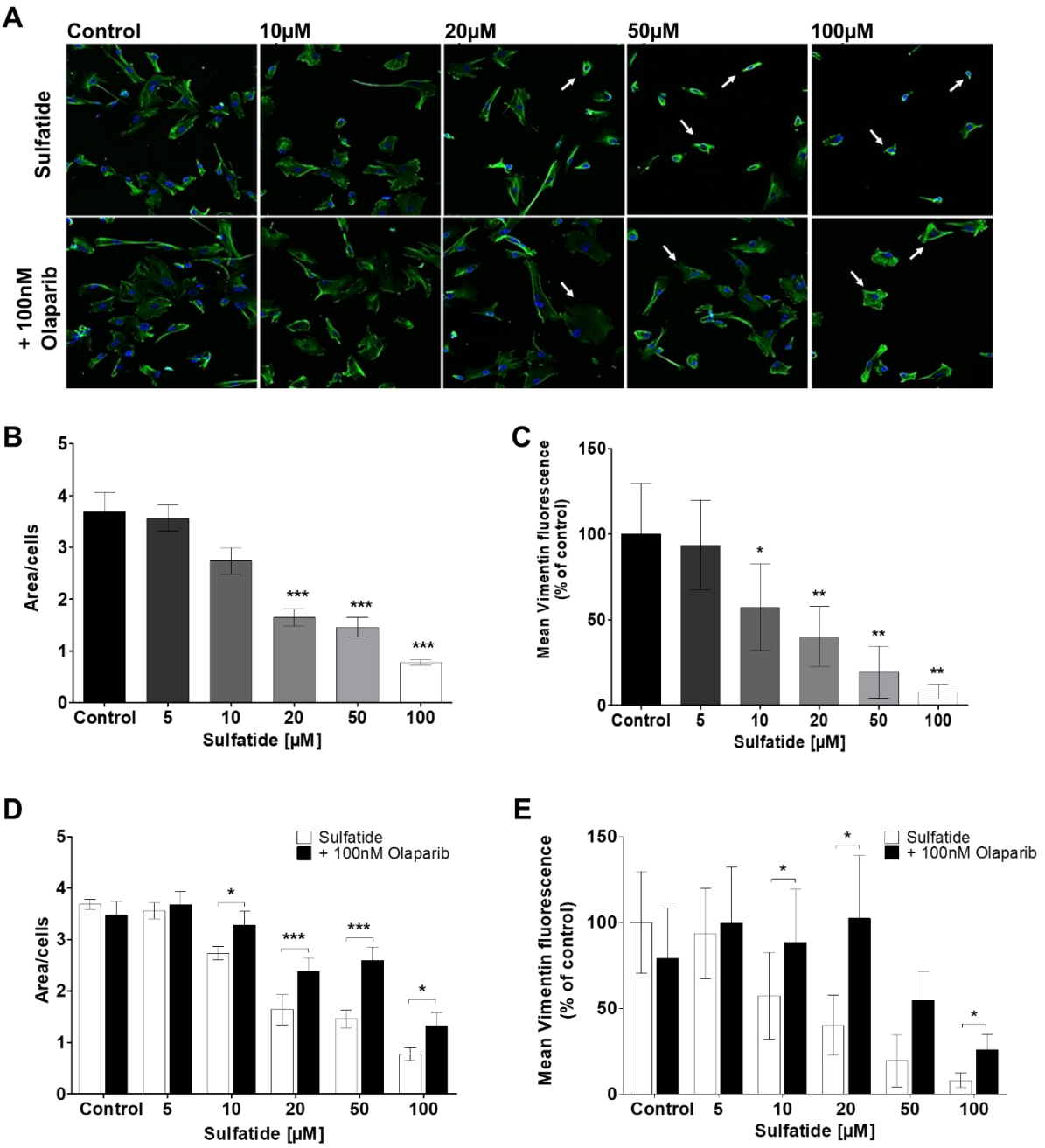
A
Control
10μM
20μM
50μM
100μM
Sulfatide
+ 100nM Olaparib
B
Area/cells
Control
5
10
20
50
100
Sulfatide [μM]
C
Mean Vimentin fluorescence (% of control)
Control
5
10
20
50
100
Sulfatide [μM]
D
Sulfatide
+ 100nM Olaparib
Area/cells
Control
5
10
20
50
100
Sulfatide [μM]
E
Sulfatide
+ 100nM Olaparib
Mean Vimentin fluorescence (% of control)
Control
5
10
20
50
100
Sulfatide [μM]

**Figure 3.5: Sulfatide-induced changes in vimentin in human astrocytes are partially reversed by Olaparib.** Human astrocytes were treated with sulfatides (5µM, 10µM, 20µM, 50µM, and 100µM for 24 hours) with or without the PARP inhibitor Olaparib (100nM for 24 hours). (**A**) Representative confocal images displaying Hoechst (blue) and vimentin (green) staining under treatment conditions indicated. Confocal images were captured at ×20 magnification showing that treatment with 100 nM Olaparib (bottom) attenuates astrocyte morphology impairment induced by sulfatides (5µM, 10µM, 20µM, 50µM, and 100µM, top). A number of 15 images were analysed per condition. (**B**) Bar graph illustrating changes in astrocytes area after the treatment with sulfatides (5µM, 10µM, 20µM, 50µM, and 100µM) for 24 hours. (**C**) Bar graph illustrating changes in the intensity of vimentin fluorescence after the treatment with sulfatides (5µM, 10µM, 20µM, 50µM, and 100µM) for 24 hours. (**D**) Bar graph illustrating changes in astrocytes area after the treatment with sulfatides (5µM, 10µM, 20µM, 50µM, and 100µM) and with or without Olaparib (100nM) for 24 hours. (**E**) Bar graph illustrating changes in the intensity of vimentin fluorescence after the treatment with sulfatides (5µM, 10µM, 20µM, 50µM, and 100µM) and with or without Olaparib (100nM) for 24 hours. Data are presented as mean ± SEM (n = 5), one-way ANOVA followed by Dunnett post hoc test, *$p<0.05$, ***$p<0.001$.

**Figure 3.6**

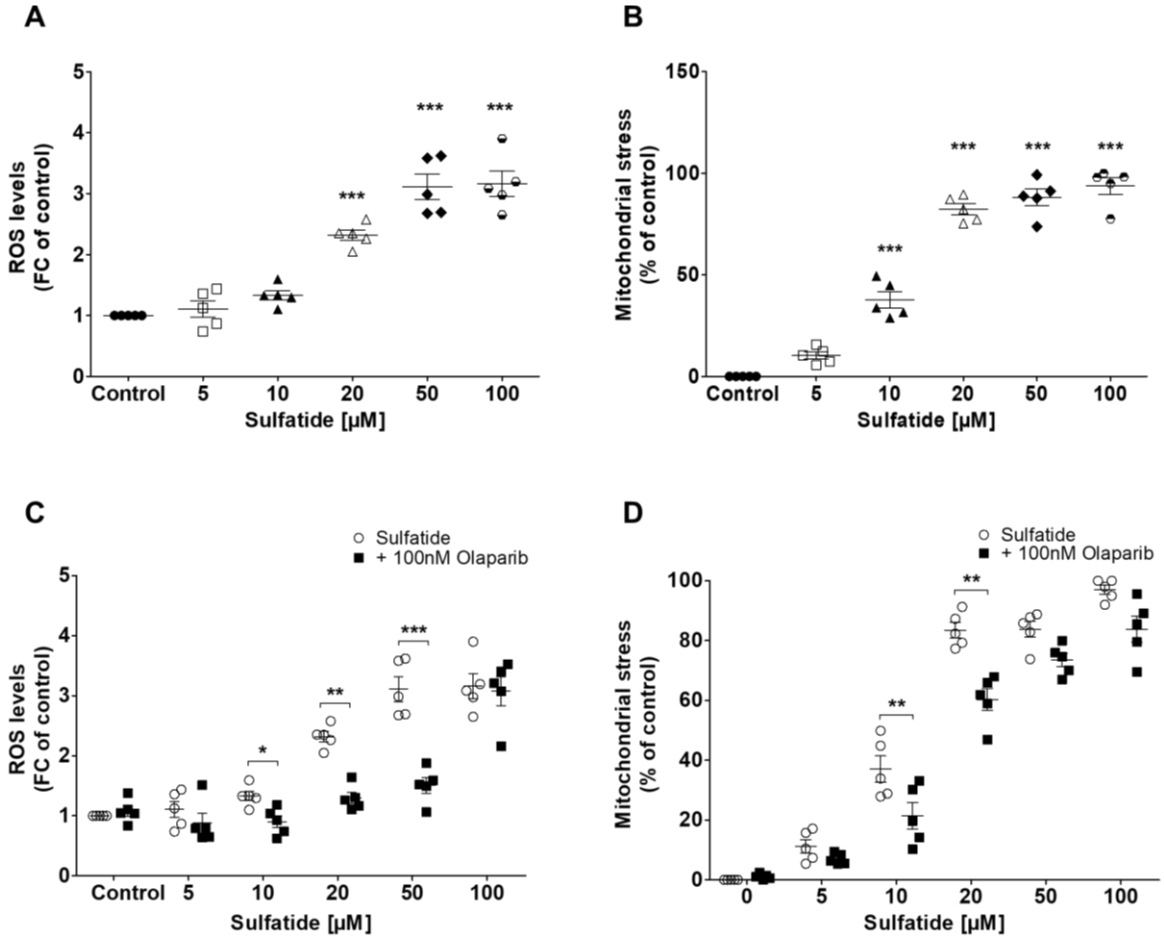


**Figure 3.6: Olaparib suppresses reactive oxygen species (ROS) generation caused by sulfatides in human astrocytes and reduces mitochondrial stress.** (**A**) Quantification of ROS levels was determined by 2'-7' dichlorofluorescin diacetate (DCFH-DA) staining in human astrocytes treated with 5µM, 10µM, 20µM, 50µM, and 100µM of sulfatides. (**B**) To confirm that PARP-1 activation had negligible effects on cellular stress, the JC-1 assay was performed to measure changes in the mitochondrial membrane potential of sulfatides (5µM, 10µM, 20µM, 50µM, and 100µM). Data are presented as the mean absorbance levels (at 570 nm). (**C**) Quantification of ROS levels in human astrocytes treated with 5µM, 10µM, 20µM, 50µM, and 100µM of sulfatides (clear circle) with or without 100 nM of Olaparib (black square). Data are presented as the mean absorbance levels (at 490 nm). (**D**) JC-1 assay was performed to measure changes in the mitochondrial membrane potential of sulfatides (5µM, 10µM, 20µM, 50µM, and 100µM) and Olaparib (100nM). Data are presented as the mean absorbance levels (at 570 nm). The measures of fluorescence signal are reported in the graphs as fold change (FC) or percentage of each condition versus the untreated and presented as mean ± SD (n = 5). Statistical significance was determined by paired t-test, *p<0.05, **p<0.01, ***p<0.001.

**Figure 3.7**

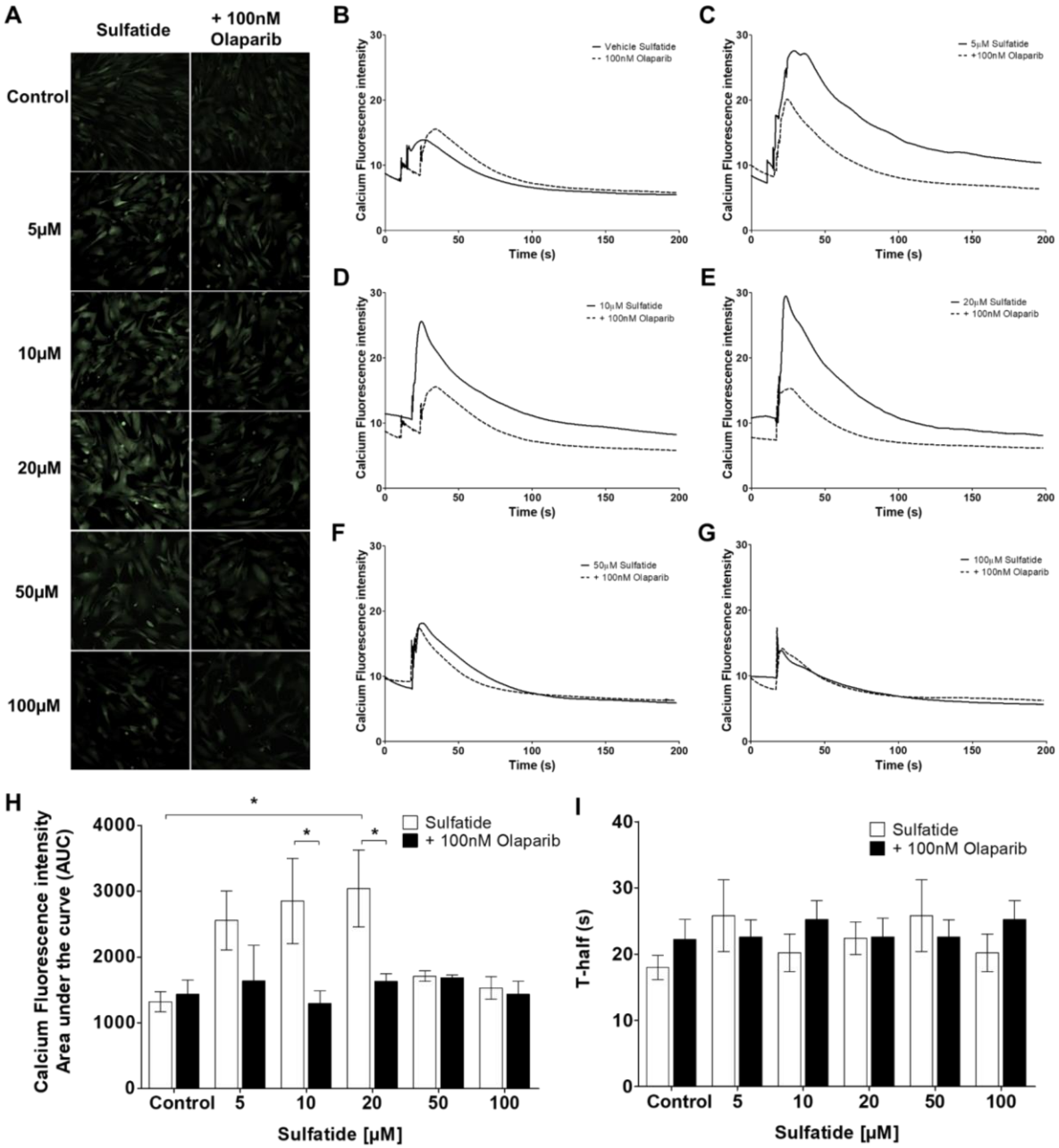
A
Sulfatide
+ 100nM Olaparib
Control
5μM
10μM
20μM
50μM
100μM
B
Vehicle Sulfatide
100nM Olaparib
C
5μM Sulfatide
+100nM Olaparib
D
10μM Sulfatide
+ 100nM Olaparib
E
20μM Sulfatide
+ 100nM Olaparib
F
50μM Sulfatide
+ 100nM Olaparib
G
100μM Sulfatide
+ 100nM Olaparib
Calcium Fluorescence intensity
Time (s)
H
Calcium Fluorescence intensity
Area under the curve (AUC)
Sulfatide
+ 100nM Olaparib
Control
5
10
20
50
100
Sulfatide [μM]
I
T-half (s)
Sulfatide
+ 100nM Olaparib
Control
5
10
20
50
100
Sulfatide [μM]

**Figure 3.7: Olaparib decreases $Ca^{2+}$ changes caused by sulfatides in human astrocytes.** Human astrocytes were treated with 5µM, 10µM, 20µM, 50µM, and 100µM sulfatides for 24 hours and with or without 100nM Olaparib and loaded with 3µM Cal-520AM calcium indicator for 2 hours in Hank's balanced salt solution (HBSS) without calcium ($Ca^{2+}$) and magnesium ($Mg^{2+}$). Immediately prior to $Ca^{2+}$ imaging experiments, astrocytes were transferred to a fresh DMEM medium. Time-lapse $Ca^{2+}$ imaging experiments were performed at a rate of 0.99 frames per second over a 3-minute 20-second period, which included 20 seconds baseline, and 3 minutes of exposure to 300µM ATP. (**A**) Representative confocal images (×20 magnification) of $Ca^{2+}$ influx in response to 300 µM ATP in untreated and reactive astrocytes pre-treated with sulfatides (5µM, 10µM, 20µM, 50µM, and 100µM) and with or without 100nM Olaparib for 24 hours. (**B-G**) Representative traces showing changes in cytosolic $Ca^{2+}$ levels in untreated and sulfatide-stimulated astrocytes (continuous line) with or without 100nM Olaparib (broken line). There was a 30-second baseline, at which point astrocytes were stimulated with ATP for a further 3 minutes. (**H-I**) Olaparib (black square) caused a larger decrease of both the peak amplitude and AUC in 10µM and 20µM sulfatide-treated astrocytes (clear circle) but didn't change the time half. Data for the total 3.20-minute treatment period are presented as mean ± SEM (n = 5) and were analysed using a two-way ANOVA followed by Bonferroni post-hoc test, *$p<0.05$.

**Figure 3.8**

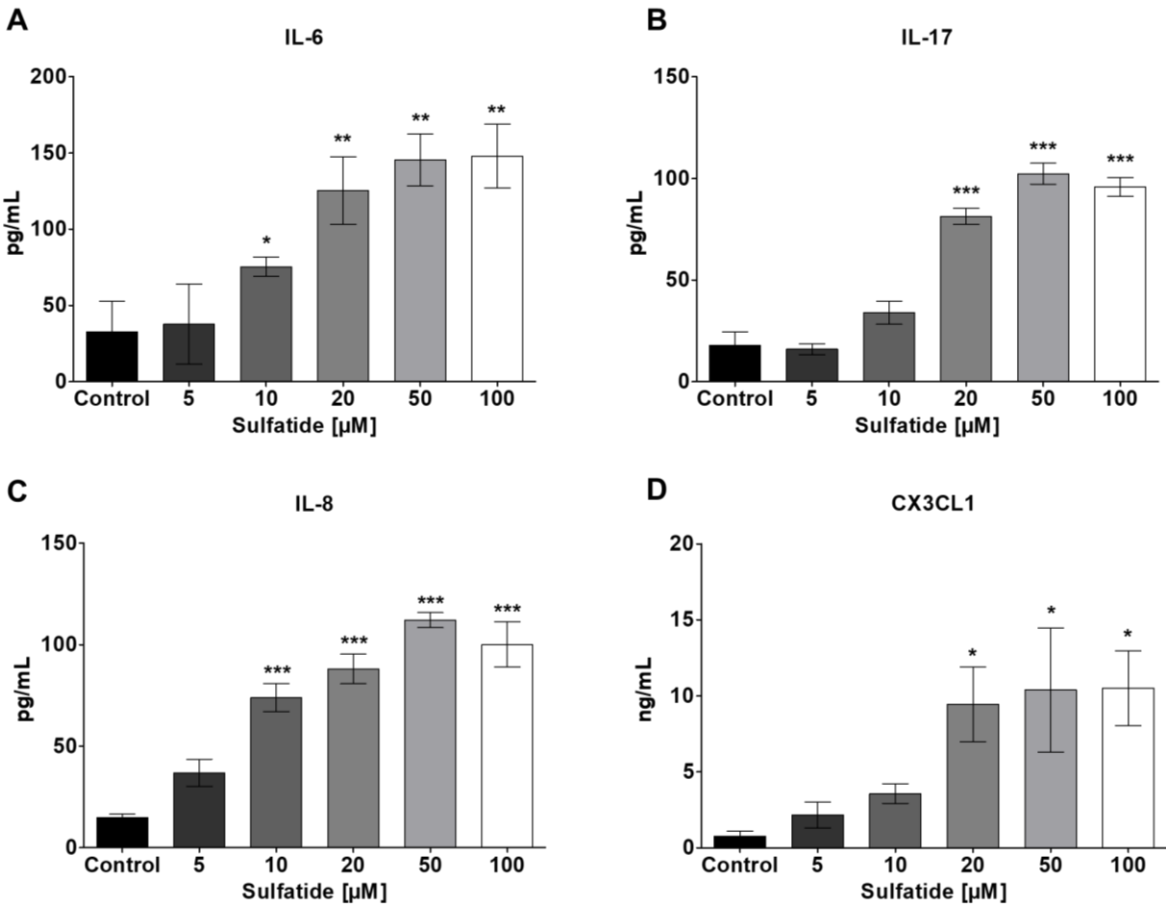


**Figure 3.8: Sulfatides induce cytokine and chemokine release from human astrocytes.** Cytokine and chemokine release from untreated and sulfatide-stimulated astrocytes were measured after 24. Sulfatide showed a significant increase in (**A**) IL-6, (**B**) IL-17, (**C**) IL-8, and (**D**) CX3CL1 release into the cell culture medium, as measured by ELISA. (**A**) Sulfatide causes a significant induction in IL-6 secretion from astrocytes when compared to the untreated group, (**B**) Sulfatide also caused a significant increase in IL-17 secretion from human astrocytes. (**C**) Sulfatide increases IL-8 secretion and (**D**) CX3CL1 from astrocytes. Data from the ELISA assays are presented as mean ± SEM. IL-6, IL-17, IL-8, and CX3CL1 ELISA's were repeated n = 5 (using supernatants generated from MTT assay experiments). Statistical analysis was performed using a paired t-test; *p<0.05, **p<0.01, ***p<0.001.

**Figure 3.9**

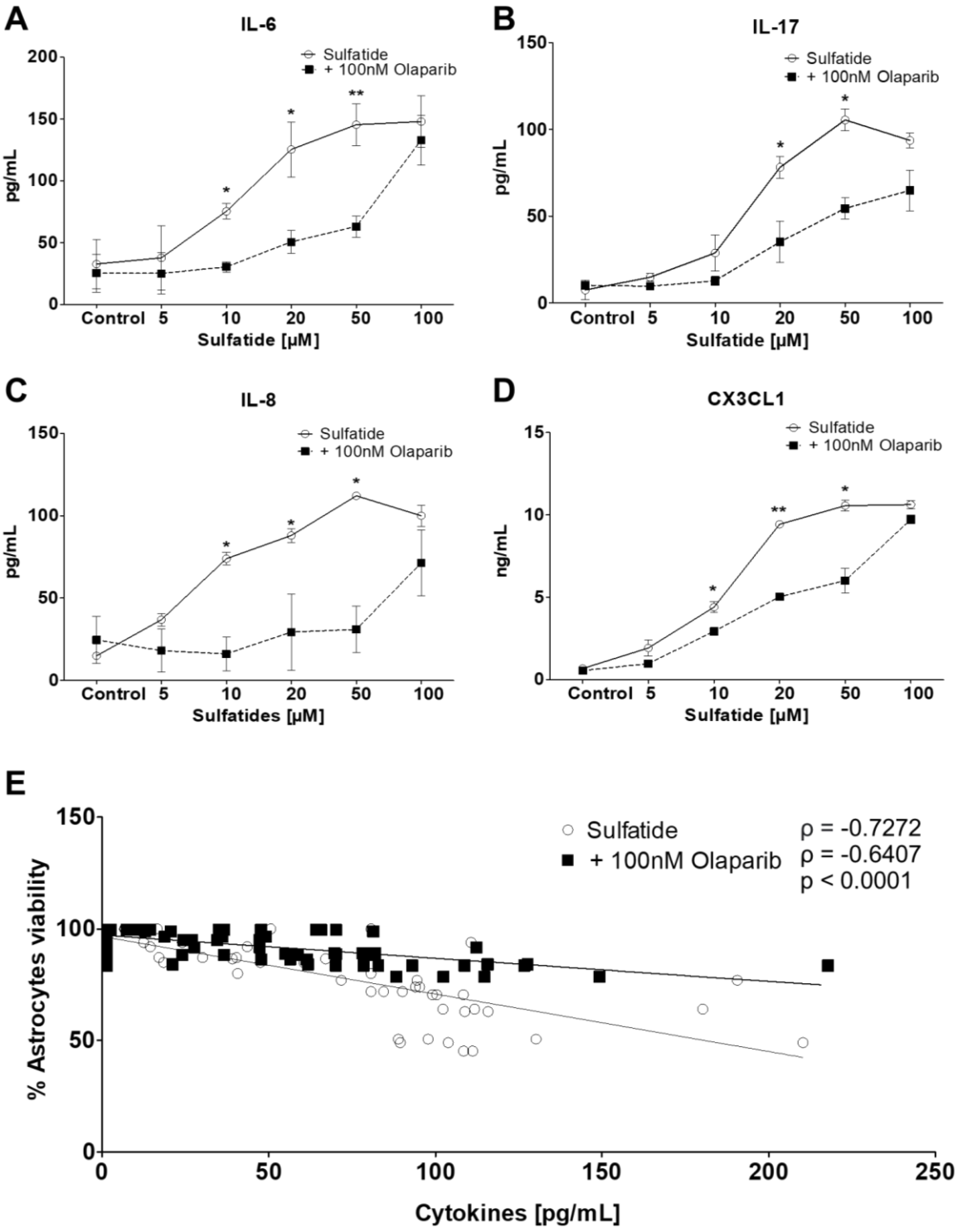
A
IL-6
Sulfatide
+ 100nM Olaparib
pg/mL
Control 5 10 20 50 100
Sulfatide [µM]
B
IL-17
pg/mL
Sulfatide [µM]
C
IL-8
pg/mL
Sulfatides [µM]
D
CX3CL1
ng/mL
Sulfatide [µM]
E
% Astrocytes viability
Cytokines [pg/mL]
ρ = -0.7272
ρ = -0.6407
p < 0.0001

**Figure 3.9: PARP-1 modulates cytokine and chemokine release from human astrocytes.** Cytokine and chemokine release from untreated and sulfatide-stimulated astrocytes (clear circle) were measured after 24 hours of Olaparib exposure (black square). Olaparib (100 nM) showed a significant decrease in (**A**) IL-6, (**B**) IL-17, (**C**) IL-8, and (**D**) CX3CL1 release into the cell culture medium, as measured by ELISA. (**A**) Olaparib causes a significant reduction in IL-6 secretion from astrocytes when compared to the sulfatides group, (**B**) Olaparib also caused a significant decrease in IL-17 secretion from sulfatide-stimulated astrocytes. (**C**) Olaparib reduces IL-8 secretion and (**D**) CX3CL1 from sulfatide-stimulated astrocytes. (**E**) Correlation between total cytokines level and astrocyte survival. The levels of the 4 cytokines were significantly positively correlated with cell death. Data from the ELISA assays are presented as mean ± SEM. IL-6, IL-17, IL-8, and CX3CL1 ELISA's were repeated n = 5 (using supernatants generated from MTT assay experiments). CX3CL1 values were multiplied by 1000 and divided by 100 to adjust Figure E. Statistical analysis was performed using a paired t-test; *$p<0.05$, **$p<0.01$.

**Figure 3.10**

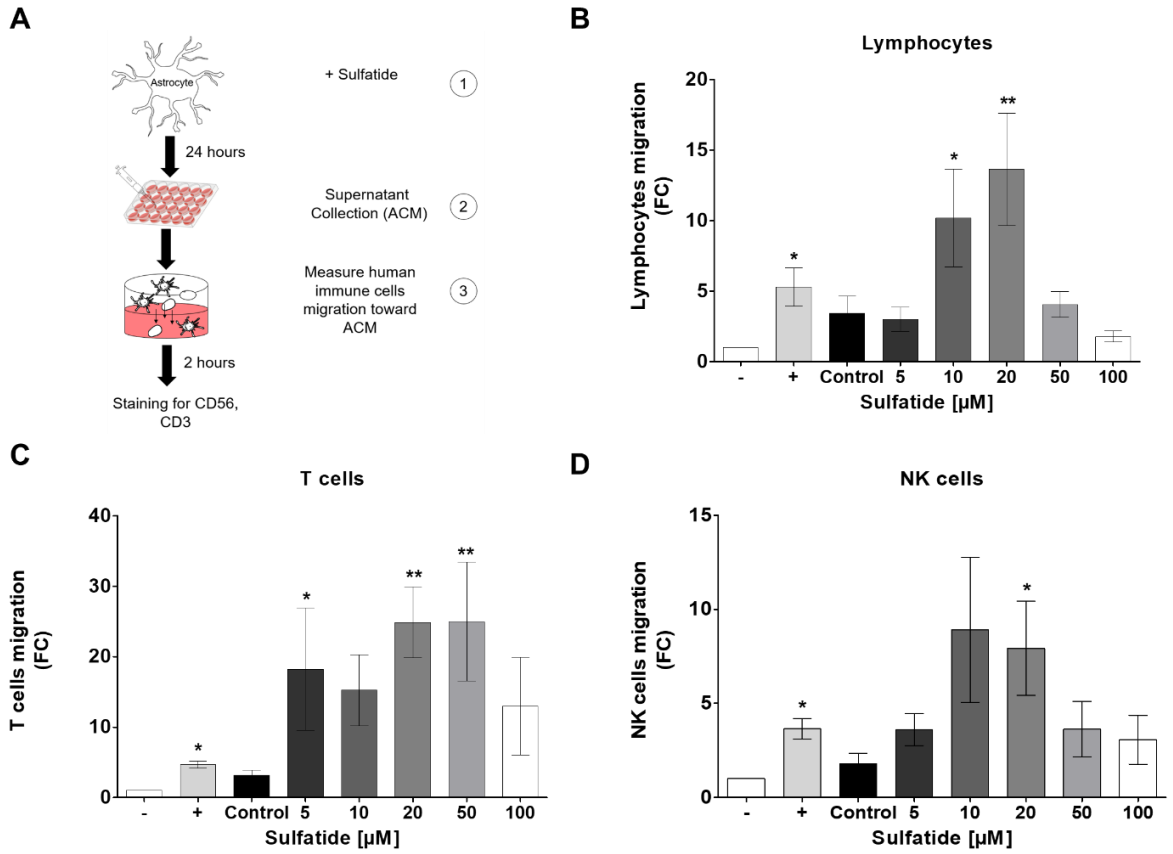


**Figure 3.10: Sulfatides induce the chemoattraction of human immune cells towards the soluble microenvironment of astrocytes.** Lymphocyte, T cell, and NK cell migration towards astrocyte-conditioned medium (ACM) from untreated and sulfatide-stimulated astrocytes were measured after 24 hours. (**A**) Diagram of experimental timeline and treatments. (**B**) Bar charts showing the fold change (FC) migration of lymphocytes towards the negative untreated (serum-free DMEM (-)), positive untreated (DMEM+20% FBS (+)), vehicle untreated (Control), or ACM from, astrocytes treated with sulfatides (5µM, 10µM, 20µM, 50µM, and 100µM). (**C**) Bar charts showing FC migration of T cells towards the negative untreated (serum-free DMEM (-)), positive untreated (DMEM+20% FBS (+)), vehicle untreated (Control), or ACM from astrocytes treated with sulfatides (5µM, 10µM, 20µM, 50µM, and 100µM). (**D**) Bar charts showing FC migration of NK cells to negative untreated (-), positive untreated (+), vehicle untreated, and ACM following treatment of sulfatides (5µM, 10µM, 20µM, 50µM, and 100µM). Data from the chemotaxis assays are presented as mean ± SEM (n = 6, using supernatants generated from MTT assay experiments). Statistical analysis was performed using a paired t-test; *p<0.05, **p<0.01 compared to negative control.

**Figure 3.11**

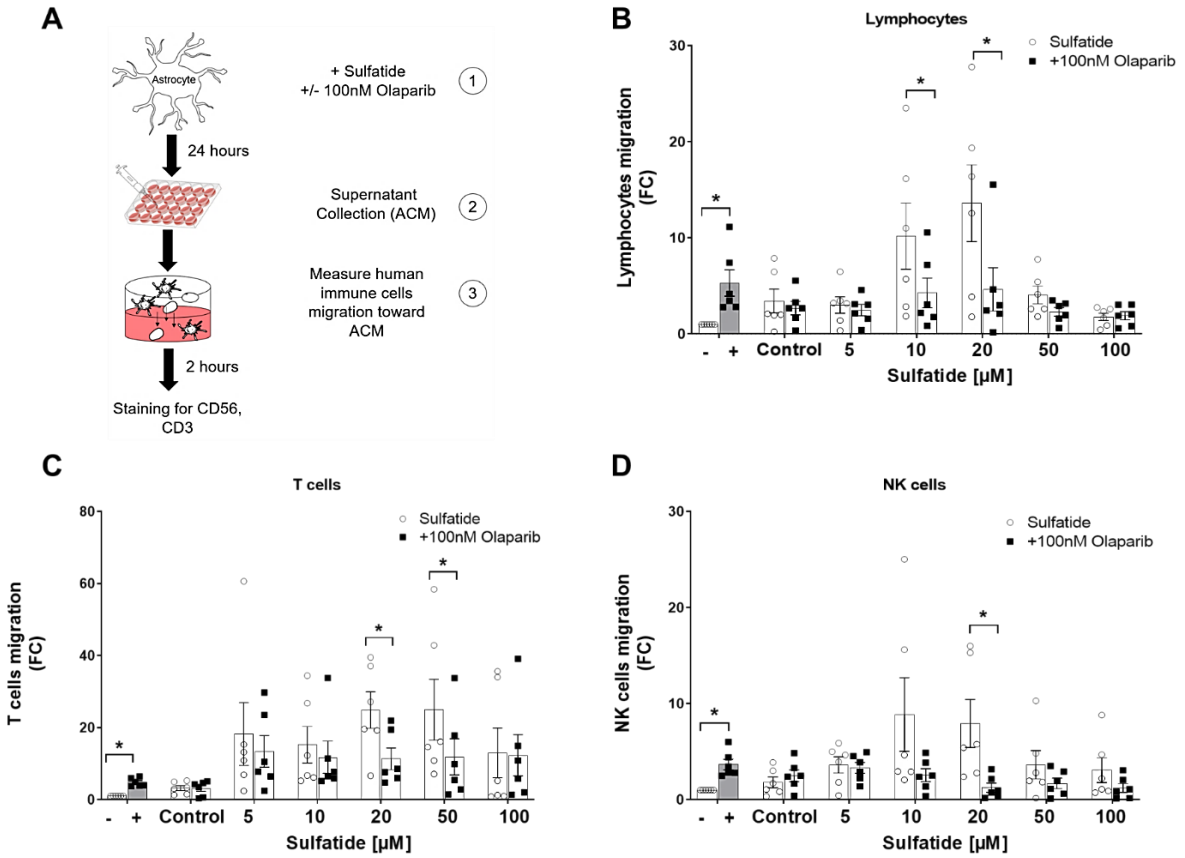


**Figure 3.11: Olaparib reduced the chemoattraction of human immune cells towards the soluble microenvironment of sulfatide-treated astrocytes.** Lymphocyte, T cell, and NK cell migration towards astrocyte-conditioned medium (ACM) from untreated and sulfatide-stimulated astrocytes were measured after 24 hours of 100nM Olaparib exposure. (**A**) Diagram of experimental timeline and treatments. (**B**) Bar charts showing the fold change migration of lymphocytes towards the negative untreated (serum-free DMEM (-)), positive untreated (DMEM+20% FBS (+)), vehicle untreated (Control), or ACM from, astrocytes treated with sulfatides (clear circle) (5µM, 10µM, 20µM, 50µM, and 100µM) with or without 100nM Olaparib (black square). (**C**) Bar charts showing fold change migration of T cells towards the negative untreated (-), positive untreated (+), vehicle untreated (Control), or ACM from astrocytes treated with sulfatides (clear circle (5µM, 10µM, 20µM, 50µM, and 100µM)) with or without 100nM Olaparib (black square). (**D**) Bar charts showing FC migration of NK cells to negative untreated (-), positive untreated (+), vehicle untreated or ACM from astrocytes treated with sulfatides (clear circle (5µM, 10µM, 20µM, 50µM, and 100µM)) with or without 100nM Olaparib (black square). Data from the chemotaxis assays are presented as mean ± SEM (n = 6, using supernatants generated from MTT assay experiments). Statistical analysis was performed using a paired t-test; *p<0.05, **p<0.01.

## 3.5 Discussion

### 3.5.1 Summary of Findings

In this current study, we demonstrated that sulfatides caused astrocyte cell death in a concentration-dependent manner, which was attenuated by treatment with Olaparib. Olaparib showed strong efficacy in rescuing sulfatide-induced astrocyte death and rescued morphology impairment caused by treatment with sulfatides. For the first time, our data show that sulfatides induced PARP-1 activation in a concentration-dependent manner, which was inhibited by Olaparib. These data also demonstrated that sulfatides increased ROS levels and mitochondrial stress in a concentration-dependent manner in human astrocytes which were dampened by treatment with Olaparib. Olaparib also mediated the dampening of ATP-induced $Ca^{2+}$ waves in astrocytes treated with sulfatides. Sulfatides increased pro-inflammatory cytokine secretion by human astrocytes, including IL-6, IL-8, IL-17, and CX3CL1, which could be suppressed by Olaparib. Lastly, the data showed that Olaparib dampened the enhanced chemo-attraction of peripheral blood-derived lymphocytes, NK cells, and T cells toward conditioned media from human astrocytes treated with sulfatides. Taken together, this research suggests that PARP-1 plays a key role in sulfatide-induced inflammation and oxidation in human astrocytes, which can be reversed by Olaparib.

### 3.5.2 Olaparib Protection from Sulfatide-Induced Astrocyte Toxicity is Likely Due to Decreased Expression of PARP-1

Previous studies have shown that sulfatide accumulation causes neuronal dysfunction and is cytotoxic to this cell type, as well as showing that these effects could be closely linked to the pathogenesis of MLD [117]. Here, we find that sulfatides induce morphological changes in

cultured human astrocytes as observed by a reduction of astrocyte size, as well as cell death as measured by MTT assay. In addition, sulfatides increase ROS levels and impair mitochondrial potential suggesting that sulfatides are a source of oxidative stress for human astrocytes. Importantly, we observed that the use of Olaparib, an FDA-approved anti-cancer therapeutic, was effective in protecting astrocytes against the cytotoxic effects of sulfatides. Olaparib targets PARP-1, a transcription factor mainly involved in the recognition and repair of DNA single-strand breaks. PARP-1 is expressed by all brain cells in the CNS, where it contributes to multiple biological processes including cell differentiation and maturation, regulation of cholinergic and glutamatergic signaling, and memory formation. PARP-1 chronic activation, which occurs in many CNS disorders, is responsible for augmented oxidative stress and cell death via apoptotic-independent pathways. Our findings showed sulfatides to cause PARP-1 overexpression and reversal by Olaparib. In sulfatide-treated astrocytes, we found that Olaparib augmented cell survival and reduced ROS production and mitochondrial damage. Overall, this set of data supports PARP-1 being a key driver of sulfatide-induced astrocyte damage and which can be effectively targeted by Olaparib to reverse sulfatide toxicity.

### 3.5.3 PARP-1 Over-Expression Impairs Calcium Release from Human Astrocytes

Under physiological conditions, calcium signaling plays a critical role in communication between astrocytes and neurons, while dysregulated cellular calcium contributes to pathophysiological conditions such as necrosis, apoptosis, autophagy deficits, and neurodegeneration [118]. Furthermore, calcium is central to many astrocytic signaling events, including mitogenic responses to growth factors, gene expression, release of signaling molecules, and responses to neurotransmitters such as ATP and glutamate [119]. The downstream pathways essential for the execution of cell death in response to PARP-1-mediated

metabolic alterations remain poorly understood, but there are some evidence that support the involvement of aberrant calcium signaling. The regulatory mechanisms controlling PARP-1 function to either promote cell survival or cell death in response to DNA damage also remain enigmatic. PARP-1 facilitates DNA repair and cell survival in response to a variety of DNA-damaging agents. PARP-1 also mediates programmed necrosis [120], as well as caspase-independent apoptotic cell death following severe levels of DNA damage [121]. Given that we found that sulfatides promoted the expression of PARP-1 and increased the levels of intracellular calcium and that these effects are dampened by Olaparib, we consider a coupling between the expression of PARP-1 and calcium signaling, which play a role in astrocyte death. We note, however, that the temporal order of these events remains to be elucidated.

### 3.5.4 Role Of PARP-1 in Neuroinflammation

In the past, PARP-1 was thought to contribute to disease pathogenesis primarily by inducing cell death [122]. However, more recently it has been recognized that PARP-1 activity may also modulate the transcription and translation of genes involved in inflammation [122,123]. In the majority of CNS disorders, inflammatory processes trigger changes in BBB function that are central to the infiltration of immune cells into CNS tissues, inflammatory responses and, ultimately, the pathogenesis of the disease [124,125]. Inflammatory processes have also been implicated in the pathogenesis of MLD while the overexpression of pro-inflammatory cytokines has been reported in the brains of MLD patients [93]. Since astrocytes are an important source of such neuromodulatory cytokine and chemokine production [126,127], the effects of sulfatides treatment on astrocyte secretion of pro-inflammatory cytokines, IL-17, IL-8, IL-6, and CX3CL1, were examined. Our data show that sulfatides increased pro-inflammatory cytokine release from sulfatide-stimulated human astrocytes while Olaparib

treatment significantly attenuated this effect. Therefore, PARP-1 inhibition may cause a general dampening of pro-inflammatory cytokine secretion in astrocytes.

In some disease models, such as multiple sclerosis, PARP-1 activity has been proposed to alter leukocyte migration by modifying the expression of adhesion molecules [128,129]. In agreement with these findings, our data show that Olaparib treatment reduced human peripheral blood immune cell migration towards the soluble microenvironment (i.e., astrocyte-conditioned media) of sulfatide-treated human astrocytes. The Olaparib-induced decreases in human lymphocyte, NK cell and T cell migration were positively correlated with the Olaparib-mediated reductions in pro-inflammatory mediators implicated in the disease pathogenesis and with an increased astrocyte survival rate. These studies go some way in translating the findings to a human setting showing that sulfatide-treated human astrocytes promote migration of immune cells, that were obtained from the peripheral blood of healthy humans.

### 3.6 Conclusion

MLD is a fatal leukodystrophy with no current curative treatment. Therefore, the need for new drugs and pharmacological approaches that can cure or improve survival and/or quality of life for these patients is urgent. Accumulation of sulfatides, propagation of pro-inflammatory cytokines, demyelination, and the widespread loss of oligodendrocytes are all hallmarks of MLD. To date, little is known about the role of astrocytes in MLD, whereas the majority of studies have mainly focused on the role of oligodendrocytes in this illness. Altered astrocytic function has gained recognition as a major contributing factor to a growing number of neurological disorders and the belief that astrocytic dysfunction significantly contributes to the development of inflammation in the CNS has gained traction in the past number of years [130,131]. In addition, the immunomodulatory functions of astrocytes are now being shown to

actively participate in the pathogenesis of several demyelinating disorders [131]. It has also been reported that astrocytic processes may closely surround demyelinating fibres and that astrocytes release a number of factors to promote myelination. This might support the idea that demyelination in MLD may not be solely attributed to oligodendrocyte dysfunction but involve a central role for astrocytes. Thus, while astrocytic reactivity in MLD may represent a secondary response to demyelination, these cells may be primary responders to sulfatides and contribute to the pathogenesis of MLD.

Here we demonstrated that sulfatide treatment alters human astrocyte cell survival, mitochondrial function, ROS levels, calcium signaling, and pro-inflammatory cytokine levels. Our data also indicate that sulfatides induce overactivation of PARP-1 in human astrocytes. Importantly, we show that sulfatide-treated human astrocytes promote migration of human peripheral blood immune cells. All these effects of sulfatides were attenuated by the PARP-1 inhibitor Olaparib. Overall, our study translates somewhat into a human cell biology setting and suggests that PARP-1 inhibition may be a therapeutic option in MLD, where marketed drugs such as Olaparib may be worthy of further investigation. Future studies should be focused on the study of the biochemical cascades involved in PARP-1-mediated sulfatide toxicity and the effect of impaired astrocytes on oligodendrocytes development and myelination.

# Chapter 4 – Olaparib attenuates demyelination and neuroinflammation in an organotypic slice culture model of Metachromatic Leukodystrophy

## 4.1 Hypothesis and Aims

Sulfatide accumulation in various nervous system cells in MLD triggers demyelination, neuroinflammation, and oxidative stress. Overactivity of PARP-1 is linked to brain disorders like Parkinson's and multiple sclerosis due to excessive PAR synthesis, leading to cell death. PARP-1 also activates NF-κB, sparking inflammation and oxidative stress. With DNA damage, oxidative stress, and inflammation in MLD, PARP-1 likely plays a key role in neurodegeneration. Targeting PARP-1 through gene deletion or drugs like Olaparib, a PARP-1 inhibitor, shows promise in reducing stress and inflammation.

**Hypothesis**

Sulfatide-induced demyelination and neuroinflammation in an *ex vivo* cerebellar organotypic slice culture model is underpinned by PARP-1 over-activation and can be attenuated by Olaparib.

**Aims**

1. Assessing the effect of sulfatides on myelin protein expression, oligodendrocyte, and neuronal survival using cerebellar organotypic slice culture.
2. Examining if the inhibition of PARP-1, with Olaparib, prevents loss of myelin protein caused by sulfatides in brain slices.
3. Analysing the effects of sulfatides and Olaparib on glial cell activation and inflammatory molecule release (IL-6, IL-17A, CCL3, TNF-α, INF-γ, and MIF).

## 4.2 Highlights

- Sulfatides induce demyelination in organotypic cerebellar slice culture in a concentration-dependent manner ($EC_{50}$~20μM at 24 hours).

- Sulfatide-induced demyelination is underpinned by PARP-1 activation, oligodendrocyte loss, pro-inflammatory cytokine expression, astrogliosis, and microgliosis.
- Sulfatide-induced effects are attenuated by Olaparib treatment ($IC_{50}$~100nM).

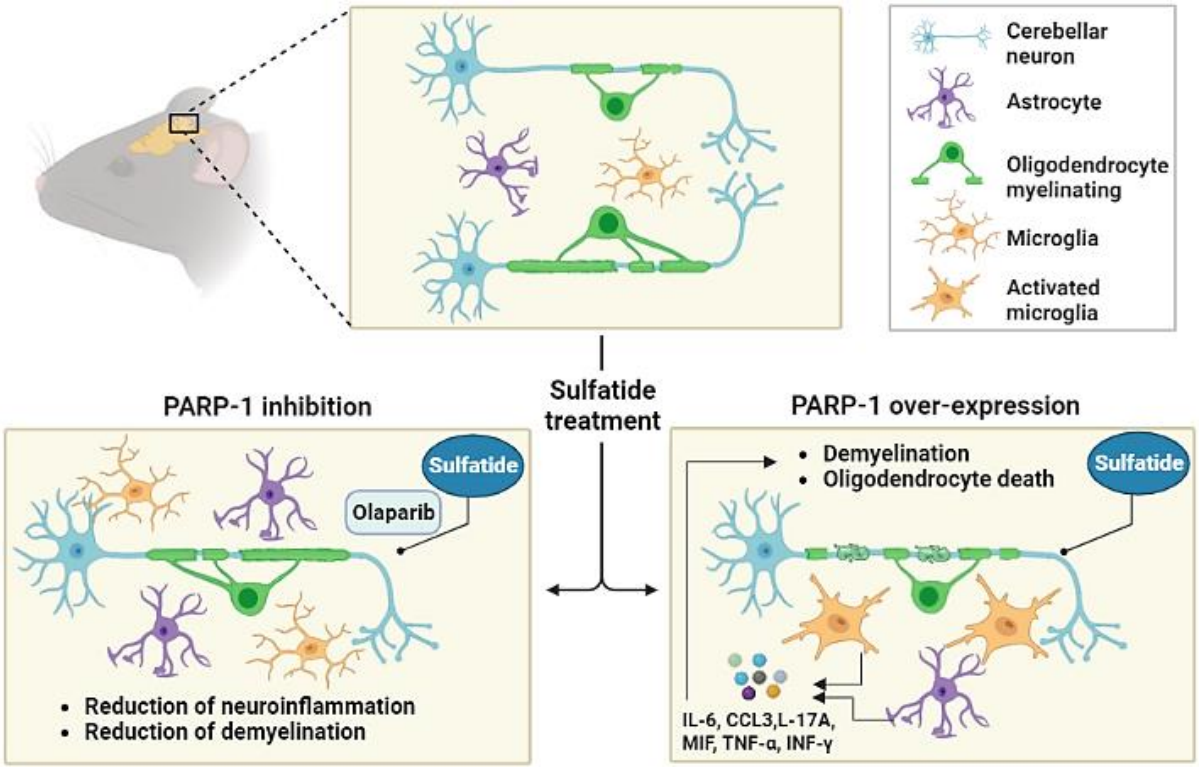


**4.1 Graphical abstract. Proposed mechanism of action of Olaparib in sulfatide-treated mouse organotypic cerebellar slice cultures.** Mouse OCS cultures treated for 24 hours with sulfatides increase PARP-1 expression. PARP-1 overexpression partly mediates oligodendrocyte loss, demyelination, and neuronal damage. Sulfatide also promotes neuroinflammation by activating glial response and increasing IL-6, IL-17A, CCL3, TNF-α, INF-γ, and MIF release from slice cultures and this is positively correlated with demyelination. Olaparib decreases cytokines and chemokine release from sulfatide-stimulated slice cultures, suggesting that PARP-1 plays a role in dampening neuroinflammation in MLD. This is confirmed by the reduction of glial reactivity. Moreover, demyelination and neuronal damage induced by sulfatides are rescued by PARP-1 inhibition. By inhibiting excessive PARP-1 expression, Olaparib may prove a useful experimental tool in myelination in MLD.

### 4.3 Introduction

MLD is a lysosomal disorder arising from recessive mutations in the ARSA gene, responsible for encoding the ASA enzyme [111]. ASA plays a crucial role in the metabolism of galactosylceramide-3-O-sulfate, commonly known as sulfatide [111]. In instances of ASA deficiency, sulfatides accumulate within lysosomal storage deposits in both the central and peripheral nervous systems. Sulfatides are a significant component of myelin, constituting approximately 4% of its composition and playing a vital role in myelin maintenance [111]. In the context of MLD, sulfatides amass in various cell types, including oligodendrocytes, Schwann cells, phagocytes, astrocytes, and neurons, resulting in demyelination [92]. This accumulation of sulfatides is closely associated with neuroinflammation and oxidative stress in MLD [96]. MLD manifests as a severe demyelinating disease characterized by the progressive loss of muscle function, cognitive abilities, and vision, with an estimated birth prevalence of around 1–2 cases per 100,000 births and an incidence of 1 in 40,000 births [90]. If left untreated, this devastating condition leads to death. Unfortunately, there is currently no curative treatment for MLD, emphasizing the urgent need for novel therapeutic approaches [90].

PARP-1 stands as the most abundant and well-studied member within the PARP nuclear enzyme superfamily, catalyzing the transfer of PAR from $NAD^+$ to a diverse array of acceptor proteins, including histones and transcription factors [3]. PARP-1 plays a pivotal role in numerous cellular processes, encompassing DNA repair, transcriptional regulation, and mitochondrial function [3]. Overactivation of PARP-1 has been implicated in the pathogenesis of various brain disorders such as Parkinson's disease, traumatic brain injury, and multiple sclerosis [36,72]. This overactivation leads to excessive PAR synthesis, depletion of $NAD^+$ and ATP, culminating in cell death [31]. Furthermore, PARP-1 is involved in disease by co-activating NF-κB, thereby promoting the transcription of genes encoding inflammatory,

oxidative stress, and cell adhesion-related proteins, including TNF-α, inducible nitric oxide synthase (iNOS), and intercellular adhesion molecule-1 (ICAM-1) [31,32]. This cascade amplifies inflammation, consequently elevating the expression of reactive oxygen species (ROS) and increasing genomic instability, as well as the susceptibility of neighboring cells to oxidative stress [114]. Given the accumulating evidence of DNA fragmentation, oxidative stress, inflammation, mitochondrial dysfunction, and BBB disruption in the pathogenesis of MLD, PARP-1 emerges as a potential central player in neurodegeneration within this context. Importantly, the deletion of the PARP-1 gene or its pharmacological inhibition could offer a neuroprotective strategy for individuals affected by MLD.

Olaparib, an FDA-approved PARP-1 inhibitor initially designed for cancer therapy, has demonstrated intriguing effectiveness in reducing oxidative stress, curbing PAR synthesis, preventing $NAD^+$ depletion, inhibiting cell death, and mitigating inflammation in various neurological diseases [36,49]. In light of these promising attributes, we have developed a novel mouse organotypic slice culture model designed to induce sulfatide-induced demyelination. This model enables us to explore the role of PARP-1 in the context of demyelination and neuroinflammation and assess the therapeutic potential of Olaparib in treating MLD.

## 4.4 Results

### 4.4.1 Sulfatide Induces Demyelination in Mouse OCS

To investigate the role of PARP-1 in MLD, we established an *ex vivo* murine organotypic slice culture (OCS) model of sulfatide-induced demyelination to simulate the disease conditions effectively. OCS specimens were exposed to increasing concentrations of sulfatides (10μM, 20μM, 50μM, and 100μM) for a duration of 24 hours [**Figure 4.2A**]. As a result, sulfatides induced a concentration-dependent demyelination, as evidenced by a reduction in MBP expression (10μM: 86.7%; 20μM: 42.3%, p=0.0009; 50μM: 34.3%, p=0.0005; and 100μM: 32.9%, p=0.0004, compared to untreated) [**Figure 4.2B and C**]. Moreover, exposure to sulfatides also led to decreased expression of NFH (10μM: 89.2%; 20μM: 84.0%; 50μM: 54.5%, p=0.0004; and 100μM: 42.6%, p=0.0007, compared to untreated) [**Figure 4.2D**]. The ratio of MBP to NFH suggested that at 20μM sulfatides, demyelination might be reversible since neuronal degeneration had not yet occurred [**Figure 4.2E**]. These findings collectively demonstrate that sulfatides induce both demyelination and neuronal toxicity in OCS cultures. Consequently, we selected a concentration of 20μM sulfatides for subsequent experiments.

Western blot analysis further confirmed that elevated sulfatide concentrations disrupt myelination, as evidenced by the overall expression levels of MBP in homogenized cerebellum tissue. OCS were exposed to increasing sulfatide concentrations (10μM, 20μM, 50μM, and 100μM) for a 24-hour period, and the protein levels of MBP in relation to the total β-actin expression were quantified [**Figure 4.2F**]. The decreases in MBP levels induced by sulfatides were found to be concentration-dependent (10μM: 71.6%; 20μM: 46.9%, p=0.006; 50μM: 43.6%, p=0.003; and 100μM: 30.5%, p=0.0003, compared to untreated) [**Figure 4.2G**].

### 4.4.2 Sulfatide-Induced Demyelination is Mediated By PARP-1 Overexpression in Mouse OCS

PARP-1 plays a pivotal role in the pathogenesis of several neurodegenerative diseases [36] and exhibits regulation during both demyelination and remyelination processes [55]. To evaluate its significance in MLD, we examined the impact of sulfatides and Olaparib on PARP-1 activation in our OCS cultures by monitoring changes in PARP-1 expression within the cell nucleus [**Figure 4.3A**].

Notably, Olaparib treatment alone led to a significant reduction in PARP-1 expression within the nuclei when compared to untreated conditions (52.4%, p=0.002) [**Figure 4.3B and C**]. On the other hand, exposure of the slice cultures to 20μM sulfatides for 24 hours induced an increase in PARP-1 expression within the nuclei of surviving cells in comparison to the untreated group (192.5%, p=0.0007) [**Figure 4.3B and C**]. Importantly, these sulfatide-induced changes in PARP-1 fluorescence were mitigated by treatment with 100nM Olaparib (Sulfatide: 192.5% vs Sulfatide + Olaparib: 121.9%, p=0.0003) [**Figure 4.3B and C**]. These findings collectively suggest that the toxicity induced by sulfatides involves, at least in part, PARP-1 overactivation, and that Olaparib holds promise in ameliorating these detrimental effects.

### 4.4.3 Olaparib Inhibits Sulfatide-Induced Demyelination in OCS

In this study, we investigated the impact of Olaparib on sulfatide-induced demyelination. OCS cultures were exposed to sulfatide (20μM) with or without Olaparib (100nM) for 24 hours [**Figure 4.4A**]. Olaparib treatment alone did not produce significant effects on myelin and neuronal conditions when compared to untreated conditions, as indicated by MBP and NFH immunostaining [**Figure 4.4B**]. However, the presence of 20μM sulfatide induced substantial

demyelination (41.21%, p=0.0005), as evidenced by the reduction in MBP staining, and this effect was significantly mitigated by Olaparib (Sulfatide: 41.21% vs Sulfatide + Olaparib: 70.19%, p=0.03) [Figure 4.3C]. While sulfatide treatment led to a modest, though not statistically significant, decrease in NFH levels [**Figure 4.4D**], the ratio of MBP to NFH indicated partial rescue of demyelination at 20μM sulfatides by Olaparib [**Figure 4.4E**]. Further assessment of the impact of 20μM sulfatide on OCS treated with or without 100nM Olaparib showed changes in MBP protein levels [**Figure 4.4F**]. Specifically, sulfatide treatment reduced MBP levels (MBP: 49.7%, p=0.02 compared to untreated), while Olaparib treatment increased MBP levels (MBP: 92.0%, p=0.05 compared to Sulfatide) **[Figure 4.4F and G**].

When examining the expression levels of MOG, similar results were observed [**Figure 4.5A**]. Treatment with 20μM sulfatide significantly reduced MOG levels (45.5%, p=0.02) compared to untreated conditions, and this reduction was attenuated by treatment with 100nM Olaparib (Sulfatide: 45.5% vs Sulfatide + Olaparib: 91.99%, p=0.01) [**Figure 4.5B**]. Notably, changes in NFH fluorescence intensity did not reach statistical significance [**Figure 4.5C and D**]. These findings strongly suggest that Olaparib has the potential to mitigate sulfatide-induced demyelination. Moreover, the total levels of MOG exhibited a similar pattern to MBP expression, indicating that PARP-1 may have a detrimental role in myelin formation, and Olaparib could serve as a rescuing agent for sulfatide-induced demyelination.

### 4.4.4 Effects of Olaparib on Oligodendrocytes in Cerebellar Slices Treated with Sulfatide

In the context of MLD, sulfatides primarily accumulate within oligodendrocytes. Therefore, we evaluated the therapeutic potential of Olaparib in OCS treated with 20μM sulfatide by analysing Olig2 staining [**Figure 4.6A**]. Notably, treatment with 100nM Olaparib alone

resulted in a significant increase in Olig2 fluorescence (72.6%, p=0.01 compared to untreated), consistent with prior studies [55] [**Figure 4.6B**]. Importantly, sulfatide exposure led to a pronounced reduction in Olig2 fluorescence (40.66%, p=0.0004 compared to untreated), and Olaparib significantly mitigated this reduction (90.5%, p=0.0007) [**Figure 4.6B**]. These findings were corroborated by Western blot analysis, which demonstrated that the decline in total Olig2 levels induced by sulfatide was significantly ameliorated by Olaparib (Olaparib: 52.8%, p=0.04; Sulfatide: 33.9%, p=0.006 compared to untreated; Sulfatide + Olaparib: 83.1%, p=0.02 compared to Sulfatide) [**Figure 4.6C**].

### 4.4.5 Olaparib Decreases Sulfatide-Induced Astrocytes Impairment in Cerebellar Slices

Astrocytes play a crucial role in supporting myelination [112], are involved in innate immune responses within the CNS, and have been implicated as instigators of neuroinflammation, a significant contributor to MLD [93]. Thus, we examined the impact of sulfatides (20µM) and Olaparib (100nM) on astrocyte activation in OCS, utilizing GFAP (mature astrocytes) and vimentin (neural progenitor cells/immature astroglia) as astrocyte markers [**Figure 4.7A and D**] [132].

In cerebellar slices, treatment with 100nM Olaparib alone resulted in a slight alteration in GFAP and vimentin fluorescence, which was not statistically significant compared to untreated (GFAP: 103.09%; vimentin: 93.4% relative to untreated) [**Figure 4.7B and E**]. However, sulfatide exposure induced a notable decrease in GFAP fluorescence (32.3%, p=0.01 compared to untreated) and induced changes in astrocyte morphology by reducing the number of branches (Untreated: 51 vs Sulfatide: 23, p=0.0003) [**Figure 4.7B and C**]. Co-treatment with Olaparib significantly mitigated sulfatide-induced astrocyte toxicity by preserving the number of

branches per astrocyte (Sulfatide: 23 vs Sulfatide + Olaparib: 38) and GFAP fluorescence intensity (32.3% vs 90.57%, p=0.03) [**Figure 4.7B and C**].

Sulfatide exposure also led to a decrease in vimentin fluorescence (61.32%, p=0.03 compared to untreated) [**Figure 4.7D and E**], which was significantly attenuated by Olaparib co-treatment (Sulfatide: 61.32% vs Sulfatide + Olaparib: 96.2%, p=0.008) [**Figure 4.7D and E**]. Furthermore, total GFAP and vimentin levels were reduced by sulfatide treatment (GFAP: 36.8%, p=0.01; Vimentin: 40.3%, p=0.03 compared to untreated) and increased by co-treatment with Olaparib (GFAP, Sulfatide: 36.8% vs Sulfatide + Olaparib: 104.4%, p=0.04; Vimentin, Sulfatide: 40.3% vs Sulfatide + Olaparib: 86.6%, p=0.01) [**Figure 4.7F and G**]. These findings collectively suggest that astrocyte number is altered in sulfatide-treated cerebellum and that Olaparib can modulate these effects.

### 4.4.6 Olaparib Attenuates Sulfatide-Induced Microglia Activation

Activation of PARP-1 has been linked to microglial activation, proliferation, and the production of pro-inflammatory molecules [59]. Furthermore, studies have shown that deleting or inhibiting PARP-1 in microglia promotes neuroprotection in injured brains [60]. Consequently, we investigated the impact of sulfatides and Olaparib on microglia. Treatment of slice cultures with 20µM sulfatides significantly increased microglial activation compared to untreated, as indicated by ionized calcium-binding adapter molecule 1 (Iba1) fluorescence (451.9%, p=0.0004 compared to untreated) [**Figure 4.8A and B**]. Importantly, Olaparib (100nM) mitigated these changes in Iba1 fluorescence induced by sulfatides (Sulfatide: 451.9% vs Sulfatide + Olaparib: 110.1%, p=0.0004) [**Figure 4.8B**]. Additionally, Olaparib reduced

sulfatide-induced microglial proliferation, as evidenced by a decrease in Iba1 cell count (Sulfatide: 32.3 vs Sulfatide + Olaparib: 18.5, p=0.0007) [**Figure 4.8C**].

Considering the well-established correlation between microglial morphology and function, where "resting" microglia have short, fine processes and are ramified, while "activated" microglia appear spherical with reduced processes [26], we examined the effects of sulfatides and Olaparib on microglial morphology. Analysis of the total surface area covered by Iba1 on the number of cells revealed a significant increase when slices were treated with 20µM sulfatides (Untreated: 2.29 vs Sulfatide: 3.38, p=0.03). Olaparib alone had no significant impact on Iba1 volume, but co-treatment with sulfatides and Olaparib significantly reduced microglial surface area compared to sulfatide treatment alone, indicating Olaparib's ability to attenuate sulfatide-induced microglial activation (Sulfatide: 3.38 vs Sulfatide + Olaparib: 1.92, p=0.0003) [**Figure 4.8D and E**].

Olaparib also mitigated the sulfatide-induced increase in total Iba1 levels, as demonstrated by western blot analysis (Sulfatide: 410.9%, p=0.006 compared to untreated; Sulfatide + Olaparib: 129.5%, p=0.003 compared to Sulfatide) [**Figure 4.8F and G**]. These findings collectively highlight elevated Iba1 expression and activation in sulfatide-treated OCS, which can be significantly reduced by Olaparib.

### 4.4.7 Increased Cytokine and Chemokine Profile in Sulfatide-Treated Cerebellar Slices

MLD patients exhibit augmented levels of pro-inflammatory cytokines and chemokines including CCL3, IL-1Ra, IL-8, and CCL4 in the cerebral spinal fluid (CSF) [93]. Since our data strongly indicate that sulfatides induce microglia activation, we next interrogated their effects on the secretion of pro-inflammatory cytokines and chemokines from OCS cultures.

Treatment of cerebellar slices with sulfatides (10μM, 20μM, 50μM, 100μM) for 24 hours resulted in increased soluble levels of IL-6, IL-17A, TNF-α, CCL3, MIF, and IFN-γ, which were significant at doses of 10μM and 20μM sulfatides, compared to untreated: IL-6 (Untreated: 8.2 pg/ml; 10μM: 182.4 pg/ml, p=0.002; 20μM: 166.5 pg/ml, p=0.01) [**Figure 4.9A**], TNF-α (Untreated: 22.3 pg/ml; 10μM: 110.4 pg/ml, p=0.0005; 20μM: 118.9 pg/ml, p=0.0003) [**Figure 4.9B**], IL-17A (Untreated: 61.5 pg/ml; 10μM: 769.4 pg/ml, p=0.0008; 20μM: 762.2 pg/ml, p=0.0009) [**Figure 4.9C**], CCL3 (Untreated: 64.7 pg/ml; 10μM: 572.2 pg/ml, p=0.004; 20μM: 629.3 pg/ml, p=0.001) [**Figure 4.9D**], MIF (Untreated: 869.2 pg/ml; 10μM: 2949.4 pg/ml, p=0.0001; 20μM: 2287.0 pg/ml, p=0.01) [**Figure 4.9E**], and IFN-γ (Untreated: 36.6 pg/ml; 10μM: 711.8 pg/ml, p=0.0004; 20μM: 426.8 pg/ml, p=0.006) [**Figure 4.9F**]. Taken together, these data demonstrate that exposure to sulfatides promotes inflammatory mediator release in OCS cultures in parallel with increased demyelination and axonal damage.

### 4.4.8 Olaparib Significantly Reduces Pro-Inflammatory Cytokine and Chemokine Release from Sulfatide-Treated Organotypic Slice Cultures

PARP-1 has a key role in chronic inflammation in the context of many inflammatory-driven pathologies [26]. Given that our data show that Olaparib attenuates sulfatide-induced microglia activation, we investigated whether Olaparib can dampen sulfatide-induced inflammatory cytokine and chemokine release. Treatment of slice cultures with 100nM Olaparib for 24 hours, in the presence of sulfatides (10μM and 20μM), significantly decreased the sulfatide-induced release of IL-6 (Untreated: 8.8 vs. Olaparib: 4.4 pg/ml; 10μM Sulfatide: 182.4 vs. 10μM Sulfatide + Olaparib: 21.6 pg/ml p=0.02; 20μM Sulfatide: 166.5 vs. 20μM Sulfatide + Olaparib: 27.7 pg/ml p=0.01) [**Figure 4.10A**], TNF-α (Untreated: 22.3 vs. Olaparib: 16.0

pg/ml; 10μM Sulfatide: 110.4 vs. 10μM Sulfatide + Olaparib: 59.1 pg/ml p=0.04; 20μM Sulfatide 118.9 vs. 20μM Sulfatide + Olaparib: 70.2 pg/ml p=0.02) [**Figure 4.10B**], IL-17A (Untreated: 61.5 vs. Olaparib: 37.2 pg/ml; 10μM Sulfatide: 769.4 vs. 10μM Sulfatide + Olaparib: 93.0 pg/ml p=0.0004; 20μM Sulfatide: 762.2 vs. 20μM Sulfatide + Olaparib: 82.2 pg/ml p=0.0007) [**Figure 4.10C**], CCL3 (Untreated: 64.7 vs. Olaparib: 87.8 pg/ml; 10μM Sulfatide: 575.2 vs. 10μM Sulfatide + Olaparib: 442.5 pg/ml; 20μM Sulfatide: 629.3 vs. 20μM Sulfatide + Olaparib: 423.2 pg/ml p=0.007) [**Figure 4.10D**], MIF (Untreated: 869.2 vs. Olaparib: 885.0 pg/ml; 10 μM Sulfatide: 2919.4 vs. 10μM Sulfatide + Olaparib: 1695.4 pg/ml p=0.002; 20μM Sulfatide 2317.0 vs. 20μM Sulfatide + Olaparib: 1259.2 pg/ml p=0.01) [**Figure 4.10E**], and IFN-γ (Untreated: 36.6 vs. Olaparib: 57.6 pg/ml; 10μM Sulfatide 711.8 vs. 10μM Sulfatide + Olaparib: 81 pg/ml p=0.0009; 20μM Sulfatide: 426.8 vs. 20μM Sulfatide + Olaparib: 49.3 pg/ml p=0.0004) [**Figure 4.10F**]. Taken together, these data show that Olaparib can attenuate sulfatide-induced secretion of pro-inflammatory cytokines and chemokines in OCS cultures. This may in part explain the protective effects of PARP inhibition on sulfatide-induced demyelination.

### 4.4.9 Positive Correlation Between Levels of Pro-Inflammatory Mediators and Demyelination

To further determine whether the elevated concentrations of cytokines and chemokines in sulfatide-treated slice cultures are associated with the severity of demyelination, a correlation analysis was conducted. Supernatants generated from organotypic slice cultures treated with 20 μM sulfatide with or without 100 nM Olaparib and stained with MBP were used to perform ELISAs. Interestingly, the overall secretion of IL-6, IL-17A, TNF-α, CCL3, MIF, and IFN-γ significantly correlated with a decrease in myelination measured by MBP staining ($\rho$=-0.3570,

p=0.0353) [**Figure 4.11**]. Treatment with Olaparib lessened this correlation by reducing both pro-inflammatory cytokine and chemokine secretion and attenuating demyelination (ρ=-0.1965, p=0.2508) [**Figure 4.11**]. These data strongly indicate that sulfatide-induced demyelination is paralleled by pro-inflammatory cytokine and chemokine release in matched samples thus implicating sulfatide-induced inflammation as a key contributor to demyelination. Furthermore, these data indicate that Olaparib holds promise to simultaneously attenuate pro-inflammatory cytokine and chemokine release and demyelination in MLD.

### 4.4.10 Olaparib Attenuates Sulfatide-Induced Levels of SMI-32

SMI-32 is a non-phosphorylated epitope of NFH and a marker of axonal damage and demyelination [133,134,135]. Here, SMI-32 was used as a biomarker to examine the effects of Olaparib on sulfatide-induced axonal damage. Murine OCSs were treated with 20μM sulfatide in the presence or absence of 100nM Olaparib for 24 hours and then fixed and stained for SMI-32. OCS treated with sulfatide displayed an increase in SMI-32 expression in the whole cerebellum (141.4% compared with untreated) [**Figure 4.12A and B**] and in the axons of cerebellar Purkinje neurons (175.8%, p=0.0003 compared with untreated) [**Figure 4.12C and D**]. Importantly, treatment with Olaparib significantly attenuated the overall increase in SMI-32 fluorescence intensity in the cerebellum (Sulfatide: 141.4% vs Sulfatide + Olaparib: 61.5%, p=0.005) [**Figure 4.12A and B**) and in the white matter tract (Sulfatide: 175.8% vs Sulfatide + Olaparib: 119.2%, p=0.02) [**Figure 4.12C and D**]. These results show for the first time that sulfatide accumulation increases SMI-32 staining within the axons of the major white matter tracts in the cerebellum, indicating axonal damage. Importantly, this axonal damage is attenuated by treatment with Olaparib.

**Figure 4.2**

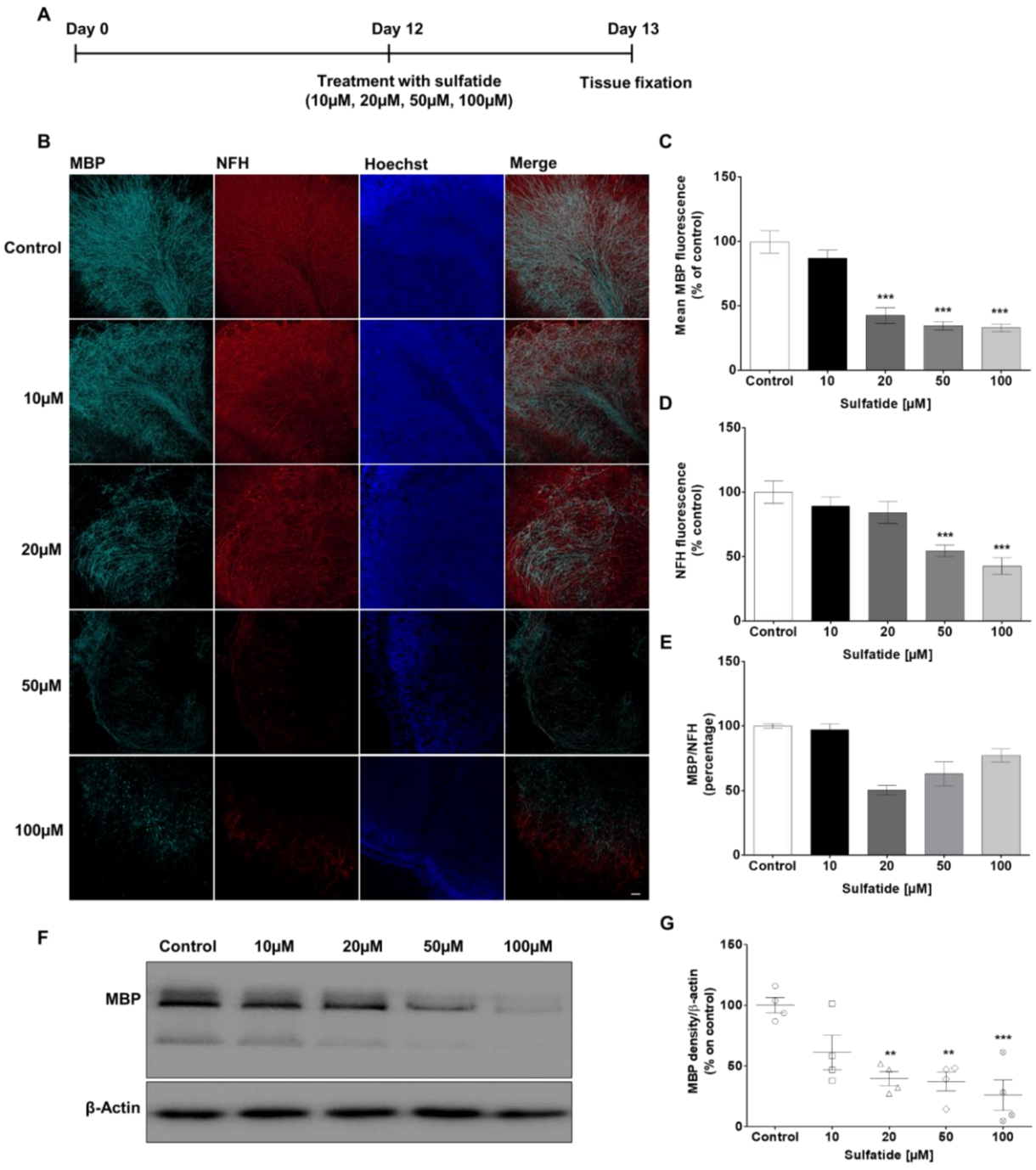
A
Day 0
Day 12
Day 13
Treatment with sulfatide
(10μM, 20μM, 50μM, 100μM)
Tissue fixation
B
MBP
NFH
Hoechst
Merge
Control
10μM
20μM
50μM
100μM
C
Mean MBP fluorescence (% of control)
Control
10
20
50
100
Sulfatide [μM]
D
NFH fluorescence (% control)
E
MBP/NFH (percentage)
F
MBP
β-Actin
G
MBP density/β-actin (% on control)

**Figure 4.2: Sulfatide induces demyelination in cerebellar slice cultures in a concentration-dependent manner.** OCS were treated with sulfatides (10μM, 20μM, 50μM, 100μM) for 24 hours. (**A**) Schematic diagram explaining the experimental protocol for pharmacological treatments of *ex vivo* brain slice cultures. Cerebellar slices were cultured for 12 days and then treated for 24 hours with sulfatides (10μM, 20μM, 50μM, 100μM) to trigger demyelination. (**B**) Representative confocal images displaying MBP (blue), NFH (red), and Hoechst (blue) immunostaining under treatment conditions indicated. Confocal images were captured at ×20 magnification. (**C**) Bar graph illustrating changes in the intensity of MBP fluorescence after the treatment with sulfatides. Quantification of confocal images shows a significant decrease in MBP fluorescence at 20μM, 50μM, and 100μM sulfatide. (**D**) Bar graph illustrating changes in the intensity of NFH fluorescence after the treatment with sulfatides. Quantification of confocal images shows a significant decrease in NFH fluorescence with 50μM and 100μM sulfatide treatment. (**E**) Bar graph illustrating the ratio of MBP on NFH. Data are expressed as a percentage of untreated and presented ± SEM compared with untreated (n = 5). Statistical significance was determined by One-way ANOVA followed by Tukey multiple comparison test, ***$p<0.001$. A number of 100 images were analysed per condition. Scale bar, 100 μm. (**F-G**) Changes in the levels of MBP were quantified using Western blotting. Myelination as measured by MBP was significantly decreased by 20μM, 50μM, and 100μM sulfatide. Data are expressed as a percentage of untreated and presented ± SEM compared with untreated (n = 4). Statistical significance was determined by One-way ANOVA followed by Newman–Keuls post-hoc test, **$p<0.01$, ***$p<0.001$.

**Figure 4.3**

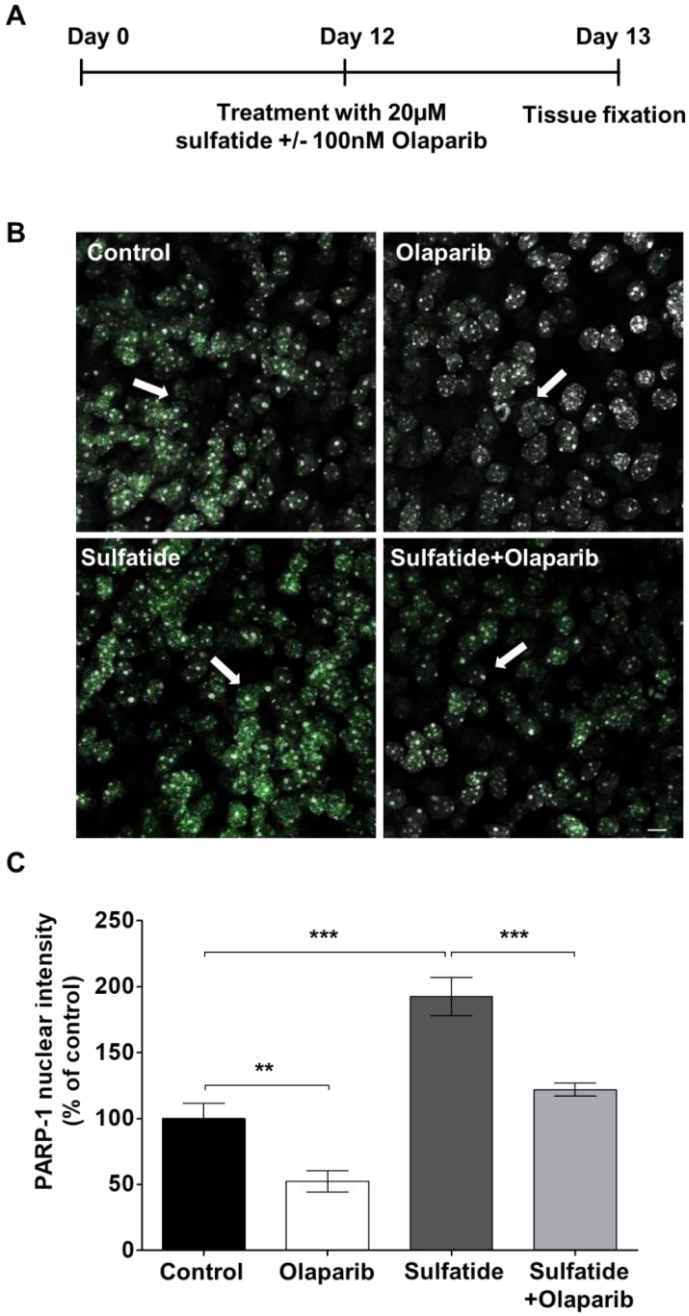


**Figure 4.3: Sulfatide-induced demyelination is mediated by PARP-1 expression in slice cultures.** (**A**) Schematic diagram explaining the experimental protocol for pharmacological treatments of *ex vivo* brain slice cultures. Cerebellar slices were cultured for 12 days and then treated for 24 hours with 20µM sulfatides in the presence or absence of 100nM Olaparib. **(B)** Representative confocal images displaying PARP-1 (green) and Hoechst (grey) immunostaining under treatment conditions indicated. Confocal images were captured at ×40 magnification. (**C**) Bar graphs showing that treatment with Olaparib (100nM) reduced sulfatide-induced PARP-1 expression in nuclei (20µM). A number of 100 images were analysed per condition. Semi-quantitative analysis of PARP-1-associated fluorescence in the nuclei. Data are expressed as a percentage of untreated and presented ± SEM compared with untreated (n = 5). Statistical significance was determined by One-way ANOVA followed by Tukey multiple comparison test, **p<0.01, ***p<0.001. A number of 100 images were analysed per condition. Scale bar, 100 µm

**Figure 4.4**

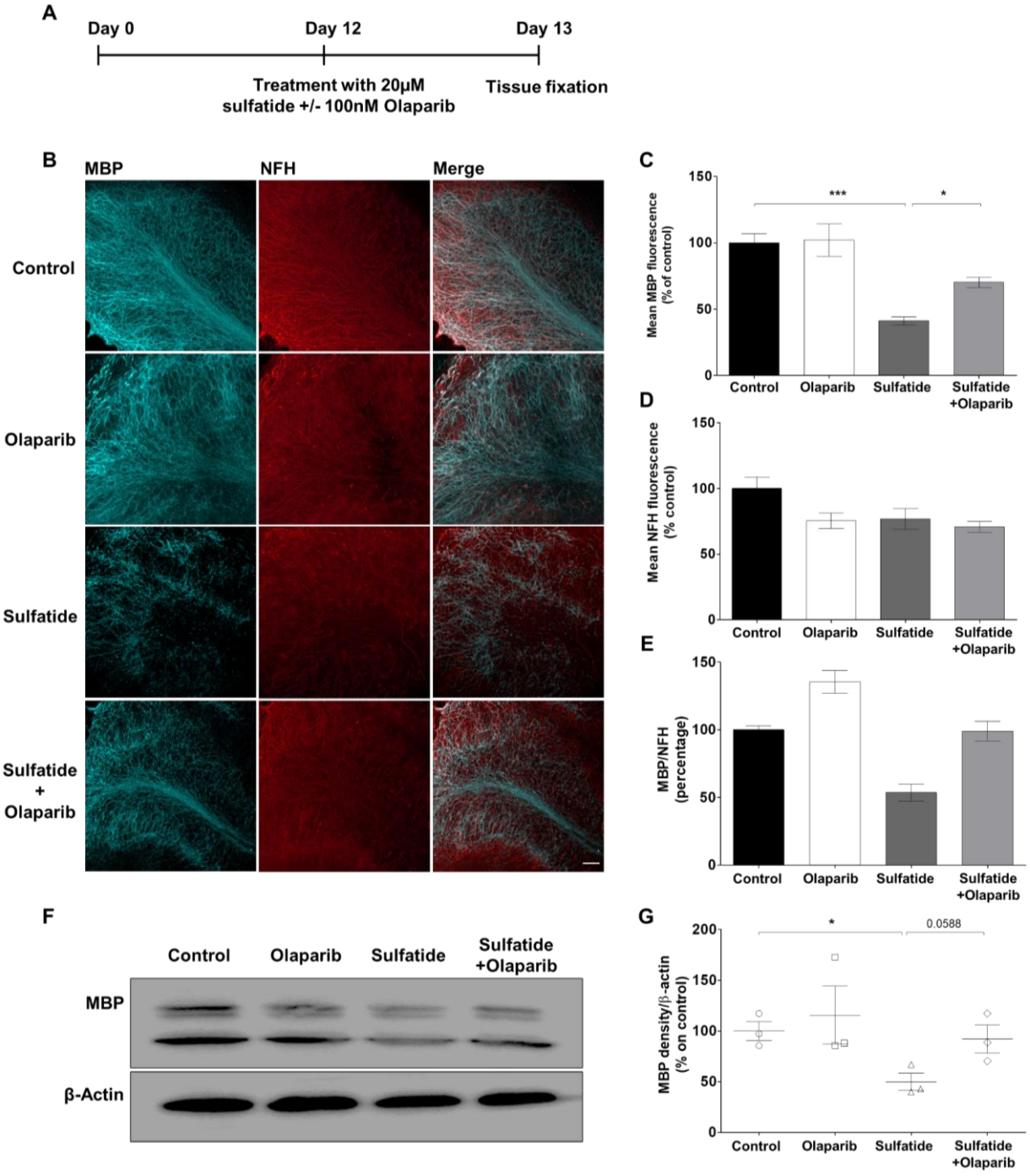
A
Day 0
Day 12
Day 13
Treatment with 20μM sulfatide +/- 100nM Olaparib
Tissue fixation
B
MBP
NFH
Merge
Control
Olaparib
Sulfatide
Sulfatide + Olaparib
C
Mean MBP fluorescence (% of control)
***
*
Control
Olaparib
Sulfatide
Sulfatide +Olaparib
D
Mean NFH fluorescence (% control)
E
MBP/NFH (percentage)
F
MBP
β-Actin
G
MBP density/β-actin (% on control)
0.0588

**Figure 4.4: Olaparib attenuates sulfatide-induced demyelination in cerebellar slice cultures.** (**A**) OCS slices were treated with sulfatides (20µM) in the presence or absence of Olaparib (100nM) for 24 hours. (**B**) Representative confocal images displaying MBP (blue) and NFH (red) immunostaining under treatment conditions indicated. Confocal images were captured at ×20 magnification. (**C**) Bar graph illustrating changes in the intensity of MBP fluorescence after the treatment with sulfatides (20µM) and with or without Olaparib (100nM). Quantification of confocal images shows a significant decrease in MBP fluorescence, which is attenuated by Olaparib. (**D**) Bar graph illustrating changes in the intensity of NFH fluorescence after the treatment with sulfatides (20µM) and with or without Olaparib (100nM). Quantification of confocal images shows no significant decrease in NFH fluorescence with sulfatide and Olaparib treatment. (**E**) Bar graph illustrating the ratio of MBP on NFH. Data are expressed as a percentage of untreated and presented ± SEM compared with untreated (n = 5). Statistical significance was determined by One-way ANOVA followed by Tukey multiple comparison test, *p<0.05, ***p<0.001. A number of 100 images were analysed per condition. Scale bar, 100 µm. (**F-G**) Total MBP protein levels were measured by western blotting. Bar graph illustrating reduced MBP protein levels following sulfatide exposure, which is attenuated by Olaparib. Data are expressed as a percentage of untreated and presented ± SEM compared with untreated (n = 3). Statistical significance was determined by One-way ANOVA followed by Newman–Keuls post-hoc test, *p<0.05.

**Figure 4.5**

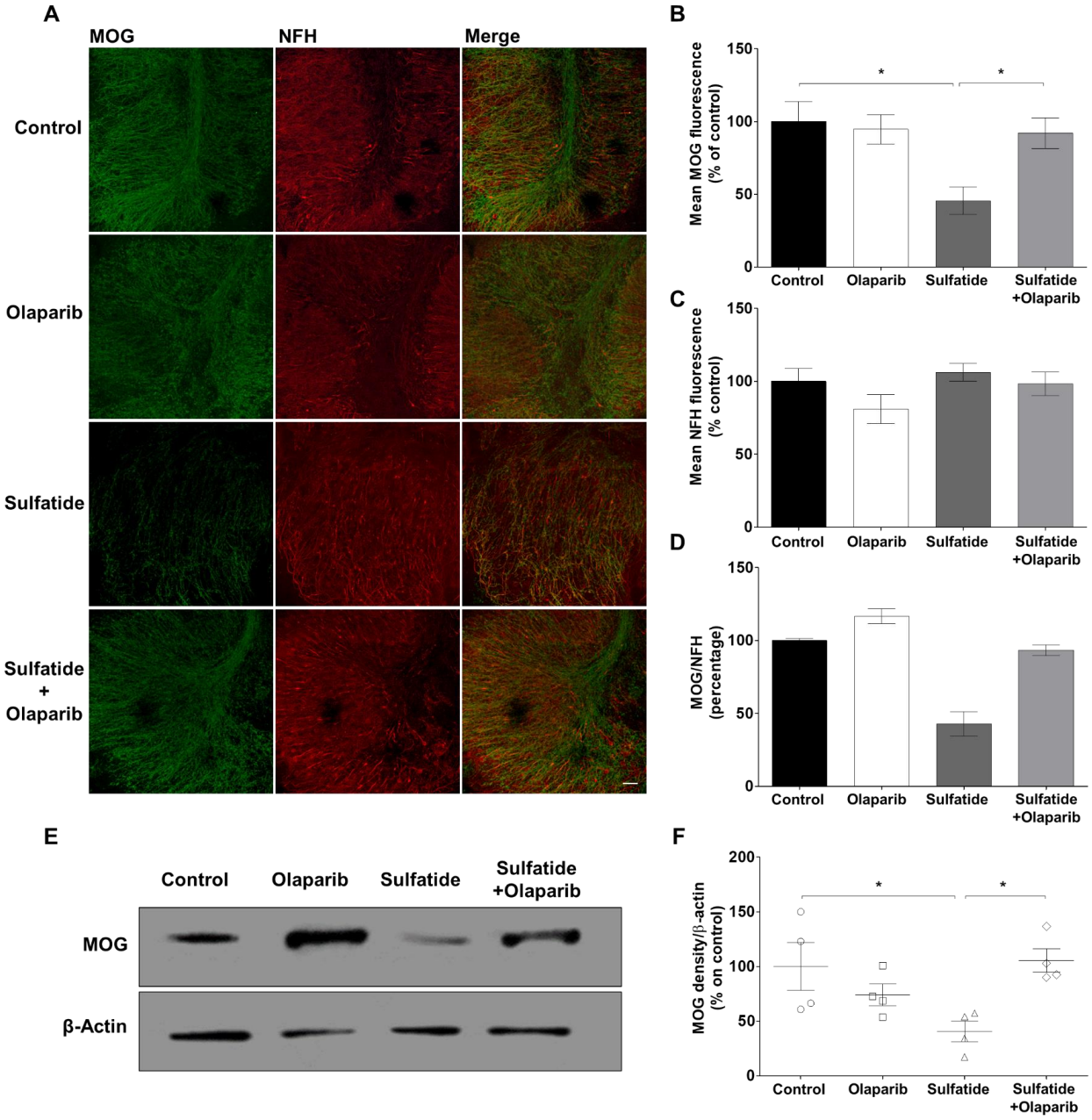
A
MOG
NFH
Merge
Control
Olaparib
Sulfatide
Sulfatide + Olaparib
B
Mean MOG fluorescence (% of control)
150
100
50
0
*
*
Control
Olaparib
Sulfatide
Sulfatide +Olaparib
C
Mean NFH fluorescence (% control)
150
100
50
0
Control
Olaparib
Sulfatide
Sulfatide +Olaparib
D
MOG/NFH (percentage)
150
100
50
0
Control
Olaparib
Sulfatide
Sulfatide +Olaparib
E
Control
Olaparib
Sulfatide
Sulfatide +Olaparib
MOG
β-Actin
F
MOG density/β-actin (% on control)
200
150
100
50
0
*
*
Control
Olaparib
Sulfatide
Sulfatide +Olaparib

**Figure 4.5: Sulfatide-mediated reduction of MOG expression is attenuated by Olaparib.** OCS were treated with sulfatides (20µM) in the presence or absence of Olaparib (100nM) for 24 hours. (**A**) Representative confocal images displaying MOG (green) and NFH (red) immunostaining under treatment conditions indicated. Confocal images were captured at ×20 magnification. (**B**) Bar graph illustrating changes in the intensity of MOG fluorescence after the treatment with sulfatides (20µM) and with or without Olaparib (100nM). Quantification of confocal images shows a significant decrease in MOG fluorescence, which is attenuated by Olaparib. (**C**) Bar graph illustrating changes in the intensity of NFH fluorescence after the treatment with sulfatides (20µM) and with or without Olaparib (100nM). Quantification of confocal images shows no significant decrease in NFH fluorescence with sulfatide and Olaparib treatment. (**D**) Bar graph illustrating the ratio of MOG on NFH. Data are expressed as a percentage of untreated and presented ± SEM compared with untreated (n = 5). Statistical significance was determined by One-way ANOVA followed by Tukey multiple comparison test, *$p<0.05$. A number of 100 images were analysed per condition. Scale bar, 100 µm. (**E-F**) Total MOG protein levels were measured by western blotting. Bar graph illustrating reduced MOG protein levels following sulfatide exposure, which is attenuated by Olaparib. Data are expressed as a percentage of untreated and presented ± SEM compared with untreated (n = 4). Statistical significance was determined by One-way ANOVA followed by Newman–Keuls post-hoc test, *$p<0.05$.

**Figure 4.6**

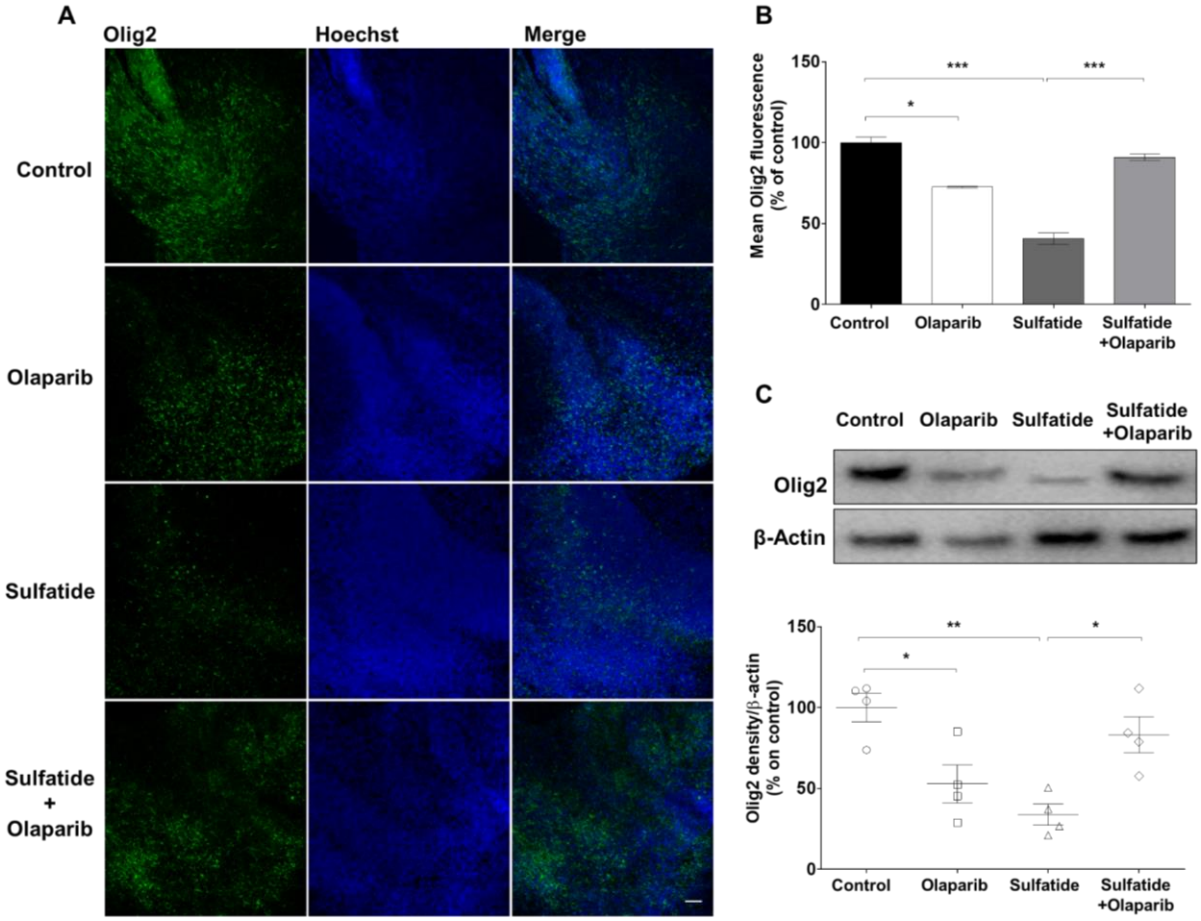


**Figure 4.6: Olaparib reduces sulfatide-induced oligodendrocyte death.** OCS were treated with sulfatides (20µM) in the presence or absence of Olaparib (100nM) for 24 hours. (**A**) Representative confocal images displaying Olig2 staining under treatment conditions indicated. Confocal images were captured at ×20 magnification. (**B**) Bar graph illustrating that treatment with Olaparib alone and sulfatides significantly decreased Olig2 fluorescence compared with untreated. Importantly, sulfatide-induced decrease is attenuated with Olaparib. Data are expressed as a percentage of untreated and presented ± SEM compared with untreated (n = 5). Statistical significance was determined by One-way ANOVA followed by Tukey multiple comparison test, *p<0.05, ***p<0.001. A number of 100 images were analysed per condition. Scale bar, 100 µm. (**C**) Changes in Olig2 expression levels were assessed by Western blotting. Sulfatide-induced Olig2 decrease was attenuated by Olaparib. Data are expressed as a percentage of untreated and presented ± SEM compared with untreated (n = 4). Statistical significance was determined by One-way ANOVA followed by Newman–Keuls post-hoc test, *p0.05, **p< 0.01.

**Figure 4.7**

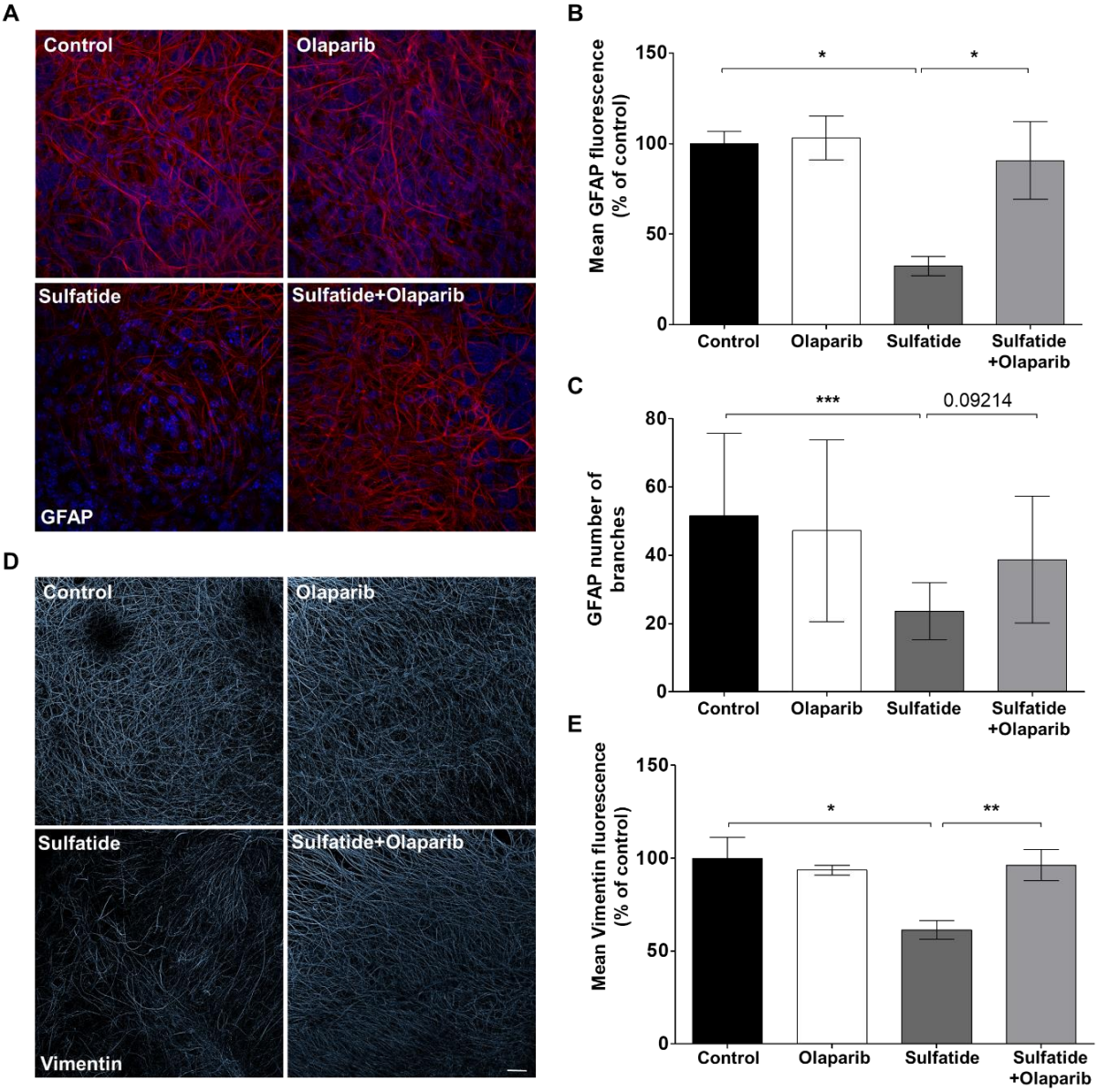
A
Control
Olaparib
Sulfatide
Sulfatide+Olaparib
GFAP
B
Mean GFAP fluorescence (% of control)
150
100
50
0
*
*
Control
Olaparib
Sulfatide
Sulfatide +Olaparib
C
GFAP number of branches
80
60
40
20
0
***
0.09214
Control
Olaparib
Sulfatide
Sulfatide +Olaparib
D
Control
Olaparib
Sulfatide
Sulfatide+Olaparib
Vimentin
E
Mean Vimentin fluorescence (% of control)
150
100
50
0
*
**
Control
Olaparib
Sulfatide
Sulfatide +Olaparib

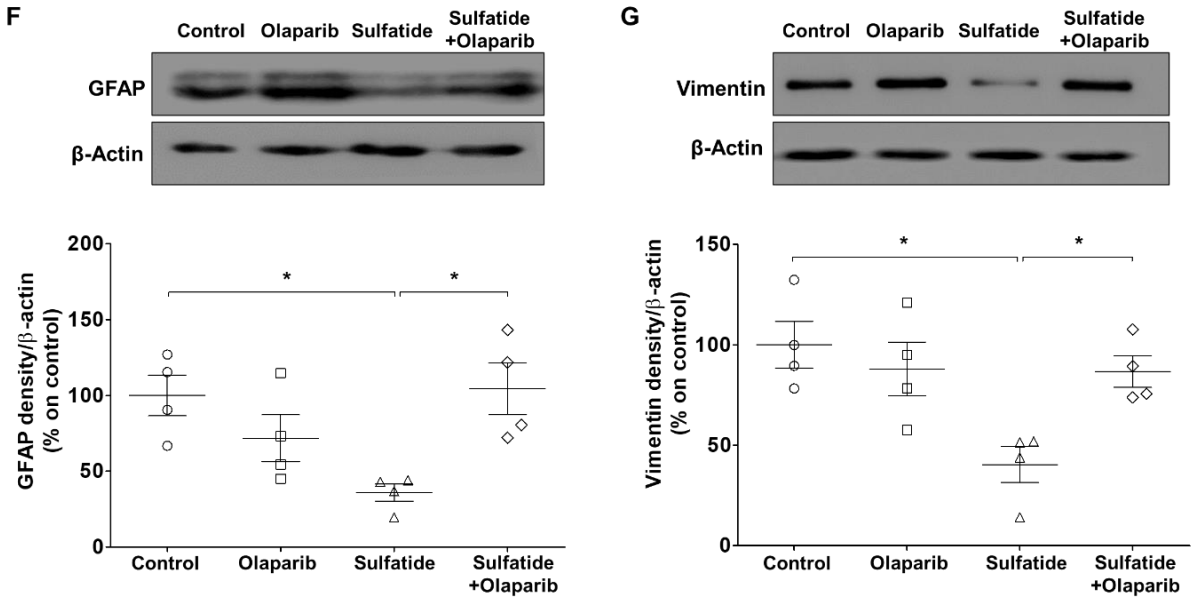


**Figure 4.7: Sulfatide-induced reductions in GFAP and vimentin in cerebellar slices is attenuated by Olaparib.** (**A**) Representative confocal images displaying GFAP staining under treatment conditions indicated. Confocal images were captured at ×40 magnification showing that treatment with 100nM Olaparib attenuates astrocyte fluorescence intensity and number of branches decrease induced by 20µM sulfatides. (**B**) Bar graph illustrating that treatment with sulfatides (20µM) for 24 hours significantly decreased GFAP fluorescence compared with untreated. Importantly, this decrease is attenuated with Olaparib (100nM). (**C**) Bar graph illustrating that Olaparib attenuates sulfatide-induced decrease in GFAP number of branches compared with untreated. (**D**) Representative confocal images displaying vimentin staining under treatment conditions indicated. Confocal images were captured at ×20 magnification showing that treatment with 100nM Olaparib attenuates vimentin fluorescence intensity decrease induced by 20µM sulfatides. (**E**) Bar graph illustrating that treatment with sulfatides (20µM) for 24 hours significantly decreased vimentin fluorescence compared with untreated. Importantly, this decrease is attenuated with Olaparib (100nM). Data are expressed as a percentage of untreated and presented ± SEM compared with untreated (n = 5). Statistical significance was determined by One-way ANOVA followed by Tukey multiple comparison test, *p<0.05, ***p<0.001, **p<0.01. A number of 100 images were analysed per condition. Scale bar, 100 µm. (**F**-**G**) Changes in GFAP and vimentin expression levels were assessed by Western blotting. Bar graph illustrating reduced GFAP (**F**) and vimentin (**G**) protein levels following sulfatide exposure, which is attenuated by Olaparib. Data are expressed as a percentage of untreated and presented ± SEM compared with untreated (n = 4). Statistical significance was determined by One-way ANOVA followed by Newman–Keuls post-hoc test, *p<0.05.

## Figure 4.8

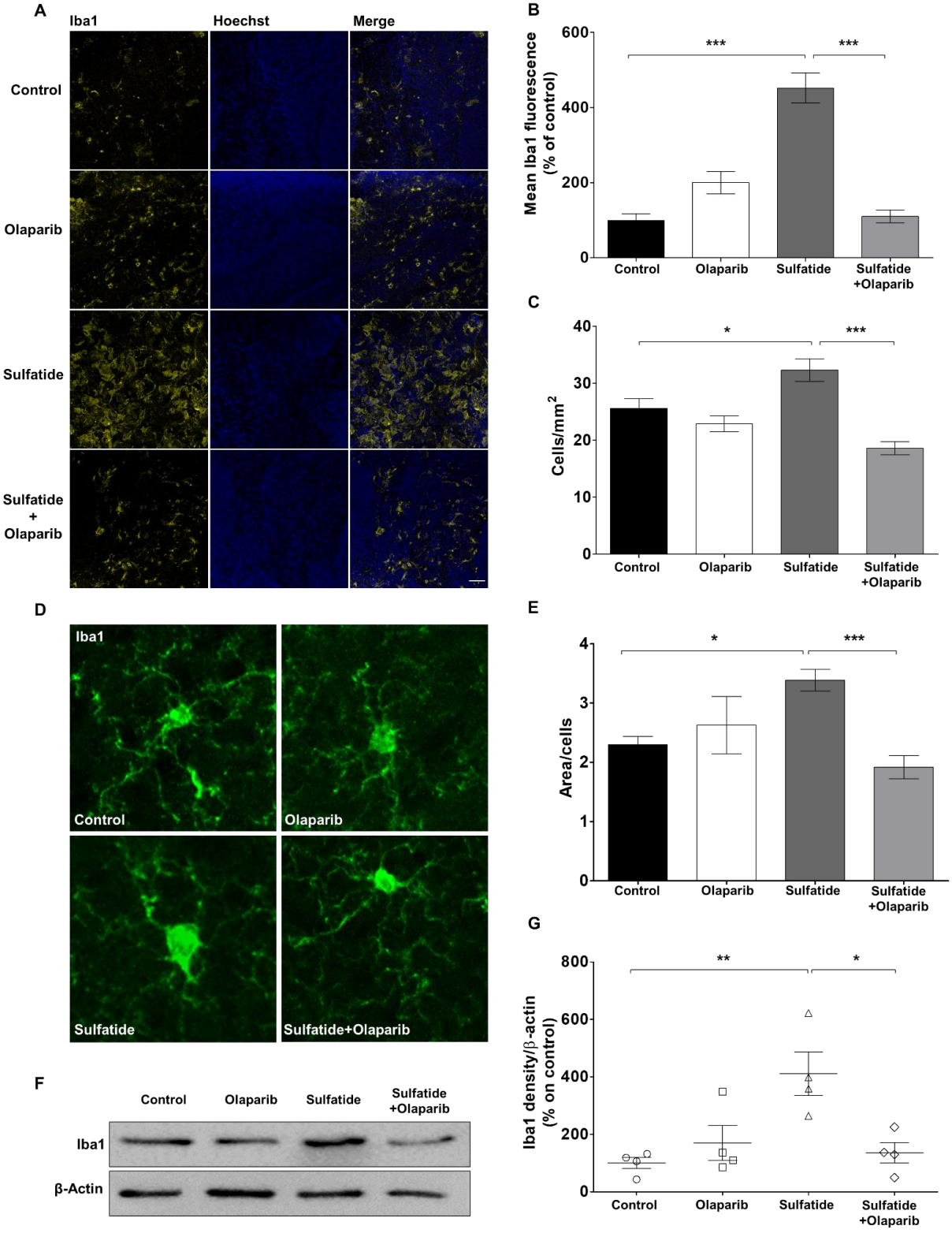
A
Iba1
Hoechst
Merge
Control
Olaparib
Sulfatide
Sulfatide + Olaparib
B
Mean Iba1 fluorescence (% of control)
600
400
200
0
***
***
Control
Olaparib
Sulfatide
Sulfatide +Olaparib
C
Cells/mm2
40
30
20
10
0
*
***
Control
Olaparib
Sulfatide
Sulfatide +Olaparib
D
Iba1
Control
Olaparib
Sulfatide
Sulfatide+Olaparib
E
Area/cells
4
3
2
1
0
*
***
Control
Olaparib
Sulfatide
Sulfatide +Olaparib
F
Control
Olaparib
Sulfatide
Sulfatide +Olaparib
Iba1
β-Actin
G
Iba1 density/β-actin (% on control)
800
600
400
200
0
**
*
Control
Olaparib
Sulfatide
Sulfatide +Olaparib

**Figure 4.8: Olaparib attenuates sulfatide-induced microglia reactivity.** OCS were treated with sulfatides (20μM) in the presence or absence of Olaparib (100nM) for 24 hours. (**A**) Representative confocal images displaying Iba1 (yellow) and Hoechst (blue) immunostaining under treatment conditions indicated. Confocal images were captured at ×20 magnification (**B**) Bar graph illustrating changes in the intensity of Iba1 fluorescence after the treatment with sulfatides (20μM) and with or without Olaparib (100nM) for 24 hours. Data are expressed as a percentage of untreated (**C**) Iba1 positive cell counting shows the sulfatides increase microglia proliferation and Olaparib reduces it. (**D**) Representative confocal images displaying Iba1 immunostaining under treatment conditions indicated. Confocal images were captured at ×40 magnification. (**E**) Quantification of cell surface on number of cells showed a significant increase in Iba1 surface in sulfatide-treated slices compared with untreated, which is attenuated by Olaparib. Data are expressed as a percentage of untreated and presented ± SEM compared with untreated (n = 5). Statistical significance was determined by One-way ANOVA followed by Tukey multiple comparison test, *p<0.05, ***p<0.001. A number of 100 images were analysed per condition. Scale bar, 100 μm. (**F-G**) Changes in Iba1 expression levels were assessed by Western blotting. Bar graph illustrating increased Iba1 protein levels following sulfatide exposure, which is attenuated by Olaparib. Data are expressed as a percentage of untreated and presented ± SEM compared with untreated (n = 4). Statistical significance was determined by One-way ANOVA followed by Newman–Keuls post-hoc test, *p<0.05, **p<0.01.

**Figure 4.9**

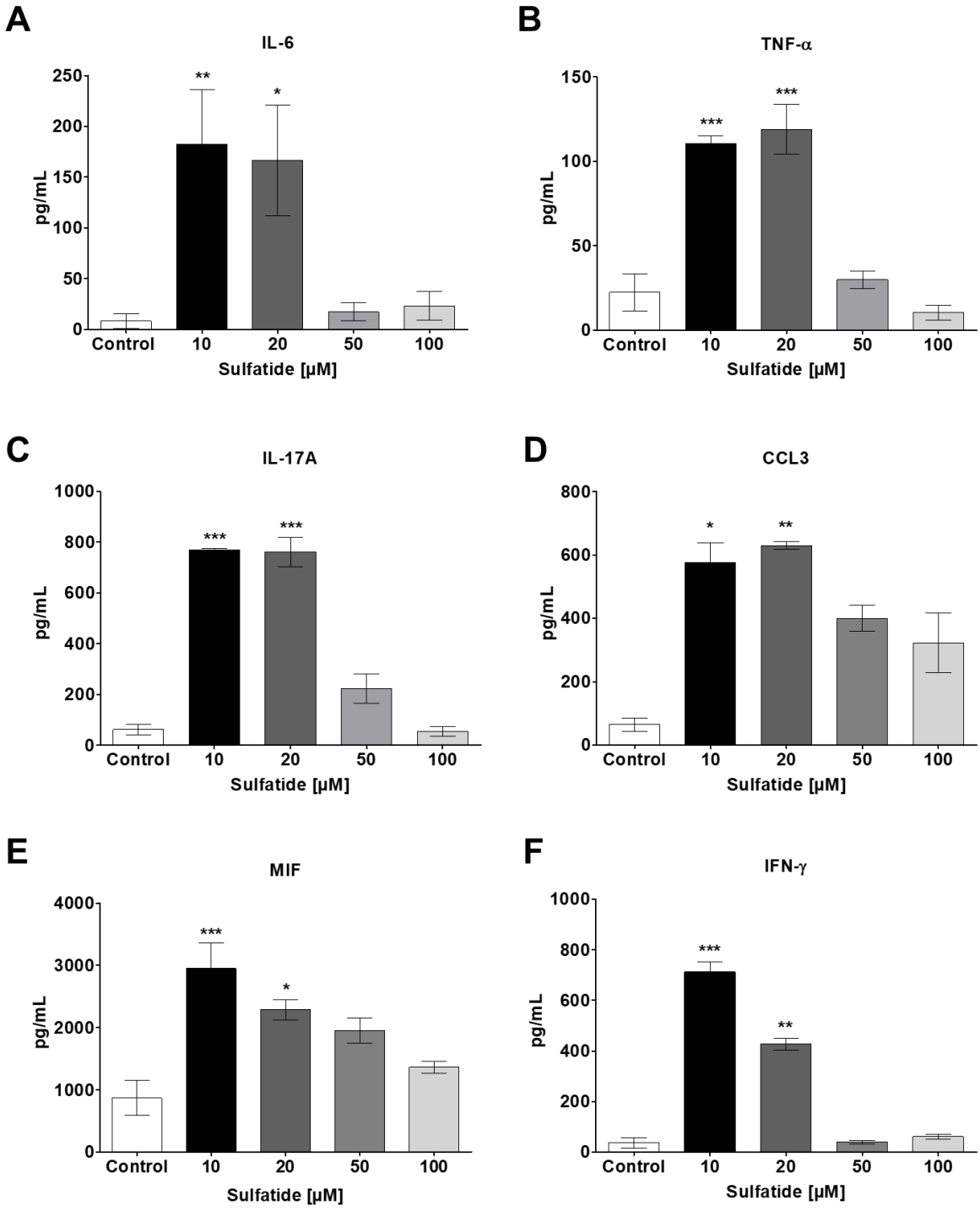


**Figure 4.9: Sulfatides increase cytokine and chemokine release from slice cultures.** Cytokine and chemokine release from untreated and sulfatide-stimulated slice cultures were measured after 24 hours. Sulfatides (10µM, 20µM, 50µM, and 100µM) showed a significant increase in (**A**) IL-6, (**B**) TNF-α, (**C**) IL-17A, (**D**) CCL3, (**E**) MIF, and (**F**) IFN-γ release into the slice culture medium, as measured by ELISA. Data from the ELISA assays are presented as mean ± SEM. IL-6, TNF-α, IL-17A, CCL3, MIF, and IFN-γ ELISA's were repeated n = 5. Statistical analysis was performed using One-way ANOVA followed by Tukey's post hoc test; *p<0.05, **p<0.01, ***p<0.001.

**Figure 4.10**

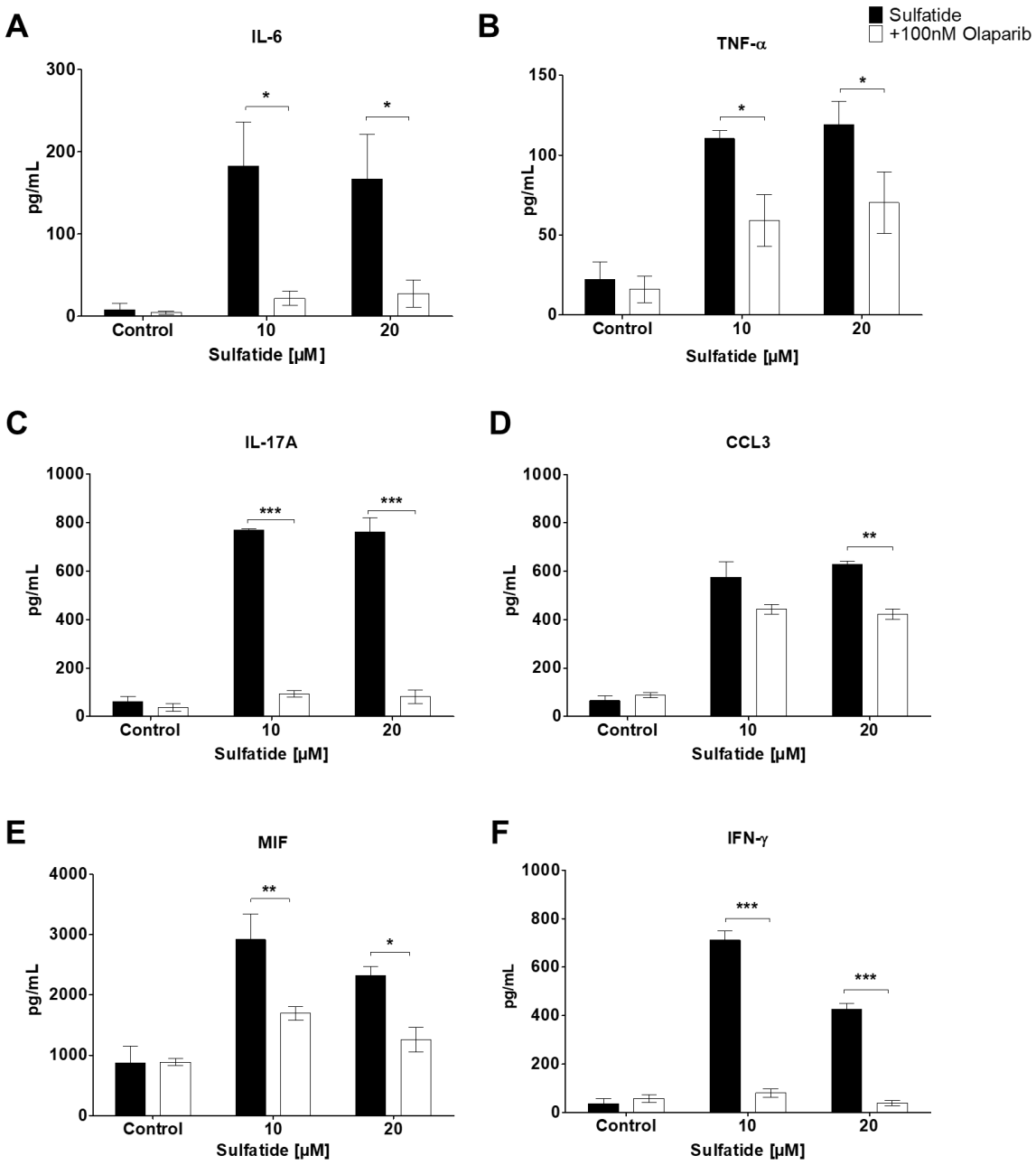


**Figure 4.10: PARP-1 modulates cytokine and chemokine release from sulfatide-treated organotypic slice cultures.** Cytokine and chemokine release from untreated and sulfatide-stimulated (10µM, 20µM) slice cultures (clear bar) were measured after 24 hours of Olaparib exposure (black bar). Olaparib (100nM) showed a significant decrease in (**A**) IL-6, (**B**) TNF-α, (**C**) IL-17A, and (**D**) CCL3, (**E**) MIF, and (**F**) IFN-γ release into the slice culture medium, as measured by ELISA. (**A**) Olaparib causes a significant reduction in IL-6 secretion from slice cultures when compared to the sulfatides group, (**B**) Olaparib also caused a significant decrease in TNF-α secretion from sulfatide-stimulated slice cultures. (**C**) Olaparib reduces IL-17A secretion, (**D**) CCL3, (**E**) MIF from sulfatide-stimulated slice cultures and (**F**) IFN-γ from sulfatide-stimulated slice cultures. Data from the ELISA assays are presented as mean ± SEM. IL-6, TNF-α, IL-17A, CCL3, MIF, and IFN-γ ELISA's were repeated n = 5. Statistical analysis was performed using a Two-way ANOVA followed by Tukey's post hoc test; *p<0.05, **p<0.01, ***p<0.001.

**Figure 4.11**

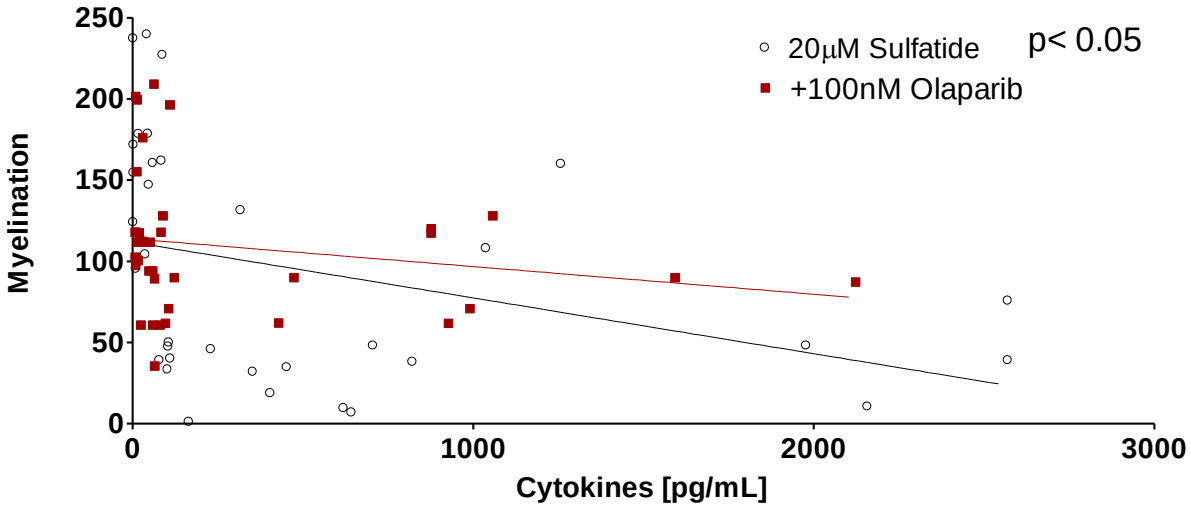


**Figure 4.11: Correlation between pro-inflammatory cytokine and chemokine release and demyelination in organotypic slice cultures.** Supernatants generated from the organotypic slice cultures treated with 20μM sulfatide with or without 10 nM Olaparib and stained with MBP were used to perform ELISAs. The levels of the IL-6, IL-17A, TNF-α, CCL3, MIF, and IFN-γ were significantly positively correlated with demyelination induced by 20μM sulfatide. Statistical analysis was performed using Correlation; *p<0.05, n = 5.

**Figure 4.12**

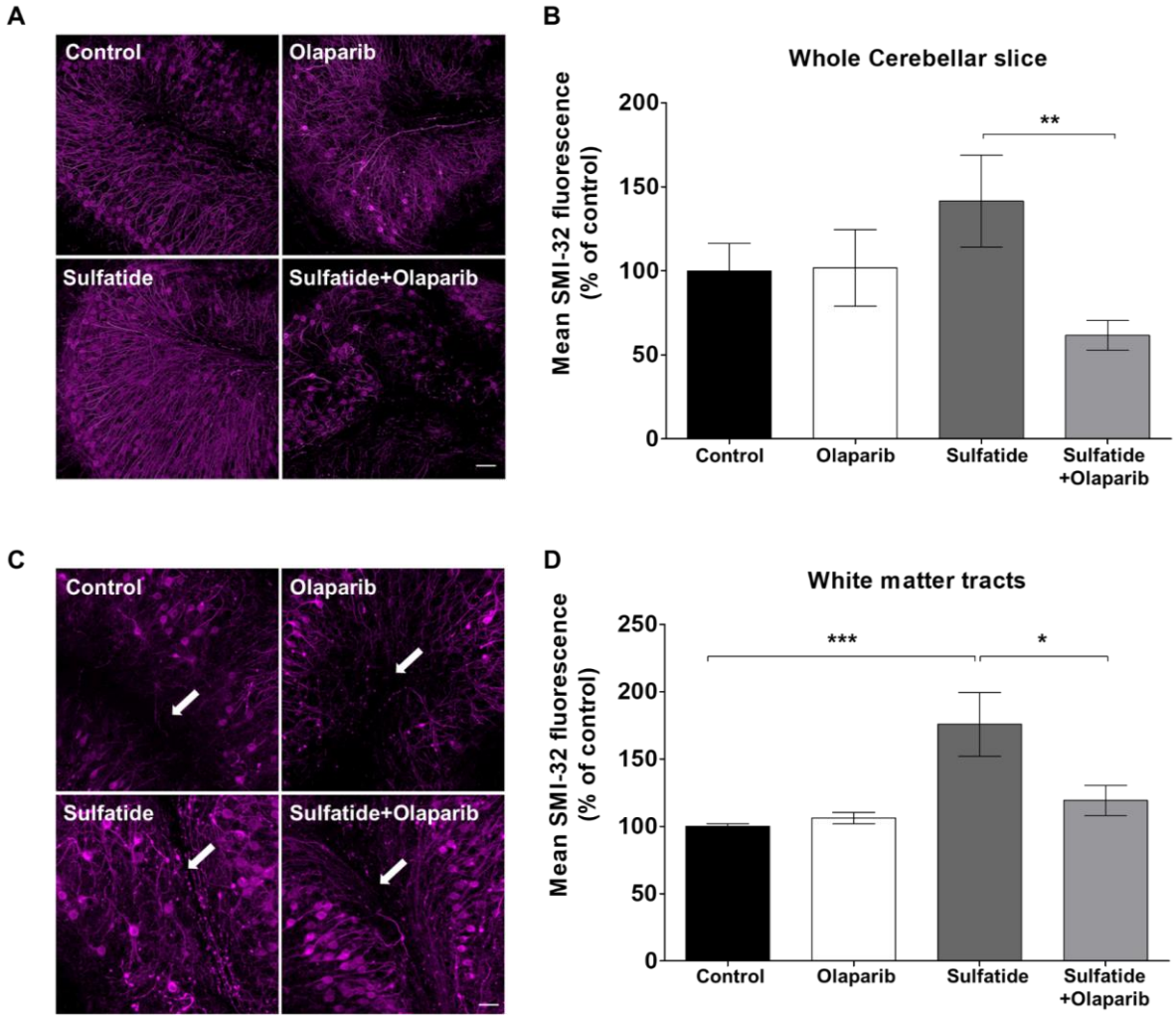


**Figure 4.12: Olaparib attenuates sulfatide-induced axonal damage.** OCS were treated with sulfatides (20µM) in the presence or absence of Olaparib (100nM) for 24 hours. (**A**) Representative confocal images displaying SMI-32 immunostaining in whole cerebellar slice under treatment conditions indicated. Confocal images were captured at ×20 magnification. (**B**) Relative fluorescent intensity of SMI-32 staining in the whole cerebellar slice shows a protective effect of Olaparib on sulfatide-induced increase in SMI-32 fluorescence. (**C**) Representative confocal images displaying SMI-32 immunostaining in white matter tract under treatment conditions indicated. Confocal images were captured at ×20 magnification. (**D**) Relative fluorescent intensity of SMI-32 staining in major white matter tract regions shows a protective effect of Olaparib on sulfatide-induced increase in SMI-32 fluorescence. Data are expressed as a percentage of untreated and presented ± SEM compared with untreated (n = 5). Statistical significance was determined by One-way ANOVA followed by Tukey multiple comparison test, *p<0.05, **p<0.01, ***p<0.001. A number of 100 images were analysed per condition. Scale bar, 100 µm.

## 4.5 Discussion

### 4.5.1 Summary of Findings

In this current study, we examined the effect of sulfatide on markers of myelination in an intact mouse organotypic cerebellar slice culture model. We report for the first time that direct application of sulfatides induces demyelination of organotypic cerebellar slices in a concentration-dependent manner. Moreover, sulfatide-treated organotypic slice cultures appear to impair oligodendrocyte viability and axonal morphology. Olaparib showed strong efficacy in rescuing sulfatide-induced demyelination and rescued axonal degeneration caused by treatment with sulfatides. For the first time, our data show that sulfatides induced PARP-1 activation in mouse organotypic slice cultures, which was significantly attenuated by Olaparib. Sulfatides increased the secretion of pro-inflammatory cytokines and chemokines IL-6, IL-17A, TNF-α, CCL3, MIF, and IFN-γ by slice cultures, which could be suppressed by Olaparib. Lastly, the data showed that Olaparib dampened the augmented microglial proliferation/activation and astrocyte impairment in slice cultures treated with sulfatides. Taken together, this research suggests that PARP-1 plays a key role in sulfatide-induced inflammation and demyelination in mouse organotypic slice culture, which can be reversed by Olaparib.

### 4.5.2 Role of Sulfatide in Demyelination

Chronic demyelination and almost complete loss of oligodendrocytes are two of the major pathological features of MLD [90]. The hypothesis that supraphysiological levels of sulfatides kill oligodendrocytes and result in widespread demyelination is now widely accepted [110]. Sulfatide levels in CSF and the sural nerve have been correlated to the severity of neuropathy

in patients with MLD [110], and in a recent publication, increased levels of CSF sulfatide correlated with worse motor function in MLD [136]. The mechanisms by which sulfatides induce demyelination in MLD remain unclear at present. Increasing evidence suggest that the widespread demyelination and loss of oligodendrocytes observed in MLD could be due to sulfatide-induced chronic inflammation underpinned by excessive cytokine and chemokine release [93,96].

Here, we examined the effect of sulfatide on markers of myelination in an intact cell culture model such as organotypic slice cultures. We report that the direct application of sulfatides induces demyelination of organotypic slice cultures in a concentration-dependent manner. These data corroborate the idea that sulfatides may directly induce demyelination in the brains of MLD patients. In addition, sulfatide-treated organotypic slice cultures show a significant oligodendrocyte death, rescued by Olaparib. Interestingly, slice cultures treated with Olaparib alone show oligodendrocyte loss suggesting that PARP-1's enzymatic activity is necessary for oligodendrocyte development in physiological conditions.

Lastly, we demonstrated that PARP-1 inhibition reduces sulfatide-induced axonal damage in mouse slice cultures. This is in agreement with data from pre-clinical models of MLD showing that elevated sulfatide levels in neurons are accompanied by a significant axonal degeneration.

### 4.5.3 Role of Sulfatide in Neuroinflammation

Sulfatides represent an important, relatively unexplored component of immune regulation in the CNS [137]. MLD patients exhibit augmented levels of pro-inflammatory cytokines and chemokines including CCL2, IL-1Ra, IL-8, and CCL4 in the CSF, and sulfatides are known to influence a variety of immune cells, such as neutrophils, dendritic cells, B cells, and microglia

in the CNS [137,138,139]. Data presented here demonstrate that sulfatide-treated organotypic slice cultures exhibit an enhanced inflammatory profile characterized by augmented microglial proliferation/activation, astrocyte impairment, and elevated levels of pro-inflammatory cytokines and chemokines such as IL-6, IL-17A, TNF-α, CCL3, MIF, and IFN-γ. Activation of pro-inflammatory pathways in the brain, including IL-6 pathway, TNF-α, IL-17A, and MIF comprises a potential point of convergence between chronic neuroinflammation and neurodegeneration in many brain diseases such as AD and MS, so it is rational to hypothesize that the elevation of these cytokines contributes to demyelination in MLD [140,141,142]. Moreover, the elevated levels of CCL3, IFN-γ, and IL-6 observed here is in line with elevated levels observed in the preclinical stages of MLD [96]. Nowadays it is generally accepted that these cytokines promote pathology by activating glial cells and by recruiting peripheral immune cells such as granulocytes and T cells [96,143]. CCL3, IFN-γ, and TNF-α are T helper 1 cytokines and they play a pathogenic role in other demyelinating diseases namely MS in which they drive the recruitment and activation of immune cells and elicit toxic or proapoptotic effects on oligodendrocytes [143]. The production of IL-17A has been demonstrated as pivotal for autoimmune demyelination and it appears to be almost exclusively T helper 17 cytokine induced by elevated levels of IL-6 [144]. Our findings together with data in the literature, strengthen the idea that neuroinflammation could be a major driver of MLD, therefore enhanced levels of myelination and less axonal degeneration could be achieved via modulation of specific soluble immune mediators, or cellular players such as microglia, and astrocytes.

### 4.5.4 Identifying the Role Of PARP-1 and the Therapeutic Utility of Olaparib In MLD

PARP-1 is expressed by all brain cells in the central nervous system (CNS) and is involved in the synthesis of PAR, cell differentiation and maturation, regulation of cholinergic and

glutamatergic signaling, and memory formation [114]. Previous studies have reported that PARP-1 chronic activation, which occurs in many demyelinating disorders, causes neuronal death, axonal degeneration, and impairment of essential myelin proteins (e.g., MOG, MBP, myelin-associated glycoprotein (MAG)) [55]. Furthermore, PAR, the marker of PARP-1 activation, accumulates in astrocytes as well as oligodendrocytes, microglia, and neurons, surrounding demyelinated plaques [59]. Our data show that sulfatide-treated slice cultures express higher levels of PARP-1, suggesting that PARP-1 may contribute to demyelination and neuroinflammation in MLD.

Given that PARP-1 inhibition with selective inhibitors lessens neurodegeneration and demyelination in several animal disease models (e.g., Parkinson's disease, AD, and MS) and improves symptoms, via a reduction in the expression of inflammatory cytokines, we investigated the effects of Olaparib, a PARP inhibitor, on our sulfatide-treated slice culture model.

Olaparib proved to reduce PARP-1 expression and prevent sulfatide-induced demyelination. It is not yet known if Olaparib exerts a direct beneficial effect on oligodendrocytes or an indirect protective mechanism of action on myelinated axons. Indeed, both scenarios are possible. Importantly, the inflammatory response associated with demyelination was deeply reduced by Olaparib as shown by the rescue in astrocyte loss, the decrease in proliferation and activation of microglial Iba1, as well as pro-inflammatory molecules levels. Taken together, these reports suggest that drugs inhibiting PARP-1 activity protect from neuroinflammatory responses in MLD via immunomodulation and direct neuroprotection and provide strong evidence for the utility of PARP-1 inhibitors in MLD. Further insights into the function of PARP-1 in brain homeostasis and dysregulation in pathological states may assist in the development of PARP-1 inhibitors for MLD.

## 4.6 Conclusion

Here we demonstrated that sulfatide treatment induces demyelination, PARP-1 expression, axonal damage, astrocyte impairment, and elevates pro-inflammatory cytokine and chemokine levels in murine organotypic slice culture. Our data also indicate that sulfatides increase microglial proliferation and promote ameboid morphology. Importantly, all the deleterious effects of sulfatides were attenuated by the PARP-1 inhibitor Olaparib. Overall, our study data suggest that PARP-1 inhibition may be a therapeutic option in MLD, where marketed drugs such as Olaparib may be worthy of further investigation. Future studies will focus on the assessment of the delivery and the effects of Olaparib on symptoms and demyelination in MLD mice.

# Chapter 5 – Elucidating whether the therapeutic utility of Olaparib can be extended to psychosine-induced astrocyte toxicity and neuroinflammation

## 5.1 Hypothesis and Aims

Globoid cell leukodystrophy, also known as Krabbe disease (KD) is a rare infantile neurodegenerative disorder. The disease is caused by a deficiency in the lysosomal enzyme galactocerebrosidase (GALC), which leads to the accumulation of a toxic metabolite called galactosylsphingosine (psychosine) in the brain at micromolar levels. While PARP inhibitors have demonstrated effectiveness in preclinical models of various neurodegenerative and inflammatory conditions, their potential for treating KD has not been explored.

**Hypothesis**

The potential therapeutic utility of PARP-1 inhibitor, Olaparib to rescue astrocyte toxicity, neuroinflammation and demyelination can be extended to a model of Krabbe Disease, which is underpinned by psychosine-induced pathology.

**Aims**

1. Investigate the utility of PARP-1 inhibitor Olaparib to reverse psychosine-induced toxicity in human astrocytes.
2. Examine the influence of PARP-1 on astrocyte survival, mitochondrial stress, and cytokine release.
3. Elucidate the effects of Olaparib on calcium signaling in human astrocytes.
4. Assess the effect of psychosine on myelin protein expression, oligodendrocyte, and neuronal survival using cerebellar organotypic slice culture.
5. Examine if the inhibition of PARP-1, with Olaparib, prevents psychosine-induced myelin protein loss in brain slices.
6. Analyse the effects of psychosine and Olaparib on glial cell activation and immune cell recruitment.

## 5.2 Highlights

- Psychosine-induced toxicity ($EC_{50}$~10µM and 20µM) is underpinned by PARP-1 activation, neuroinflammation, and immune cell recruitment and abundance *in vitro* and *ex vivo*.
- Olaparib treatment ($IC_{50}$~100nM) ameliorates disruptions caused by psychosine, including ROS production, $Ca^{2+}$ signaling, axonal degeneration, demyelination, and oligodendrocyte loss.

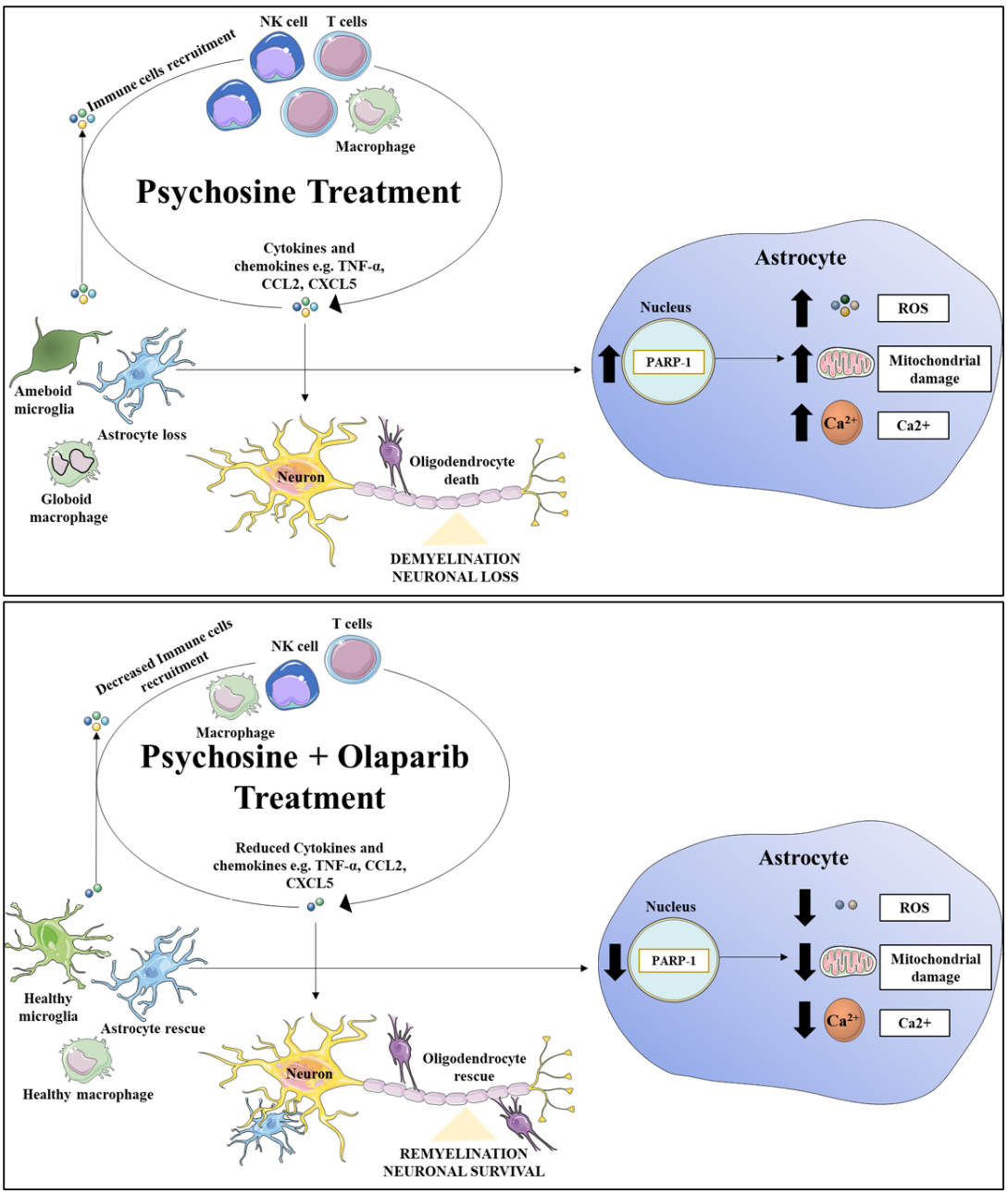


**5.1 Graphical abstract. Proposed mechanism of action of Olaparib in psychosine-treated astrocytes and mouse organotypic cerebellar slice cultures.** Human astrocytes treated for 24 hours with psychosine increase PARP-1 expression and die. PARP-1 overexpression is modulated by $Ca^{2+}$ release from the endoplasmic reticulum, thus enhancing intracellular $Ca^{2+}$ concentration. PARP-1 inhibition with Olaparib reduces $Ca^{2+}$ influx and cell death. Olaparib also decreases mitochondrial stress and ROS production induced by sulfatides. Mouse OCS cultures treated for 24 hours with psychosine increased PARP-1 expression. PARP-1 overexpression partly mediates oligodendrocyte loss, demyelination, and neuronal damage. Psychosine also promotes neuroinflammation by increasing CCL3, TNF-α, and CXCL5 release from slice cultures and inducing immune cell migration such as macrophages, NK cells, and T cells towards psychosine-treated slice cultures. Olaparib decreases cytokines and chemokine release from psychosine-stimulated slice cultures and immune cell migration, suggesting that PARP-1 plays a role in dampening neuroinflammation in KD. This is confirmed by the reduction of glial morphology impairment. Moreover, demyelination and neuronal damage induced by psychosine are rescued by PARP-1 inhibition. By inhibiting excessive PARP-1 expression, Olaparib may prove a useful experimental tool in myelination in KD.

## 5.3 Introduction

KD is a rare and severe neurodegenerative condition that mainly affects infants [145]. This genetic disorder, inherited in an autosomal recessive manner, is characterized by a deficiency in the lysosomal enzyme GALC, leading to the accumulation of a harmful metabolite called psychosine in the brain [146]. The progressive neurodegeneration seen in KD results in severe neurological symptoms, including developmental regression, loss of motor skills, muscle weakness, and impairments in vision and hearing [145]. Unfortunately, effective treatments for KD are currently limited.

In recent years, there has been a growing interest in unravelling the molecular mechanisms responsible for neurodegeneration in KD and identifying potential targets for therapy. One intriguing candidate is PARP-1, a nuclear enzyme involved in DNA repair and cell death pathways. PARP-1 has been implicated in various neurodegenerative disorders such as Alzheimer's, Parkinson's, and Huntington's disease, but its role in KD and associated neurodegeneration has not been extensively explored.

PARP-1 becomes activated in response to DNA damage, initiating the production of PARylation and promoting DNA repair processes [3]. However, excessive activation of PARP-1 can deplete cellular $NAD^+$ and ATP levels, leading to energy depletion and cell death [11]. Furthermore, PARP-1 activation has been linked to the release of pro-inflammatory molecules, fostering neuroinflammation, which can worsen neuronal damage [114].

Emerging evidence suggests that PARP-1 may have a significant role in the development of leukodystrophies. We have observed heightened PARP-1 activation in brain tissues of mice treated with sulfatide, a toxin that accumulates in a related disorder called MLD [147]. This increased PARP-1 activity may contribute to the neurodegenerative processes observed in KD through several mechanisms. Firstly, the build-up of psychosine, a characteristic feature of KD,

can induce DNA damage, triggering PARP-1 activation. Secondly, excessive PARP-1 activation may result in energy depletion and exacerbate cell death in affected brain regions. Lastly, PARP-1 activation may set off a chain reaction involving neuroinflammation and immune cell activation, further driving neurodegeneration.

Given the potential involvement of PARP-1 in the pathogenesis of KD, targeting this enzyme could offer a promising therapeutic avenue. PARP-1 inhibitors, originally designed for cancer treatment, have shown effectiveness in preclinical models of various neurodegenerative disorders [76,83]. These inhibitors have demonstrated the ability to mitigate DNA damage, reduce neuroinflammation, and protect against neuronal cell death [73,79]. Nevertheless, the therapeutic potential of PARP-1 inhibition in the context of KD remains largely unexplored.

This study aims to investigate the potential role of PARP-1 in the neurodegenerative processes associated with KD. We will assess PARP-1 activation in both *in vivo* and *ex vivo* models of KD and evaluate the impact of PARP-1 inhibition on neurotoxicity related to the disease. Furthermore, we will delve into the underlying mechanisms through which PARP-1 influences neurodegeneration in KD, with a focus on neuroinflammation and immune cell activation. These findings will contribute to our understanding of the pathophysiology of KD and may offer valuable insights into the development of novel therapeutic approaches targeting PARP-1 to alleviate neurodegeneration in this devastating disorder.

## 5.4 Results

### 5.4.1 The Administration of Olaparib Significantly Ameliorates the Toxic Effects of Psychosine in Human Astrocytes

Previous studies from our group and others have established the cytotoxic effects of psychosine on astrocytes [134,135]. In this study, we provide evidence that Olaparib can attenuate psychosine-induced cell toxicity and limit psychosine-induced morphological changes in human astrocytes. Cultured human astrocytes were subjected to treatment with psychosine (10µM, 20µM) and Olaparib (100nM) at specified time points [**Figure 5.2A**]. After 24 hours of psychosine treatment, astrocyte cell survival was significantly reduced (10µM Psychosine: 79.0%, p=0.04; 20 µM Psychosine: 42.4%, p=0.005, compared with control). However, Olaparib exhibited a protective effect against psychosine-induced astrocyte cell death (10µM Psychosine: 79.0% vs 10µM Psychosine + Olaparib: 115.2%, p=0.002; 20 µM Psychosine: 42.4% vs 10µM Psychosine + Olaparib: 107.8%, p=0.004) [**Figure 5.2B and C**].

To further investigate the cytotoxic effects of psychosine and the potential rescue by Olaparib, we examined their impact on astrocyte morphology. Specifically, we evaluated the protective role of Olaparib by performing immunocytochemistry using vimentin, a type III intermediate filament marker involved in cytoskeleton formation in astrocytes. Treatment of human astrocytes with psychosine (10µM, 20µM) for 24 hours led to a reduction in vimentin expression, particularly in the cell processes (Control: 2.9; 10µM Psychosine: 1.7; 20µM Psychosine: 0.8, p=0.007, compared with control) [**Figure 5.2D and E**]. Importantly, Olaparib treatment attenuated the psychosine-induced changes in vimentin localization (Control: 2.9 vs Olaparib: 3.0; 10 µM Psychosine: 1.7 vs 10µM Psychosine + Olaparib: 2.6, p=0.04; 20µM Psychosine: 0.8 vs 20µM Psychosine + Olaparib: 2.7, p=0.04) [**Figure 5.2E**]. Analysis of vimentin fluorescence intensity further confirmed that psychosine changes astrocyte

morphology at 10µM (14.6%, p=0.02, compared with control) and 20µM (8.03%, p=0.01, compared with control), while Olaparib attenuated these effects (10µM Psychosine: 14.6% vs 10µM Psychosine + Olaparib: 69.8%, p=0.03; 20µM Psychosine: 8.03% vs 20µM Psychosine + Olaparib: 68.1%, p=0.008) [**Figure 5.2F**].

In summary, our findings provide strong evidence that Olaparib can attenuate psychosine-induced toxicity in human astrocytes.

### 5.4.2 Inhibition of Psychosine-Induced PARP-1 Activation in Human Astrocytes by Olaparib

Activation of PARP-1 plays a pivotal role in the activation and survival of astrocytes [66]. Consequently, we explored the influence of psychosine and Olaparib on PARP-1 activation within human astrocytes by examining changes in PARP-1 expression within the cell nucleus. When human astrocytes were treated with psychosine (10µM or 20µM) for 24 hours, we observed an increase in PARP-1 expression within the nuclei of astrocytes (10µM Psychosine: 159.2%, p=0.01; 20µM Psychosine: 178.0%, p=0.01, compared to the control) [**Figure 5.3A and B**]. Significantly, co-treatment with Olaparib (100nM) led to a reduction in the fluorescence intensity of PARP-1, indicating a decrease in its activation (10µM Psychosine: 159.2% vs 10µM Psychosine + Olaparib: 96.3%, p=0.02; 20µM Psychosine: 178.0% vs 20µM Psychosine + Olaparib: 115.1%, p=0.01) [**Figure 5.3B**]. These findings provide evidence that psychosine-induced toxicity involves excessive activation of PARP-1 and demonstrate that Olaparib can mitigate these effects.

### 5.4.3 Suppression of Psychosine-Induced Calcium Influx in Astrocytes by Olaparib

Previous studies have indicated that psychosine triggers calcium influx, mitochondrial depolarization, and increased levels of reactive oxygen species (ROS), leading to astrocyte apoptosis [134,135]. PARP-1 activation has been observed to facilitate the expression of calcium-permeable channels during brain injury and to be involved in mitochondrial membrane potential ($\Delta\Psi m$) loss [16,47,116]. To investigate the role of calcium in psychosine-induced astrocyte death, human astrocytes were treated with psychosine (10μM, 20μM) in the presence or absence of Olaparib (100nM) for 24 hours. Cal-520AM calcium dye was used to load cells, and time-lapse $Ca^{2+}$ imaging was performed. After a 20-second baseline recording, cells were exposed to 300μM ATP, and imaging was conducted for an additional 3 minutes to assess ATP-induced $Ca^{2+}$ oscillations. The activation and oscillations of $Ca^{2+}$ were analysed. Astrocytes treated with psychosine exhibited larger ATP-induced $Ca^{2+}$ peaks compared to astrocytes co-treated with psychosine and Olaparib [**Figure 5.4A-D**]. Measurement of the area under the curve (AUC) for the 10μM and 20μM psychosine groups revealed a higher AUC $Ca^{2+}$ response to ATP perfusion compared to the control group (Control: 1167; 10μM Psychosine: 1895, p=0.01; 20μM Psychosine: 2950, p=0.0003). Olaparib significantly reduced the psychosine-induced AUC $Ca^{2+}$ response to ATP perfusion (10μM Psychosine: 1895 vs 10μM Psychosine + Olaparib: 1286, p=0.03; 20μM Psychosine: 2950 vs 20μM Psychosine + Olaparib: 1753, p=0.009) [**Figure 5.4E**].

The levels of oxidative stress in human astrocytes following exposure to psychosine (10μM, 20μM) were assessed using DCFH-DA. Psychosine treatment led to an increase in the fluorescence intensity of DCFH-DA (10μM Psychosine: 1.92, p=0.004; 20μM Psychosine: 2.15, p=0.0007 compared to the control group) [**Figure 5.4F**]. Treatment with 100nM Olaparib significantly mitigated psychosine-induced ROS levels (10μM Psychosine: 1.92 vs 10μM

Psychosine + Olaparib: 1.22, p=0.005; 20μM Psychosine: 2.15 vs 20μM Psychosine + Olaparib: 1.87) [**Figure 5.4F**].

Furthermore, mitochondrial membrane potential (ΔΨm) was measured using the membrane-permeant dye tetraethylbenzimidazolylcarbocyanine iodide (JC-1), which accumulates in mitochondria in a potential-dependent manner. An increase in JC-1 monomers indicates mitochondrial membrane potential loss. After treatments, cells were loaded with 1μM JC-1, and emission spectra were measured after 30 minutes. Psychosine treatment of astrocytes resulted in increased mitochondrial stress (10μM Psychosine: 1.90, p=0.0005; 20μM Psychosine: 1.65, p=0.007 compared to the control group) [**Figure 5.4G**]. Treatment with Olaparib reduced the psychosine-induced mitochondrial stress (10μM Psychosine: 1.90 vs 10μM Psychosine + Olaparib: 1.16, p=0.003; 20μM Psychosine: 1.65 vs 20μM Psychosine + Olaparib: 1.1, p=0.01) [**Figure 5.4G**].

These findings further substantiate the detrimental effects of psychosine on astrocytes and support the involvement of PARP-1 in modulating calcium signaling, oxidative stress, and mitochondrial dysfunction. Furthermore, we demonstrate that Olaparib treatment can alleviate these effects.

### 5.4.4 Attenuation of Psychosine-Induced Demyelination in OCS by Olaparib

Our *in vitro* experiments have revealed that Olaparib exerts a protective effect on astrocytes exposed to psychosine. Subsequently, we delved into the role of PARP-1 within the context of OCS, a complex microenvironment where the effects of both Olaparib and psychosine on various types of brain cells can be investigated. Previous studies have established that psychosine induces demyelination in OCS [134,135]. In this study, our primary goals were to validate psychosine-induced demyelination in OCS and explore the therapeutic potential of

Olaparib. We exposed cerebellar slices to psychosine (10μM) with or without Olaparib (100nM) for a duration of 24 hours [**Figure 5.5A**].

Consistent with our earlier findings, psychosine induced a moderate reduction in NFH levels (87.3% compared to control) [**Figure 5.5B and E**]. This was accompanied by significant demyelination, as evidenced by reduced expression of myelin basic protein (MBP) (47.6%, *$p<0.05$ compared to control) [**Figure 5.5B and C**] and MOG (55.6%, $p=0.008$ compared to control) [**Figure 5.5B and D**]. Olaparib, when administered alone, did not induce any significant alterations in myelin or neuronal status compared to the control group, as indicated by MBP (93.1%), MOG (102.2%), and NFH (102.1%) immunostaining [**Figure 5.5C-E**].

Importantly, Olaparib (100nM) significantly alleviated the psychosine-induced demyelination (MBP, Psychosine: 47.6% vs. Psychosine + Olaparib: 79.5%, $p=0.04$; MOG, Psychosine: 55.6% vs. Psychosine + Olaparib 99.0%, $p=0.005$) [**Figure 5.5C and D**]. These findings further substantiate the idea that PARP-1 plays a role in psychosine-induced cellular toxicity and exerts a multifaceted impact on both astrocytes and oligodendrocytes. Additionally, our data strongly indicate that Olaparib can mitigate the demyelination resulting from the accumulation of psychosine.

### 5.4.5 Reduction of Psychosine-Induced SMI-32 Levels by Olaparib

In light of a non-significant decrease observed in total NFH staining [**Figure 5.5**], a comprehensive investigation was conducted to examine the impact of psychosine and 100 nM Olaparib on the levels of SMI-32, a non-phosphorylated epitope of NFH and a marker indicative of axonal damage, within slice cultures, subjected to 10μM psychosine treatment for 24 hours. Slice cultures treated with psychosine exhibited a notable increase in SMI-32

expression throughout the cerebellum (201.6%, p=0.03 compared to the control) [**Figure 5.6A and B**], as well as an enlargement in the surface area expression of axons belonging to the major white matter tracts in the cerebellum (284.8%, p=0.0004 compared to the control) [**Figure 5.6A and C**]. Significantly, treatment with Olaparib effectively mitigated the overall increase in SMI-32 fluorescence intensity within the cerebellum (Psychosine: 201.6% vs Psychosine + Olaparib: 134.2%, p=0.01) [**Figure 5.6B**] and reduced the surface area expansion in the white matter tract (Psychosine: 201.6% vs Psychosine + Olaparib: 138.7%, p=0.002) [**Figure 5.6C**]. These findings represent the first evidence that Olaparib attenuates psychosine-induced axonal damage in OCS.

### 5.4.6 Olaparib Limits Psychosine-Induced Astrocyte Cell Death and Oxidative Stress in Cerebellar Slice Cultures

In our group's previous investigations, we have elucidated that psychosine-induced demyelination in OCS is partly mediated by the loss of astrocytes and an elevation in oxidative stress levels [134]. Therefore, we sought to explore the potential beneficial effects of Olaparib on the expression of GFAP (a marker for mature astrocytes) and vimentin (a marker for neural progenitor cells/immature astroglia), as well as the oxidative stress marker 8-hydroxy-2'-deoxyguanosine (8-OHdG), using brain slice cultures treated with 10μM psychosine.

Consistent with our previous findings, psychosine treatment led to a reduction in GFAP fluorescence intensity (68.4%, p=0.001 compared to control) and altered astrocyte morphology by decreasing the number of branches per astrocyte (Control: 32 vs Psychosine: 15, p=0.01) [**Figure 5.7A-C**]. Co-treatment with Olaparib effectively mitigated psychosine-induced astrocyte toxicity by attenuating the reduction in the number of branches per astrocyte (Psychosine: 15 vs Psychosine + Olaparib: 30, p=0.01) and GFAP fluorescence intensity

(68.4% vs 102.5%, p=0.0008) [**Figure 5.7B and C**]. Psychosine also induced a decrease in vimentin fluorescence (42.1%, p=0.006 compared to control), and Olaparib significantly attenuated this effect (Psychosine: 42.1% vs Psychosine + Olaparib: 96.0%, p=0.04) [**Figure 5.7D and E**]. Moreover, psychosine treatment resulted in reduced levels of total GFAP and vimentin (GFAP: 58.4%, p=0.0007; Vimentin: 67.5%, p=0.005 compared to control), while co-treatment with Olaparib elevated their expression (GFAP, Psychosine: 58.4% vs Psychosine + Olaparib: 97.2%, p=0.0002; Vimentin, Psychosine: 40.3% vs Psychosine + Olaparib: 93.2%, p=0.02) [**Figure 5.7F-I**]. These results, combined with our previous investigations in human astrocyte cultures, further support the notion that psychosine compromises astrocyte viability. Notably, Olaparib attenuated the decrease in GFAP and vimentin expression induced by psychosine in OCS.

Psychosine is known to induce oxidative stress in cultured cells and in the Twitcher mouse model of KD [148]. Although targeting oxidative stress in Twitcher mice has not led to clinical improvements, it has shown improvements in immunohistochemical markers of the disease. Considering the involvement of PARP-1 in neuroinflammation and oxidative stress, we further assessed the impact of Olaparib on oxidative stress in psychosine-treated slice cultures. 8-hydroxy-2'-deoxyguanosine (8-OHdG) is a widely utilized biomarker for oxidative stress resulting from free radical-induced oxidative lesions [149]. OCS treated with 10μM psychosine exhibited a significant increase in 8-OHdG expression (222.0%, p=0.0007 compared to control), which was ameliorated by Olaparib co-treatment (Psychosine: 222.0% vs Psychosine + Olaparib: 136.5%, p=0.03) [**Figure 5.7L and M**]. High concentrations of psychosine trigger cellular signaling pathways that induce oxidative stress, mitochondrial dysfunction, apoptosis, demyelination, and neuronal and axonal damage. It is plausible that Olaparib may ameliorate symptoms of KD by targeting multiple aspects of the disease or possibly synergizing with other therapies or therapeutic combinations.

### 5.4.7 Olaparib Ameliorates Psychosine-Induced Toxicity in Oligodendrocytes in Cerebellar Slices

We assessed the therapeutic impact of Olaparib on oligodendrocytes within OCS exposed to 10μM psychosine, the primary site of psychosine accumulation in KD. To examine these effects, we used Olig2 staining [**Figure 5.8A**]. Our findings revealed a significant change in Olig2 fluorescence in cerebellar slices treated with 100nM Olaparib alone (61.2%, p=0.02 compared to the control), consistent with prior research [147]. Moreover, psychosine induced a more pronounced decrease in Olig2 fluorescence (48.1%, p=0.003 compared to the control), but Olaparib effectively mitigated this decrease (97.0%, p=0.03) [**Figure 5.8B**].

We further validated these results through western blot analysis, which showed that Olaparib significantly counteracted the sulfatide-induced reduction in total Olig2 levels (Olaparib: 44.3%, p=0.01; Psychosine: 24.7%, p=0.007 compared to control; Psychosine + Olaparib: 105.6%, p=0.005 compared to Psychosine) [**Figure 5.8C and D**].

### 5.4.8 Olaparib Modulates Psychosine-Induced Demyelination via Alterations in Microglia and Macrophage Morphology

Multinucleated microglia/macrophages are a prominent feature in the pathology of KD and represent early characteristic changes in CNS tissue. Thus, we investigated the impact of psychosine and Olaparib on microglia and macrophage morphology using Ionised calcium-binding adapter molecule 1 (Iba1) and F4/80 as markers for microglia and macrophages, respectively. Treatment of OCS with psychosine (10μM) for 24 hours did not result in significant alterations in the expression of Iba1 [**Figure 5.9A and B**] or F4/80 in our model [**Figure 5.9C and D**]. These findings from immunofluorescence analysis were corroborated

by Western blot, which showed no detectable changes in Iba1 and F4/80 protein levels in OCS following 24-hour psychosine exposure (Iba1: 96.7%, p=0.2; F4/80: 95.1%, p=0.2 compared with control). Furthermore, no subsequent changes were observed after treatment with Olaparib (Iba1, Psychosine: 96.7% vs Psychosine + Olaparib: 91.6%, p=0.8; F4/80, Psychosine: 95.4% vs Psychosine + Olaparib: 85.6%, p=0.5) [**Figure 5.9E-H**].

To assess potential morphological changes in Iba1- and F4/80-expressing cells as indicators of an immune response to treatment, high-resolution z-stack images of cerebellar slices stained with Iba1 and F4/80 were prepared [**Figure 5.9I and M**]. Using Imaris software, we calculated the total volume of these markers under different conditions. Our analysis revealed a significant increase in the average volume of Iba1 and F4/80 staining in the number of cells when slices were treated with 10µM psychosine (Iba1, Control: 12.7 vs Psychosine: 24.7, p=0.005; F4/80, Control: 4.6 vs Psychosine: 7.9, p=0.03) (**Figure 5.9L and N**). However, this morphological alteration in microglia and macrophages was attenuated when 100nM Olaparib was added concurrently with the treatment (Iba1, Psychosine: 24.7 vs Psychosine + Olaparib: 14.4, p=0.02; F4/80, Psychosine: 7.9 vs Psychosine + Olaparib: 5.3, p=0.01) [**Figure 5.9L and N**]. Although no differences were observed in the number of microglia and macrophages or in the total protein expression, likely due to the early treatment of slice cultures, psychosine induced a change in the morphology of these cells, transforming them into globoid cells [150]. Importantly, Olaparib appeared to revert microglia and macrophage morphology back to the control state.

### 5.4.9 Lower Levels of NK and T Cell Migration Towards the Soluble Microenvironment of OCS Treated with Both Olaparib and Psychosine, Compared to Those Slices Treated with Psychosine Alone

Leukodystrophies often exhibit neuroinflammation, marked by the activation of innate immune elements within the nervous system, followed by an adaptive immune response and the infiltration of lymphocytes into the central nervous system (CNS). This phenomenon typically aligns with white matter abnormalities, disease progression, and increased morbidity.

To investigate the impact of psychosine accumulation and Olaparib treatment on immune cell infiltration into the inflamed CNS, murine splenocytes were isolated, and the migration of macrophages (F4/80), NK cells (NK1.1), and T cells (CD3) towards conditioned media of OCS (OCSCM) was examined. Slice cultures were treated with 10μM psychosine with or without 100nM Olaparib for 24 hours to generate the OCSCM. A transwell chemotaxis assay was employed to measure the migration of isolated murine immune cells towards the lower chamber containing OCSCM [**Figure 5.10A**]. The data shown here are presented as fold-change (FC) migration of T cells, NK cells, and macrophages towards the lower chamber of the transwell, compared to Negative Control (DMEM). Firstly, migration of immune cells towards the positive control (DMEM + 20% FBS) was significantly higher compared to the negative control (DMEM), validating the functionality of the chemotaxis system (T cells, Negative Control vs Positive Control: 1 vs 35.7, p=0.02) [**Figure 5.10B**], (NK cells, Negative Control vs Positive Control: 1 vs 15.1, p=0.02) [**Figure 5.10C**], (Macrophages, Negative Control vs Positive Control: 1 vs 3.7, p=0.03) [**Figure 5.10D**]. No significant changes were observed in the migration of T cells, NK cells, and macrophages towards the OCSCM from control and Olaparib-treated slices [**Figure 5.10B-D**]. However, OCSCM generated from psychosine-treated slices recruited significantly more immune cells compared to control OCSCM (T cells, Control vs Psychosine: 7.6 vs 51.6, p=0.04) [**Figure 5.10B**], (NK cells, Control vs Psychosine:

6.7 vs 31.5, p=0.05) [**Figure 5.10C**], (Macrophages, Control vs Psychosine: 0.87 vs 5.6, p=0.007) [**Figure 5.10D**]. Importantly, OCSCM from psychosine and Olaparib co-treated slices recruited significantly less immune cells compared to psychosine alone-treated slices: (T cells, Psychosine vs Psychosine + Olaparib: 51.6 vs 12.3, p=0.01) [**Figure 5.10B**]; (NK cells, Psychosine vs Psychosine + Olaparib: 31.5 vs 6.2, p=0.005) [**Figure 5.10C**]; (Macrophages, Psychosine vs Psychosine + Olaparib: 5.6 vs 3.2, p=0.07) [**Figure 5.10D**].

In summary, the findings presented in this section underscore the significant impact of psychosine in triggering immune responses and inflammatory pathways within murine slice cultures. Treatment with Olaparib effectively diminishes the chemoattraction of T cells, NK cells, and macrophages towards the psychosine-exposed slice culture microenvironment. These results emphasize the potential of Olaparib as a therapeutic intervention for mitigating neuroinflammatory processes and immune cell-mediated damage in the context of leukodystrophies and related disorders. Further investigations are needed to elucidate the underlying mechanisms and evaluate the clinical implications of Olaparib in the treatment of these conditions.

### 5.4.10 Olaparib Reverses Psychosine-Induced Changes T-Cell Abundance in OCS

Elevated T cell frequencies have been observed in various neurodegenerative conditions, including Alzheimer's disease, Parkinson's disease, and their contribution to demyelination in multiple sclerosis is well-documented [151,152,153]. In section 5.4.9, we have shown that psychosine promotes recruitment of T cells towards the OCS and here, we assessed whether resident OCS T cells expanded in response to psychosine treatment. To investigate the impact of psychosine treatment on OCS T cells, we stimulated slice cultures with 10µM psychosine for 24 hours and subsequently conducted CD3e staining [**Figure 5.11A**].

Initially, we examined the effect of psychosine on CD3e fluorescence intensity, revealing a significant increase (131.9%, p=0.02 compared to control), which was mitigated by co-treatment with 100nM Olaparib (Psychosine: 131.9% vs Psychosine + Olaparib: 87.2%, p=0.0006) [**Figure 5.11B**]. Subsequently, we determined the total T-cell count in the cerebellum, demonstrating a similar increase induced by psychosine (Control: 120.5; Psychosine: 324.2, p=0.02), which was attenuated by Olaparib (Psychosine: 324.2 vs Psychosine + Olaparib: 157.2, p=0.04) [**Figure 5.11C**].

T cells proliferate and are recruited to damaged nerves in response to fibroblast-produced chemokines CCL2 and CXCL5 following Schwann cell demyelination [154,155]. Since our data strongly indicate both T cell recruitment and proliferation in response to psychosine, we proceeded to evaluate the effect of psychosine and Olaparib on the expression of several key T cell cytokines and chemokines.

### 5.4.11 Olaparib Significantly Reduces Psychosine-Induced Release of Pro-inflammatory Cytokines and Chemokines in OCS

When we exposed organotypic slice cultures to psychosine (10μM) for 24 hours, we observed a significant increase in the release of pro-inflammatory molecules compared to untreated slice cultures (control): CXCL5 (1.7, p=0.01 compared to control) [**Figure 5.12A**], CCL2 (2.9, p=0.003 compared to control) [**Figure 5.12B**], and the pro-inflammatory cytokine TNF-α (3.8, p=0.0009 compared to control) [**Figure 5.12C**]. Interestingly, there was no significant alteration observed in IL-6 expression, possibly due to the early treatment of slice cultures (1.3, p=0.07 compared to control) [**Figure 5.12D**]. However, the addition of Olaparib (100nM) significantly reduced the psychosine-induced increase in CXCL5 (Psychosine: 1.7 vs. Psychosine + Olaparib: 0.8, p=0.007) [**Figure 5.12A**], CCL2 (Psychosine: 2.9 vs. Psychosine

+ Olaparib: 1.8, p=0.004) [**Figure 5.12B**], TNF-α (Psychosine: 3.8 vs. Psychosine + Olaparib: 1.7, p=0.0006) [**Figure 5.12C**], and IL-6 (Psychosine: 1.3 vs. Psychosine + Olaparib: 1.2, p=0.3) [**Figure 5.12D**].

These findings provide further evidence that exposure to psychosine induces inflammatory cytokine and chemokine secretion in organotypic slice cultures, while Olaparib significantly inhibits this effect. This mechanism may contribute to the protective effects of PARP inhibition against psychosine-induced demyelination, NK and T cell recruitment and T-cell activation.

**Figure 5.2**

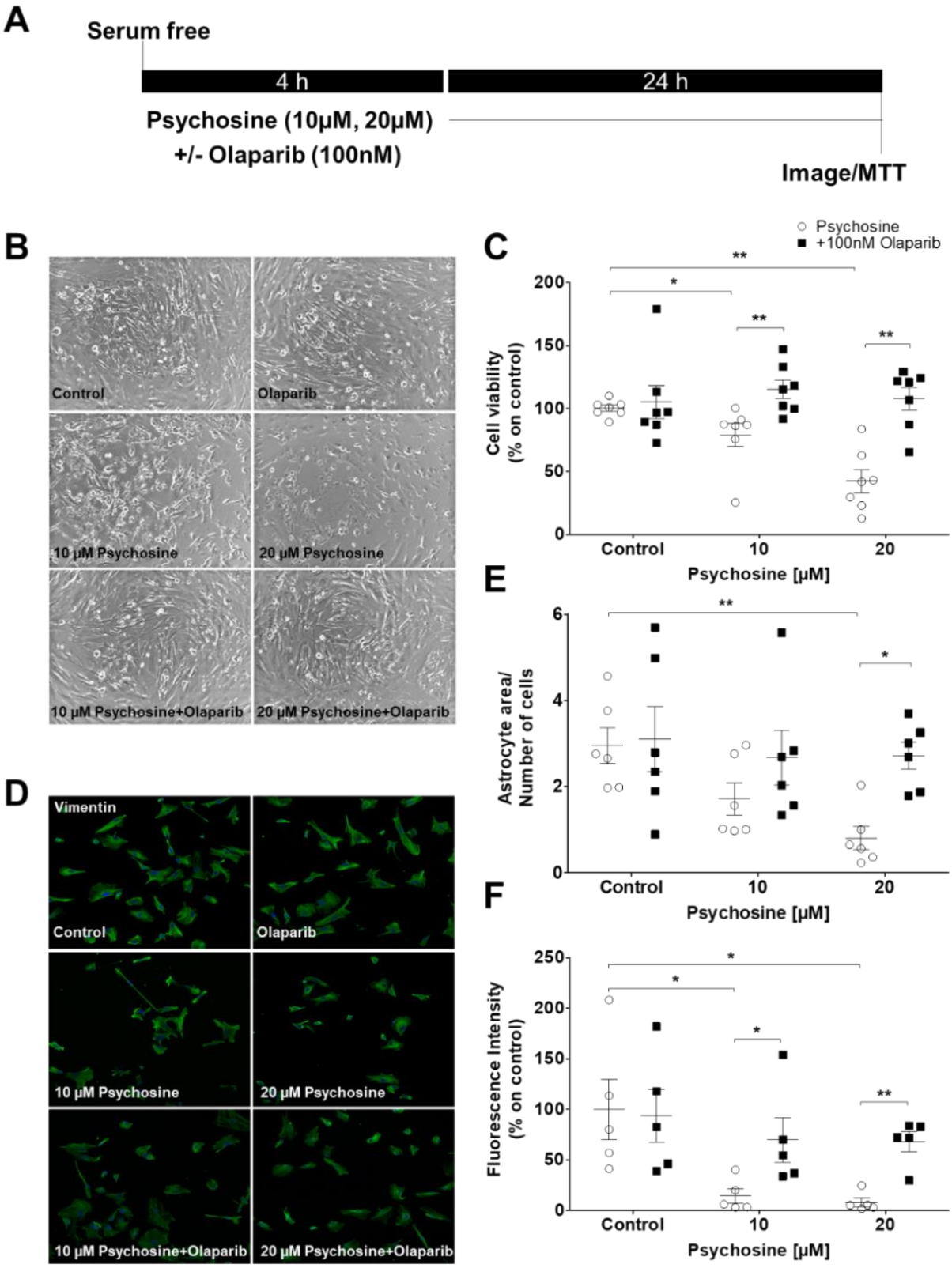
A
Serum free
4 h
24 h
Psychosine (10μM, 20μM)
+/- Olaparib (100nM)
Image/MTT
B
Control
Olaparib
10 μM Psychosine
20 μM Psychosine
10 μM Psychosine+Olaparib
20 μM Psychosine+Olaparib
C
Psychosine
+100nM Olaparib
Cell viability (% on control)
Control
10
20
Psychosine [μM]
D
Vimentin
Control
Olaparib
10 μM Psychosine
20 μM Psychosine
10 μM Psychosine+Olaparib
20 μM Psychosine+Olaparib
E
Astrocyte area/ Number of cells
Control
10
20
Psychosine [μM]
F
Fluorescence Intensity (% on control)
Control
10
20
Psychosine [μM]

**Figure 5.2: Olaparib reduces sulfatide-induced human astrocyte cell death and partially reverses changes in astrocyte morphology.** (**A**) Diagram of experimental timeline and treatments. Human astrocytes were treated with 10µM, 20µM psychosine for 24 hours with or without 100nM Olaparib. (**B**) Representative images of astrocytes treated with psychosine with or without Olaparib. Cells were imaged under light microscopy. (**C**) Graph showing changes in astrocyte viability after treatment with psychosine (10µM, 20µM, clear circle) with or without Olaparib treatment (100nM, black square) for 24 hours (n = 5). Cell viability was quantified using an MTT assay (Vybrant® MTT Cell Proliferation Assay Kit, Life technologies). (**D**) Representative confocal images displaying Hoechst (blue) and vimentin (green) staining under treatment conditions indicated. Confocal images were captured at ×20 magnification showing that treatment with 100nM Olaparib attenuates astrocyte morphology changes induced by psychosine (10µM, 20µM). A number of 15 images were analysed per condition. (**E**) Bar graph illustrating changes in astrocyte area after the treatment with psychosine and with or without Olaparib for 24 hours. (**F**) Bar graph illustrating changes in the intensity of vimentin fluorescence after the treatment with psychosine and with or without Olaparib for 24 hours. Data are presented as mean ± SEM (n = 5 or 6). One-way ANOVA followed by Tukey post-hoc test, *$p<0.05$, **$p<0.01$ compared with control or psychosine.

**Figure 5.3**

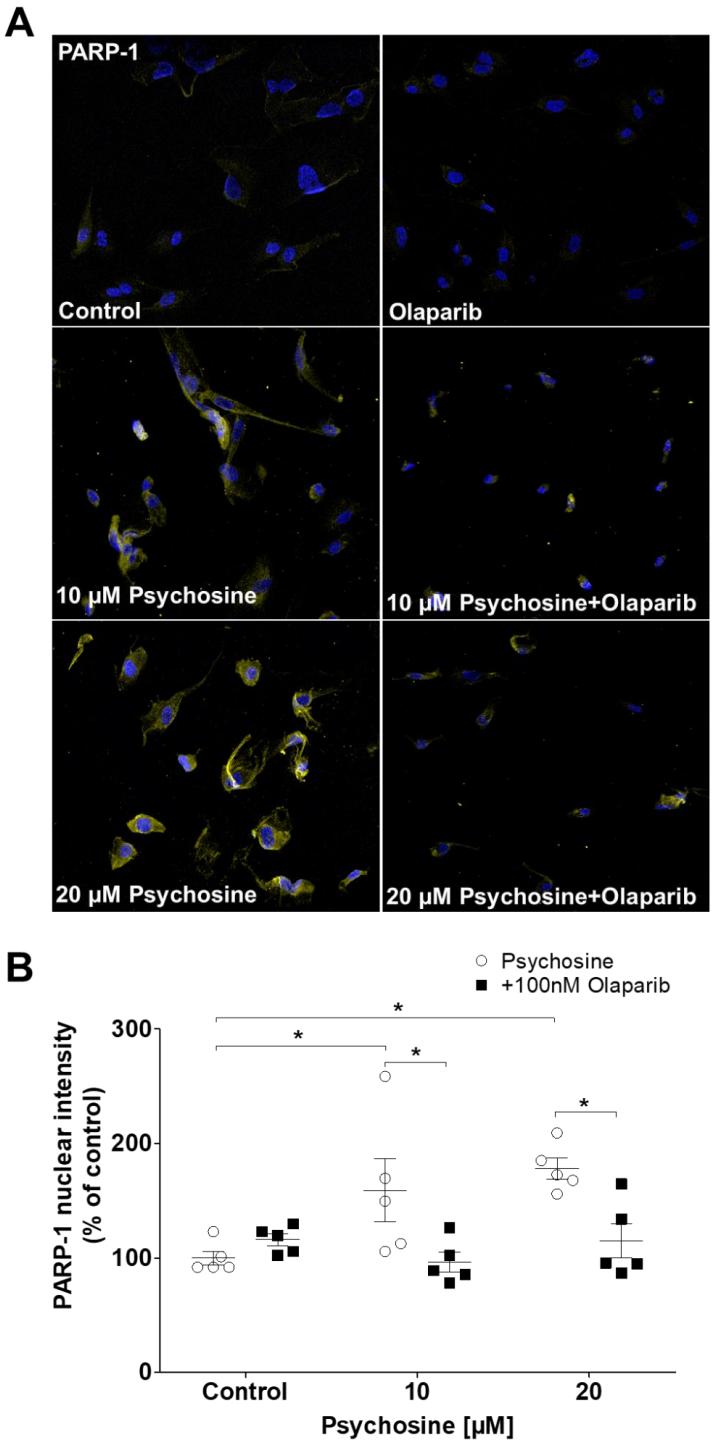


**Figure 5.3: Olaparib decreases psychosine-induced PARP-1 expression in human astrocytes. (A)** Representative confocal images displaying PARP-1 (yellow) and Hoechst (blue) immunostaining under treatment conditions indicated. Confocal images were captured at ×40 magnification. **(B)** Treatment with Olaparib (100nM) reduced psychosine-induced PARP-1 translocation to nuclei (10µM, 20µM). A number of 15 images were analysed per condition. Semi-quantitative analysis of PARP-1-associated fluorescence in the nuclei of astrocytes. Data are presented as mean ± SEM (n = 5), One-way ANOVA followed by Tukey post-hoc test, *p<0.05 compared with control or psychosine.

**Figure 5.4**

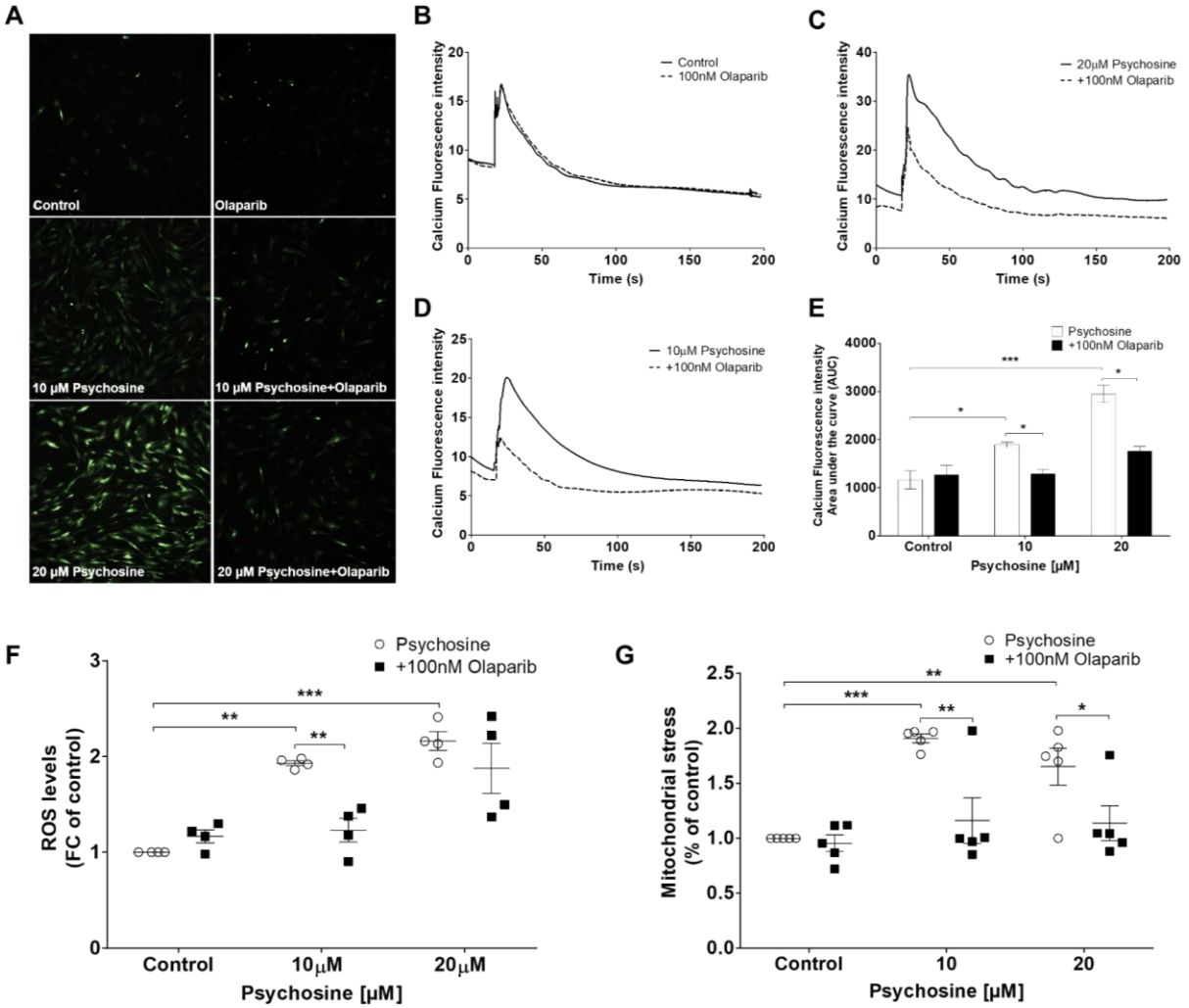


**Figure 5.4: Olaparib decreases $Ca^{2+}$ changes, suppresses ROS generation caused by psychosine in human astrocytes and reduces mitochondrial stress.** Human astrocytes were treated with 10μM, 20μM psychosis for 24 hours and with or without 100nM Olaparib and loaded with 3 μM Cal-520AM calcium indicator for 2 hours in Hank's balanced salt solution (HBSS) without calcium ($Ca^{2+}$) and magnesium ($Mg^{2+}$). Immediately prior to $Ca^{2+}$ imaging experiments, astrocytes were transferred to a fresh DMEM medium. Time-lapse $Ca^{2+}$ imaging experiments were performed at a rate of 0.99 frames per second over a 3 minutes 20 seconds period, which included 20 seconds baseline, and 3 minutes of exposure to 300μM ATP. (**A**) Representative confocal images (×20 magnification) of $Ca^{2+}$ influx in response to 300μM ATP in control and reactive astrocytes pre-treated with psychosine (10μM, 20μM) and with or without 100nM Olaparib for 24 hours. (**B-D**) Representative traces showing changes in cytosolic $Ca^{2+}$ levels in controls and psychosine-stimulated astrocytes (continuous line) with or without 100nM Olaparib (broken line). There was a 30-second baseline, at which point astrocytes were stimulated with ATP for a further 3 minutes. (**E**) Bar graph illustrating that Olaparib caused a larger decrease of both the peak amplitude and AUC in 10μM and 20μM psychosine-treated astrocytes. (**F**) Quantification of ROS levels was determined by 2'-7' dichlorofluorescin diacetate (DCFH-DA) staining in human astrocytes treated with 10μM, 20μM of psychosine (clear circle) with or without 100nM of Olaparib (black square). Data are presented as the fold change (FC) versus control of mean absorbance levels (at 490 nm). (**G**) To confirm that PARP-1 activation had negligible effects on cellular stress, the JC-1 assay was performed to measure changes in the mitochondrial membrane potential of psychosine (10μM, 20μM) and Olaparib (100nM). Data are presented as the mean absorbance levels

(at 570 nm). The measures of fluorescence signal are reported in the graph as a percentage of each condition versus the control and presented as mean ± SEM (n = 4 or 5). Statistical significance was determined using a one-way ANOVA followed by Tukey post-hoc test, *$p<0.05$, **$p<0.01$, ***$p<0.001$ compared with control or psychosine.

## Figure 5.5

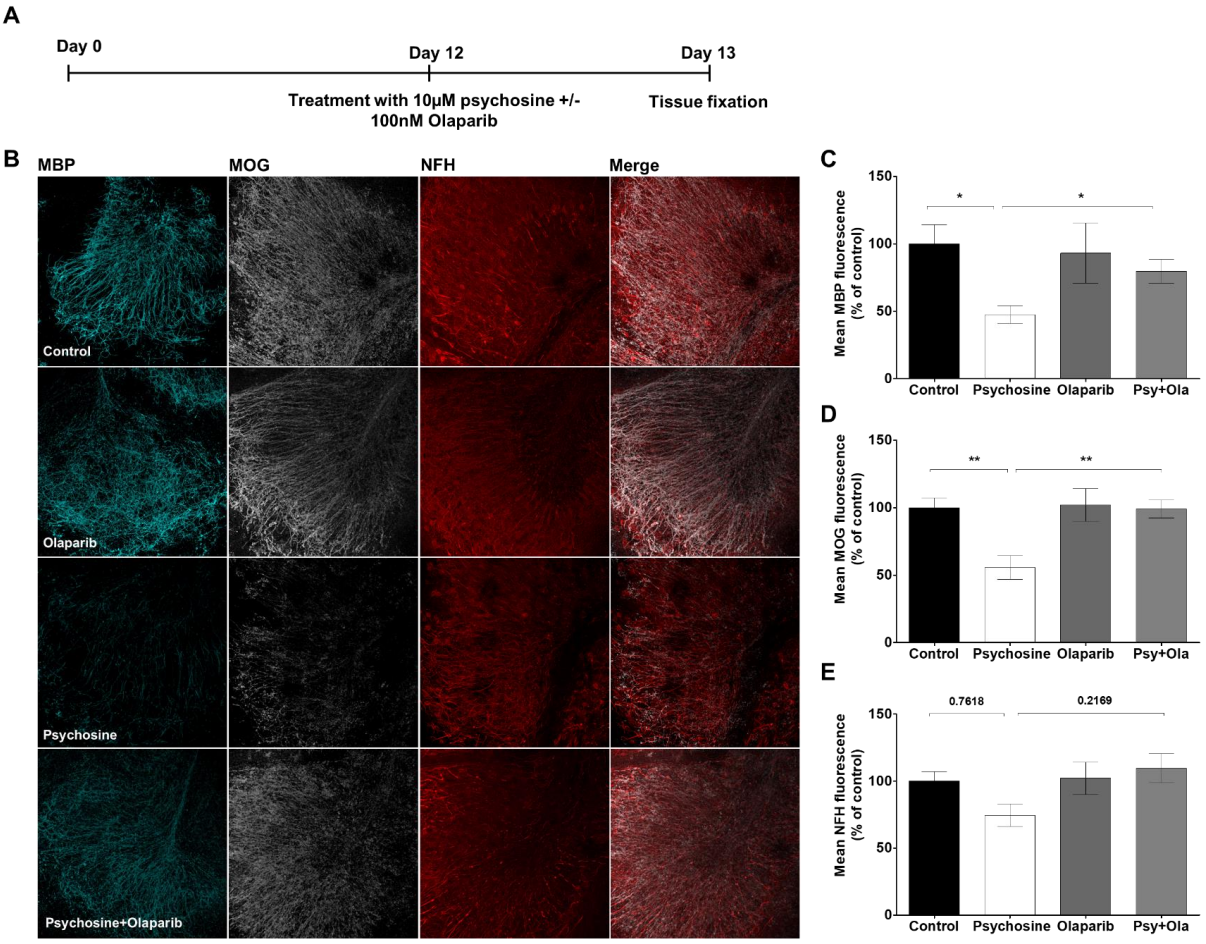


**Figure 5.5: Olaparib attenuates psychosine-induced demyelination in cerebellar slice cultures.** (**A**) Diagram of experimental timeline and treatments. OCS were treated with psychosine (10μM) in the presence or absence of Olaparib (100nM) for 24 hours. (**B**) Representative confocal images displaying MBP (blue), MOG (grey), and NFH (red) immunostaining under treatment conditions indicated. Confocal images were captured at ×20 magnification. (**C**) Bar graph illustrating changes in the intensity of MBP fluorescence after the treatment with psychosine (10μM) and with or without Olaparib (100nM). Quantification of confocal images shows a significant decrease in MBP fluorescence, which is attenuated by Olaparib. (**D**) Bar graph illustrating changes in the intensity of MOG fluorescence after the treatment with psychosine (10μM) and with or without Olaparib (100nM). Quantification of confocal images shows a significant decrease in MOG fluorescence, which is attenuated by Olaparib. (**E**) Bar graph illustrating changes in the intensity of NFH fluorescence after the treatment with psychosine (10μM) and with or without Olaparib (100nM). Quantification of confocal images shows no significant decrease in NFH fluorescence with psychosine and Olaparib treatment. Data are expressed as a percentage of control and presented ± SEM (n = 5). Statistical significance was determined by One-way ANOVA followed by Tukey multiple comparison test, *p<0.05, **p<0.01. A number of 100 images were analysed per condition. Scale bar, 100 μm.

**Figure 5.6**

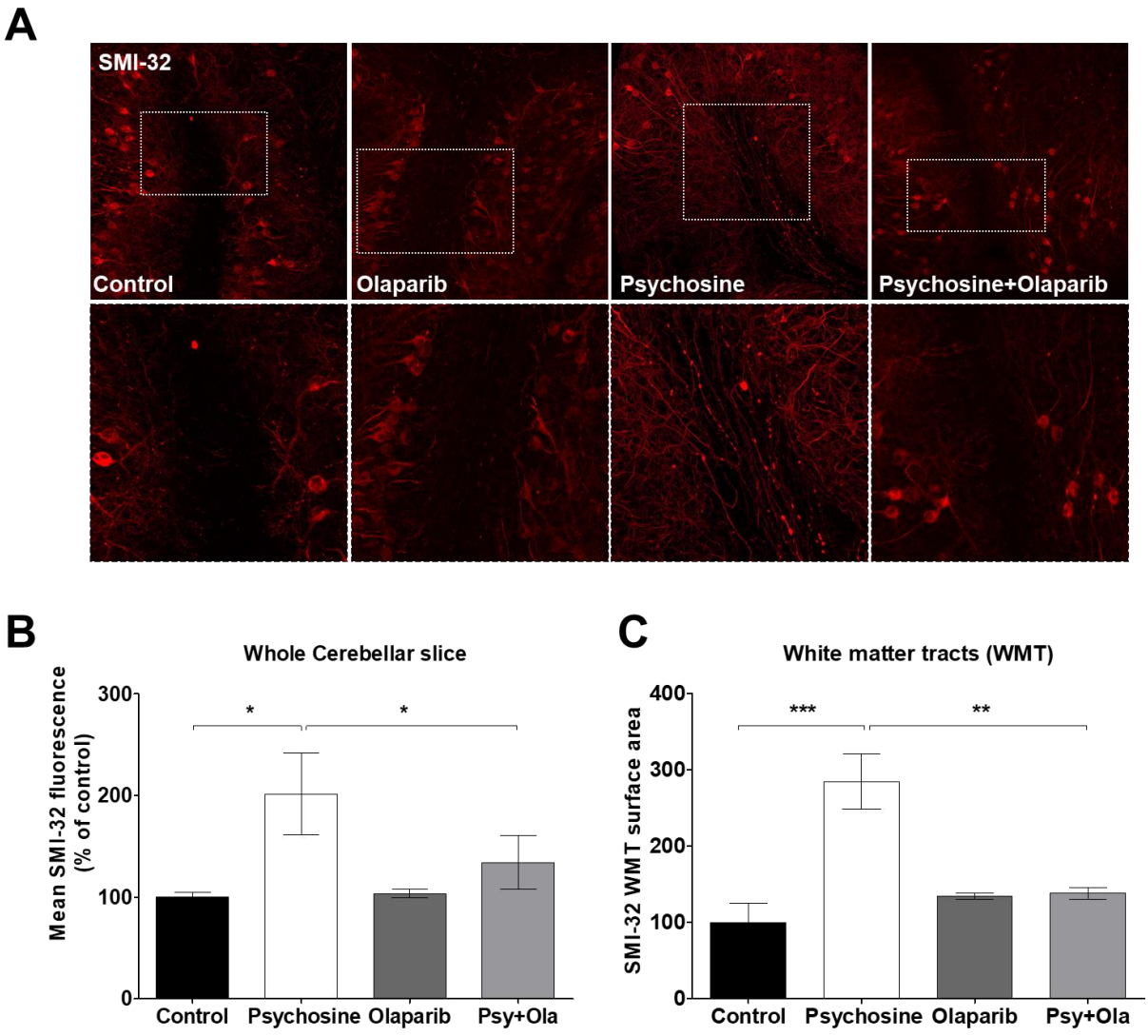


**Figure 5.6: Olaparib attenuates psychosine-induced axonal damage.** OCS were treated with psychosine (10µM) in the presence or absence of Olaparib (100nM) for 24 hours. (**A**) Representative confocal images displaying SMI-32 immunostaining in white matter tract under treatment conditions indicated. Confocal images were captured at ×20 magnification. (**B**) Relative fluorescent intensity of SMI-32 staining in the whole cerebellar slice shows a protective effect of Olaparib on psychosine-induced increase in SMI-32 fluorescence. (**C**) Relative fluorescent intensity of SMI-32 staining in major white matter tract regions shows a protective effect of Olaparib on psychosine-induced increase in SMI-32 fluorescence. Data are expressed as a percentage of control and presented ± SEM (n = 5). Statistical significance was determined by One-way ANOVA followed by Tukey multiple comparison test, *p< 0.05, ***p< 0.001. A number of 100 images were analysed per condition. Scale bar, 100 µm.

## Figure 5.7

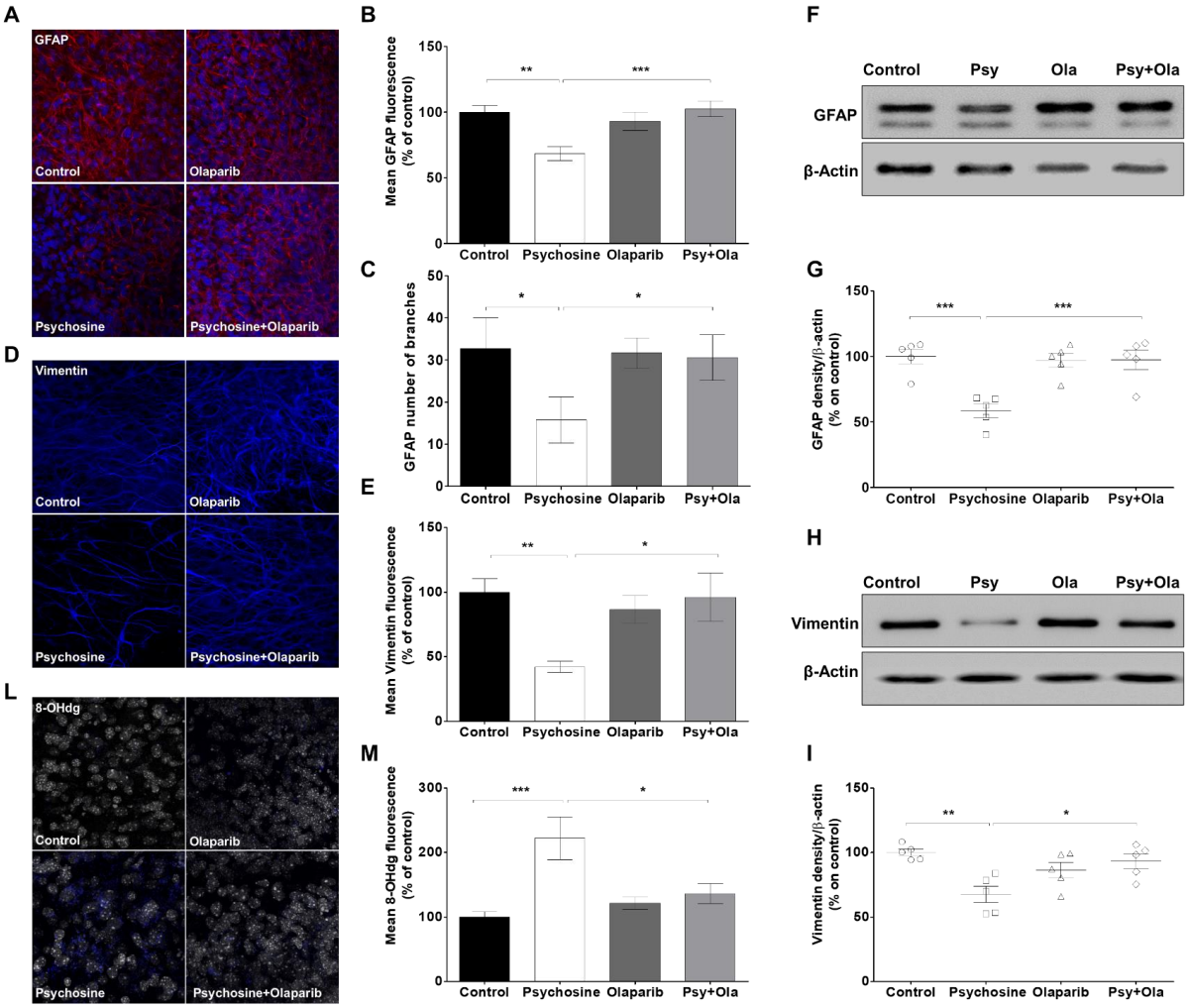


**Figure 5.7: Psychosine-induced death of astrocytes and increase of oxidative stress in cerebellar slices is limited by Olaparib.** (**A**) Representative confocal images displaying GFAP staining under treatment conditions indicated. Confocal images were captured at ×40 magnification showing that treatment with 100nM Olaparib attenuates astrocyte fluorescence intensity and number of branches decrease induced by 10µM psychosine. (**B**) Bar graph illustrating that treatment with psychosine (10µM) for 24 hours significantly decreased GFAP fluorescence compared with control. Importantly, this decrease is attenuated with Olaparib (100nM). (**C**) Bar graph illustrating that Olaparib attenuates psychosine-induced decrease in GFAP number of branches compared with control. (**D**) Representative confocal images displaying vimentin staining under treatment conditions indicated. Confocal images were captured at ×20 magnification showing that treatment with 100nM Olaparib attenuates vimentin fluorescence intensity decrease induced by 10µM psychosine. (**E**) Bar graph illustrating that treatment with psychosine (10µM) for 24 hours significantly decreased vimentin fluorescence compared with control. Importantly, this decrease is attenuated with Olaparib (100nM). Data are expressed as a percentage of control and presented ± SEM compared with control (n = 5). Statistical significance was determined by One-way ANOVA followed by Tukey multiple comparison test, *p<0.05, ***p<0.001, **p<0.01. A number of 100 images were analysed per condition. Scale bar, 100 µm. (**F-I**) Changes in GFAP and vimentin expression levels were assessed by Western blotting. Bar graph illustrating reduced GFAP (**F-G**) and vimentin (**H-I**) protein levels following psychosine exposure, which is attenuated by

Olaparib. (**L**) Representative confocal images displaying 8-OHdg staining under treatment conditions indicated. Confocal images were captured at ×40 magnification showing that treatment with 100 nM Olaparib attenuates oxidative stress induced by 10 µM psychosine. (**M**) Bar graph illustrating that treatment with psychosine (10µM) for 24 hours significantly increased 8-OHdg fluorescence compared with control. Importantly, this decrease is attenuated with Olaparib (100nM). Data are expressed as a percentage of control and presented ± SEM (n = 5). Statistical significance was determined by One-way ANOVA followed by Tukey post-hoc test, *p<0.05, **p<0.01, ***p<0.001.

**Figure 5.8**

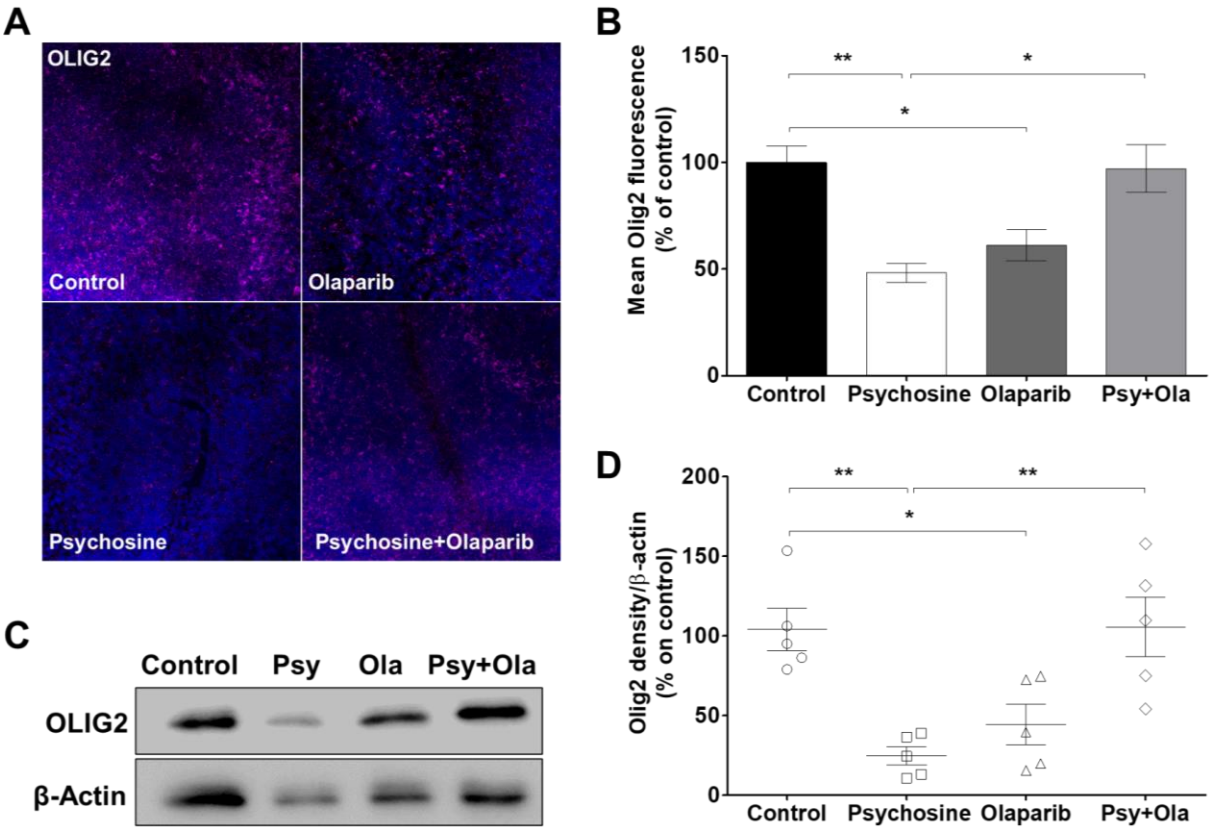


**Figure 5.8: Olaparib significantly limits psychosine-induced oligodendrocyte death.** OCS were treated with psychosine (10µM) in the presence or absence of Olaparib (100nM) for 24 hours. (**A**) Representative confocal images displaying Olig2 staining under treatment conditions indicated. Confocal images were captured at ×20 magnification. (**B**) Bar graph illustrating that treatment with Olaparib alone and psychosine significantly decreased Olig2 fluorescence compared with control. Importantly, psychosine-induced decrease is attenuated by Olaparib. Data are expressed as a percentage of control and presented ± SEM compared with control (n = 5). A number of 100 images were analysed per condition. Scale bar, 100 µm. (**C**) Changes in Olig2 expression levels were assessed by Western blotting. (**D**) Psychosine-induced Olig2 decrease was attenuated by Olaparib. Data are expressed as a percentage of control and presented ± SEM (n = 5). Statistical significance was determined by One-way ANOVA followed by Tukey multiple comparison test, *p<0.05, **p<0.01.

**Figure 5.9**

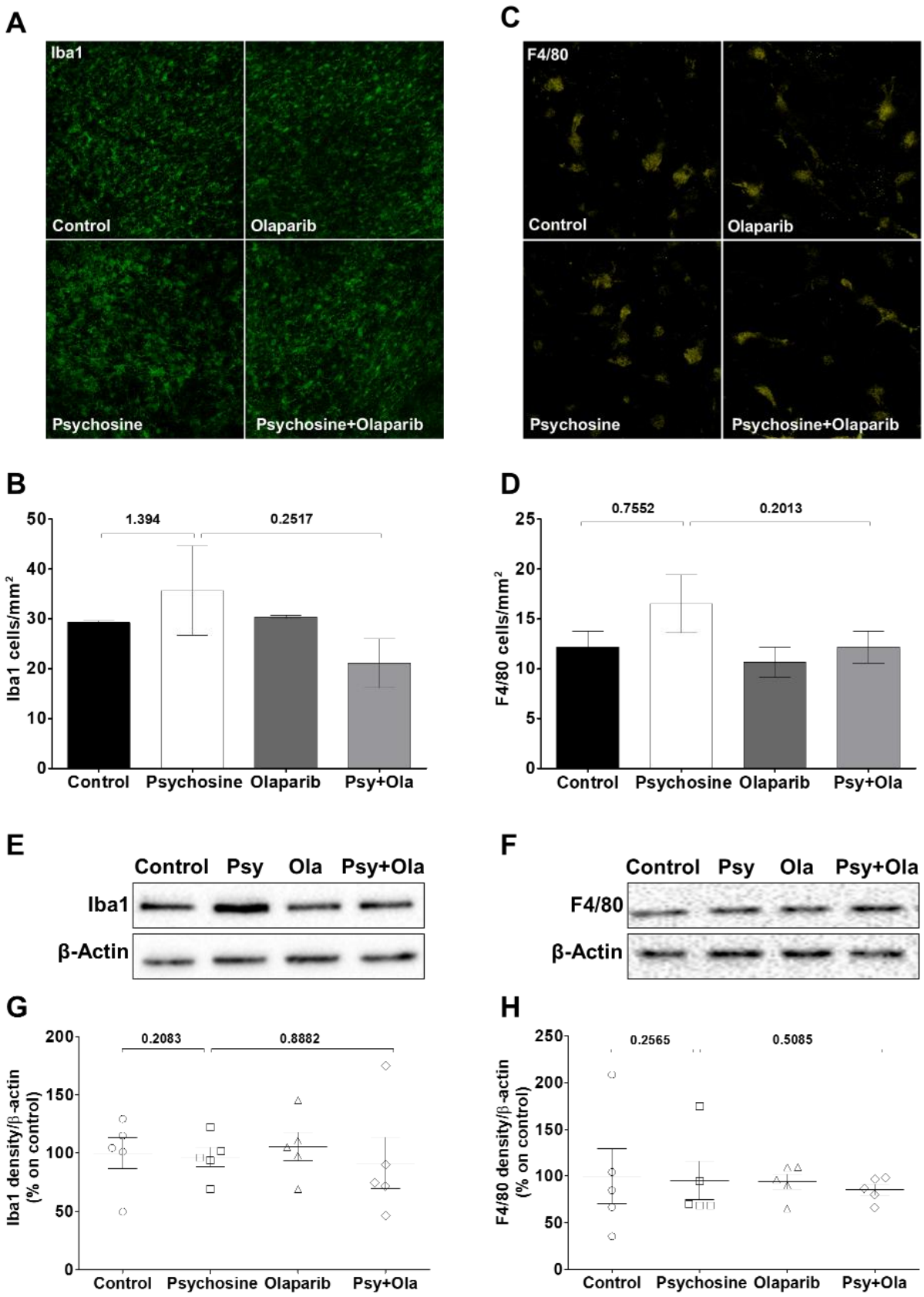
A
Iba1
Control
Olaparib
Psychosine
Psychosine+Olaparib
C
F4/80
Control
Olaparib
Psychosine
Psychosine+Olaparib
B
Iba1 cells/mm²
1.394
0.2517
Control
Psychosine
Olaparib
Psy+Ola
D
F4/80 cells/mm²
0.7552
0.2013
Control
Psychosine
Olaparib
Psy+Ola
E
Control
Psy
Ola
Psy+Ola
Iba1
β-Actin
F
Control
Psy
Ola
Psy+Ola
F4/80
β-Actin
G
Iba1 density/β-actin (% on control)
0.2083
0.8882
Control
Psychosine
Olaparib
Psy+Ola
H
F4/80 density/β-actin (% on control)
0.2565
0.5085
Control
Psychosine
Olaparib
Psy+Ola

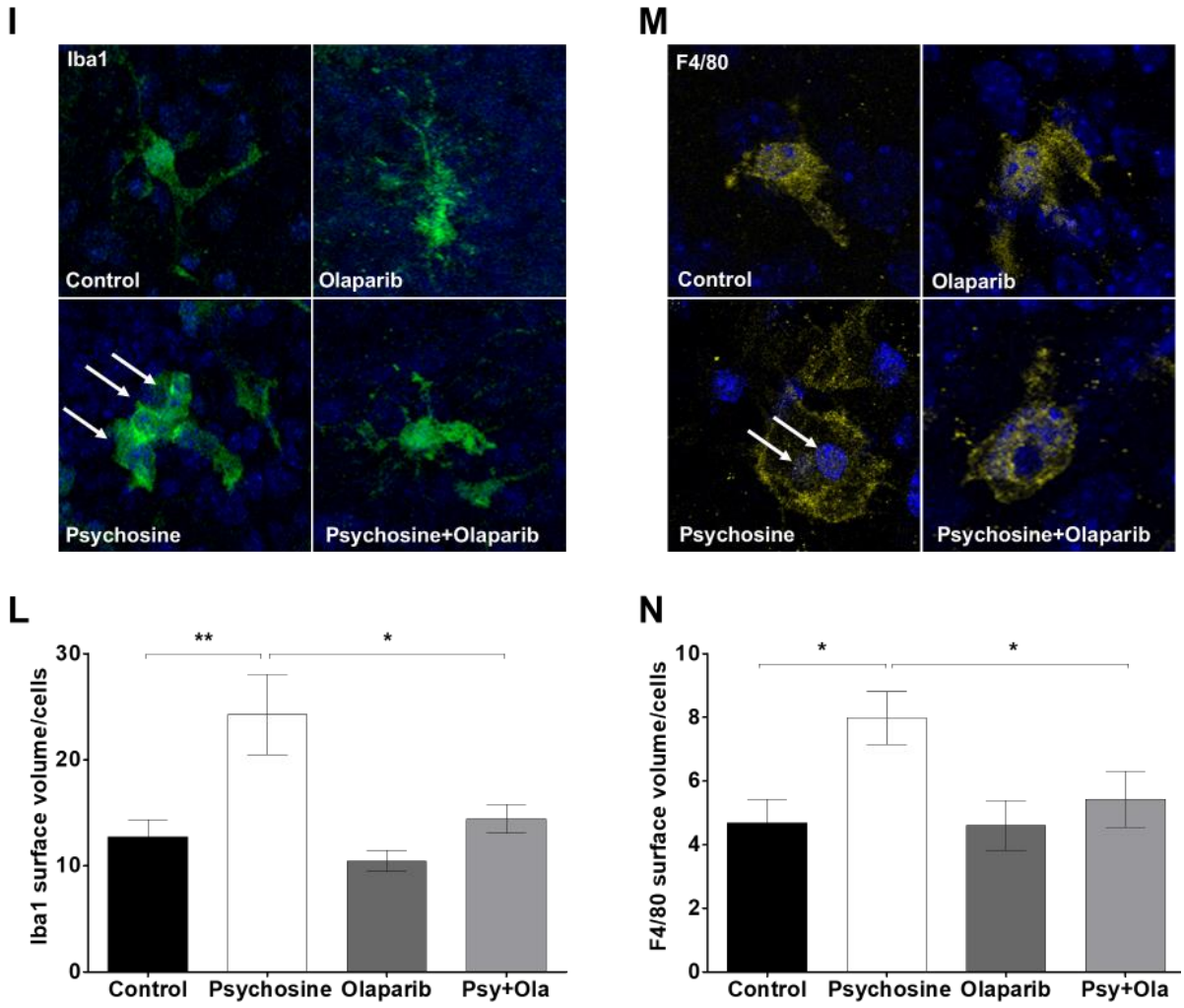


**Figure 5.9: Olaparib attenuates psychosine-induced microglia and macrophage change in morphology.** OCS were treated with psychosine (10µM) in the presence or absence of Olaparib (100nM) for 24 hours. (**A**) Representative confocal images displaying Iba1 (green) immunostaining under treatment conditions indicated. Confocal images were captured at ×20 magnification. (**B**) Bar graph illustrating changes in cell count of Iba1 after the treatment with psychosine (10µM) and with or without Olaparib (100nM) for 24 hours. Data are expressed as a percentage of control (**C**) Representative confocal images displaying F4/80 (yellow) immunostaining under treatment conditions indicated. Confocal images were captured at ×20 magnification (**D**) Bar graph illustrating changes in the cell count of F4/80 after the treatment with psychosine (10 µM) and with or without Olaparib (100 nM) for 24 hours. Data are expressed as a percentage of control. (**E**-**H**) Changes in Iba1 and F4/80 expression levels were assessed by Western blotting. Bar graph illustrating increased Iba1 and F4/80 protein levels following psychosine and Olaparib exposure. (**I**) Representative confocal images displaying Iba1 (green) and Hoechst (blue) immunostaining under treatment conditions indicated. Confocal images were captured at ×40 magnification. (**L**) Quantification of cell surface on number of cells showed a significant increase in Iba1 surface in sulfatide-treated slices compared with control, which is attenuated by Olaparib. (**M**) Representative confocal images displaying F4/80 (yellow) and Hoechst (blue) immunostaining under treatment conditions indicated. Confocal images were captured at ×40 magnification. (**N**) Quantification of cell surface on number of cells showed a significant increase in F4/80 surface in sulfatide-treated slices compared with control, which is attenuated by Olaparib. Data are presented ± SEM (n = 5). Statistical significance was determined by One-way ANOVA followed by Tukey multiple comparison test, *$p<0.05$, **$p<0.01$. A number of 100 images were analysed per condition. Scale bar, 100 µm.

**Figure 5.10**

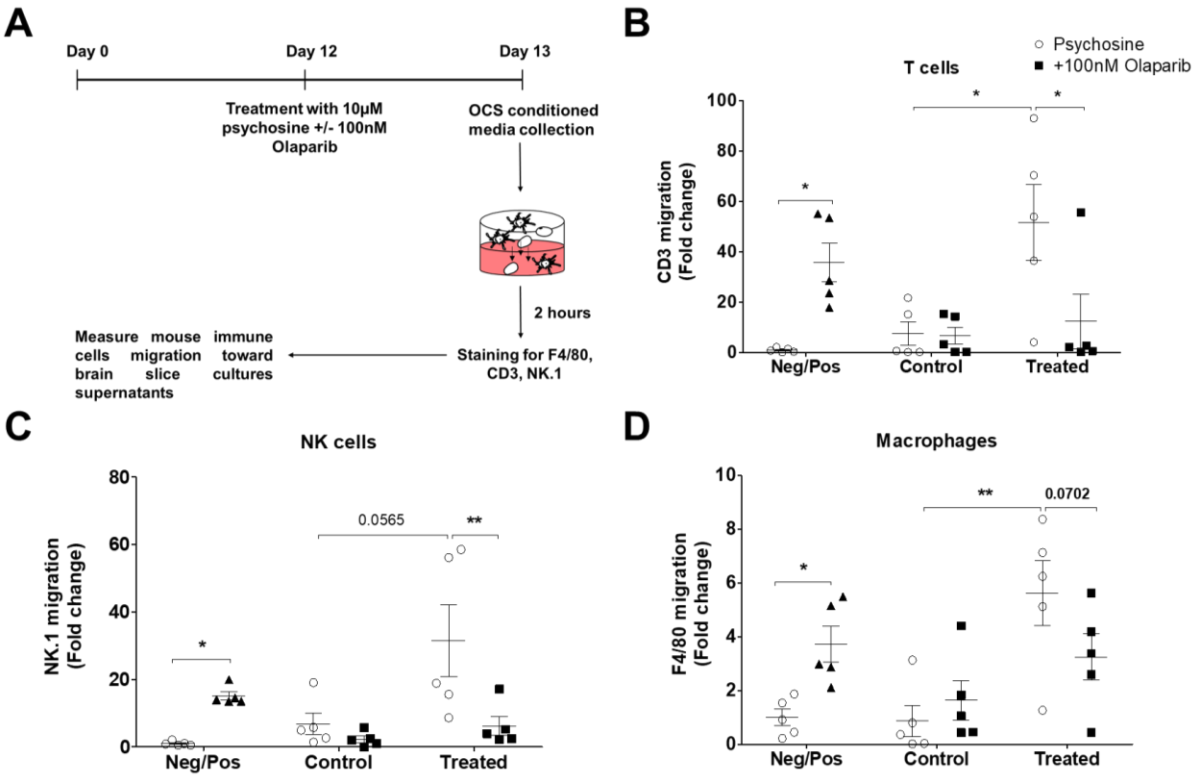


**Figure 5.10: Olaparib reduced the chemoattraction of NK and T cells towards the soluble microenvironment of psychosine-treated OCS.** T cell, NK cell, and macrophage migration towards slice cultures-conditioned medium from control and psychosine-stimulated OCS were measured after 24 hours of 100nM Olaparib exposure. (**A**) Diagram of experimental timeline and treatments. (**B**) Bar charts showing the fold change migration of T cells towards the negative control (serum-free DMEM (-)), positive control (DMEM+20% FBS (+)), vehicle control (Control), or slice cultures-conditioned medium from, OCS treated with 10 µM psychosine (clear circle) with or without 100nM Olaparib (black square). (**C**) Bar charts showing fold change migration of NK cells towards the negative control (-), positive control (+), vehicle control (Control), or slice cultures-conditioned medium from, OCS treated with 10 µM psychosine (clear circle) with or without 100nM Olaparib (black square). (**D**) Bar charts showing FC migration of macrophages to negative control (-), positive control (+), vehicle control (Control) or slice cultures-conditioned medium from, OCS treated with 10µM psychosine (clear circle) with or without 100 nM Olaparib (black square). Data from the chemotaxis assays are expressed as fold change versus negative control and are presented as mean ± SEM (n = 5). Statistical analysis was performed using a Two-way ANOVA followed by Tukey's post hoc test; *p<0.05, **p<0.01.

**Figure 5.11**

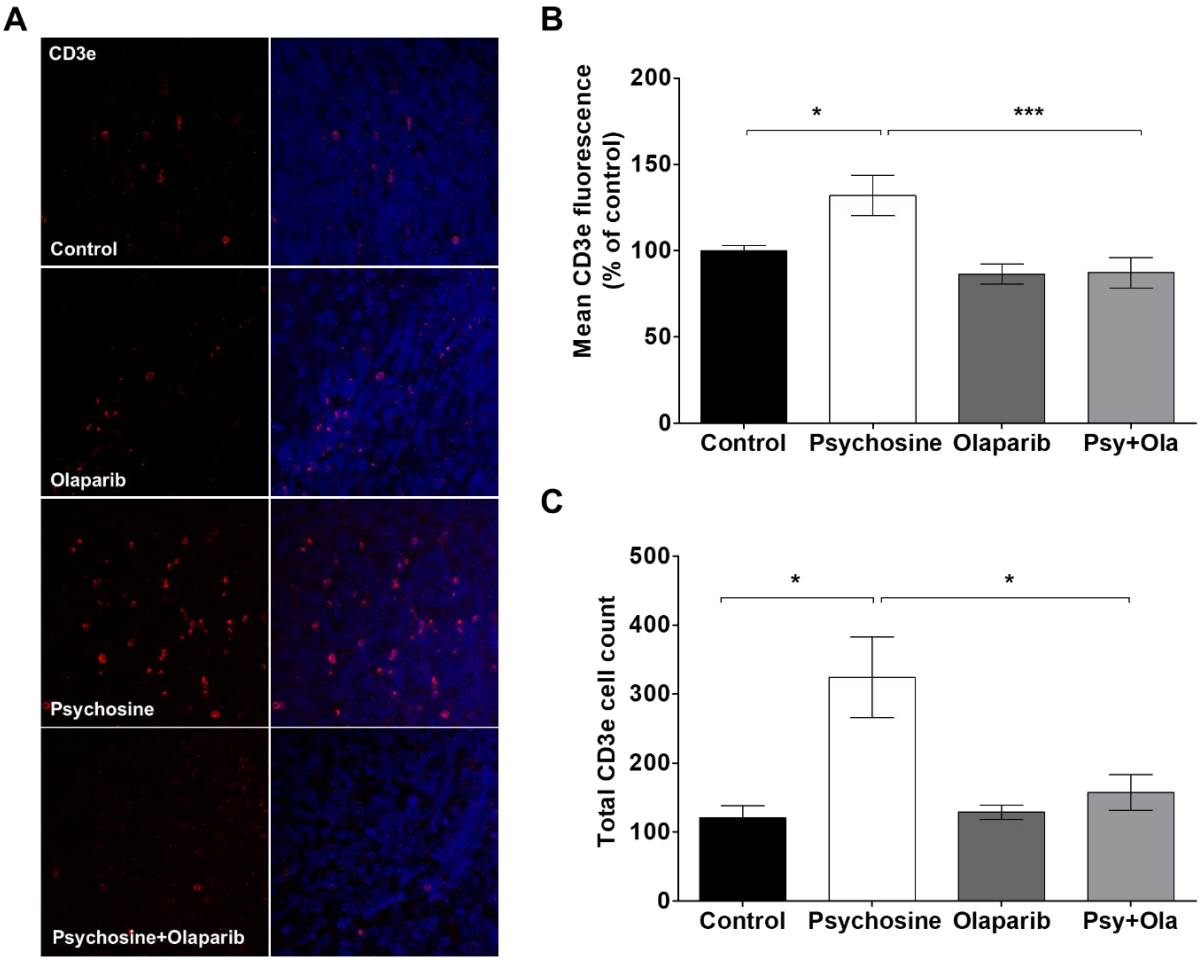


**Figure 5.11: Olaparib reduces psychosine-induced CD3e fluorescence intensity.** OCS were treated with psychosine (10µM) in the presence or absence of Olaparib (100nM) for 24 hours. (**A**) Representative confocal images displaying CD3e (red) and Hoechst (blue) immunostaining under treatment conditions indicated. Confocal images were captured at ×20 magnification. (**B**) Bar graph illustrating changes in the intensity of CD3e fluorescence after the treatment with psychosine (10µM) and with or without Olaparib (100nM) for 24 hours. Data are expressed as a percentage of control. (**C**) CD3e positive cell counting shows that psychosine increases T-cell proliferation and Olaparib reduces it. Data are presented ± SEM (n = 5). Statistical significance was determined by One-way ANOVA followed by Tukey multiple comparison test, *p<0.05, ***p<0.001. A number of 100 images were analysed per condition. Scale bar, 100 µm.

**Figure 5.12**

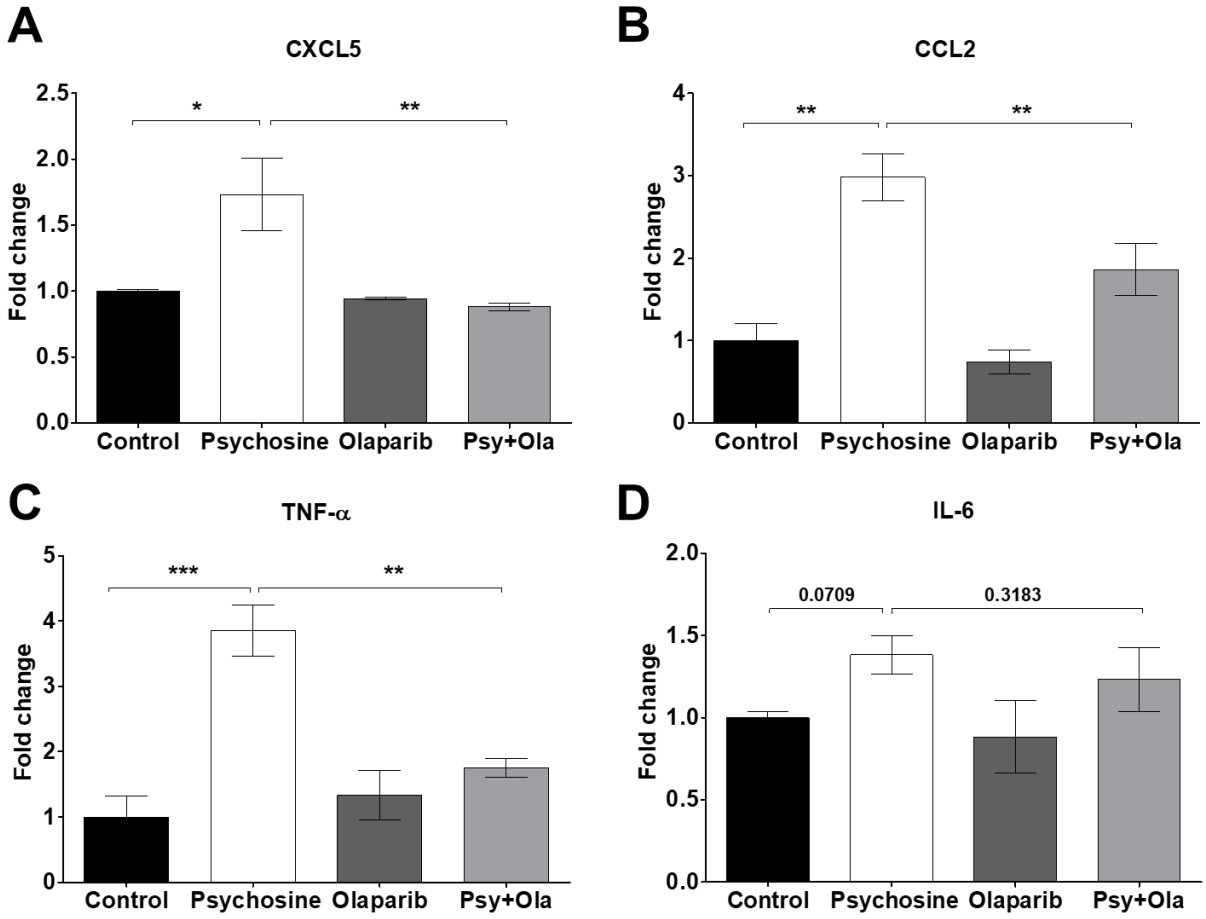


**Figure 5.12: PARP-1 ameliorates psychosine-induced inflammatory cytokine and chemokine release in organotypic slice cultures.** Cytokine and chemokine release from control and psychosine-stimulated (10μM) slice cultures were measured after 24 hours of Olaparib exposure. Olaparib (100nM) showed a significant decrease in (**A**) CXCL5, (**B**) CCL2, (**C**) TNF-α, and doesn't significantly affect (**D**) IL-6 release into the slice culture medium, as measured by ELISA. (**A**) Olaparib causes a significant reduction in CXCL5 secretion from slice cultures when compared to the psychosine group, (**B**) Olaparib also caused a significant decrease in CCL2 secretion from psychosine-stimulated slice cultures. (**C**) Olaparib reduces TNF-α secretion. (**D**) Neither treatment with psychosine nor Olaparib significantly affects IL-6 secretion from slice cultures. Data from the ELISA assays are presented as mean ± SEM (n = 5). Statistical analysis was performed using a One-way ANOVA followed by Tukey's post hoc test; *$p<0.05$, **$p<0.01$, ***$p<0.001$.

## 5.5 Discussion

### 5.5.1 Summary of Findings

Krabbe Disease (KD) arises from the deficiency of the lysosomal enzyme GALC, leading to the accumulation of psychosine, a toxic metabolite. This study delves into the role of PARP-1 in psychosine-induced astrocyte toxicity, immune cell functionality, and demyelination, along with exploring the therapeutic potential of the PARP-1 inhibitor Olaparib. Here, we demonstrate that psychosine treatment inflicts cytotoxicity and morphological alterations in human astrocytes, in alignment with prior research [134,135]. Crucially, Olaparib effectively alleviated psychosine-induced astrocyte toxicity, enhancing cell viability and preventing morphological changes, suggesting its protective effect.

The study also examined PARP-1's involvement in psychosine-induced toxicity. Results revealed that psychosine treatment activated PARP-1 in human astrocytes, marked by heightened PARP-1 expression in the cell nuclei. Co-treatment with Olaparib mitigated PARP-1 activation, indicating its ability to counteract psychosine-induced PARP-1 activation, potentially diminishing its detrimental effects on astrocytes. In addition to astrocyte toxicity, the study explored psychosine and Olaparib's effects on calcium influx and reactive oxygen species (ROS) levels in astrocytes. Psychosine heightened calcium influx and ROS levels in human astrocytes, however Olaparib co-treatment effectively suppressed psychosine-induced calcium influx and mitigated ROS levels, suggesting Olaparib's protective mechanisms may involve regulating calcium homeostasis and ROS levels.

To comprehend the broader implications of psychosine-induced toxicity and Olaparib's therapeutic potential, the study utilized organotypic cerebellar slice cultures from mice. Olaparib treatment attenuated psychosine-induced demyelination, axonal degeneration, and oligodendrocyte loss. Additionally, Olaparib ameliorated psychosine-induced immune cell

recruitment, prevalence, and reduced pro-inflammatory cytokine expression, hinting at its capacity to limit toxin-induced demyelination and modulate immune responses in KD.

In summary, this study sheds light on PARP-1's role in psychosine-induced astrocyte toxicity, impaired immune cell function, and demyelination in KD. Olaparib emerges as a promising candidate for mitigating psychosine's harmful effects on human astrocytes, encompassing cell toxicity, morphological changes, PARP-1 activation, calcium influx, and ROS levels. These findings highlight Olaparib's potential to ameliorate the adverse impacts of KD.

### 5.5.2 Regulation of Astrocytes by Olaparib

Previous research has linked psychosine accumulation to astrocyte dysfunction and cytotoxicity, suggesting its involvement in the development of KD [134,135]. This study confirms that psychosine induces adverse changes in human astrocytes, including reduced astrocyte size, cell death, increased oxidative stress, and mitochondrial damage. Remarkably, Olaparib proves effective in protecting astrocytes from psychosine-induced toxicity. It is worth noting that PARP-1, expressed in all brain cells, plays a crucial role in various biological processes and can be chronically activated in CNS disorders, leading to increased oxidative stress and cell death. The study also investigates the relationship between calcium signaling and PARP-1-mediated metabolic changes in astrocyte death. Dysregulated calcium signaling is associated with several pathological conditions, and this research suggests a potential link between PARP-1 expression and calcium signaling in astrocyte death. However, the precise temporal order of events remains to be determined.

### 5.5.3 Exploring the Role of PARP-1 and Olaparib's Therapeutic Potential in KD

PARP-1 is a ubiquitous presence in all brain cells within the central nervous system (CNS). Its functions encompass PAR synthesis, cell differentiation, maturation, regulation of cholinergic and glutamatergic signaling, and memory formation [39,40]. Notably, previous investigations have revealed that chronic activation of PARP-1, a phenomenon observed in various demyelinating disorders, leads to neuronal demise, axonal degeneration, and disruption of critical myelin-related proteins such as MOG, MBP, and MAG [55,147]. Additionally, the marker of PARP-1 activation, PAR, accumulates in multiple cell types including astrocytes, oligodendrocytes, microglia, and neurons surrounding demyelinated plaques [72]. Our findings indicate heightened levels of PARP-1 expression in psychosine-treated slice cultures, implying a potential role for PARP-1 in contributing to demyelination and neuroinflammation in KD. Given the documented reduction in neurodegeneration and demyelination achieved through PARP-1 inhibition in various animal disease models such as Parkinson’s disease, Alzheimer’s disease, and multiple sclerosis, resulting in symptom improvement via decreased inflammatory cytokine expression, we embarked on an investigation into the effects of Olaparib, a PARP inhibitor, using our psychosine-treated slice culture model. Olaparib effectively lowered PARP-1 expression and thwarted psychosine-induced demyelination. The precise mechanism through which Olaparib exerts its benefits on oligodendrocytes or myelinated axons remains undetermined. Significantly, Olaparib substantially mitigated the inflammatory response associated with demyelination, as evidenced by the rescue of astrocyte loss, decreased oxidative stress, reduced T cell recruitment and abundance, and reductions in pro-inflammatory molecule levels. In summation, these findings strongly advocate for the use of PARP-1 inhibitors in KD and neuroinflammation, emphasizing their capacity to shield against neuroinflammation in KD models through a combination of immunomodulation and direct neuroprotection. Furthermore, a deeper comprehension of PARP-1's role in maintaining brain

homeostasis and its dysregulation in pathological states may pave the way for the development of PARP-1 inhibitors specifically tailored for KD treatment.

## 5.6 Conclusion

Here we demonstrated that psychosine treatment induces demyelination, PARP-1 expression, axonal damage, astrocyte impairment, and elevates pro-inflammatory cytokine and chemokine levels in murine organotypic slice culture. Our data also indicate that psychosine increases immune cell abundance and promotes the globoid morphology of microglia and macrophages. Importantly, all the deleterious effects of psychosine were attenuated by the PARP-1 inhibitor Olaparib. Overall, our study data suggest that PARP-1 inhibition may be a therapeutic option in KD, where marketed drugs such as Olaparib may be worthy of further investigation. Future studies will focus on evaluating the delivery and therapeutic effects of Olaparib on symptoms and demyelination in KD mice.

# Chapter 6 – Discussion

## 6.1 Summary of findings

The role of PARP-1 has been quite topical across a wide range of inflammatory and neurological diseases since PARP inhibitors have emerged as a promising targeted therapy for brain cancer. PARP-1 is expressed by all brain cells in the CNS and mediates several different vital cell functions including cell apoptosis, differentiation, and memory formation. However, the expression and function of PARP-1 in CNS pathologies have both remained relatively unclear, specifically in rare demyelinating diseases such as MLD and KD. Here, we investigated the role of PARP-1 in these pathologies:

- We first investigated the role of PARP-1 in astrocytes and showed it to be overexpressed in response to toxic stimuli, such as sulfatides. We also demonstrated that pharmacological inhibition of PARP-1, by Olaparib, regulated the reactive state of astrocytes by; (1) reducing the levels of proinflammatory molecules such as IL-6, IL-8, CX3CL1, and TNF-α in astrocytes, (2) decreasing the chemoattraction of human immune cells towards the soluble microenvironment of sulfatide-treated astrocytes, (3) regulating sulfatide-induced oxidative stress and mitochondrial damage, and (4) altering Ca2+ signalling response upon PARP-1 inhibition *in vitro* (Chapter 3).
- Next, we investigated the role of PARP-1 *ex vivo*, using organotypic cerebellum slice cultures treated with a toxic concentration of sulfatide, in the presence or absence of Olaparib. Corroborating our *in vitro* data, we observed that PARP-1 over-expression induced by sulfatide led to astrocyte death. We also validated the myelin state and microglia reactivity of this model, observing that sulfatide induces demyelination and oligodendrocyte death and Olaparib mitigates them. PARP-1 inhibition also attenuates neuroinflammation induced by sulfatide by decreasing the release of pro-inflammatory molecules and microglia proliferation (Chapter 4).

- Lastly, based on our previous studies showing that psychosine is toxic for astrocytes *in vitro*, we hypothesized and examined a potential role for PARP-1 in the regulation of psychosine-treated astrocytes. We showed that PARP-1 inhibition with Olaparib is protective towards astrocyte viability and reduces oxidative stress and Ca2+ signalling induced by psychosine. Our previous studies also showed that psychosine directly induces demyelination in the CNS. Therefore, we examined the potential role of PARP-1 in the regulation of myelination. Using an organotypic cerebellum slice culture *ex vivo* model, we showed that inhibition of PARP-1 with Olaparib reduced psychosine-induced demyelination. Moreover, Olaparib attenuated the psychosine-induced microglia reactivity, neuronal loss, and immune cell activation *ex vivo*. In agreement with our *in vitro* studies on astrocytes, we observed that Olaparib caused an increase in astrocyte viability *ex vivo* (Chapter 5).

These findings report, for the first time, a role for the transcription factor PARP-1 in the modulation of astrocytic reactivity upon inflammatory or toxic stimuli across 2 demyelinating diseases. Furthermore, we suggest PARP-1 as a regulator of myelination, likely playing a role as a modulator in the crosstalk between oligodendrocytes and neurons.

### 6.2 The effect of sulfatide or psychosine on astrocyte functionality and inflammation

Evidence is emerging that astrocyte dysfunction can be the direct cause of neurodegeneration, as shown in Alexander's disease where myelin degeneration is caused by mutations in the gene encoding the astrocyte-specific cytoskeleton protein glial fibrillary acidic protein [130]. Recent studies point to a primary role for astrocytes in the pathogenesis of other genetic leukodystrophies such as megalencephalic leukoencephalopathy with subcortical cysts and vanishing white matter disease. In this setting of diseases, astrocyte dysfunction and loss are

suggested to cause disruption of astrocyte-oligodendrocyte interactions and lead to the pathological mechanism of these diseases.

There is limited research on the role of astrocytes in MLD and KD. Many studies suggest that peripheral neuropathy is a significant symptom of MLD and KD, but the reasons for its persistence after treatment are not fully understood and might be adduced to persistent astrogliosis [76,141].

Our research unveiled the effects of sulfatide and psychosine on astrocytes' viability and functionality and shows that they are at least in part mediated by the transcription factor PARP-1. In our current study, we obtained data that demonstrated a direct effect of psychosine or sulfatide on astrocyte cell death and attenuation by Olaparib. We investigated the effect of the cytotoxic lipid on cultures of human astrocytes. Sulfatide caused a time- and concentration-dependent decrease in astrocyte cell numbers. Our JC-1 experiments show that psychosine or sulfatide induces mitochondrial dysfunction and increased ROS levels. Hence, we suggest, the astrocytic cell death induced by toxin is likely to occur via an apoptotic process. Importantly, Olaparib attenuated psychosine or sulfatide-induced cell death as well as restoring mitochondrial dysfunction. Moreover, we found that sulfatide induces increased levels of pro-inflammatory cytokines such as IL-6, IL-8, CX3CL1, and TNF-α, and these effects were again reduced by Olaparib. We also evaluated the chemoattraction of human immune cells towards the soluble microenvironment of sulfatide-treated astrocytes. Our data show that the sulfatide-induced changes in the pro-inflammatory response of human astrocytes are paralleled by an increased potential to recruit NK cells and T cells. Therefore, correcting neuroinflammation, in addition to correcting ASA deficiency, might have positive effects on demyelination as observed in MLD mouse models [96]. However, convincing preclinical and clinical evidence for a neuroinflammatory role in the pathology and treatment of peripheral neuropathy in MLD and KD has yet to be shown.

### 6.3 Sulfatide or psychosine change intracellular calcium signalling in human astrocytes

Studies in the literature show that the production of pro-inflammatory molecules is mediated by NF-κB [27]. Historically, it has been regarded that activation of NF-κB is positively regulated by intracellular $Ca^{2+}$ signals [118]. However, $Ca^{2+}$ regulation of the activation of NF-κB is complex and dependent on time, amplitude, duration and frequency of the $Ca^{2+}$ signal [118]. Thus, we suggest that sulfatide and psychosine could increase levels of $Ca^{2+}$, and consequently, activation of NF-κB as transcription factor for proinflammatory molecule production, supporting our findings on the levels of cytokine and chemokine release in stimulated astrocytes following treatment with sulfatide and psychosine. We have demonstrated that sulfatide and psychosine can alter $Ca^{2+}$ signalling in astrocytes. The importance of $Ca^{2+}$ homeostasis is central in disease, where despite specific etiopathology and progression, most neurological conditions including Parkinson's disease, Alzheimer's disease, multiple sclerosis, Huntington's disease or amyotrophic lateral sclerosis, have $Ca^{2+}$ dysregulation as a common feature [118].

### 6.4 PARP-1 mediates sulfatide or psychosine toxicity in human astrocytes

In all of the studies performed with sulfatide and psychosine, Olaparib, a PARP-1 inhibitor, was able to attenuate the cytotoxic damage induced by the toxic lipid metabolites to varying degrees. The mechanisms of action through which it exerts its protective effects however are unknown. PARP-1 has a key role in chronic inflammation in the context of many inflammatory-driven pathologies [26]. PARP-1′s pro-inflammatory effects are not limited to immune cells and have been observed in astrocytes, endothelial cells, and fibroblasts, contributing to the inflammatory process in nearly all tissues [29,30]. PARP-1 achieves this mainly via the co-activation of NF-κB, which induces the transcription of genes encoding

proteins such as iNOS, TNF-α, IL-1, IL-6, and pro-metastatic cytokines [31,32]. Together these molecules enhance inflammation, which in turn augments the expression of ROS and increases genomic instability as well as the sensitivity of surrounding cells to oxidation [26,32]. In addition, NF-κB induces further PARP-1 activation, thus creating a chronic oxidative loop [33].

Many examples exist in the literature describing the pro-survival and protective effects of PARP-1 inhibitors in varies cell types [34,35]. Our study demonstrates that Olaparib reduces astrocyte death via a decrease of oxidative stress, mitochondria damage, inflammation, and calcium signalling. Hence, although the exact mechanism by which Olaparib attenuates sulfatide or psychosine-induced astrocytic cell death in the current study has not been fully elucidated, it is likely to involve the activation of PARP-1 and NF-κB. The inhibition of this pathway with Olaparib might be protective against those toxins. Olaparib is also a known immunomodulator and hence may attenuate cell damage via the dampening of proinflammatory processes.

### 6.5 Effect of sulfatide or psychosine on demyelination in OCS

Demyelination and oligodendrocyte loss, induced by sulfatide or psychosine, are two major pathological features of MLD and KD brains respectively.

Sulfatide is a critical molecule in the complex process of myelination within the CNS and PNS [92]. Sulfatide molecules interact with other lipids and proteins, such as MBP and proteolipid protein (PLP), to form a dense, multi-layered structure that insulates axons [114]. This insulation allows for rapid saltatory conduction of nerve impulses, a fundamental process for proper neurological function. Sulfatide's role extends beyond mere structural support. It also participates in axon-glial interactions that are essential for myelin formation [110,111]. Oligodendrocytes in the CNS and Schwann cells in the PNS rely on sulfatide to establish and

maintain intimate contact with axons, a prerequisite for successful myelination. On the flip side, sulfatide dysfunction can lead to demyelination, a hallmark of diseases like MLD and multiple sclerosis [106,147]. Contrary, psychosine is a minor compound in a normal brain and its concentration is elevated in white matter of humans and animal models with GALC deficiency [146]. Psychosine toxicity is mainly adduced to its accumulation in lipid rafts which leads to mitochondria damage and apoptosis [145].

Interestingly, sulfatide as well as psychosine could trigger morphological changes in microglia and induce inflammation-associated molecules including NO and cytokines [145,146]. Additionally, treatment resulted in the activation of intracellular signaling pathways including MAPKs and representative inflammation-associated transcription factors [150]. These observations suggest that sulfatide and psychosine may cause and exacerbate inflammatory conditions in demyelinating brain. Understanding the intricate relationship between these two toxins and myelination is vital for developing therapeutic interventions for demyelinating diseases. In the present thesis, we show for the first time that high concentrations of sulfatide induce demyelination, oligodendrocyte loss, and axonal degeneration in brain slice cultures. Our data provide an interesting clue regarding sulfatide's pathogenic action, which requires microglia activation and proliferation, increased pro-inflammatory cytokines, and astrocyte loss. We also show that psychosine alone induces demyelination *ex vivo* through oligodendrocyte loss and glia impairment. Interestingly, Olaparib rescues demyelination in both MLD and KD models.

### 6.6 Olaparib-mediated attenuation of toxin-induced inflammation is observed across MLD and KD

The effects of sulfatide or psychosine on myelin and oligodendrocytes are attenuated by Olaparib, suggesting a predominant role of PARP-1 in MLD and KD. Olaparib likely prevents demyelination through immunomodulation of glial cells. Many now believe that astrocytes and microglia play a prominent role in myelin dysfunction [112]. Astrocytes and microglia physically communicate via receptor-ligand interactions as well as communication via several connexins [130]. Disruption of this interaction activates microglia that enhance proinflammatory responses in the CNS and has been implicated in the pathogenesis of several models of demyelinating disease [112]. Treatment of brain slice cultures with sulfatide induced the production of pro-inflammatory molecules including IL-6, TNF-α, IL-17, INF-γ, and MIF. Activation of pro-inflammatory pathways in the brain, including IL-6 pathway, TNF-α, IL-17A, and MIF comprises a potential point of convergence between chronic neuroinflammation and neurodegeneration in many brain diseases such as AD and MS, so it is rational to hypothesize that the elevation of these cytokines contributes to demyelination in MLD [140,141,142]. Moreover, the elevated levels of CCL3, IFN-γ, and IL-6 observed here are in line with elevated levels observed in the preclinical stages of MLD [96]. Nowadays it is generally accepted that these cytokines promote pathology by activating glial cells and by recruiting peripheral immune cells such as granulocytes and T cells [96,143]. Sulfatide also induced microglia proliferation and astrocyte activation in slice cultures, strengthening the idea that neuroinflammation could be a major driver of MLD, therefore enhanced levels of myelination and less axonal degeneration could be achieved via modulation of immune pathways, microglia, and astrocytes.

Neuroinflammation plays a significant role also in the pathophysiology of KD, by contributing to damage to myelin and neurons. In advanced stages of KD, immune cells from the peripheral

blood, such as macrophages and T lymphocytes, may infiltrate the brain. These immune cells exacerbate the neuroinflammatory response, leading to further damage to myelin and neurons. Brain slice cultures treated with psychosine showed astrocyte loss, increased oxidative stress, and increased production of pro-inflammatory molecules such as TNF-α, CXCL5, and CCL2. Moreover, psychosine induces an increase in T cells abundance which is in line with previous studies. In our studies, we did not observe overt microglial activation as well as macrophage proliferation in our slice cultures or increased levels of IL-6 in response to psychosine-induced demyelination. In contrast, we observe changes in microglia and macrophage morphology turning into globoid cells. We acknowledge, however, that these slice culture studies may differ from *in vivo* settings, where demyelination observed in KD may involve an intricate balance between astrocytes and microglia.

## 7. Limitations and Future Directions

Our findings on the expression of PARP-1 in astrocytes treated with sulfatide or psychosine suggest its role in the modulation of reactivity of astrocytes through cytokine release and metabolic changes. Recent studies have shown a phenotype for activated astrocytes, termed A1 astrocytes, that differentiates under inflammatory conditions such as LPS and that have neurotoxic effects [156]. In order to assess whether the expression of PARP-1 is linked to reactive astrocytes, studies of colocalization of PARP-1 and the A1 phenotype marker C3 are suggested. If PARP-1 were expressed in reactive astrocytes, the decrease in the levels of IL-6, IL-8, CX3CL1, and TNF-α after sulfatide treatment might be linked to a change in the astrocytes' reactive phenotype and likely on their neurotoxic effects as well, maybe then proposing PARP-1 as a target to treat detrimental neuroinflammation derived from astrocytes. We have also hypothesized the mechanisms of action through which PARP-1 could sulfatide-induces toxicity of astrocytes. However, to corroborate the biochemical pathways underlying these processes, different approaches could be considered. Western-Blot analysis could help define the cascades involved in the regulation of astrocytic reactivity. In addition, immunoprecipitation followed by Liquid Chromatography Mass Spectrometry analysis would help elucidate any binding partners of PARP-1.

The current study also examined the protective effects of PARP-1 modulation in KD and MLD, using murine brain slice culture as an *ex vivo* model. We highlighted several beneficial effects on myelination and inflammation with PARP-1 inhibition in the CNS. We are aware that, although we have shown that inhibition of PARP-1 attenuates the decrease of myelin markers caused by psychosine or sulfatide, we cannot know whether this attenuation is due to an increase of the remyelination process, or due to protection against demyelination. In order to examine whether PARP-1 has a regulatory effect on the maturation of oligodendrocytes,

analysis of the mature oligodendrocyte marker NOGO-A would be advisable. We also note that this study measures fluorescence intensity of myelin markers, which does not necessarily correspond to the levels of myelination, as these markers are also detected in the non-myelinating oligodendrocytes and in myelin debris. Moreover, we note that the increase in myelin caused by Olaparib can be non-functional or aberrant. Therefore, electron microscopy studies showing the thickness and structure of the myelin sheath would corroborate and support our findings.

In addition, studies on MLD and KD animals should be performed, where we could analyse the delivery of Olaparib through the blood-brain barrier. We suggest that PARP-1 plays an actual role in the process of myelination, as its inhibition by Olaparib leads to demyelination *ex vivo*. However, we cannot assure that the effects observed with Olaparib are solely due to PARP-1 activity, and not due to PARP-2. Thus, in other to corroborate whether Olaparib exerts its protective effects through PARP-1 or through off-targets, experiments in which PARP-1 is knockout or specifically blocked would be needed.

Finally, we proposed that Olaparib could be used as a potential treatment in other demyelinating animal models. Our lab has ongoing studies on KD model, twitcher mouse. We hypothesize that co-treatment of Olaparib with FTY720 could be a potential efficient approach to prevent demyelination in the twitcher model, and thus the progression of the pathology.

## 8. Conclusion

This novel study investigated the potential role of PARP-1 and utility of Olaparib in debilitating diseases of the central nervous system. Here, we have shown that PARP-1 is over-expressed in astrocytes in response to psychosine or sulfatide treatment and that this is paralleled by altered intracellular $Ca^{2+}$ signalling and cytokine release. Moreover, our data reveal that sulfatide or psychosine treatment lowers myelin protein expression without affecting neuronal markers. On the contrary, PARP-1 inhibition with Olaparib rescues demyelination in toxin-treated organotypic slice cultures and this is paralleled by a reduction in neuroinflammation and gliosis. Thus, for the first time, our data uncover PARP-1 as a master regulator of the neuroinflammatory state of glia and myelination regulation in KD and MLD and identify Olaparib as a promising therapeutic for these pathologies.

**References**


1. Mata-Garrido J., Tapia O., Casafont I., Berciano M.T., Cuadrado A., Lafarga M. Persistent accumulation of unrepaired DNA damage in rat cortical neurons: Nuclear organization and ChIP-seq analysis of damaged DNA. *Acta Neuropathol. Commun.* 2018;6:68. doi: 10.1186/s40478-018-0573-6.
2. Heuvel D.V.D., van der Weegen Y., Boer D.E., Ogi T., Luijsterburg M.S. Transcription-Coupled DNA Repair: From Mechanism to Human Disorder. *Trends Cell Biol.* 2021;31:359–371. doi: 10.1016/j.tcb.2021.02.007.
3. Feng F.Y., de Bono J.S., Rubin M., Knudsen K.E. Chromatin to Clinic: The Molecular Rationale for PARP1 Inhibitor Function. *Mol. Cell.* 2015;58:925–934. doi: 10.1016/j.molcel.2015.04.016.
4. Engbrecht M., Mangerich A. The Nucleolus and PARP1 in Cancer Biology. *Cancers.* 2020;12:1813. doi: 10.3390/cancers12071813.
5. Jubin T., Kadam A., Jariwala M., Bhatt S., Sutariya S., Gani A., Gautam S., Begum R. The PARP family: Insights into functional aspects of poly (ADP-ribose) polymerase-1 in cell growth and survival. *Cell Prolif.* 2016;49:421–437. doi: 10.1111/cpr.12268.
6. Alemasova E.E., Lavrik O.I. Poly(ADP-ribosyl)ation by PARP1: Reaction mechanism and regulatory proteins. *Nucleic Acids Res.* 2019;47:3811–3827. doi: 10.1093/nar/gkz120.
7. Chaudhuri A.R., Nussenzweig A. The multifaceted roles of PARP1 in DNA repair and chromatin remodelling. *Nat. Rev. Mol. Cell Biol.* 2017;18:610–621. doi: 10.1038/nrm.2017.53.
8. Houl J.H., Ye Z., Brosey C.A., Balapiti-Modarage L.P.F., Namjoshi S., Bacolla A., Laverty D., Walker B.L., Pourfarjam Y., Warden L.S., et al. Selective small molecule

PARG inhibitor causes replication fork stalling and cancer cell death. *Nat. Commun.* 2019;10:5654. doi: 10.1038/s41467-019-13508-4.

9. Noordermeer S.M., van Attikum H. PARP Inhibitor Resistance: A Tug-of-War in BRCA-Mutated Cells. *Trends Cell Biol.* 2019;29:820–834. doi: 10.1016/j.tcb.2019.07.008.
10. Curtin N.J., Szabo C. Poly(ADP-ribose) polymerase inhibition: Past, present and future. *Nat. Rev. Drug Discov.* 2020;19:711–736. doi: 10.1038/s41573-020-0076-6.
11. Koehler R.C., Dawson V.L., Dawson T.M. Targeting Parthanatos in Ischemic Stroke. *Front. Neurol.* 2021;12:622. doi: 10.3389/fneur.2021.662034.
12. Lüscher B., Ahel I., Altmeyer M., Ashworth A., Bai P., Chang P., Cohen M., Corda D., Dantzer F., Daugherty M.D., et al. ADP-ribosyltransferases, an update on function and nomenclature. *FEBS J.* 2021 doi: 10.1111/febs.16142.
13. Pascal J.M. The comings and goings of PARP-1 in response to DNA damage. *DNA Repair.* 2018;71:177–182. doi: 10.1016/j.dnarep.2018.08.022.
14. Berger N.A., Besson V.C., Boulares A.H., Bürkle A., Chiarugi A., Clark R.S., Curtin N.J., Cuzzocrea S., Dawson T.M., Dawson V.L., et al. Opportunities for the repurposing of PARP inhibitors for the therapy of non-oncological diseases. *Br. J. Pharmacol.* 2018;175:192–222. doi: 10.1111/bph.13748.
15. Pazzaglia S., Pioli C. Multifaceted Role of PARP-1 in DNA Repair and Inflammation: Pathological and Therapeutic Implications in Cancer and Non-Cancer Diseases. *Cells.* 2019;9:41. doi: 10.3390/cells9010041.
16. Wang L., Liang C., Li F., Guan D., Wu X., Fu X., Lu A., Zhang G. PARP1 in Carcinomas and PARP1 Inhibitors as Antineoplastic Drugs. *Int. J. Mol. Sci.* 2017;18:2111. doi: 10.3390/ijms18102111.

17. Schiewer M.J., Knudsen K.E. Transcriptional Roles of PARP1 in Cancer. *Mol. Cancer Res.* 2014;12:1069–1080. doi: 10.1158/1541-7786.MCR-13-0672.
18. Bryant H.E., Schultz N., Thomas H.D., Parker K.M., Flower D., Lopez E., Kyle S., Meuth M., Curtin N.J., Helleday T. Specific killing of BRCA2-deficient tumours with inhibitors of poly(ADP-ribose) polymerase. *Nature.* 2005;434:913–917. doi: 10.1038/nature03443. Erratum in *Nature* **2007**, *447*, 346.
19. Farmer H., McCabe N., Lord C.J., Tutt A.N.J., Johnson D.A., Richardson T.B., Santarosa M., Dillon K.J., Hickson I., Knights C., et al. Targeting the DNA repair defect in BRCA mutant cells as a therapeutic strategy. *Nature.* 2005;434:917–921. doi: 10.1038/nature03445.
20. Steffen J.D., Brody J.R., Armen R.S., Pascal J.M. Structural Implications for Selective Targeting of PARPs. *Front. Oncol.* 2013;3:301. doi: 10.3389/fonc.2013.00301.
21. Rose M., Burgess J.T., O'Byrne K., Richard D.J., Bolderson E. PARP Inhibitors: Clinical Relevance, Mechanisms of Action and Tumor Resistance. *Front. Cell Dev. Biol.* 2020;8:564601. doi: 10.3389/fcell.2020.564601.
22. Yu J., Luo L., Hu T., Cui Y., Sun X., Gou W., Hou W., Li Y., Sun T. Structure-based design, synthesis, and evaluation of inhibitors with high selectivity for PARP-1 over PARP-2. *Eur. J. Med. Chem.* 2021;227:113898. doi: 10.1016/j.ejmech.2021.113898.
23. Wang Y.-Q., Wang P.-Y., Wang Y.-T., Yang G.-F., Zhang A., Miao Z.-H. An Update on Poly(ADP-ribose)polymerase-1 (PARP-1) Inhibitors: Opportunities and Challenges in Cancer Therapy. *J. Med. Chem.* 2016;59:9575–9598. doi: 10.1021/acs.jmedchem.6b00055.
24. Farrés J., Martín-Caballero J., Martínez C., Lozano J.J., Llacuna L., Ampurdanés C., Ruiz-Herguido C., Dantzer F., Schreiber V., Villunger A., et al. Parp-2 is required to

maintain hematopoiesis following sublethal γ-irradiation in mice. *Blood.* 2013;122:44–54. doi: 10.1182/blood-2012-12-472845.

25. Papeo G., Posteri H., Borghi D., Busel A.A., Caprera F., Casale E., Ciomei M., Cirla A., Corti E., D'Anello M., et al. Discovery of 2-[1-(4,4-Difluorocyclohexyl)piperidin-4-yl]-6-fluoro-3-oxo-2,3-dihydro-1H-isoindole-4-carboxamide (NMS-P118): A Potent, Orally Available, and Highly Selective PARP-1 Inhibitor for Cancer Therapy. *J. Med. Chem.* 2015;58:6875–6898. doi: 10.1021/acs.jmedchem.5b00680.
26. Ke Y., Wang C., Zhang J., Zhong X., Zeng X., Ba X. The Role of PARPs in Inflammation—and Metabolic—Related Diseases: Molecular Mechanisms and Beyond. *Cells.* 2019;8:1047. doi: 10.3390/cells8091047.
27. Oliver F., Murcia J.M., Nacci C., Decker P., Andriantsitohaina R., Muller S., De La Rubia G., Stoclet J.C., De Murcia G. Resistance to endotoxic shock as a consequence of defective NF-kappa B activation in poly (ADP-ribose) polymerase-1 deficient mice. *EMBO J.* 1999;18:4446–4454. doi: 10.1093/emboj/18.16.4446.
28. Mabley J.G., Jagtap P., Perretti M., Getting S.J., Salzman A.L., Virág L., Szabó É., Soriano F.G., Liaudet L., Abdelkarim G.E., et al. Anti-inflammatory effects of a novel, potent inhibitor of poly (ADP-ribose) polymerase. *Agents Actions.* 2001;50:561–569. doi: 10.1007/PL00000234.
29. Carrillo A. Transcription regulation of TNF- -early response genes by poly(ADP-ribose) polymerase-1 in murine heart endothelial cells. *Nucleic Acids Res.* 2004;32:757–766. doi: 10.1093/nar/gkh239.
30. Chiarugi A. Inhibitors of poly(ADP-ribose) polymerase-1 suppress transcriptional activation in lymphocytes and ameliorate autoimmune encephalomyelitis in rats. *J. Cereb. Blood Flow Metab.* 2002;137:761–770. doi: 10.1038/sj.bjp.0704934.

31. Swindall A.F., Stanley J.A., Yang E.S. PARP-1: Friend or Foe of DNA Damage and Repair in Tumorigenesis? *Cancers.* 2013;5:943–958. doi: 10.3390/cancers5030943.
32. Schreiber V., Dantzer F., Ame J.-C., De Murcia G. Poly(ADP-ribose): Novel functions for an old molecule. *Nat. Rev. Mol. Cell Biol.* 2006;7:517–528. doi: 10.1038/nrm1963.
33. Peralta-Leal A., Rodríguez-Vargas J.M., Aguilar-Quesada R., Rodríguez M.I., Linares J.L., de Almodóvar M.R., Oliver F.J. PARP inhibitors: New partners in the therapy of cancer and inflammatory diseases. *Free Radic. Biol. Med.* 2009;47:13–26. doi: 10.1016/j.freeradbiomed.2009.04.008.
34. Gariani K., Ryu D., Menzies K.J., Yi H.-S., Stein S., Zhang H., Perino A., Lemos V., Katsyuba E., Jha P., et al. Inhibiting poly ADP-ribosylation increases fatty acid oxidation and protects against fatty liver disease. *J. Hepatol.* 2017;66:132–141. doi: 10.1016/j.jhep.2016.08.024.
35. Sachdev E., Tabatabai R., Roy V., Rimel B.J., Mita M.M. PARP Inhibition in Cancer: An Update on Clinical Development. *Target. Oncol.* 2019;14:657–679. doi: 10.1007/s11523-019-00680-2.
36. Sriram C.S., Jangra A., Kasala E.R., Bodduluru L.N., Bezbaruah B.K. Targeting poly(ADP-ribose)polymerase1 in neurological diseases: A promising trove for new pharmacological interventions to enter clinical translation. *Neurochem. Int.* 2014;76:70–81. doi: 10.1016/j.neuint.2014.07.001.
37. Laudisi F., Sambucci M., Pioli C. Poly (ADP-ribose) polymerase-1 (PARP-1) as immune regulator. *Endocr. Metab. Immune Disord.-Drug Targets.* 2011;11:326–333. doi: 10.2174/187153011797881184.
38. Kim J.-E., Kim Y.-J., Kim J.-Y., Kang T.-C. PARP1 activation/expression modulates regional-specific neuronal and glial responses to seizure in a hemodynamic-independent manner. *Cell Death Dis.* 2014;5:e1362. doi: 10.1038/cddis.2014.331.

39. Jacewicz M., Czapski G.A., Katkowska I., Strosznajder R.P. Systemic administration of lipopolysaccharide impairs glutathione redox state and object recognition in male mice. The effect of PARP-1 inhibitor. *Folia Neuropathol.* 2009;47:20054784.
40. Goldberg S., Visochek L., Giladi E., Gozes I., Cohen-Armon M. PolyADP-ribosylation is required for long-term memory formation in mammals. *J. Neurochem.* 2009;111:72–79. doi: 10.1111/j.1471-4159.2009.06296.x.
41. Pieper A., Blackshaw S., Clements E.E., Brat D.J., Krug D.K., White A.J., Pinto-Garcia P., Favit A., Conover J.R., Snyder S.H., et al. Poly(ADP-ribosyl)ation basally activated by DNA strand breaks reflects glutamate-nitric oxide neurotransmission. *Proc. Natl. Acad. Sci. USA.* 2000;97:1845–1850. doi: 10.1073/pnas.97.4.1845.
42. Wang H., Shimoji M., Yu S.-W., Dawson T.M., Dawson V.L. Apoptosis inducing factor and PARP-mediated injury in the MPTP mouse model of Parkinson's disease. *Ann. N. Y. Acad. Sci.* 2006;991:132–139. doi: 10.1111/j.1749-6632.2003.tb07471.x.
43. Meinertzhagen I.A., Takemura S.-Y., Lu Z., Huang S., Gao S., Ting C.-Y., Lee C.-H. From Form to Function: The Ways to Know a Neuron. *J. Neurogenet.* 2009;23:68–77. doi: 10.1080/01677060802610604.
44. Hocsak E., Szabo V., Kalman N., Antus C., Cseh A., Sumegi K., Eros K., Hegedus Z., Gallyas F., Sumegi B., et al. PARP inhibition protects mitochondria and reduces ROS production via PARP-1-ATF4-MKP-1-MAPK retrograde pathway. *Free Radic. Biol. Med.* 2017;108:770–784. doi: 10.1016/j.freeradbiomed.2017.04.018.
45. Dawson T.M., Dawson V.L. *Advances in Pharmacology.* Volume 82. Elsevier; Amsterdam, The Netherlands: 2018. Nitric oxide signaling in neurodegeneration and cell death; pp. 57–83.

46. Alano C.C., Garnier P., Ying W., Higashi Y., Kauppinen T., Swanson R. $NAD^+$ Depletion Is Necessary and Sufficient forPoly(ADP-Ribose) Polymerase-1-Mediated Neuronal Death. *J. Neurosci.* 2010;30:2967–2978. doi: 10.1523/JNEUROSCI.5552-09.2010.

47. Gerace E., Masi A., Resta F., Felici R., Landucci E.C.T., Mello T., Pellegrinigiampietro D.E., Mannaioni G., Moroni F. PARP-1 activation causes neuronal death in the hippocampal CA1 region by increasing the expression of $Ca^{2+}$-permeable AMPA receptors. *Neurobiol. Dis.* 2014;70:43–52. doi: 10.1016/j.nbd.2014.05.023.

48. Weiss J.H. $Ca^{2+}$ Permeable AMPA Channels in Diseases of the Nervous System. *Front. Mol. Neurosci.* 2011;4:42. doi: 10.3389/fnmol.2011.00042.

49. Stoica B.A., Loane D., Zhao Z., Kabadi S.V., Hanscom M., Byrnes K., Faden A.I. PARP-1 Inhibition Attenuates Neuronal Loss, Microglia Activation and Neurological Deficits after Traumatic Brain Injury. *J. Neurotrauma.* 2014;31:758–772. doi: 10.1089/neu.2013.3194.

50. Brochier C., Jones J.I., Willis D.E., Langley B. Poly(ADP-ribose) polymerase 1 is a novel target to promote axonal regeneration. *Proc. Natl. Acad. Sci. USA.* 2015;112:15220–15225. doi: 10.1073/pnas.1509754112.

51. Zhou B., Zhu Z., Ransom B.R., Tong X. Oligodendrocyte lineage cells and depression. *Mol. Psychiatry.* 2021;26:103–117. doi: 10.1038/s41380-020-00930-0.

52. Elbaz B., Popko B. Molecular Control of Oligodendrocyte Development. *Trends Neurosci.* 2019;42:263–277. doi: 10.1016/j.tins.2019.01.002.

53. Domingues H.S., Cruz A., Chan J.R., Relvas J., Rubinstein B., Pinto I.M. Mechanical plasticity during oligodendrocyte differentiation and myelination. *Glia.* 2018;66:5–14. doi: 10.1002/glia.23206.

54. Bercury K.K., Macklin W.B. Dynamics and Mechanisms of CNS Myelination. *Dev. Cell.* 2015;32:447–458. doi: 10.1016/j.devcel.2015.01.016.

55. Wang Y., Zhang Y., Zhang S., Kim B., Hull V.L., Xu J., Prabhu P., Gregory M., Martinez-Cerdeno V., Zhan X., et al. PARP1-mediated PARylation activity is essential for oligodendroglial differentiation and CNS myelination. *Cell Rep.* 2021;37:109695. doi: 10.1016/j.celrep.2021.109695.

56. Veto S., Acs P., Bauer J., Lassmann H., Berente Z., Setalo G., Borgulya G., Sumegi B., Komoly S., Gallyas F., et al. Inhibiting poly(ADP-ribose) polymerase: A potential therapy against oligodendrocyte death. *Brain.* 2010;133:822–834. doi: 10.1093/brain/awp337.

57. Domercq M., Mato S., Soria F.N., Sánchez-Gómez M.V., Alberdi E., Matute C. Zn2+-induced ERK activation mediates PARP-1-dependent ischemic-reoxygenation damage to oligodendrocytes. *Glia.* 2013;61:383–393. doi: 10.1002/glia.22441.

58. Baldassarro V.A., Marchesini A., Giardino L., Calzà L. PARP activity and inhibition in fetal and adult oligodendrocyte precursor cells: Effect on cell survival and differentiation. *Stem Cell Res.* 2017;22:54–60. doi: 10.1016/j.scr.2017.05.011.

59. Kauppinen T.M., Swanson R.A. Poly(ADP-Ribose) Polymerase-1 Promotes Microglial Activation, Proliferation, and Matrix Metalloproteinase-9-Mediated Neuron Death. *J. Immunol.* 2005;174:2288–2296. doi: 10.4049/jimmunol.174.4.2288.

60. Mehrabadi A.R., Korolainen M.A., Odero G., Miller D.W., Kauppinen T.M. Poly(ADP-ribose) polymerase-1 regulates microglia mediated decrease of endothelial tight junction integrity. *Neurochem. Int.* 2017;108:266–271. doi: 10.1016/j.neuint.2017.04.014.

61. Ullrich O., Diestel A., Eyüpoglu I.Y., Nitsch R. Regulation of microglial expression of integrins by poly(ADP-ribose) polymerase-1. *Nat. Cell Biol.* 2001;3:1035–1042. doi: 10.1038/ncb1201-1035.
62. Raghunatha P., Vosoughi A., Kauppinen T.M., Jackson M.F. Microglial NMDA receptors drive pro-inflammatory responses via PARP-1/TRMP2 signaling. *Glia.* 2020;68:1421–1434. doi: 10.1002/glia.23790.
63. Guillamón-Vivancos T., Gómez-Pinedo U., Matías-Guiu J. Astrocitos en las enfermedades neurodegenerativas (I): Función y caracterización molecular. *Neurología.* 2015;30:119–129. doi: 10.1016/j.nrl.2012.12.007.
64. Kim Y., Park J., Choi Y.K. The Role of Astrocytes in the Central Nervous System Focused on BK Channel and Heme Oxygenase Metabolites: A Review. *Antioxidants.* 2019;8:121. doi: 10.3390/antiox8050121.
65. Martínez-Zamudio R.I., Ha H.C. PARP 1 enhances inflammatory cytokine expression by alteration of promoter chromatin structure in microglia. *Brain Behav.* 2014;4:552–565. doi: 10.1002/brb3.239.
66. Phulwani N.K., Kielian T. Poly (ADP-ribose) polymerases (PARPs) 1-3 regulate astrocyte activation. *J. Neurochem.* 2008;106:578–590. doi: 10.1111/j.1471-4159.2008.05403.x.
67. Alano C.C., Ying W., Swanson R. Poly(ADP-ribose) Polymerase-1-mediated Cell Death in Astrocytes Requires $NAD^+$ Depletion and Mitochondrial Permeability Transition. *J. Biol. Chem.* 2004;279:18895–18902. doi: 10.1074/jbc.M313329200.
68. Tang K.S., Suh S.W., Alano C.C., Shao Z., Hunt W.T., Swanson R.A., Anderson C.M. Astrocytic poly(ADP-ribose) polymerase-1 activation leads to bioenergetic depletion and inhibition of glutamate uptake capacity. *Glia.* 2009;58:446–457. doi: 10.1002/glia.20936.

69. Sinha A., Katyal S., Kauppinen T.M. PARP-DNA trapping ability of PARP inhibitors jeopardizes astrocyte viability: Implications for CNS disease therapeutics. *Neuropharmacology.* 2021;187:108502. doi: 10.1016/j.neuropharm.2021.108502.
70. Mao K., Zhang G. The role of PARP1 in neurodegenerative diseases and aging. *FEBS J.* 2021 doi: 10.1111/febs.15716.
71. Ghasemi N., Razavi S., Nikzad E. Multiple Sclerosis: Pathogenesis, Symptoms, Diagnoses and Cell-Based Therapy. *Cell J.* 2017;19:1–10.
72. Kauppinen T.M., Suh S.W., Genain C.P., Swanson R.A. Poly(ADP-ribose) polymerase-1 activation in a primate model of multiple sclerosis. *J. Neurosci. Res.* 2005;81:190–198. doi: 10.1002/jnr.20525.
73. Scott G., Hake P., Kean R., Virág L., Szabó C., Hooper D. Role of poly(ADP-ribose) synthetase activation in the development of experimental allergic encephalomyelitis. *J. Neuroimmunol.* 2001;117:78–86. doi: 10.1016/S0165-5728(01)00329-0.
74. Scott G.S., Kean R.B., Mikheeva T., Fabis M.J., Mabley J., Szabó C., Hooper D.C. The Therapeutic Effects of PJ34 [N-(6-Oxo-5,6-dihydrophenanthridin-2-yl)-N,N-dimethylacetamide.HCl], a Selective Inhibitor of Poly(ADP-Ribose) Polymerase, in Experimental Allergic Encephalomyelitis Are Associated with Immunomodulation. *J. Pharmacol. Exp. Ther.* 2004;310:1053–1061. doi: 10.1124/jpet.103.063214.
75. Cavone L., Chiarugi A. Targeting poly(ADP-ribose) polymerase-1 as a promising approach for immunomodulation in multiple sclerosis? *Trends Mol. Med.* 2012;18:92–100. doi: 10.1016/j.molmed.2011.10.002.
76. Cavone L., Aldinucci A., Ballerini C., Biagioli T., Moroni F., Chiarugi A. PARP-1 inhibition prevents CNS migration of dendritic cells during EAE, suppressing the

encephalitogenic response and relapse severity. *Mult. Scler. J.* 2011;17:794–807. doi: 10.1177/1352458511399113.

77. Rom S., Zuluaga-Ramirez V., Reichenbach N.L., Dykstra H., Gajghate S., Pacher P., Persidsky Y. PARP inhibition in leukocytes diminishes inflammation via effects on integrins/cytoskeleton and protects the blood-brain barrier. *J. Neuroinflamm.* 2016;13:254. doi: 10.1186/s12974-016-0729-x.
78. Goedert M. Alpha-synuclein and neurodegenerative diseases. *Nat. Rev. Neurosci.* 2001;2:492–501. doi: 10.1038/35081564.
79. Kam T.-I., Mao X., Park H., Chou S.-C., Karuppagounder S.S., Umanah G.E., Yun S.P., Brahmachari S., Panicker N., Chen R., et al. Poly(ADP-ribose) drives pathologic α-synuclein neurodegeneration in Parkinson's disease. *Science.* 2018;362:eaat8407. doi: 10.1126/science.aat8407.
80. Salech F., Ponce D.P., Sanmartín C.D., Rogers N.K., Henríquez M., Behrens M.I. Cancer Imprints an Increased PARP-1 and p53-Dependent Resistance to Oxidative Stress on Lymphocytes of Patients That Later Develop Alzheimer's Disease. *Front. Neurosci.* 2018;12:58. doi: 10.3389/fnins.2018.00058.
81. Salech F., Ponce D.P., Paula-Lima A.C., Sanmartin C.D., Behrens M.I. Nicotinamide, a Poly [ADP-Ribose] Polymerase 1 (PARP-1) Inhibitor, as an Adjunctive Therapy for the Treatment of Alzheimer's Disease. *Front. Aging Neurosci.* 2020;12:255. doi: 10.3389/fnagi.2020.00255.
82. Michelena J., Lezaja A., Teloni F., Schmid T., Imhof R., Altmeyer M. Analysis of PARP inhibitor toxicity by multidimensional fluorescence microscopy reveals mechanisms of sensitivity and resistance. *Nat. Commun.* 2018;9:2678. doi: 10.1038/s41467-018-05031-9.

83. Green K.N., Steffan J.S., Martínez-Coria H., Sun X., Schreiber S.S., Thompson L.M., LaFerla F.M. Nicotinamide Restores Cognition in Alzheimer's Disease Transgenic Mice via a Mechanism Involving Sirtuin Inhibition and Selective Reduction of Thr231-Phosphotau. *J. Neurosci.* 2008;28:11500–11510. doi: 10.1523/JNEUROSCI.3203-08.2008.

84. Cosi C., Colpaert F., Koek W., Degryse A., Marien M. Poly(ADP-ribose) polymerase inhibitors protect against MPTP-induced depletions of striatal dopamine and cortical noradrenaline in C57B1/6 mice. *Brain Res.* 1996;729:264–269. doi: 10.1016/0006-8993(96)00571-9.

85. Cosi C., Guerin K., Marien M., Koek W., Rollet K. The PARP inhibitor benzamide protects against kainate and NMDA but not AMPA lesioning of the mouse striatum *in vivo*. *Brain Res.* 2004;996:1–8. doi: 10.1016/j.brainres.2003.09.072.

86. Liu D., Pitta M., Jiang H., Lee J.-H., Zhang G., Chen X., Kawamoto E.M., Mattson M.P. Nicotinamide forestalls pathology and cognitive decline in Alzheimer mice: Evidence for improved neuronal bioenergetics and autophagy procession. *Neurobiol. Aging.* 2013;34:1564–1580. doi: 10.1016/j.neurobiolaging.2012.11.020. Erratum in *Neurobiol. Aging* **2013**, *34*, e3.

87. Czapski G.A., Cieślik M., Wencel P.L., Wójtowicz S., Strosznajder R.P., Strosznajder J.B. Inhibition of poly(ADP-ribose) polymerase-1 alters expression of mitochondria-related genes in PC12 cells: Relevance to mitochondrial homeostasis in neurodegenerative disorders. *Biochim. Biophys. Acta Mol. Cell Res.* 2018;1865:281–288. doi: 10.1016/j.bbamcr.2017.11.003.

88. Martire S., Fuso A., Rotili D., Tempera I., Giordano C., De Zottis I., Muzi A., Vernole P., Graziani G., Lococo E., et al. PARP-1 Modulates Amyloid Beta Peptide-Induced Neuronal Damage. *PLoS ONE.* 2013;8:e72169. doi: 10.1371/journal.pone.0072169.

89. Xu J.-C., Fan J., Wang X., Eacker S.M., Kam T.-I., Chen L., Yin X., Zhu J., Chi Z., Jiang H., et al. Cultured networks of excitatory projection neurons and inhibitory interneurons for studying human cortical neurotoxicity. *Sci. Transl. Med.* 2016;8:333ra48. doi: 10.1126/scitranslmed.aad0623.
90. Gieselmann V. Metachromatic Leukodystrophy: Recent Research Developments. *J. Child Neurol.* 2003;18:591–594. doi: 10.1177/08830738030180090301.
91. Biffi A., Cesani M., Fumagalli F., Del Carro U., Baldoli C., Canale S., Gerevini S., Amadio S., Falautano M., Rovelli A., et al. Metachromatic leukodystrophy—Mutation analysis provides further evidence of genotype-phenotype correlation. *Clin. Genet.* 2008;74:349–357. doi: 10.1111/j.1399-0004.2008.01058.x.
92. Rosenberg J.B., Kaminsky S., Aubourg P., Crystal R.G., Sondhi D. Gene therapy for metachromatic leukodystrophy. *J. Neurosci. Res.* 2016;94:1169–1179. doi: 10.1002/jnr.23792.
93. Thibert K.A., Raymond G.V., Tolar J., Miller W.P., Orchard P.J., Lund T.C. Cerebral Spinal Fluid levels of Cytokines are elevated in Patients with Metachromatic Leukodystrophy. *Sci. Rep.* 2016;6:24579. doi: 10.1038/srep24579.
94. Eichler F., Van Haren K. Immune Response in Leukodystrophies. *Pediatr. Neurol.* 2007;37:235–244. doi: 10.1016/j.pediatrneurol.2007.06.011.
95. Bergner C.G., van der Meer F., Winkler A., Wrzos C., Türkmen M., Valizada E., Fitzner D., Hametner S., Hartmann C., Pfeifenbring S., et al. Microglia damage precedes major myelin breakdown in X-linked adrenoleukodystrophy and metachromatic leukodystrophy. *Glia.* 2019;67:1196–1209. doi: 10.1002/glia.23598.
96. Stein A., Stroobants S., Gieselmann V., D'Hooge R., Matzner U. Anti-inflammatory Therapy with Simvastatin Improves Neuroinflammation and CNS Function in a Mouse

Model of Metachromatic Leukodystrophy. *Mol. Ther*. 2015;23:1160–1168. doi: 10.1038/mt.2015.69.

97. Teng F., Zhu L., Su J., Zhang X., Li N., Nie Z., Jin L. Neuroprotective Effects of Poly(ADP-ribose)polymerase Inhibitor Olaparib in Transient Cerebral Ischemia. *Neurochem. Res.* 2016;41:1516–1526. doi: 10.1007/s11064-016-1864-6.
98. Moroni F., Cozzi A., Chiarugi A., Formentini L., Camaioni E., Pellegrini-Giampietro D., Chen Y., Liang S., Zaleska M., Gonzales C., et al. Long-lasting neuroprotection and neurological improvement in stroke models with new, potent and brain permeable inhibitors of poly(ADP-ribose) polymerase. *J. Cereb. Blood Flow Metab.* 2012;165:1487–1500. doi: 10.1111/j.1476-5381.2011.01666.x.
99. Matsushima G.K., Morell P. The Neurotoxicant, Cuprizone, as a Model to Study Demyelination and Remyelination in the Central Nervous System. *Brain Pathol.* 2006;11:107–116. doi: 10.1111/j.1750-3639.2001.tb00385.x.
100. D'Avila J.C., I Lam T., Bingham D., Shi J., Won S.J., Kauppinen T.M., Massa S., Liu J., Swanson R.A. Microglial activation induced by brain trauma is suppressed by post-injury treatment with a PARP inhibitor. *J. Neuroinflamm.* 2012;9:31. doi: 10.1186/1742-2094-9-31.
101. Waldman A.T. Leukodystrophies. *Contin. Lifelong Learn. Neurol.* 2018;24:130–149. doi: 10.1212/CON.0000000000000560.
102. Ashrafi M.R., Amanat M., Garshasbi M., Kameli R., Nilipour Y., Heidari M., Rezaei Z., Tavasoli A.R. An update on clinical, pathological, diagnostic, and therapeutic perspectives of childhood leukodystrophies. *Expert Rev. Neurother.* 2020;20:65–84. doi: 10.1080/14737175.2020.1699060.
104. Perlman S.J., Mar S. Leukodystrophies. *Adv. Exp. Med. Biol.* 2012;724:154–171. doi: 10.1007/978-1-4614-0653-2_13.

105. van der Knaap M.S., Schiffmann R., Mochel F., Wolf N. Diagnosis, prognosis, and treatment of leukodystrophies. *Lancet Neurol.* 2019;18:962–972. doi: 10.1016/S1474-4422(19)30143-7.

106. Béchet S., O'Sullivan S.A., Yssel J., Fagan S.G., Dev K.K. Fingolimod Rescues Demyelination in a Mouse Model of Krabbe's Disease. *J. Neurosci.* 2020;40:3104–3118. doi: 10.1523/JNEUROSCI.2346-19.2020.

107. Steffen JD, Brody JR, Armen RS, Pascal JM. Structural Implications for Selective Targeting of PARPs. Front Oncol. 2013 Dec 20;3:301. doi: 10.3389/fonc.2013.00301. PMID: 24392349; PMCID: PMC3868897.

108. Elain G, Jeanneau K, Rutkowska A, Mir AK, Dev KK. The selective anti-IL17A monoclonal antibody secukinumab (AIN457) attenuates IL17A-induced levels of IL6 in human astrocytes. Glia. 2014 May;62(5):725-35. doi: 10.1002/glia.22637. PMID: 24677511.

109. Rutkowska A, Preuss I, Gessier F, Sailer AW, Dev KK. EBI2 regulates intracellular signaling and migration in human astrocyte. Glia. 2015 Feb;63(2):341-51. doi: 10.1002/glia.22757. Epub 2014 Oct 9. PMID: 25297897.

110. Dali CÍ, Barton NW, Farah MH, Moldovan M, Månsson JE, Nair N, Dunø M, Risom L, Cao H, Pan L, Sellos-Moura M, Corse AM, Krarup C. Sulfatides levels correlate with severity of neuropathy in metachromatic leukodystrophy. Ann Clin Transl Neurol. 2015 May;2(5):518-33. doi: 10.1002/acn3.193. Epub 2015 Mar 27. PMID: 26000324; PMCID: PMC4435706.

111. Takahashi T, Suzuki T. Role of sulfatides in normal and pathological cells and tissues. J Lipid Res. 2012 Aug;53(8):1437-50. doi: 10.1194/jlr.R026682. Epub 2012 May 22. PMID: 22619219; PMCID: PMC3540844.

112. Camargo, N.; Goudriaan, A.; Van Deijk, A.-L.F.; Otte, W.; Brouwers, J.F.; Lodder, H.; Gutmann, D.; Nave, K.-A.; Dijkhuizen, R.M.; Mansvelder, H.; et al. Oligodendroglial myelination requires astrocyte-derived lipids. PLoS Biol. 2017, 15, e1002605.

113. Abbott, N.J.; Rönnbäck, L.; Hansson, E. Astrocyte–endothelial interactions at the blood–brain barrier. Nat. Rev. Neurosci. 2006, 7, 41–53.

114. Mekhaeil M, Dev KK, Conroy MJ. Existing Evidence for the Repurposing of PARP-1 Inhibitors in Rare Demyelinating Diseases. Cancers (Basel). 2022 Jan 29;14(3):687. doi: 10.3390/cancers14030687. PMID: 35158955; PMCID: PMC8833351.

115. Bai P. Biology of Poly(ADP-Ribose) Polymerases: The Factotums of Cell Maintenance. Mol Cell. 2015 Jun 18;58(6):947-58. doi: 10.1016/j.molcel.2015.01.034. PMID: 26091343.

116. Vosler PS, Sun D, Wang S, et al. Calcium dysregulation induces apoptosis-inducing factor release: cross-talk between PARP-1- and calpain-signaling pathways. *Exp Neurol*. 2009;218(2):213-220. doi:10.1016/j.expneurol.2009.04.032

117. Molander-Melin M, Pernber Z, Franken S, Gieselmann V, Mansson JE, Fredman P. Accumulation of sulfatides in neuronal and glial cells of arylsulfatase A deficient mice. *J Neurocytol.* 2004;33:417–427.

118. Bezprozvanny I. Calcium signaling and neurodegenerative diseases. Trends Mol Med. 2009 Mar;15(3):89-100. doi: 10.1016/j.molmed.2009.01.001. Epub 2009 Feb 21. PMID: 19230774; PMCID: PMC3226745.

119. Bezzi P, Carmignoto G, Pasti L, Vesce S, Rossi D, Rizzini BL, Pozzan T, Volterra A. Prostaglandins stimulate calcium-dependent glutamate release in

astrocytes. Nature. 1998 Jan 15;391(6664):281-5. doi: 10.1038/34651. PMID: 9440691.

120. Zong WX, Ditsworth D, Bauer DE, Wang ZQ, Thompson CB. Alkylating DNA damage stimulates a regulated form of necrotic cell death. Genes Dev. 2004 Jun 1;18(11):1272-82. doi: 10.1101/gad.1199904. Epub 2004 May 14. PMID: 15145826; PMCID: PMC420353.

121. Yu SW, Wang H, Poitras MF, Coombs C, Bowers WJ, Federoff HJ, Poirier GG, Dawson TM, Dawson VL. Mediation of poly(ADP-ribose) polymerase-1-dependent cell death by apoptosis-inducing factor. Science. 2002 Jul 12;297(5579):259-63. doi: 10.1126/science.1072221. PMID: 12114629.

122. Szabó C (2002b) Role of poly(ADP-ribose) synthetase in inflammation.

123. Kraus WL and Lis JT (2003) PARP goes transcription. Cell **113:** 677-683.

124. Hooper DC, Scott GS, Zborek A, Mikheeva T, Kean RB, Koprowski H, and Spitsin SV (2000) Uric acid, a peroxynitrite scavenger, inhibits CNS inflammation, blood-CNS barrier permeability changes and tissue damage in a mouse model of multiple sclerosis. FASEB J **14:** 691-698.

125. Kean RB, Spitsin SV, Mikhaeva T, Scott GS, and Hooper DC (2000) The peroxynitrite scavenger uric acid prevents inflammatory cell invasion into the CNS in experimental allergic encephalomyelitis through maintenance of blood-CNS barrier integrity. J Immunol **165:** 6511-6518.

126. Lieberman, A. P., Pitha, P. M., Shin, H. S., & Shin, M. L. (1989). Production of tumor necrosis factor and other cytokines by astrocytes stimulated with lipopolysaccharide or a neurotropic virus. Proceedings of the National Academy of Sciences of the United States of America, 86(16), 6348–6352.

127. Rothhammer, V., & Quintana, F. J. (2015). Control of autoimmune CNS inflammation by astrocytes. Seminars in Immunopathology, 37(6), 625–638.

128. Zingarelli B, Salzman AL, and Szabó C (1998) Genetic disruption of poly(ADP-Ribose) synthetase inhibits the expression of P-selectin and intercellular adhesion molecule-1 in myocardial ischemia/reperfusion injury. Circ Res **83:** 85-94.

129. Sharp C, Warren A, Oshima T, Williams L, Li JH, and Alexander JS (2001) Poly ADP-ribose-polymerase inhibitors prevent the upregulation of ICAM-1 and E-selectin in response to Th1 cytokine stimulation. Inflammation **25:** 157-163.

130. Claycomb, K., Johnson, K., Winokur, P., Sacino, A. and Crocker, S. (2013). Astrocyte regulation of CNS inflammation and remyelination. Brain Sci. 3, 1109-1127.

131. Sharma, R., Fischer, M.-T., Bauer, J., Felts, P. A., Smith, K. J., Misu, T., Fujihara, K., Bradl, M. and Lassmann, H. (2010). Inflammation induced by innate immunity in the central nervous system leads to primary astrocyte dysfunction followed by demyelination. Acta Neuropathol. 120, 223-236.

132. Heimfarth L, Loureiro SO, Dutra MF, Petenuzzo L, de Lima BO, Fernandes CG, da Rocha JB, Pessoa-Pureur R. Disrupted cytoskeletal homeostasis, astrogliosis and apoptotic cell death in the cerebellum of preweaning rats injected with diphenyl ditelluride. Neurotoxicology. 2013 Jan;34:175-88. doi: 10.1016/j.neuro.2012.10.015. Epub 2012 Nov 24. PMID: 23182946.

133. Louis ED, Ma K, Babij R, Cortés E, Liem RK, Vonsattel JP, Faust PL. Neurofilament protein levels: quantitative analysis in essential tremor cerebellar cortex. Neurosci Lett. 2012 Jun 14;518(1):49-54. doi: 10.1016/j.neulet.2012.04.054. Epub 2012 May 4. PMID: 22561033; PMCID: PMC3364538.

134. Misslin C, Velasco-Estevez M, Albert M, O'Sullivan SA, Dev KK. Phospholipase A2 is involved in galactosylsphingosine-induced astrocyte toxicity,

neuronal damage and demyelination. PLoS One. 2017 Nov 2;12(11):e0187217. doi: 10.1371/journal.pone.0187217. PMID: 29095858; PMCID: PMC5667767.

135. O'Sullivan SA, Dev KK. The chemokine fractalkine (CX3CL1) attenuates H2O2-induced demyelination in cerebellar slices. J Neuroinflammation. 2017 Aug 15;14(1):159. doi: 10.1186/s12974-017-0932-4. PMID: 28810923; PMCID: PMC5558650.

136. Cao KH, Zhang G, Jacobsen L, Wu J. LC-MS/MS assays to quantify sulfatides and lysosulfatide in cerebrospinal fluid of metachromatic leukodystrophy patients. Bioanalysis. 2020 Nov;12(22):1621-1633. doi: 10.4155/bio-2020-0200. Epub 2020 Nov 5. PMID: 33151743.

137. Jeon SB, Yoon HJ, Park SH, Kim IH, Park EJ. Sulfatide, a major lipid component of myelin sheath, activates inflammatory responses as an endogenous stimulator in brain-resident immune cells. J Immunol. 2008 Dec 1;181(11):8077-87. doi: 10.4049/jimmunol.181.11.8077. PMID: 19018000.

138. Konno A, Nunogami K, Wada T, Yachie A, Suzuki Y, Takahashi N, Suzuki T, Miyamoto D, Kiso M, Hasegawa A, Miyawaki T. Inhibitory action of sulfatide, a putative ligand for L-selectin, on B cell proliferation and Ig production. Int Immunol. 1996 Dec;8(12):1905-13. doi: 10.1093/intimm/8.12.1905. PMID: 8982775.

139. Kanamori M, Tasumi Y, Iyoda T, Ushida M, Inaba K. Sulfatide inhibits α-galactosylceramide presentation by dendritic cells. Int Immunol. 2012 Feb;24(2):129-36. doi: 10.1093/intimm/dxr108. Epub 2012 Jan 12. PMID: 22247226.

140. Lyra E, Silva NM, Gonçalves RA, Pascoal TA, Lima-Filho RAS, Resende EPF, Vieira ELM, Teixeira AL, de Souza LC, Peny JA, Fortuna JTS, Furigo IC, Hashiguchi D, Miya-Coreixas VS, Clarke JR, Abisambra JF, Longo BM, Donato J Jr, Fraser PE, Rosa-Neto P, Caramelli P, Ferreira ST, De Felice FG. Pro-inflammatory interleukin-6

signaling links cognitive impairments and peripheral metabolic alterations in Alzheimer’s disease. Transl Psychiatry. 2021;11(1):251. PMID: 33911072; PMCID: PMC8080782.

141. Muhammad M. Tumor necrosis factor alpha: a major cytokine of brain neuroinflammation. Cytokines. 2019;861231.

142. Nasiri E, Sankowski R, Dietrich H, Oikonomidi A, Huerta PT, Popp J, Al-Abed Y, Bacher M. Key role of MIF-related neuroinflammation in neurodegeneration and cognitive impairment in Alzheimer's disease. Mol Med. 2020 Apr 17;26(1):34. doi: 10.1186/s10020-020-00163-5. PMID: 32303185; PMCID: PMC7164357.

143. Sospedra M, Martin R. Immunology of multiple sclerosis. Annu Rev Immunol. 2005;23:683–747.

144. Bettelli E, Korn T, Oukka M, Kuchroo VK. Induction and effector functions of T(H)17 cells. Nature. 2008 Jun 19;453(7198):1051-7. doi: 10.1038/nature07036. PMID: 18563156; PMCID: PMC6280661.

145. Graziano AC, Cardile V. History, genetic, and recent advances on Krabbe disease. Gene. 2015 Jan 15;555(1):2-13. doi: 10.1016/j.gene.2014.09.046. Epub 2014 Sep 26. PMID: 25260228.

146. Suzuki K, Suzuki Y. Globoid cell leucodystrophy (Krabbe's disease): deficiency of galactocerebroside beta-galactosidase. Proc Natl Acad Sci U S A. 1970 Jun;66(2):302-9. doi: 10.1073/pnas.66.2.302. PMID: 5271165; PMCID: PMC283044.

147. Mekhaeil M, Conroy MJ, Dev KK. Olaparib Attenuates Demyelination and Neuroinflammation in an Organotypic Slice Culture Model of Metachromatic Leukodystrophy. Neurotherapeutics. 2023 Sep;20(5):1347-1368. doi: 10.1007/s13311-023-01409-w. Epub 2023 Jul 31. PMID: 37525026; PMCID: PMC10480139.

148. Hawkins-Salsbury JA, Qin EY, Reddy AS, Vogler CA, Sands MS. Oxidative stress as a therapeutic target in globoid cell leukodystrophy. Exp Neurol. 2012 Oct;237(2):444-52. doi: 10.1016/j.expneurol.2012.07.013. Epub 2012 Jul 28. PMID: 22849820; PMCID: PMC3443330.

149. Valavanidis A, Vlachogianni T, Fiotakis C. 8-hydroxy-2' -deoxyguanosine (8-OHdG): A critical biomarker of oxidative stress and carcinogenesis. J Environ Sci Health C Environ Carcinog Ecotoxicol Rev. 2009 Apr;27(2):120-39. doi: 10.1080/10590500902885684. PMID: 19412858.

150. Ijichi K, Brown GD, Moore CS, Lee JP, Winokur PN, Pagarigan R, Snyder EY, Bongarzone ER, Crocker SJ. MMP-3 mediates psychosine-induced globoid cell formation: implications for leukodystrophy pathology. Glia. 2013 May;61(5):765-77. doi: 10.1002/glia.22471. Epub 2013 Feb 13. PMID: 23404611; PMCID: PMC3804069.

151. Machhi J, Yeapuri P, Lu Y, Foster E, Chikhale R, Herskovitz J, Namminga KL, Olson KE, Abdelmoaty MM, Gao J, Quadros RM, Kiyota T, Jingjing L, Kevadiya BD, Wang X, Liu Y, Poluektova LY, Gurumurthy CB, Mosley RL, Gendelman HE. CD4+ effector T cells accelerate Alzheimer's disease in mice. J Neuroinflammation. 2021 Nov 19;18(1):272. doi: 10.1186/s12974-021-02308-7. PMID: 34798897; PMCID: PMC8603581.

152. Williams GP, Schonhoff AM, Jurkuvenaite A, Gallups NJ, Standaert DG, Harms AS. CD4 T cells mediate brain inflammation and neurodegeneration in a mouse model of Parkinson's disease. Brain. 2021 Aug 17;144(7):2047-2059. doi: 10.1093/brain/awab103. PMID: 33704423; PMCID: PMC8370411.

153. van Langelaar J, Rijvers L, Smolders J, van Luijn MM. B and T Cells Driving Multiple Sclerosis: Identity, Mechanisms and Potential Triggers. Front Immunol. 2020

May 8;11:760. doi: 10.3389/fimmu.2020.00760. PMID: 32457742; PMCID: PMC7225320.

154. Zhou Q, Schneider IC, Edes I, Honegger A, Bach P, Schönfeld K, Schambach A, Wels WS, Kneissl S, Uckert W, Buchholz CJ. T-cell receptor gene transfer exclusively to human CD8(+) cells enhances tumor cell killing. Blood. 2012 Nov 22;120(22):4334-42. doi: 10.1182/blood-2012-02-412973. Epub 2012 Aug 16. PMID: 22898597.

155. Martini R, Willison H. Neuroinflammation in the peripheral nerve: Cause, modulator, or bystander in peripheral neuropathies? Glia. 2016 Apr;64(4):475-86. doi: 10.1002/glia.22899. Epub 2015 Aug 6. PMID: 26250643; PMCID: PMC4832258.

156. Liddelow SA, Guttenplan KA, Clarke LE, Bennett FC, Bohlen CJ, Schirmer L, Bennett ML, Münch AE, Chung WS, Peterson TC, Wilton DK, Frouin A, Napier BA, Panicker N, Kumar M, Buckwalter MS, Rowitch DH, Dawson VL, Dawson TM, Stevens B, Barres BA. Neurotoxic reactive astrocytes are induced by activated microglia. Nature. 2017 Jan 26;541(7638):481-487. doi: 10.1038/nature21029. Epub 2017 Jan 18. PMID: 28099414; PMCID: PMC5404890.